**Université des Sciences et Technologies de Lille**

**Laboratoire de Mécanique de Lille**

**EDF R&D**

**Département Mécanique des Fluides, Energies et Environnement**

# Couplages fluide structure

**Elisabeth LONGATTE LACAZEDIEU**

## Habilitation à Diriger des Recherches

*Mécanique - Energétique*

*Soutenue lundi 3 juillet 2006 devant le jury composé de :*

Monsieur Franscico CHINESTA
Monsieur Aziz HAMDOUNI
Monsieur Dominique LAURENCE
Monsieur Roger OHAYON
Monsieur Serge PIPERNO
Monsieur Olivier PIRONNEAU
Monsieur Michaël SCHAEFER
Monsieur Mhamed SOULI

# REMERCIEMENTS

# REMERCIEMENTS

# SOMMAIRE

# SOMMAIRE

# SYNTHESE

# SYNTHESE

## 1. Résumé

Sur le parc nucléaire, le respect des critères de sûreté, l'optimisation de la maintenance et la maîtrise de la durée de vie des composants passent par une prévision fiable des mécanismes de vieillissement et d'endommagement, comme l'usure ou la fatigue vibratoire des structures mécaniques que les seules approches expérimentales actuelles ne permettent pas de prévoir dans leur globalité. La mise au point de nouvelles méthodes s'inscrit dans une perspective d'amélioration continue des processus de conception, d'exploitation et de maintenance des matériels. Elle fait l'objet d'un projet[1] engagé depuis 2001 à EDF R&D et consacré à la **préparation d'outils numériques prédictifs pour les études des composants de REP**[2], en particulier les études faisant intervenir des **couplages multi-physiques** comme les couplages fluide structure.

Ce document est consacré à la présentation de nouvelles méthodologies numériques pour la simulation des interactions fluide structure et des vibrations induites par les écoulements dans les REP. Il propose une classification des méthodologies en fonction de la nature des problèmes multi-physiques considérés de trois types :

1. **Physiques découplées**
2. **Physiques chaînées ou faiblement couplées**
3. **Physiques fortement couplées.**

Ces trois thématiques sont développées successivement. Après une présentation des méthodologies, des premiers éléments de qualification des méthodes sont proposés sur la base de cas tests semi-industriels, représentatifs de tout ou partie des composants de REP considérés. Quelques résultats marquants obtenus sur des applications industrielles sont présentés. Enfin, l'apport de la simulation numérique est mis en évidence, tout particulièrement l'accès à des informations nouvelles, fondamentales pour la compréhension des phénoménologies intervenant dans les couplages fluide structure et inaccessibles au travers des modélisations semi-empiriques mises en œuvre actuellement.

Dans la mesure du possible, le **caractère généraliste** des méthodes utilisées et des outils développés est souligné. Les exemples cités relèvent de domaines aussi diversifiés que : **l'interaction fluide structure, la vibration de structure induite par écoulement, l'acoustique, l'aéroacoustique, la thermohydraulique, la mécanique vibratoire, la dynamique, la dynamique rapide, la machine tournante, la thermique, la thermo-mécanique.**

Après un rappel du contexte industriel et des objectifs du programme de recherche qui a donné lieu à ces travaux, le document est décomposé en trois chapitres consacrés aux trois types de physiques considérés. Les principales perspectives de ces travaux sont abordées en conclusion.

[1] Projet NATIFS, Nouvelles Approches et Traitements en Interactions Fluide Structure, puis Lot IFS du Projet JUPITER.

[2] Réacteur à Eau Pressurisée.

Le chapitre I s'intéresse aux **physiques découplées** et à leurs modélisations en vue de leur couplage. L'objectif est de montrer l'importance des modélisations mono-physiques adoptées et de leur compatibilité aux interfaces. Pour ce faire, le document s'appuie sur plusieurs études réalisées dans le domaine de la modélisation de la turbulence. Deux applications sont illustrées :

- La simulation des écoulements turbulents en faisceaux de tubes fixes et l'estimation des chargements pariétaux induits par la turbulence avec une approche L.E.S.[3] en prévision des études vibratoires de tubes mobiles en présence d'écoulements transverses, axiaux ou obliques.
- La modélisation de la génération d'instabilités au niveau des couches de mélange par résolution d'équations fluides non linéaires et le lien avec l'identification de sources potentielles de bruit induites par la turbulence.

Dans tous les cas, les résultats numériques présentés font l'objet d'une validation par rapport à des données expérimentales ou analytiques et on s'attache à montrer l'impact du choix du modèle de turbulence sur les résultats au niveau de l'interface multi-physique en vue de la simulation des couplages.

Les problématiques **de chaînage et de couplage faible** sont abordées dans le chapitre II. L'objectif est de montrer la faisabilité et la pertinence de calculs chaînés fluide structure dans des configurations où les couplages forts peuvent être négligés, ou au moins contrôlés. Plusieurs exemples sont cités, relevant des domaines des vibrations sous écoulements, de l'aéroacoustique et de la dynamique.

Dans chaque cas, la procédure de **chaînage de codes** mise en œuvre est décrite, les méthodes numériques spécifiques à chacune des disciplines sont rappelées et des comparaisons calculs / mesures expérimentales / théories analytiques sont utilisées pour évaluer les performances des méthodologies de chaînage pour le traitement de configurations semi-industrielles représentatives des composants de REP.

Enfin le chapitre III est consacré à la simulation de **couplages faibles ou forts par couplages de codes**. Les principales applications présentées sont relatives au calcul des vibrations de structures induites par écoulements. La procédure de couplage retenue consiste en un couplage externe entre les codes fluide et structure avec une gestion adaptée de l'interface pouvant reposer sur une formulation fluide de type A.L.E.[4]. Les problématiques posées par la modélisation de la physique au niveau de l'interface des systèmes couplés et les méthodes numériques associées sont abordées.

Les développements réalisés ont abouti à l'élaboration d'un **coupleur** fluide structure appelé ***Cosmethyc***[5]. Quelques résultats obtenus avec l'outil sont présentés, comme l'identification numérique des caractéristiques vibratoires de tubes et faisceaux de tubes en présence de fluide et d'écoulements en termes de fréquences et d'amortissements vibratoires. Sur la base de confrontations calculs / mesures expérimentales / théories analytiques, on conclut que le coupleur développé et en cours d'évolution constitue un outil à caractère prédictif pour des configurations académiques. Les développements à venir des capacités de calculs permettront d'envisager son exploitation dans le cadre plus large des études industrielles.

[3] Large Eddy Simulation.

[4] Arbitraire Lagrange Euler.

[5] COupleur pour la Simulation MEcanique et ThermoHYdrauliQUE.

On peut dire que les **outils de chaînages et de couplages conçus, développés et mis en œuvre** seront opérationnels à court ou moyen terme pour la réalisation d'études locales des composants de REP faisant intervenir simultanément des problématiques aussi diverses que l'acoustique, la thermohydraulique, la mécanique, la dynamique, la thermique. Ils fourniront des informations nouvelles qui permettront de progresser dans la compréhension des phénoménologies en interaction fluide structure et favoriseront l'identification de paramètres inaccessibles par la mesure et cependant fondamentaux pour raison de sûreté. On peut citer la vitesse critique de départ en instabilité des tubes de générateurs de vapeur ou les caractéristiques de dimensionnement des grilles de mélange des assemblages combustibles.

Parmi les principales perspectives de ces travaux, outre l'amélioration des performances des codes, via le parallélisme notamment, et leurs nombreuses applications potentielles dans le cadre d'études industrielles, on peut mentionner la généralisation de ces développements au cas des écoulements diphasiques, domaine dans lequel on dispose également de nombreuses données expérimentales qui pourront être à la base de campagnes de qualification des outils numériques. L'extension des méthodes numériques et le recours à des méthodes alternatives seront également envisagés pour la simulation de nouveaux types de **phénomènes de couplages multi-physiques multi-échelles non linéaires**. Les couplages de modèles et de méthodes numériques pourront être à la base de ces généralisations d'outils, avec une gestion adaptée des interfaces associées.

Une présentation succincte du contexte fait office de préambule à ce document et propose une description des activités de recherche, d'enseignement et d'encadrement qui sont à l'origine des résultats exposés.

## 2. Summary

In nuclear power plants, maintaining systems in operating and safety conditions requires reliable prediction methods of possible wear and damage of components, especially for mechanical structures whose vibrations can not be perfectly forecast by the only experimental current techniques. Using new predictive approaches may provide improvement for designing, exploiting and maintaining installations. A project[6] devoted to preparation of new numerical methods has been created in 2001 in EDF R&D Division. The purpose is to prepare numerical tools for future studies on components, especially studies involving multi-physics problems, like fluid structure coupling.

This document presents new numerical methods for **simulation of fluid structure interactions and flow-induced vibrations** in PWR[7]. It gives a classification of methods according to the strength of multi-physics problems to be considered. They are of three kinds :

1. **Un-coupling**
2. **Chaining or weak coupling**
3. **Strong coupling.**

These three issues are successively developed. After a presentation of methodologies, examples for qualification of methods are given based on semi-industrial test cases featuring parts of PWR components. Main results in industrial applications are mentioned. Finally one

[6] Project NATIFS, New Approaches and Treatments in Fluid Structure Interactions, and Part FSI of Project JUPITER.

[7] Pressurized Water Reactor.

points out the interest of numerical simulation methods for predicting new information and understanding physics involving fluid structure interactions.

As far as possible, it is shown that numerical methods to be used and tools to be developed are **generalist**. Several examples of application are given in various areas like : **fluid structure interaction, flow-induced vibration, acoustics, aeroacoustics, thermohydraulics, mechanics, dynamics, fast dynamics, rotating machine, heat tranfer, thermo-mechanics.**

First context and objectives are recalled. Then the document is split into three parts devoted to the three kinds of physics to be considered. Finally outlooks and perspectives of this work are given as concluding remarks.

Part I is devoted to **uncoupled physics** and to their modelling before coupling. The purpose is to show how relevant the compatibility of each single-physic modelling at the interface is for coupling. The document presents specific studies dealing with turbulence and two main applications are illustrated on this issue :

- Simulation of turbulent cross flows in non-moving tube bundles and prediction of near-wall fluid loading induced by turbulence with a L.E.S.[8] approach for further studies on flexible tube vibrations induced by flows.
- Modelling of shear layer instability development by solving non linear fluid equations for further identification of noise sources generated by turbulence.

In all cases, numerical results are discussed and compared to experimental or analytical data. Effects of turbulence modelling on results are shown and its importance for coupled calculations is pointed out.

**Chaining and weak coupling** is investigated in chapter II. The purpose is to illustrate fluid structure chaining computations in configurations where strong coupling effects can be neglected or at least controlled. Several examples are developed related to flow-induced vibrations, aeroacoustics and dynamics.

In each case, the **code chaining** procedure is described, numerical methods for each physical problem are recalled and comparisons of computations / experiments / theories are performed for validation of methodologies in semi-industrial configurations modelling parts of PWR components.

Finally chapter III is devoted to simulation of **weak and strong coupling** problems by using **code coupling** procedure. Main applications to be presented are related to structure flow-induced vibrations. The coupling process consists in an external coupling of fluid and structure codes with a convenient computation of the interface possibly relying on a fluid A.L.E.[9] formulation. Issues dealing with interface modelling and associated numerical methods are investigated.

This work led to the development of a **coupling tool** called ***Cosmethyc***[10]. Results obtained with the tool are presented, like the identification of frequency and damping of tubes and tube bundles vibrating in the presence of fluid and flow. According to comparisons of calculations / experiments / theories, the tool is reliable in academic configurations. Improvement of computation capacities will enable further applications of the tool to industrial studies.

[8] Large Eddy Simulation

[9] Arbitrary Lagrange Euler.

[10] COupling for MEchanics and ThermoHYdrauliCs Simulation.

**Code chaining and coupling** procedures will be efficient for further local vibration studies on PWR components involving in the same time various areas like acoustics, thermohydraulics, mechanics, dynamics, heat transfer. Numerical results will provide new information enabling better understanding of physics involved by fluid structure interactions. Identification of significant parameters for safety will be possible, for example : critical flow velocity of steam generator tube bundles or dimension parameters of fuel assembly mixing grids.

Among the main outlooks of this work, one can mention the improvement of the tool performances by using parallelism, applications to industrial studies and extension of these development to two-phase flows. In this area, many experimental data also available and will be useful for qualification of numerical tools. New methods will also be considered like physical model coupling or numerical method coupling for simulation of new **multi-physics multi-scale non linear coupling problems,** with a specific attention paid to model interface treatment.

Before this work is presented, the document provides a short presentation of the context. It shows the aim and motivation of this work and gives a description of my research, teaching and managing activity.

# PARCOURS PROFESSIONNEL

# PARCOURS PROFESSIONNEL

## 1. Activités de recherche

### 1.1. Fonctions

| | |
|---|---|
| Ingénieur Chercheur Docteur ECP 98 à EDF R&D, au sein du Département Mécanique des Fluide, Energies et Environnement, dans le Pôle Interactions Fluide Structure du Groupe VIbrations et THermohydraulique dans les Echangeurs et les Cœurs. Pilotage de projets de recherche et participation à des activités sur la thermohydraulique et les vibrations induites par écoulements dans les composants de REP de centrales nucléaires. | *1999 – 2006* |
| Pilote du projet NATIFS Nouvelles Approches et Traitements en Interactions Fluide Structure puis du lot IFS du projet JUPITER consacrés à la simulation numérique des interactions fluide structure et des vibrations induites par écoulements dans les composants de REP par chaînage et couplage des codes de thermohydraulique (*Code_Saturne*) et de mécanique des structures (*Code_Aster*). Développements d'outils de chaînage et de couplage de codes en interactions fluide structure dans *Code_Saturne* et *Code_Aster*. Développement d'un outil prototype *Cosmethyc* COupleur pour la Simulation MEcanique et ThermoHYdraulique. Gestion de problématiques multi-physiques. Réalisation de travaux de validation et de qualification des outils sur la base de solutions théoriques et de données expérimentales. Applications aux études numériques des composants filaires de types générateurs de vapeur, grappes de commande, assemblages combustibles. | *2001 – 2006* |
| Pilote du projet CERAMHYC consacré à la préparation des méthodologies et outils destinés aux études de sûreté et de dimensionnement en thermohydraulique dans les cuves de réacteurs de conception EPR. | *2004 – 2006* |
| Chargée d'affaires et intervenant dans le projet SAGRAPPE puis CACHEMIRE sur la simulation du temps de chute des grappes de commande dans les REP. Développement d'un opérateur de calcul des chargements thermohydrauliques exercés sur les grappes en cours de chute dans *Code_Aster*. | *2001 – 2006* |
| Chargée d'affaires et intervenant dans plusieurs projets consacrés à l'étude du comportement vibratoire et des mécanismes d'endommagement par choc, usure, frottement, contact des grappes de commande des REP avec | *1999 – 2006* |

les composants antagonistes (assemblages combustibles, guides de grappe, mécanismes de commande) dans le cadre des projets UTRILO, Vibrations et usure des grappes de commande, Vibrations et usure des assemblages combustibles, PACHYDERME, CACHEMIRE, Suivi de Réseau avec *Code_Saturne*, *Code_Aster* et les outils d'analyse modale sous excitation non évaluée *Imene* et *Meidee* avec exploitation de la base de données expérimentales obtenues sur le banc d'essais *Phacetie*.

Doctorant au sein du Département Acoustique et Mécanique Vibratoire à EDF R&D sous la direction de Sébastien CANDEL avec le Laboratoire CNRS EM2C de l'Ecole Centrale Paris. *1995 – 1998*

### 1.2. Domaines de recherche

***Thématiques abordées***

Thermohydraulique, mécanique des fluides, mécanique des structures, dynamique linéaire, dynamique non linéaire, vibrations, interations fluide structure, écoulements turbulents, acoustique, aéroacoustique, couplages de codes, chaînages, couplages multi-physiques.

***Domaines d'application***

Durée de vie, tenue en service, endommagement par fatigue et usure des composants du domaine nucléaire : grappes de commande, générateurs de vapeur, assemblages combustibles, composants de cuve de réacteur, tuyauteries, singularités de réseaux de tuyauteries (robinetteries, vannes, soupapes).

### 1.3. Collaborations

Laboratoire de Mécanique de Lille, Université de Lille : co-encadrement de la thèse CIFRE de Fabien HUVELIN dirigée par Mhamed SOULI en interactions fluide structure sur le couplage de codes et le développement d'un coupleur fluide structure. *2005 – 2006*

Laboratoire DYN CEA Saclay : projet en collaboration EDF CEA en interactions fluide structure sur l'analyse adimensionnelle et la compréhension des instabilités fluide-élastiques dans les générateurs de vapeur. *2003 – 2006*

| | |
|---|---|
| GDR en interactions fluide structure : participation au pilotage d'un thème sur les méthodes numériques ; participation à la création du GDR en collaboration avec Mhamed SOULI et Aziz HAMDOUNI ; participation à l'organisation du 1er colloque du GDR en 2005 ; pilotage de la contribution du Département MFEE d'EDF R&D au GDR. | *2004 – 2006* |
| Ecole Polytech'Lille : participation au Conseil Scientifique. | *2005 – 2006* |
| Participation au Comité Directeur du Multiphysics Journal. | *2006* |
| Institut de Mécanique des Fluides de Toulouse : projet de collaboration sur les calculs thermohydrauliques pour les couplages fluide structure | *2006* |
| Université Paris VI : projet en cours de préparation dans le cadre de l'Ecole d'été organisée par le CEMRACS sur la propagation des incertitudes sur les chargements thermohydrauliques dans les calculs vibratoires. | *2006* |
| Université Paris XI : intervenant en Master Pro en interactions fluide structure et méthodes numériques. | *2001 – 2006* |
| Conférences, journaux : review d'articles de journaux, chairman de sessions. | *2001 – 2006* |
| Laboratoire de Mécanique de Lille, Université de Lille : co-encadrement de la thèse CIFRE de Zaky BENDJEDDOU dirigée par Mhamed SOULI en interactions fluide structure sur la simulation numérique des vibrations induites par écoulements dans les générateurs de vapeur. | *2001 – 2005* |

## 2. Activités d'enseignement

| | | |
|---|---|---|
| Création d'un cours associé à des travaux dirigés d'introduction à la simulation numérique en interactions fluide structure<br>(40 heures/an pendant 5 ans : 200 heures) | Master pro Paris XI | *2001 – 2006* |

| | | |
|---|---|---|
| Cours et travaux pratiques sur les couplages fluide structure<br>(10 heures) | Master pro La Rochelle | *2005 – 2006* |
| Création d'un atelier et de travaux pratiques sur la simulation des couplages fluide structure avec le coupleur *Cosmethyc*<br>(10 heures) | 3ème année ENPC | *2005 – 2006* |
| Cours et travaux dirigés sur la méthode des éléments finis et ses applications en mécanique<br>(40 heures/an pendant 3 ans : 120 heures) | Master pro Paris XI | *2003 – 2005* |
| Cours et travaux dirigés sur la méthode des éléments finis et ses applications en mécanique<br>(50 heures) | Master Mines de Douai | *2002 – 2003* |
| Travaux dirigés en mathématiques générales : analyse, algèbre, analyse complexe<br>(130 heures) | Licence Paris XII | *1998 – 1999* |
| Travaux dirigés en mathématiques générales : analyse, probabilités<br>(100 heures) | Tronc commun ECP | *1997 – 1998* |

# 3. Activités d'encadrement

## 3.1. Participation aux jurys de soutenances de thèses

| | |
|---|---|
| Examinateur et co-encadrant de la thèse de Zaky BENDJEDDOU, Université de Lille, sous la direction de Mhamed SOULI, intitulée : Méthodologie pour la simulation numérique des vibrations induites par écoulements dans les faisceaux de tubes. | *2005* |

| | |
|---|---|
| Examinateur de la thèse de Nicolas ACQUELET, Université de Lille, sous la direction de Mhamed SOULI, intitulée : Modélisation de l'impact hydrodynamique par un couplage fluide structure. | *2004* |

### 3.2. Co-encadrement de thèses

| | |
|---|---|
| Thèse CIFRE de Fabien HUVELIN, Université de Lille, sous la direction de Mhamed SOULI, sur le couplage de codes et le développement du coupleur fluide structure *Cosmethyc*. Contribution au développement d'un coupleur généraliste intégrant des méthodes de projection conservatives pour les échanges de données entre solveurs fluide et structure, avec modèles de structures quelconques, linéaires ou non linéaires, pour un couplage quasi-statique ou transitoire. Contribution à l'optimisation de l'outil avec le développement de formulations ALE pour la gestion de maillages mobiles adaptées aux configurations à traiter, avec gestion du parallélisme au niveau du couplage. Simulation de couplages forts comme le départ en instabilité d'un tuyau d'arrosage et d'un faisceau de tubes périodique soumis à un écoulement transverse de vitesse supérieure à la vitesse critique. | *2005 – 2006* |
| Thèse CIFRE de Zaky BENDJEDDOU, Université de Lille, sous la direction de Mhamed SOULI, sur la simulation numérique des vibrations induites par écoulements dans les générateurs de vapeur. Contribution au développement, à la validation et à l'application d'un coupleur entre le code de thermohydraulique *Code_Saturne* et un module d'interactions fluide structure monodimensionnel « masse, ressort, amortissement ». Etude des propriétés des schémas de couplage. Réalisation de cas tests théoriques et analytiques en tubes et faisceaux de tubes avec et sans écoulements. | *2001 – 2005* |

### 3.3. Encadrement de stages de fin d'études

| | |
|---|---|
| Stage de Valérie VERREMAN, Université Paris VI, 5 mois : Comparaison des méthodes de couplages mises en œuvre dans le coupleur *Cosmethyc* et dans un code aux éléments spectraux *Nektar* pour les applications de types vibrations de tubes et faisceaux de tubes en écoulements. Identification de la cellule optimale pour les calculs périodiques en faisceaux. | *2006* |
| Stage de Valérie VERREMAN, ENPC, 12 mois : Mise en œuvre, validation et extension du coupleur *Cosmethyc* : application à la prévision des coefficients de masse et d'amortissement ajoutés par un fluide pour des tubes concentriques et excentrés séparés par un fluide et pour des faisceaux de tubes périodiques pour plusieurs nombres de Stokes et différentes | *2004-2005* |

| | |
|---|---|
| configurations géométriques. Validations sur la base de comparaisons calculs / mesures / théories. Préparation de l'extension des modules de projections de données du coupleur à des géométries quelconques 1D, 2D ou 3D, non nécessairement filaires. Premières applications à la simulation du mouvement d'une structure de géométrie complexe en présence d'un écoulement : cas des robinetteries. Réflexion sur les stratégies de validation et de qualification industrielle de l'outil. | |
| Stage de Wilfrid FAILLY, Université Paris XI, 6 mois : Mise en œuvre d'un module d'interaction fluide structure monodimensionnel « masse, ressort, amortissement » introduit dans *Code_Saturne* en présence d'un écoulement. Application à l'identification des fréquences et amortissements vibratoires d'un tube en faisceau en présence d'écoulements transverses à faibles nombres de Stokes et nombres de Reynolds. Mise en évidence de l'importance du choix de la cellule périodique utilisée pour représenter un faisceau de tubes et de l'influence des conditions aux limites. Validations sur la base de comparaisons calculs / mesures / théories. Obtention d'un module d'IFS monodimensionnel couplé avec *Code_Saturne* applicable pour la simulation de problèmes d'interactions fluide structure en présence d'écoulements et de structures à un degré de liberté. | *2004* |
| Stage de Fabien MORINEAUX, ENSMA, Poitiers, 6 mois : Contribution à la validation du module d'IFS monodimensionnel « masse, ressort, amortissement » introduit dans *Code_Saturne* pour la simulation numérique d'une paroi mobile de mouvement libre, induit par les écoulements pariétaux et représentant le mouvement d'une masse supportée par un ressort avec amortissement couplée avec le fluide environnant. Mise en œuvre pour la prévision des masses et amortissements ajoutés par le fluide d'un tube vibrant et d'un tube en faisceau en présence d'un fluide au repos. Comparaisons calculs / théories et études paramétriques en fonction du nombre de Stokes et de la géométrie du tube et du faisceau. Obtention d'un module mécanique d'IFS monodimensionnel dans *Code_Saturne* couplé avec le calcul fluide en temporel et validé en fluide au repos sans écoulement permanent. | *2003* |
| Stage de Xavier KERBRAT, LEA, Poitiers, 6 mois : Contribution à la validation du module A.L.E. introduit dans *Code_Saturne* pour la simulation numérique des écoulements en présence de parois mobiles. Comparaisons calculs / mesures des champs de pression, vitesse pour un piston en compression, expansion. Mise en oeuvre d'une méthode de phase basée sur l'introduction d'un mouvement imposé de la structure en présence d'un fluide au repos et un post-traitement des signaux de forces et de déplacements permettant d'identifier les coefficients de masses et d'amortissements ajoutés par le fluide au repos. Application à l'identification des masses et amortissements ajoutés pour un tube vibrant en présence d'un fluide au repos. Validations sur la base de comparaisons calculs / théories. Obtention d'un module A.L.E. validé dans | *2002* |

| | |
|---|---|
| *Code_Saturne*, adapté à la prise en compte de parois mobiles à mouvement imposé et applicable pour des problèmes d'interactions fluide structure. | |
| Stage de Aminata DIAGNE, Université Paris VI, 3 mois : Calculs de chargements turbulents pariétaux exercés sur des tubes en faisceaux de tubes fixes en présence d'écoulements transverses par une approche L.E.S. avec *Code_Saturne*. Utilisation de cellules de faisceaux de tubes périodiques pour simuler des faisceaux de dimension infinie. Comparaisons calculs / mesures des coefficients de portances et traînées en faisceaux. Mise en évidence des limites des calculs L.E.S. bidimensionnels et de l'importance de la longueur d'extrusion du maillage du domaine de calcul suivant la direction longitudinale des tubes. | *2001* |
| Stage de Mohammed YAMANI, IMFT, Toulouse, 6 mois : Réalisation d'une passerelle de chaînage entre le code de thermohydraulique locale (*Code_Saturne*) et le code de dynamique des structures (*Code_Aster*) en spectral. Prévision par une approche L.E.S. des spectres de chargements turbulents pariétaux exercés sur un tube sous écoulement turbulent d'incidence axiale en l'absence de forts couplages fluide-élastiques. Application à l'étude de l'usure par choc et fatigue vibratoire d'un tube sous l'effet de sollicitations thermohydrauliques induites par la turbulence. Validation de la démarche numérique sur la base d'une comparaison calculs / mesures de la réponse vibratoire de la structure. Obtention d'un outil numérique prototype pour la réalisation de calculs chaînés fluide structure sur des configurations semi-industrielles. | *2000* |

# 4. Publications

## 4.1. Revues internationales avec comité de lecture

1. **Longatte, E.,** Verreman, V., Souli, M. (2006). Numerical tool for simulation of flow-induced vibrations, part I : Theory. *Journal of Fluids and Structures, soumis*.
2. **Longatte, E.,** Verreman, V., Souli, M. (2006). Numerical tool for simulation of flow-induced vibrations, part II : Application. *Journal of Fluids and Structures, soumis*.
3. Abouri, D., Parry, A., Hamdouni, A., **Longatte, E.** (2006). A stable fluid structure interaction algorithm: application to industrial problems. *Journal of Pressure Vessel Technology, accepté*.
4. **Longatte, E.**, Bendjeddou, Z., Souli, M. (2003). Application of Lagrangian Eulerian formulations to flow-induced vibration problems. *Journal of Pressure Vessel Technology*, 125 (4), 411-417.
5. **Longatte, E.**, Bendjeddou, Z., Souli, M. (2003). Methods for numerical study of tube bundle vibrations in cross flows. *Journal of Fluids and Structures*, 18, 513-528.
6. **Longatte, E.**, Lafon, P., Candel S. (2000). Computation of acoustic propagation in two-dimensional sheared ducted flows. *AIAA Journal*, 38, 389-394.

### 4.2. Congrès internationaux avec actes et comité de lecture

7. Huvelin, F., **Longatte, E.**, Verreman, V., Souli, M. (2006). Numerical simulation of dynamic instability for a pipe conveying fluid. *PVP Conference*, Vancouver.
8. **Longatte, E.**, Verreman, V., Bendjeddou, Z., Souli, M. (2005). Comparison of strong and partitioned fluid structure code coupling methods. *PVP Conference*, Denver.
9. **Longatte, E.**, Bendjeddou, Z., Verreman, V., Souli, M. (2005). Explicit and implicit code coupling schemes in fluid structure interaction. *PVP Conference*, Denver.
10. **Longatte, E.**, Bendjeddou, Z., Souli, M. (2005). Numerical simulation of flow induced vibrations in tube bundles. *NURETH 11*, Avignon.
11. Andriambololona, H., Bosselut, D., **Longatte, E.** (2005). Insertion of a slim structure into a channel : simulation and parametric analysis. *EURODYN*, Paris.
12. **Longatte, E.**, Bendjeddou, Z., Souli, M. (2004). Application of LES and DNS to prediction of tube bundle flow-induced vibrations. *FIV 4 Conference*, Paris.
13. **Longatte, E.**, Bendjeddou, Z., Souli, M. (2004). Comparison of code coupling scheme for simulation of fluid structure problems. *PVP Conference*, San Diego.
14. **Longatte, E.**, Bendjeddou, Z., Adobes, A., Souli, M. (2003). Steam generator tube vibrations : experimental determination versus ALE computation of fluidelastic forces. *PVP Conference*, Cleveland.
15. **Longatte, E.**, Bendjeddou, Z., Souli, M. (2003). Application of DNS and LES to prediction of tube flow-induced vibrations. *DLES 5 Workshop*, Munich.
16. **Longatte, E.**, Bendjeddou, Z., Souli, M. (2003). Application of fluid structure code coupling to numerical simulation of tube bundles vibrations in cross flows. *SNA Conference*, Paris.
17. **Longatte, E.**, Bendjeddou, Z., Souli, M. (2002). Numerical simulation of tube bundle vibrations in cross flows. *IMECE*, New Orleans.
18. Bendjeddou, Z., **Longatte, E.**, Souli, M. (2002). Application of Lagrangian Eulerian formulations to flow-induced vibration problems. *PVP Conference*, Vancouver.
19. **Longatte, E.**, Laurence, D., Barré, F., Ledac, P. (2001). Application of Large Eddy Simulation to a flow-induced vibration problem. *PVP Conference*, Atlanta.
20. **Longatte E.**, Lafon P., Candel S. (2001). Linear and non linear development of instabilities in a shear layer. *7th AIAA/CEAS Aeroacoustics Conference*, Maastricht.
21. **Longatte, E.**, Nhili, R., Weiss, T. (2000). Prediction of flow-induced vibrations of PWR drive line assembly. *PVP Conference*, Seattle.
22. **Longatte, E**., Lafon, P. and Candel, S. (1998). Computation of noise generation by turbulence in internal flows. *4th AIAA/CEAS Aeroacoustics Conference*, Toulouse.
23. **Longatte, E.**, Lafon, P. and Candel, S. (1997). Acoustic wave propagation in two dimensional sheared ducted flows. *18th AIAA Aeroacoustics Conference*, Atlanta.

### 4.3. Prix du meilleur papier de congrès internationaux

24. **Longatte, E.**, Adobes, A., Souli, M. (2003). Steam generator tube vibrations : experimental determination versus ALE computation of fluidelastic forces. *PVP Conference*, Cleveland.

### 4.4. Congrès français avec actes et comité de lecture

25. **Longatte, E.**, Huvelin, F., Souli, M. (2005). Code coupling for simulation of flow-induced vibrations. *1er Colloque du GDR Interactions Fluide Structure*, Sophia-Antipolis.
26. Bendjeddou, Z., **Longatte, E.**, Souli, M. (2003). Méthodologie pour la simulation numérique des vibrations induites par les écoulements dans les faisceaux de tubes. *CANUM*, Montpellier.
27. Candel, S., Lafon, P., **Longatte, E.** (2000). Acoustique en écoulements. *Ecole CEA, EDF, INRIA,* Rocquencourt.
28. **Longatte, E.**, Lafon, P., Candel, S. (1996). Modélisation de la propagation acoustique en écoulement cisaillé confiné. *4ème Congrès Français d'Acoustique*, Marseille.

### 4.5. Rapports internes EDF R&D

29. **Longatte, E.** (2005). Le Coupleur *Code_Saturne Code_Aster* : *Cosmethyc* : documentation. *EDF R&D, HI-84/05/021/P*.
30. **Longatte, E.** (2005). L'ALE dans *Code_Saturne* : Documentation. *EDF R&D, HI-84/05/020/P.*
31. **Longatte, E.,** Failly., W. (2004). Simulation numérique des couplages fluide structure de la maquette Amovi. *EDF R&D, HI-86/04/017/A*.
32. **Longatte, E.**, Bendjeddou, Z., Souli, M. (2004). Schémas de couplage explicites et implicites en IFS. *EDF R&D, HI-86/04/024/A*.
33. **Longatte, E.**, Souli, M., Adobes, A. (2004). Comparaison des approches numériques et expérimentales pour la prévision des vibrations de tubes de générateur de vapeur. *EDF R&D, HI-86/04/004/A*.
34. **Longatte, E.**, Daguse, S., Fontes, J.P. (2004). Note d'opportunité du projet CERAMHYC Concept de Réacteurs Evolutionnaires et Aide à la Maîtrise de la Thermohydraulique dans la Cuve. *EDF R&D, HI-86/04/B*.
35. **Longatte, E.**, Boyère E., Vivan L. (2003). Module de calcul de cinétique de chute de grappe de ommande dans Code_Aster : documentation. *EDF R&D, HI-86/03/024/A*.
36. Archambeau, F., **Longatte, E.** et al. (2003). Texte du projet JUPITER R&D en thermohydraulique 3D locale. *EDF R&D, HI-83/03/028/A*.
37. **Longatte, E.** et al. (2003). Bilan du projet NATIFS Nouvelles Approches et Traitements en Interactions Fluide Structure. *EDF R&D, HI-86/03/026/A*.
38. Rupp, I., **Longatte, E.** et al. (2003). Bilan du projet EMOTHIF Evaluation de Modèles pour la Thermohydraulique Industrielle Fine. *EDF R&D, HI-83/03/010/A*.
39. **Longatte, E.**, Bendjeddou, Z., Souli, M. (2002). Simulation numérique des vibrations d'un faisceau de tubes sous écoulements transverses. *EDF R&D, HI-86/02/030/A*.

40. **Longatte, E.**, Bendjeddou, Z., Souli, M. (2002). Application de *Saturne_ALE* aux études vibratoires des faisceaux de tubes de générateurs de vapeur. *EDF R&D, HI-86/02/031/A*.
41. Bosselut, D., **Longatte, E.**, et al. (2002). Note d'opportunité du projet SAGRAPPE Simulation et Analyse du comportement des GRAPPes vis-à-vis du temps de chute et de l'Endommagement. *EDF R&D, HT-62/02/019/A*.
42. **Longatte, E.**, Laurence, D., Barré, F. (2001). Exemple d'application de la LES en interactions fluide structure. EDF R&D, *HI-86/01/020/A*.
43. **Longatte, E.**, Kerbrat, X. (2001). Simulation numérique du comportement vibratoire de tubes sous écoulements transverses par une méthode ALE dans Code_Saturne. EDF R&D, *HI-86/01/019/A*.
44. **Longatte, E.** (2000). Note d'opportunité du projet NATIFS Nouvelles Approches et Traitements en Interactions Fluide Structure. *EDF R&D, HI-86/00/019/B*.
45. **Longatte, E.**, Mezoul, B. (2000). Identification des sources d'excitation exercées sur les grappes de commande. *EDF R&D, HT-32/00/024/A*.
46. **Longatte, E.**, Mezoul, B. (2000). Identification des forces de plaquage exercées sur les grappes de commande. *EDF R&D, HT-32/00/012/A*.
47. **Longatte, E.**, Mezoul, B. (2000). Estimation des pertes de charge au niveau des grappes de commande. *EDF R&D, HT-32/00/010/A*.
48. **Longatte, E.** (1998). Modélisation de la propagation et de la génération du bruit au sein des écoulements turbulents internes. *Thèse de doctorat*, Ecole Centrale Paris.
49. **Longatte, E.**, Lafon, P., Candel, S. (1997). Etude de la propagation acoustique non linéaire en écoulement non uniforme. *EDF R&D, HP-53/97/005/A*.
50. **Longatte, E.**, Lafon, P., Candel, S. (1997). Propagation d'une onde acoustique danns un écoulement bidimensionnel cisaillé en conduit. *EDF R&D, HP-53/97/023/A*.
51. **Longatte, E.**, Lafon, P., Candel, S. (1996). Etude des modélisations aéroacoustiques fondées sur les équations d'Euler. *EDF R&D, HP-53/96/016/A*.

# CONTEXTE INDUSTRIEL

# CONTEXTE INDUSTRIEL

## 1. Introduction

Sur le parc nucléaire, le respect des critères de sûreté, l'optimisation de la maintenance et la maîtrise de la durée de vie des composants passent par une prévision fiable des mécanismes de vieillissement et d'endommagement. Pour les structures soumises à de fortes sollicitations d'origines hydrodynamiques et thermohydrauliques comme les faisceaux de tubes de générateurs de vapeur, les assemblages combustibles, les grappes de commande des REP ou les circuits de tuyauteries et leurs singularités, la rupture par usure et la fatigue vibratoire des structures constituent des problématiques à enjeux majeurs pour l'exploitant. A ce titre, la mise au point d'outils prédictifs permettant de reproduire les phénomènes observés sur site répond à un besoin fort tant sur le plan technique que financier.

Les outils actuellement mis en œuvre dans le cadre des études vibratoires des composants reposent principalement sur des approches expérimentales, semi-empiriques ou numériques simplifiées, vu l'impossibilité à modéliser avec les seuls codes numériques mono-disciplinaires des physiques complexes couplées comme les vibrations induites par écoulements. La simulation numérique des couplages multi-physiques requiert la mise en place de couplages entre codes disciplinaires. Ainsi la simulation des couplages fluide structure ou des couplages écoulement structure passe par un couplage entre codes de thermohydraulique et codes de mécanique des structures. Inaccessible il y a quelques années, ce type d'approche est désormais possible pour des configurations quasi-industrielles grâce au développement récent des codes de calculs, à la mise en place de techniques de couplages de codes et à l'amélioration des performances des calculateurs. Flexibles, peu onéreuses pour la réalisation d'études paramétriques et efficaces pour modéliser des phénomènes locaux, les méthodes basées sur la simulation numérique deviennent un complément indissociable des approches classiques, alimentées par des données expérimentales, basées sur des modèles analytiques et produisant souvent des solutions simplifiées souvent découplées ou partiellement couplées.

Ce document est consacré à la présentation de méthodologies pour la simulation numérique des couplages fluide structure. Il propose une classification des méthodologies en fonction de la nature des problèmes considérés, découplés, chaînés, faiblement ou fortement couplés. Il souligne l'importance de la stratégie de qualification des outils multi-physiques, adhérente à la physique couplée des phénomènes mis en jeu. Enfin il illustre quelques résultats obtenus dans des configurations représentatives de composants de REP, montrant l'apport de la simulation numérique pour la compréhension de phénoménologies jusqu'alors inexpliquées par la seule mesure expérimentale.

## 2. Projet de recherche

### 2.1. Etat de l'art

Partant fin 2000 des trois constats suivants :

(1) une maîtrise parfois imparfaite des incertitudes sur les résultats fournis par les méthodes semi-expérimentales en interaction fluide structure, alimentées par des données expérimentales ou analytiques entachées d'erreurs,

(2) un niveau de maturation significatif en matière de qualification des codes disciplinaires en thermohydraulique (Archambeau et al. 2004, Benhamadouche 2001, Laurence 2002) et en mécanique des structures (Durand 2005, Greffet 2001),

(3) enfin une progression importante au niveau des algorithmes de résolution de problèmes multi-physiques multi-échelles par couplages de codes,

il est apparu opportun d'initier un projet[11] visant développer des outils de simulation numérique des interactions fluide structure et des vibrations de structures induites par écoulements.

Le présent document fournit une synthèse des principales conclusions de ce projet qui ont été obtenues au sein d'EDF R&D depuis 2001. Ces travaux ont porté sur les trois types de physiques, découplées, chaînées et couplées, qui font l'objet des trois chapitres du document. Ils se sont appuyés sur la mise en place de partenariats dont des collaborations avec des laboratoires extérieurs pour l'encadrement de thèses et de travaux de recherche. Ils ont donné lieu à la rédaction de plusieurs documents cités en référence dont des publications dans des revues et des actes de congrès.

## 2.2. Enjeux

Les écoulements et les sollicitations thermohydrauliques autour des composants mécaniques peuvent être à l'origine de comportements vibratoires des structures préjudiciables pour la sûreté, pouvant conduire à des dommages par usure, frottement, chocs entre éléments, fatigue des matériaux constituants ou tout autre mécanisme de dégradation progressive ou brutale, comme des phénomènes de résonance, des instabilités ou des couplages vibroacoustiques.

Dans le cadre des travaux réalisés, on s'intéresse tout particulièrement à des configurations faisant intervenir des couplages fluide structure en présence d'écoulements externes comme pour les composants filaires tubulaires de types faisceaux de tubes, ou d'écoulements internes comme les tuyauteries, les réseaux de tuyauteries et leurs singularités.

Dans les REP, les grandes vitesses des écoulements s'accompagnent de constitutions de zones de turbulences et de fluctuations de pression agissant sur les structures en présence. Les faisceaux de tubes, dotés d'une géométrie destinée en premier lieu à optimiser les échanges de chaleur au niveau des surfaces de contact, sont particulièrement sujets aux vibrations sous l'effet des sollicitations thermohydrauliques pariétales (Figure 1). De faible diamètre (quelques centimètres) et de grande longueur (plusieurs mètres), ils sont flexibles et se déplacent sous l'effet des écoulements. Dans leur mouvement, ils modifient ainsi les champs de pression locaux et peuvent réagir avec les éléments voisins. La dynamique de ces structures trouve donc à la fois des causes externes, sous l'effet de sollicitations extérieures, comme celles induites par un séisme ou une dépressurisation brusque en réacteur par exemple, mais également des causes internes, liées aux couplages fluide écoulement structure au sein du composant lui-même.

Dans les tuyauteries (Figure 2), les singularités rencontrées comme les coudes, vannes, pompes, diaphragmes et autres obstacles perturbent les écoulements, modifient localement leurs caractéristiques et peuvent conduire à des couplages écoulement structure avec introduction d'éventuels effets de compressibilité, d'élasticité ou des effets thermiques.

Aussi le dimensionnement des composants doit-il prendre en compte les effets de l'ensemble des phénomènes de couplages fluide structure qui revêtent une importance toute particulière

[11] Projet NATIFS, Nouvelles Approches et Traitements en Interactions Fluide Structure, et Lot IFS du Projet JUPITER.

dans les installations vis-à-vis de la sûreté nucléaire. Les nombreux travaux engagés dans le domaine des faisceaux de tubes durant les vingt dernières années (Pettigrew et Taylor 2004, Axisa 2001, Weaver et al. 1986, Païdoussis 2004, Granger et Perotin 1997, Granger et Gay 1996, Granger et Païdoussis 1996, Chen 1987, Price et Païdoussis 1984, 1986, 1989, 1997, Blevins 1990, Gibert 1988, Feenstra et al. 2003, Hadj-Sadok 1994, Hémon 1999, Mureithi et al. 2004, Tanaka et al. 1981, Adobes et al. 2001) se sont traduits par des campagnes de mesures expérimentales visant à caractériser les écoulements en faisceaux et leur comportement vibratoire en terme de fréquences et d'amortissements. Ils ont abouti à l'élaboration de modèles semi-empiriques performants dans plusieurs configurations mais ils n'ont pas permis d'expliquer toutes les phénoménologies observées à ce jour. Les outils numériques apporteront des réponses complémentaires grâce à la mise en oeuvre d'études locales paramétriques. Leur qualification sera facilitée par l'utilisation des bases de données expérimentales disponibles.

Parmi les problèmes ouverts qui relèvent du domaine des couplages fluide structure en faisceaux, on peut citer :

- L'identification de la vitesse critique de départ en instabilité fluide-élastique dans les faisceaux de tubes de générateurs de vapeur en présence d'écoulements transverses.
- La caractérisation des effets de grilles sur le comportement vibratoire des crayons combustibles et leur usure.
- L'identification des chargements exercés sur les grappes de commande et responsables de mécanismes d'usure, de frottement ou de plaquage hydraulique des crayons absorbants dans leurs guidages.
- La prise en compte du comportement dynamique non linéaire des structures avec chocs en présence d'écoulements turbulents
- La simulation numérique de phénomènes de dynamique rapide comme la cinétique de chute des grappes d'arrêt en cours de chute.

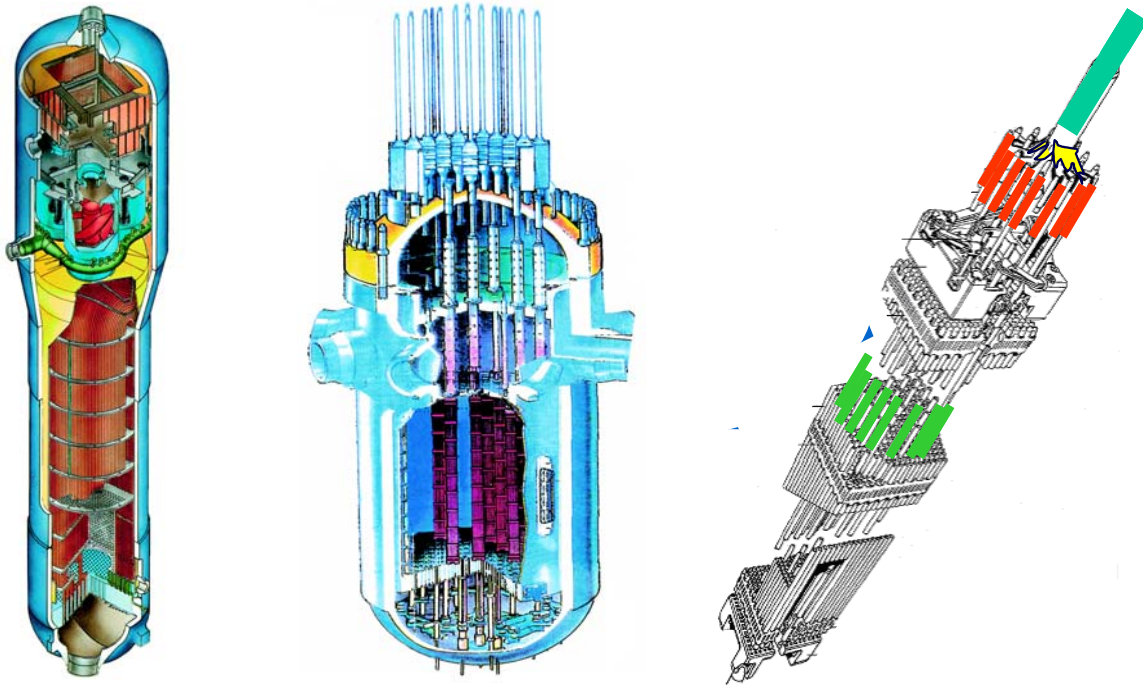

*Figure 1 : Générateur de vapeur (à gauche), cuve de réacteur (au milieu), grappe de commande insérée dans un assemblage combustible (à droite).*

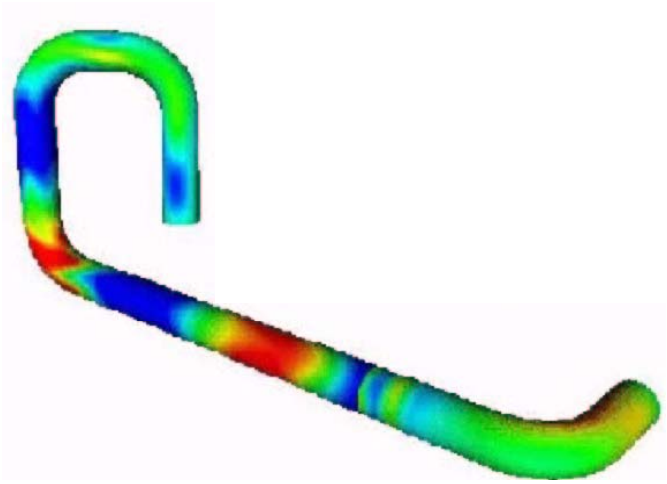

*Figure 2 : Portion de réseau de tuyauterie.*

Dans les réseaux de tuyauteries, les méthodologies sont souvent basées sur des formulations monodimensionnelles avec des modélisations simplifiées des singularités non aptes à reproduire les couplages et leurs effets. La simulation numérique est également fortement attendue dans ce domaine.

### 2.3. Objectifs

Les méthodologies à mettre en œuvre dépendent du type de problème considéré, en particulier de la « force » du couplage physique mis en jeu. Comment évaluer cette force ? Elle peut être estimée à partir de paramètres adimensionnels, dépendant des caractéristiques du fluide, de la structure et de rapports d'échelles entre les deux systèmes. Par exemple, le rapport des vitesses caractéristiques du fluide et de la structure, ou vitesse réduite, est l'une des grandeurs clefs indiquant si les deux problèmes sont fortement corrélés ou non. D'autres paramètres renseignent sur la nature du couplage (nombres de masse, de déplacement, de Stokes, de Froude, de Cauchy). Un inventaire des paramètres adimensionnels fondamentaux de couplages fluide structure est donné par De Langre (2002). En se basant sur une analyse adimensionnelle, on peut ainsi établir une classification des problématiques physiques et des méthodologies à mettre en œuvre pour les simuler (Figure 3). Ainsi, un chaînage physique peut être simulé par un chaînage de codes ; pour un couplage physique fort, un couplage entre codes disciplinaires est nécessaire.

Tout l'enjeu de la simulation numérique des couplages fluide structure est de représenter fidèlement les échanges d'énergie entre les systèmes couplés aux interfaces. La mise en place des méthodologies numériques passe par leur qualification, et tout particulièrement par la vérification de la validité des données transférées entre les codes. En interaction fluide structure, ces données sont d'une part les chargements thermohydrauliques responsables des vibrations, d'autre part les déplacements de la structure modifiant la position de l'interface.

Ce document présente une synthèse des travaux de qualification engagés sur les méthodes numériques. Il aborde les problématiques suivantes :

1. la gestion des interfaces entre systèmes couplés et découplés et les transferts des données associées
2. la résolution de problèmes chaînés ou faiblement couplés fluide structure par chaînage de codes
3. la résolution de problèmes faiblement ou fortement couplés fluide structure par couplage de codes

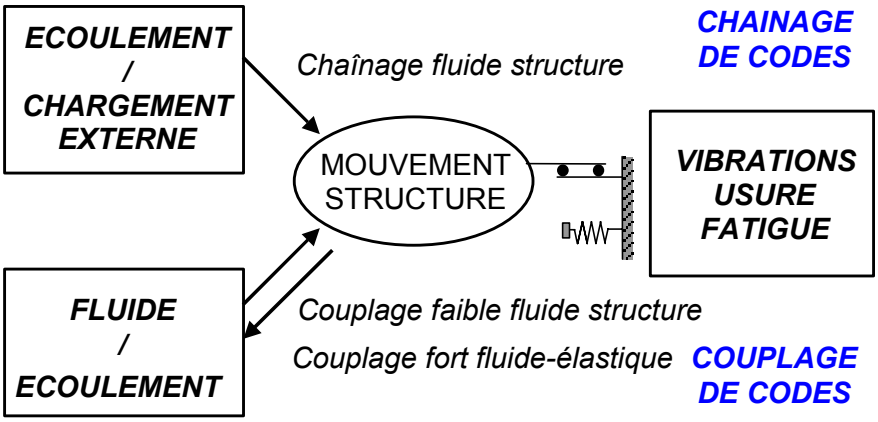


*Figure 3 : Classification des problématiques de chaînage fluide structure, couplage fluide structure et couplage fluide-élastique.*

Pour chaque problématique, la méthodologie proposée est rappelée. Des exemples de qualification des méthodes sont illustrés. Enfin les méthodes sont appliquées à des configurations représentatives de parties de composants de REP et les résultats sont interprétés et validés sur la base de confrontations calculs / mesures ou calculs / théories.

Les publications présentées en annexe de chaque partie illustrent la progression et la cohérence des développements qui ont été réalisés entre 2000 et 2005 et ont abouti à la création d'un nouvel outil généraliste de simulation numérique des couplages multi-physiques en mécanique et thermohydraulique baptisé *Cosmethyc*[12].

## 3. Problématique industrielle

Un exemple de problématique industrielle est illustré en Annexe 1. L'article présenté au PVP en 2000 à Seattle est consacré à l'étude vibratoire d'un composant de REP soumis à de fortes sollicitations thermohydrauliques. Il s'agit des crayons absorbants de grappe de commande, structures filaires vibrant dans une configuration géométrique modérément confinée, en présence de non linéarités fluides induites par la turbulence et de non linéarités dynamiques de la structure induites par des chocs et des chargements externes. L'étude proposée met en oeuvre une approche semi-expérimentale basée sur des observations physiques, sur l'exploitation de données de mesures expérimentales et sur des lois de transposition permettant d'adopter une démarche semi-empirique.

L'intérêt des techniques expérimentales pour les études vibratoires en présence d'écoulements est souligné au travers des quelques résultats cités qui témoignent du caractère prédictif des outils mis en oeuvre dans des configurations d'intérêt industriel. Leurs limites sont également mises en évidence. Fondées sur des modélisations analytiques ou empiriques des couplages fluide structure, ces techniques reposent sur des hypothèses fondamentales qui, dans certains cas, peuvent être mises en défaut dans la pratique. De plus, elles sont alimentées par des données expérimentales qui peuvent être entachées d'incertitudes liées aux dispositifs de mesure mis en place pour les obtenir. Les travaux présentés dans cet article ouvrent donc des perspectives sur les besoins et les attentes vis-à-vis des nouvelles méthodes de prévision des couplages fluide structure. Ces nouvelles méthodes, basées sur la simulation numérique, font l'objet des chapitres suivants.

[12] COupleur pour la Simulation MEcanique et ThermoHYdrauliQUE.

## Annexe 1 : Etudes vibratoires semi-déterministes en REP

Longatte, E., Nhili, R., Weiss, T. (2000). Prediction of flow-induced vibrations of PWR drive line assembly. *PVP Conference*, Seattle.

# PREDICTION OF FLOW INDUCED VIBRATIONS OF PWR DRIVE LINE ASSEMBLY

**Elisabeth LONGATTE**
Electricité de France
R&D Division - Fluid Mechanics and Heat Transfer Department
Chatou – France
elisabeth.longatte@edf.fr

**Régis NHILI**
Electricité de France
R&D Division - Fluid Mechanics and Heat Transfer Department
Chatou – France
regis.nhili@edf.fr

**Thomas WEISS**
Electricité de France
Basic Design Department
Structural Mechanics Section
Lyon – France
thomas.weiss@edf.fr

## Abstract

In many industrial applications, mechanical structures such as PWR components are submitted to complex flows causing possible vibrations and damage. Part of fluid forces are due to turbulence and affect the dynamical behavior. For industrial concerns, it is important to be able to predict these forces and their consequences on structure wear work rate. A semi-numerical approach has been developed by the Heat Transfer and Aerodynamics research section of EDF in order to predict the physical phenomena in many cases involving flow induced vibrations.

In the framework of indirect approaches, the model provides an estimation of turbulent excitations acting on dynamic systems without any assumption about force spectral density. Physical parameters such as vibratory responses are determined from experimental data. They are introduced into the model relying on a structure modal analysis and a spatial orthonormal decomposition of fluid forces.

The full computation is described in the first section of the article. The second part provides a presentation of the indirect method used for the force identification. Main recent results related to flow induced vibrations of PWR rod cluster control assembly are finally reported in the last section. The structure behavior near the exit of continuous guidance is predicted in many configurations in terms of fluid force spectrum and magnitude. Finally one can deduce vibration effects on life duration of PWR RCCA.

## Introduction

Main PWR components are submitted to complex flows causing possible vibrations and damage. PWR rod cluster control assembly (RCCA) may be particularly excited by turbulence near the intermittent guidance bottom. As far as nuclear security is concerned, it is necessary to prevent fatigue and wear problems occurring in mechanical structures. Many experiments have been carried out in order to predict the turbulent forces responsible for vibratory fatigue. They can sometimes be measured directly by transducers but it is difficult to stand between the different physical mechanisms involved when a distributed external loading is considered. In spite of recent improvements on Computational Fluid Dynamic codes, numerical simulation of fluid structure coupling is still impracticable for industrial purposes. Hence, no direct approach is available to study flow induced vibrations.

Indirect prediction methods have shown their ability to provide an estimation of fluid forces. However, most of them rely on analytical models of force density depending themselves on unknown spectral scaled parameters (Corcos 1963, Blevins 1990, Chen 1987; Lin 1987, Gagnon and Païdoussis 1994, Axisa et al. 1990, Granger 1990, 1991). They are thus not always reliable, especially in the presence of complex turbulent flows.

A more advanced indirect approach has been developed by EDF. It relies on the measurement of structure vibratory

response and does not feature the previously mentioned disadvantages because any assumption about force cross spectral density is required. Using transfer function calculation and data processing, the method provides an estimation of turbulent excitations acting on dynamic structures. A modal model of the mechanical system is used and a spatial orthonormal decomposition of force fields is combined with a regularization process ensuring the closure system.

In this article, the method is presented and applied to the prediction of the turbulent forces acting on RCCA. The full computation is described in first section. The second part provides a theoretical derivation of the force inverse identification process. Finally, the model is applied to the prediction of RCCA behavior and main recent results are discussed in the last section.

## 1. Full computation

If one assumes flexible structure vibrations are linear, the mechanical system in flow may be characterized by its transfer function. Then, the vibratory response measurement allows the computation of turbulent excitations that are independent of the structure motion. They are expressed in the frequency domain and although in the physical space according to a suitable modal decomposition.

The full computation is described in the present section. There are three steps in the process: (1) the measurement of the structure vibratory response using an experimental mockup according to suitable scaling laws, (2) the modal analysis of the mechanical structure, (3) the fluid force rederivation using the indirect model. Finally, one gets an estimation for the characteristic physical parameters of the system in terms of excitation spectra, wear work rate, life duration.

### 1.1 Experimental scaling laws

The approach consists in identifying turbulent forces acting on a flexible multi-supported beam submitted to a complex flow. The configuration is depicted in Figure 1. Direct force measurement is difficult to perform, hence an indirect approach has been developed that uses only measured experimental data : the structure vibratory response $u(x,t)$. These measurements are performed on an experimental mockup describing the real structure geometry with its hydraulic environment. Turbulent forces $f(x,t)$ are considered

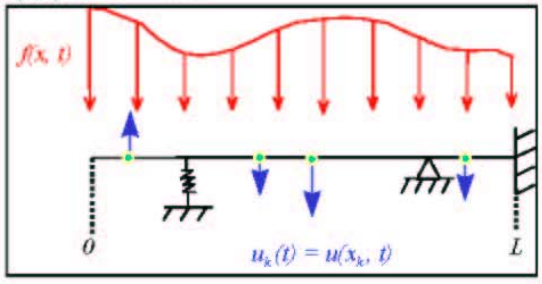


***Figure 1: Flexural vibration of a multi-supported beam subjected to a distributed external loading.***

as a stationary gaussian random process with zero mean, characterized by its cross-spectral density $S_{ff}(x_1,x_2,\omega)$. They are assumed to be independent on the structure motion. The model relies on a non-dimensional formulation. Exact values of characteristic parameters, such as flow rate, velocity, are kept in the experimental setup, except the Reynolds number. However, it has been shown that turbulent source distribution is independent of Reynolds number range. So, a scaling law may be applied in order to translate the results obtained in normal conditions of pressure and temperature into the PWR real conditions (Granger and Perotin 1997). Finally, the cross-spectral density deduced from experiment depends only on the mockup geometry scaling factor, the flowrate square and the Strouhal number. For a bidimensional system, one gets:

$$S_{ff} = \left(\frac{1}{2}\rho U^2 L\right)^2 \frac{L}{U}\tilde{S}\left(\frac{x_1}{L},\frac{x_2}{L},\omega_d\right) \qquad \textit{Eq. 1-1}$$

where $L$ designates the structure characteristic length, $\omega_d$ the reduced frequency and $(x_1,x_2)$ give the spatial locations on the rod. Using this formulation, the purpose is to compute these cross-spectral densities by using available experimental data: the rod vibratory response measured on the mockup describing the mechanical component.

### 1.2 Modal identification

Assuming the rod motion is linear, the dynamic system admits a modal representation. The vibrational displacement of the structure $u(x,t)$ can be measured at a finite number of locations and may be expressed in terms of modal parameters. In the presence of axial movement, the response is given by the following expression in terms of mode shapes $\phi_i(x)$ and modal coordinates $q_i(x)$:

$$u(x,t) = \sum_i \phi_i(x) q_i(t) \qquad \textit{Eq. 1-2}$$

where the mode shapes satisfy the following orthogonality property:

$$\int_0^L m(x)\phi_i(x)\phi_j(x)dx = m_i\delta_{ij} \qquad \textit{Eq. 1-3}$$

$m(x)$ denotes the mass per unit length of the structure in flow, including added mass, and $\delta_{ij}$ the Kronecker delta .

### 1.3 Turbulent force identification

With this convention, the generalized equation of motion can be written in the modal basis as follows (Clough 1980, Landau 1971):

$$m_i(\ddot{q}_i + 2\xi_i\omega_i\dot{q}_i + \omega_i^2 q_i) = Q_i(t) \qquad \textit{Eq. 1-4}$$

with $\xi_i$, $\omega_i$, $m_i$ and $Q_i$ respectively the modal damping ratios, natural circular frequencies, modal masses and generalized excitations. In practice, modal parameters can be estimated for the structure in flow by a modal identification method using the response measurements. Such a method is implemented in the IMENE code (Granger 1988) and provides the number of modes N, and, for each mode and in each useful frequency band, the modal damping ratio, the natural frequency and the shape values at the measurement points. The mode shape may be then interpolated at any point by using a theoretical mechanical model fitted by the identified local shape values. This model can be analytically derived or built with finite element method in the case of complex structures. Modal masses are then deduced from relation (1.3). Finally modal excitations $Q_i(t)$ are related to physical forces $f(x,t)$ by:

$$Q_i(t) = \int_0^L f(x,t)\phi_i(x)dx \qquad \textit{Eq. 1-5}$$

They are considered as a stationary gaussian process (Gibert 1988). They are totally defined by their cross-spectral density $S_{QQ}(\omega)$ and the computation of modal parameters provides an estimate of physical turbulent forces. The full indirect identification process is described in the following section.

## 2. The inverse identification process

In what follows, we describe the inverse method used for the turbulent force identification. According to equation (1.4), there are three steps in the computation: (1) the computation of modal coordinates using experimental vibratory responses, (2) the estimation of modal excitations, (3) finally the recombinaison of turbulent forces in the space domain. The modal problem to be solved is first presented. A regularization process is applied providing modal parameters. Force recombinaison in physical basis is finally described.

### 2.1 Identification of modal coordinates

Modal coordinates are related to measured displacements by equation (1.2) and although by the following decomposition in the modal basis:

$$u(t) = \sum_{i=1}^{N} \phi_i(x)q_i(t) + \varepsilon(x,t) \qquad \textit{Eq. 2-1}$$

where $\varepsilon(x,t)$ corresponds to the error induced by modal troncature and external noise. In order to compute the modal coordinates $q_i(t)$, the purpose is then to minimize the term $\|\phi q - u\|^2$ where the norm is defined by:

$$\|x\|^2 = \frac{1}{2\pi}\int_{-\infty}^{+\infty} tr\left(\left[S_{xx}(\omega)\right]\right)d\omega \qquad \textit{Eq. 2-2}$$

From the solution of least-squares problem, the cross-spectral densities $S_{\hat{q}\hat{q}}(\omega)$ can be derived from measured responses as follows:

$$\left[S_{\hat{q}\hat{q}}(\omega)\right] = \left(\left[\phi\right]^T\left[\phi\right]\right)^{-1}\left[\phi\right]^T\left[S_{uu}(\omega)\right]\left[\phi\right]\left(\left[\phi\right]^T\left[\phi\right]\right)^{-1} \qquad \textit{Eq. 2-3}$$

### 2.2 Identification of modal excitations

The basic system to be solved is given by relation (1.4). Using a direct approach, this equation is integrated to deduce modal responses from modal excitations. Conversely, here, the inverse problem consists in estimating modal excitations from the knowledge of modal responses. We denote $B(\omega)$ a diagonal matrix $N \times N$ whose components are (for $i = 1,\ldots,N$)

$$B_i(\omega) = m_i\omega_i^2\left[1 - \left[\frac{\omega}{\omega_i}\right]^2 + 2j\xi_i\left[\frac{\omega}{\omega_i}\right]\right] \qquad \textit{Eq. 2-4}$$

Then equation (1.4) yields the relation between estimates of response and excitation cross-spectral matrices:

$$\left[S_{\hat{Q}\hat{Q}}(\omega)\right] = \left[\overline{B}(\omega)\right]\left[S_{\hat{q}\hat{q}}(\omega)\right]\left[B(\omega)\right] \qquad \textit{Eq. 2-5}$$

In practice, the minimization problem to be solved is replaced by a constrained optimization problem which would guarantee that $Q(t)$ is sufficiently regular. This regularization process yields to the following problem (Ciarlet 1982):

$$\min_q \|Bq\|^2 \qquad \textit{Eq. 2-6}$$

under the following condition:

$$\|\phi q - u\|^2 \le \delta\|u\|^2 \qquad \textit{Eq. 2-7}$$

with $\delta$ the relative error magnitude (Granger and Perotin 1997). This process allows filtering and distributing the measurement error throughout the frequency domain

### 2.3 Identification of turbulent distributed excitations

Forces $f(x,t)$ are related to modal excitations $Q(t)$ by equation (1-5). Furthermore it is possible to use a Fourier expansion to express $f(x,t)$ in an orthonormal function basis as follows:

$$f(x,t) = \sum_{i=1}^{N} \alpha_i(t)\varphi_i(x) \qquad \textit{Eq. 2-8}$$

To avoid any matrix inversion, we chose to define a new set of functions $\{\varphi_i, i = 1\ldots N\}$ deduced from the mode shapes

$\{\phi_i, i = 1...N\}$:

$$\varphi_i(x) = \frac{m(x)}{\sqrt{m_i}}\phi_i(x) \qquad \textit{Eq. 2-9}$$

According to the mode shape properties, this set of functions $\varphi_i$ is an orthonormal basis associated with following inner product:

$$(v, w) = \int_0^L \frac{v(x).w(x)}{m(x)}dx \qquad \textit{Eq. 2-10}$$

This formulation yields an estimate of the Fourier coefficients of $f(x,t)$ (for $i = 1,...,N$):

$$\hat{f}(x,t) = \sum_{i=1}^{N} \frac{m(x)}{m_i}\phi_i(x)\hat{Q}_i(t) \qquad \textit{Eq. 2-11}$$

Finally, the cross-spectral density of turbulent forces is given by:

$$S_{\hat{f}\hat{f}}(x_1, x_2, \omega) = m(x_1)m(x_2)\sum_{i=1}^{N}\sum_{j=1}^{N}\frac{\phi_i(x_1)\phi_j(x_2)}{m_i m_j}S_{\hat{Q}_i\hat{Q}_j}(\omega)$$

*Eq. 2-12*

for any $\omega$ and any locations $(x_1, x_2)$. Then, one gets an estimate of turbulent excitations acting on a dynamical structure submitted to a flow.

## 3. Application

Granger and Perotin (1997) applied this model to a straight tube submitted to a complex three-dimensional turbulent water flow. The results turned out to be correct and had been used to validate the inverse identification process in the presence of linear or non linear structure supports.

More recently, the indirect approach has been applied to the prediction of PWR component behavior. The most recent results are related to RCCA vibrations and are reported in the present section. After a presentation of experimental facilities, main results are discussed and further developments are suggested.

### 3.1 Experimental setup

In practice, we want to study RCCA vibrations induced by turbulent flow near the intermittent guidance bottom (Borsoi 1997). According to the previously mentioned scaling laws, it is necessary to perform measurements on a mockup describing the main hydraulic and geometric properties of the real fluid-structure system. Many fluid forces are applied on RCCA, in the housing plate passage and in the continuous guidance (Figure 2).

In the present article, we focus our attention on turbulent excitation induced by fluid near the intermittent guidance bottom. The experimental setup is shown in Figure 3. It contains the full continuous guidance, the intermittent guidance bottom and the top of a fuel assembly including the upper core plate and the top nozzle. The mockup provides a realistic description of the hydraulics and of the RCCA geometry for different PWR configurations (900 and 1300 Mwe for example).

The structure is placed in a 1m square and 4 m high flow channel. The test section thus defined is fitted with water inlet at the bottom. Lateral outlets are dimensioned to describe the leak rates through guide plates and continuous guidance apertures. The general top outlet parameters are scaled in order to take into account the environment effects. The geometry scaling factor is set to 1. Flow rates are set to the real values measured in PWR conditions.

Concerning Reynolds number conditions, it has been shown that, in the turbulent Reynolds number range, this parameter does not affect turbulent forces. Some tests have been done to confirm this assumption, hence measurements are carried out under normal pressure and temperature conditions.

Concerning the internal components, 24 flexible tubes accounting for the control rods are linearly supported by 3 guide plates respectively in the top, middle and bottom of the intermittent guidance of the test facility. The vibratory response of 3 tubes may be measured with strain gauges located at 20 different positions along the tubes. The instumented control rods may be displaced and one gets enough information to compare tube behavior according to their position in the guidance. The different positions are described in Figure 4. Using the measured dynamic responses of tubes in flow, one may compute the modal parameters of the structure and apply the inverse method in order to identify the turbulent forces.

Rod cluster control assembly

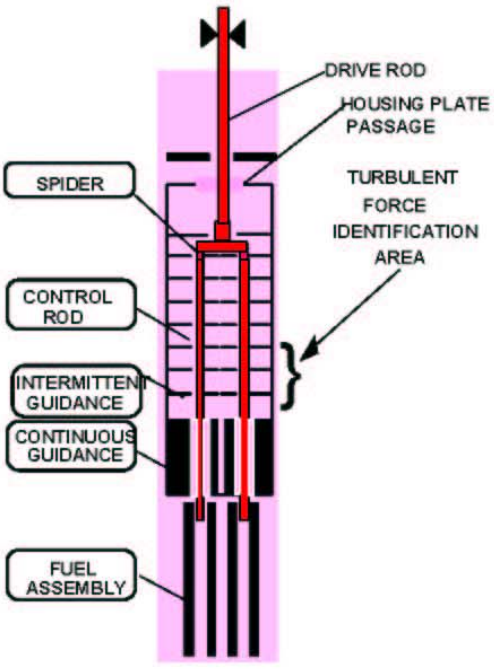


4

*Figure 2: Identification of turbulent forces acting on PWR RCCA near the intermittent guidance bottom.*

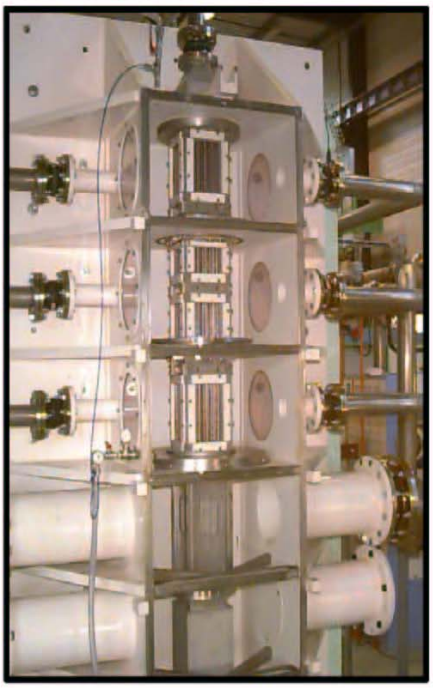

*Figure3 : Experimental mockup describing rod cluster control assemblies in configurations 900 or 1300 Mwe.*

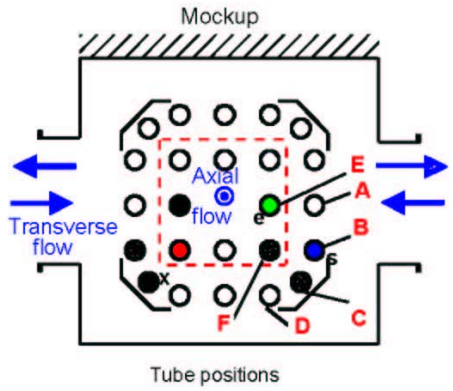


*Figure 4: Control rod positions in the intermittent guidance.*

### 3.2 Main results

Main results obtained in different configurations are presented below. Modal parameters of tubes are reported. Fluid forces are identified with the indirect approach and expressed in the physical space in terms of spectra and magnitudes.

- ***Modal parameters :***

In the first step, a modal identification is performed to estimate the modal parameters of each instrumented tube subjected to the flow. The tubes used in the experiment do not have got necessarily the same modal frequencies as the real control rods, indeed the turbulent forces to be identified are independent of structure motion and characteristics. Exploration of the frequency band 0-1000 Hz enables the characterization of the first vibratory modes. The natural frequencies and modal damping ratios obtained with the IMENE software are reported in table 1. The results turn out to be correct because the identified natural frequencies, mode shapes and modal masses are consistent with those obtained by calculation. According to the axisymmetry of the problem, each mode has an orthogonal component at about the same frequency, which corresponds to a double mode.

Moreover, to fit the numerical model with experimental data, it is necessary to check the linear properties of the mechanical system used for measurements. In particular, tube mode supports must be carefully examined because of the very slight values of damping ratios. Many tests involving impacts of different magnitudes in air and water have been carried out and the results turned out to be correct.

***Table 1: Natural frequencies and modal damping ratios identified experimentally with soft set of springs for the rod in position E (900 Mwe).***

| | Modes in the plane of flow outlet (odd) | | modes orthogonal to the plane of flow outlet (even) | |
|---|---|---|---|---|
| | f (Hz) | $\xi$ (%) | f (Hz) | $\xi$ (%) |
| Modes 1, 2 | 47,0 | 1,16 | 46,6 | 0,92 |
| Modes 3, 4 | 70,1 | 0,76 | 70,6 | 1,13 |
| Modes 5, 6 | 179,1 | 0,49 | 179,2 | 1,16 |
| Modes 7, 8 | 217,2 | 0,10 | 219,1 | 0,79 |

As soon as the system modal parameters have been calculated, the indirect method implemented in the MEIDEE software is used to estimate modal vibratory responses and excitations.

- ***Modal cross-spectral response densities :***

Modal response cross-spectral densities $S_{qq}$ are deduced from measured response cross-spectral densities $S_{uu}$ according to the aforementioned regularization process. Both physical and modal densities are illustrated in Figures 5 and 6. The first eight modes are significant. According to the level of higher order modes, their effects may be neglected. Hence, the eighth mode can be considered as the order of troncature for the representation of turbulent excitations.

- ***Modal excitations :***

Finally modal excitation cross-spectral densities may be computed. The solutions are depicted in Figure 7. They feature a slowly decreasing behavior up to a cutoff frequency and sharp drops characteristic of the Kolmogorov cascade. The

cutoff frequency range depends on the mode order and the mode shapes correspond to the spatial distribution of the turbulent excitation.

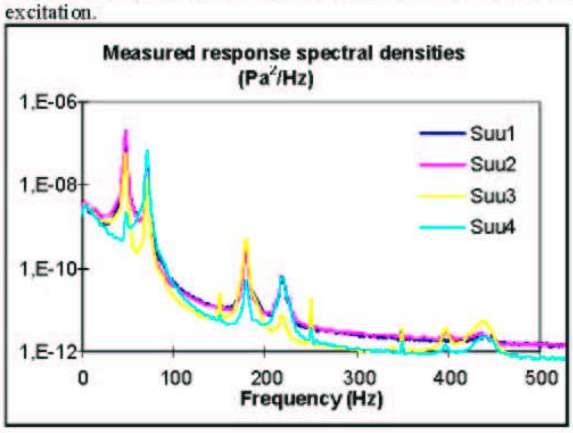


***Figure 5: Typical measured response spectral densities $S_{uu}$ for strain gauges located at one point on the intermittent guidance, for the rod in position E (900 Mwe).***

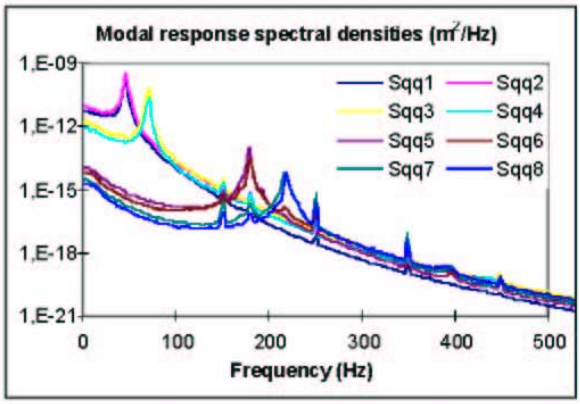


***Figure 6: Typical modal response spectral densities $S_{qq}$ for the rod in position E (900 Mwe).***

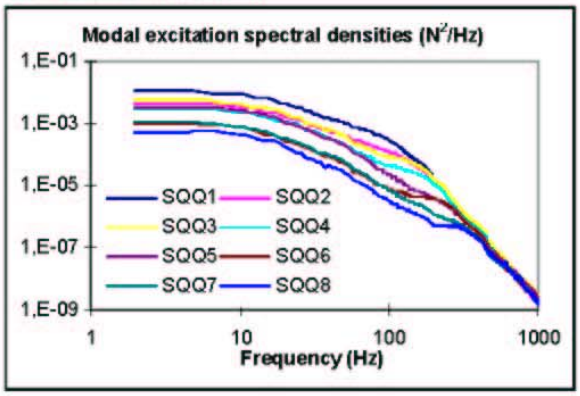


***Figure 7: Typical modal excitation spectral densities $S_{QQ}$ associated with odd and even modes (1 to 8) for the rod in position E (900 Mwe).***

- ***Physical turbulent excitations :***

Moreover, physical excitations are deduced from modal responses and may be represented in the space domain. The spectral densities of turbulent excitations applied near the first four bottom guide plates are shown in figure 8. One can conclude from these results that the excitation magnitude is very important near the first two guide plates whether it decreases near the upper ones. The same conclusion can be deduced from figure 9 depicting excitation RMS values along the rod. The structure is more excited near the continuous guidance than near the fourth guide plate in the middle of the intermittent guidance.

- ***Rod wear work rate :***

Finally, these data are used to estimate the RCCA wear work rate with the ASTER code developed by EDF (Bosselut 1997). They are illustrated in figure 10. The magnitudes are consistent with the previous results because the excitations are significant near the top of the continuous guidance, generating wear work rate maxima.

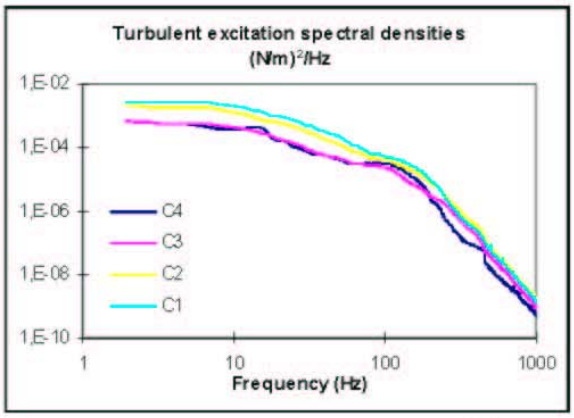


***Figure 8: Turbulent excitation spectral densities $S_{ff}$ of the rod in position E near the first four bottom guide plates (C1 to C4). (900 Mwe)***

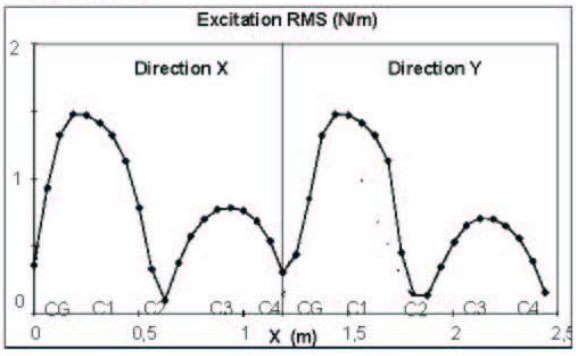


***Figure 9: Turbulent excitation RMS (900 Mwe, tube E).***

6

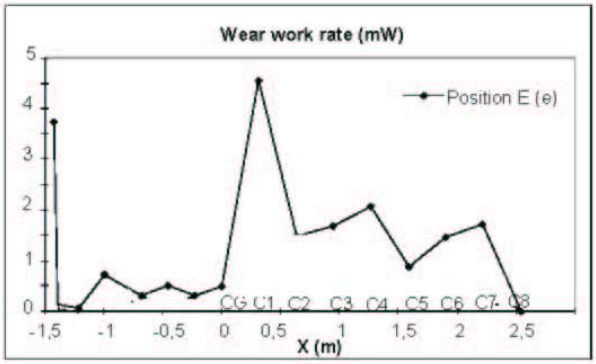


***Figure 10 : Wear work rate estimation for the rod in position E (900 Mwe).***

### 3.3 Discussion

Several tests have been carried out in order to check the influence of different parameters on turbulent excitations: number of tube supports, 900 or 1300 Mwe configurations, tube positions, transverse flow rate.

- ***Influence of tube supports number :***

As we previously mentioned, turbulent excitation is independent of the structure motion and although of mechanical support conditions. To check the good properties of identified forces, it is then possible to compare the results obtained with different supporting modes. Many tests have been carried out in the presence of 3, 4 and 5 supports located in the guide plates and at the continuous guidance top (Figure 11). Excitation RMS and phases are given in table 2 in the three cases. The results turn out to be correct. Excitations are of the same order of magnitude in the presence of 3, 4 or supports. Hence, identified excitations are independent of support conditions, that is to say of structure behavior.

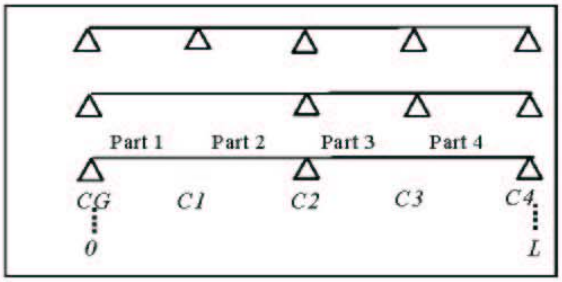


***Figure 11: 3 tube support conditions: with 5 supports (top), with 4 supports (middle), with 3 supports (bottom). Supports are located at the continuous guidance top (GC) and at the fourth inferior guide plates of intermittent guidance (C1, C2, C3, C4).***

***Table 2: Comparison of turbulent force RMS and phases on 4 intermittent guidance parts in the presence of 3 support conditions: with 3, 4 or 5 supports.***

| | | Part 4 | Part 3 | Part 2 | Part 1 |
|---|---|---|---|---|---|
| 3 supports | RMS (N) | 0,05 | 0,05 | 0,10 | 0,19 |
| | Phase (°) | 0 | 180 | 180 | 0 |
| 4 supports | RMS (N) | 0,02 | 0,03 | 0,09 | 0,17 |
| | Phase (°) | 0 | 180 | 180 | 0 |
| 5 supports | RMS (N) | 0,05 | 0,04 | 0,08 | 0,20 |
| | Phase (°) | 0 | 180 | 180 | 0 |

- ***Comparison of 900 Mwe and 1300 Mwe results :***

The experimental facilities used for measurements enable the representation of different PWR RCCA such as 900 and 1300 Mwe components. It is then possible to compare the excitation estimated in both cases. Figure 12 features force RMS values for a tube in position E. According to the solutions, excitation level is the same near C1 and C2 but the magnitude near C3 and C4 is more important in 900 Mwe than in 1300 Mwe configuration. This difference is due to the internal hydraulic distribution. The 900 and 1300 Mwe component geometries are different and the flow rate through the intermittent guidance is higher in the first case which justifies the high excitation level.

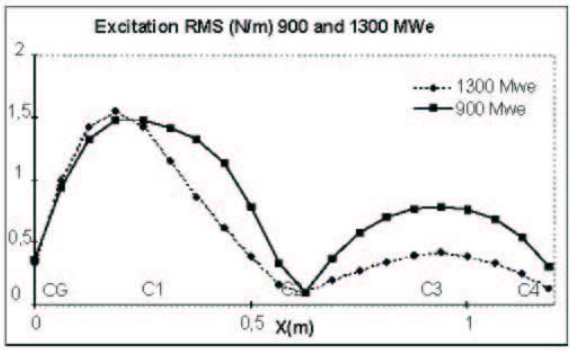


***Figure 12: Excitation RMS values for a tube in position E in 900 and 1300 Mwe configurations.***

- ***Influence of tube position :***

Many configurations have been tested for different types of configurations. For each case, it was shown that the fluid force distribution depends on the rod position in the guide. Internal and external tube excitations feature specific patterns, particularly, in terms of force magnitude. RMS values computed for two tubes located in positions s (external right class B) and e (internal right class E) are plotted in figure 13. According to the results, internal tubes are more excited than external ones and the difference corresponds to a factor 2. This result seems to be consistent with the mockup structure because internal hydraulics may be very complex and generate high turbulent fluctuations near internal rods.

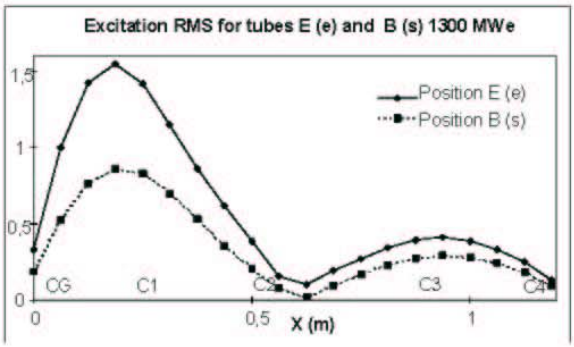


***Figure 13 : Comparison of excitation RMS obtained for internal (position E) and external (position B) tubes. 1300 Mwe***

- ***Influence of transverse flow rate :***

Another parameter effect on fluid sources has been examined by acting on the transverse flow rate. The experimental setup is built to describe the guide which may be submitted to transverse flows generated by other guides in the reactor. It is then possible to introduce transverse flow on lateral apertures of continuous guidance by acting on the corresponding left or right flow rates. In figure 14, excitation magnitudes obtained with and without transverse flows are compared. The tubes are more excited in the presence of transverse flows and rods located far from the transverse inlet are the most affected.

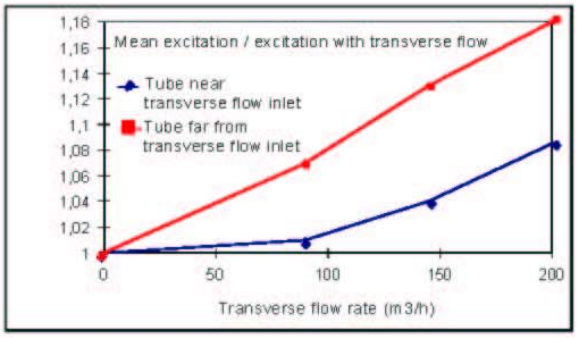


***Figure 14 : Comparison of excitation RMS magnitudes with and without transverse flow, for tubes located near and far from the transverse flow inlet 1300 Mwe.***

## Conclusion

A flow induced force identification method has been presented and applied to the prediction of PWR RCCA vibratory responses. The first two parts of the paper provide a theoretical derivation of the full inverse identification process. An application is illustrated in the third section. Fluid excitation sources acting on rod cluster control assembly are examined and numerical results turn out to be correct in terms of wear work rate estimates.

This approach requires no specific assumption regarding the force spatial distribution. As indicated in the present document, the method is convenient for the treatment of complex structures embedded in real 3D turbulent flows. Other PWR component dynamical behaviors (not shown here) have been considered and results were consistent with predictions. The numerical process used for the identification has been implemented and integrated into a sophisticated code including regularization procedures. The tool provides good performances and the applications go far beyond the flow induced vibration field. The model is fitted with experimental data. Then, for each component, a realistic mockup is built to simulate the fluid structure system. The experimental facilities may although be used for identifying other kind of excitation sources. Static force component acting near the guide plates may be identified.

Furthermore, new developments will be carried out in order to provide a force prediction numerical tool relying on Computational Fluid Dynamics (CFD) models. By using hydraulic computations in the presence of tubes or tube bundles, with Large Eddy Simulation (LES) for example, it will be possible to estimate wall pressure fields and spectra. The turbulent excitations responsible for the structure motion will be estimated without any experimental device.

## Acknowledgements

Authors would like to express their sincere thanks to Mr PEROTIN and Mr GUICHARD for their significant contribution in the present work.

## References

AXISA F., ANTUNES J., VILLARD B. (1990), Random excitation of heat exchanger tubes by cross-flow, *Journal of Fluids and Structures*, vol. 4, pp. 321-342.

BLEVINS R.D. (1990), Flow-induced vibration, *2nd edition*, Van Nostrand Reinhold.

BORSOI L., CANTENEUR C., BARBE G. (1997), Experimental and computaional investigation into vibration wear of control rods in french PWRs, *ASME, Flow-Induced Vibration and Noise*, Vol. 2, pp. 249-256.

BOSSELUT D., REGNIER G, SOULIER B. (1997), FEM of PWR's control rod cluster. Parametrical study of vibrating behavior by an experimental design method. *SMIRT 14, 14th International Conference on Structural Mechanics in reactor thechnology*, Vol. 10, pp. 63-70.

CHEN S.S. (1987), Flow-induced vibration of circular cylindrical structures, *Hemisphere Publishing Corporation*.

CIARLET P..G. (1982), Introduction à l'analyse numérique matricielle et à l'optimisation. *Editions Masson*.

CLOUGH R.N., PENZIEN J. (1980), Dynamique des structures. *Editions Pluralis*.

CORCOS G.M., (1963), Resolution of pression in turbulence. *Journal Acoust. Soc. Am.*, Vol. 35, pp. 192-199.

GAGNON J.O., PAÏDOUSSIS M.P. (1990), Fluid coupling charactristic and vibration of cylinder clusters in axial flow. Part 1: Theory, *Journal of Fluids and Structures*, Vol. 8, pp. 257-291.

GIBERT R.J. (1988), Vibrations des structures, interactions avec les fluides, sources d'excitation aléatoire. *Editions Eyrolles*.

GRANGER S., (1988), Time domain method for estimation of damping in flow induced vibration problems, *ASME PVP Conference, International Symposium on damping*.

GRANGER S. (1990), A new signal processing method for investigating fluidelastic phenomena, *Journal of Fluids and Structures*, Vol. 4, pp. 73-97.

GRANGER S. (1991), A global model for flow-induced vibration of tube bundles in cross-flow, ASME, *Journal of Pressure Vessel Technology*, Vol. 113, pp. 446-458.

GRANGER S., CAMPISTRON R., LEBRET J.(1993), Motion-dependent excitation mechanisms in a square in-line tube bundle subject to water cross-flow: an experimental modal analysis, *J. Fluids Struct.*, Vol. 7, pp. 521-550.

GRANGER S., GAY N. (1995), An unsteady semi-analytical model for cross-flow induced vibration of the tube bundle: comparison with experiment. *Flow-Induced Vibration*, Bearman ed., Balkema, pp. 327-338.

GRANGER S., PAÏDOUSSIS M.P. (1996), An improvement to the quasi-steady model with application to cross-flow-induced vibration of tube arrays, *J. Fluid Mech.*, Vol. 320, pp. 163-184.

GRANGER S., PEROTIN L. (1997), An inverse method for the identification of a distributed random excitation acting on a vibrating structure: Part 1: Theory, *ASME Fluid-Structure Interactions*.

LANDAU L., LIFCHITZ E. (1971), Mécanique des fluides, *Editions Mir*.

LIN W.H., (1987), Response of a circular rod to an axial turbulent flow, *ASME, Flow-induced Vibration PVP*, Vol. 122.

PEROTIN L., GRANGER S. (1997), An inverse method for the identification of a distributed random excitation acting on a vibrating structure: Part 2: Flow-induced vibration application, *ASME Fluid-Structure Interactions*.

# CHAPITRE I

# -

# DECOUPLAGE FLUIDE STRUCTURE

# CHAPITRE I - DECOUPLAGE FLUIDE STRUCTURE

## 1. Multi-physiques et interfaces

### 1.1. Du découplage au couplage

Tout couplage entre sous-systèmes passe par une analyse découplée préalable, a minima pour modéliser chaque sous-système et si possible évaluer la force du couplage dont la connaissance peut orienter le choix de la modélisation du système couplé global. Sur quelles bases construire le modèle couplé ? L'analyse dimensionnelle proposée par De Langre (2002) constitue la première étape clef. Elle est suivie de la phase de modélisation physique. C'est cette phase qui est examinée ici.

La modélisation du système couplé doit satisfaire deux types de conditions (Figure 4): (1) d'une part **modéliser l'interface entre les sous-systèmes**, ce qui constitue sa fonction principale, (2) d'autre part **être compatible avec les modélisations des sous-systèmes couplés**. Les deux exemples présentés ci-dessous abordent ces problématiques et montrent l'importance de ces deux conditions.

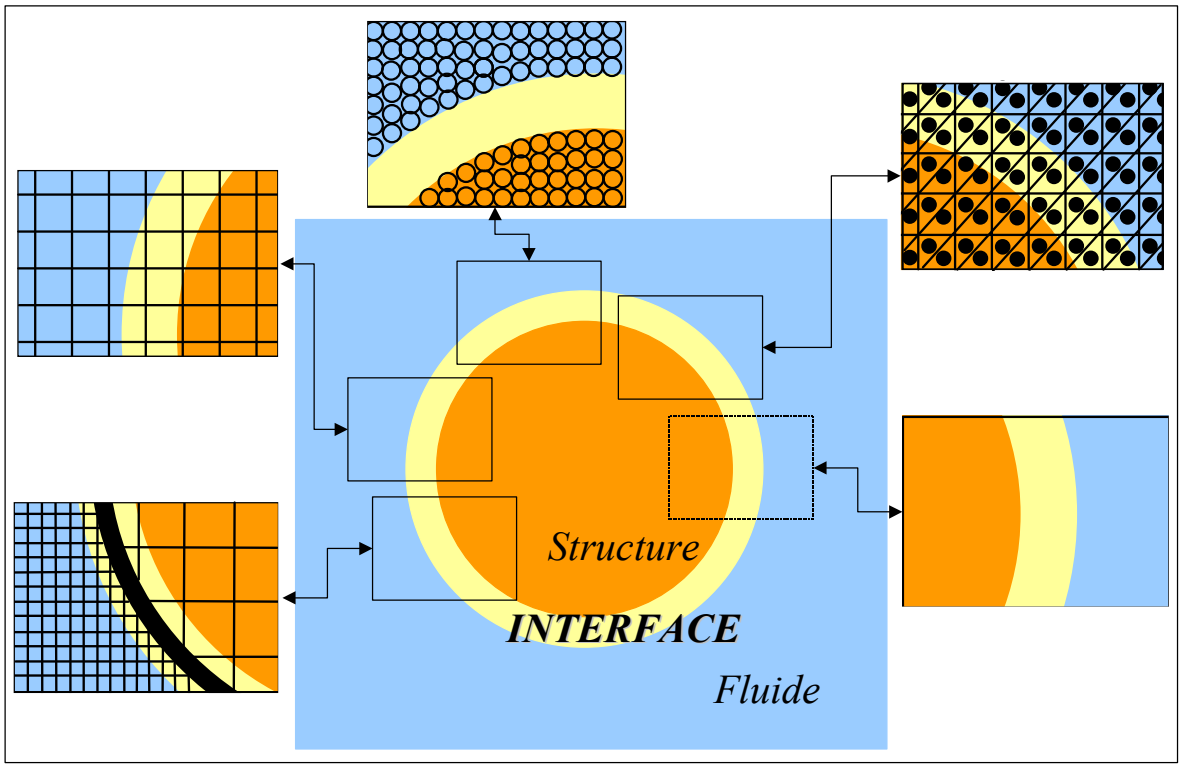


*Figure 4 : Modélisation de l'interface fluide structure.*

### 1.2. Interfaces entre physiques

Le premier exemple a pour objet de montrer l'importance du choix de la modélisation des sous-systèmes pour assurer la représentativité de l'interface. Les résultats d'un calcul couplé ne sont pas indépendants des modélisations adoptées pour les sous-systèmes couplés et **la modélisation de l'interface dépend des modélisations des sous-systèmes qui la constituent**.

### 1.3. Compatibilité des modélisations

Le second exemple traite de la problématique de compatibilité entre modélisations qui est à la base de l'une des principales difficultés rencontrées dans la modélisation des couplages. **Une modélisation d'un sous-système, valable en l'absence de couplage, peut devenir obsolète en présence de l'interface avec un deuxième sous-système**. La modélisation d'un système couplé n'est pas la superposition des modélisations des sous-systèmes couplés. C'est ce qui constitue la base des couplages comme le souligne De Langre (2002) : à partir d'une comparaison entre les analyses dimensionnelles couplées et découplées des équations de continuité à l'interface, il établit l'existence de paramètres représentatifs du couplage, indépendants des paramètres propres aux sous-systèmes, fluide et structure.

Les exemples de découplages ci-dessous en apportent quelques illustrations. Le premier exemple relève du domaine des vibrations induites par écoulements en faisceaux de tubes et porte sur la représentativité des chargements pariétaux modélisés par le solveur fluide et destinés à être transmis à l'interface avec un solveur structure. Le second exemple d'aéroacoustique est relatif à un découplage fluide fluide et traite du choix des modélisations à adopter pour représenter la propagation du bruit généré par un écoulement turbulent en respectant les modélisations des deux sous-systèmes fluides : écoulement turbulent et son généré.

## 2. Exemple des vibrations en faisceau

### 2.1. Conditions de découplage

La simulation numérique des vibrations induites par écoulements en faisceau passe par la modélisation des chargements thermohydrauliques pariétaux en faisceau. Deux options peuvent être envisagées suivant que le mouvement des tubes est pris en compte ou non dans l'identification des chargements. Le découplage fluide structure consiste à adopter la seconde option et à considérer le faisceau de tubes fixe, en négligeant l'effet de la dynamique de la structure sur les écoulements qui la sollicitent. Cette approche est pertinente tant que les déplacements de la structure restent de faible amplitude. Lorsque les conditions sont réunies pour que les déplacements de la structure en présence d'écoulement soient significatifs, l'approche découplée n'est plus possible. Sa mise en oeuvre constitue toutefois une étape préliminaire intéressante pour l'étude des vibrations induites par écoulements en ce sens que la comparaison calcul couplé / calcul découplé peut renseigner sur la force du couplage. Si les résultats fournis par les deux approches sont concordants, on peut considérer que les couplages physiques sont négligeables, ou a minima contrôlables. Dans le cas contraire, la physique n'est pas décrite par le découplage et une méthodologie de couplage doit être envisagée.

Les travaux présentés dans cette partie sont consacrés à l'identification numérique des écoulements et des chargements thermohydrauliques pariétaux en faisceaux de tubes fixes. Il s'agit d'une étude préliminaire dont l'objectif est de montrer l'importance du choix des modélisations des systèmes découplés avant d'envisager leur couplage. Tout résultat de calcul numérique dépend de la modélisation physique adoptée. **A fortiori tout calcul couplé dépend des modélisations des sous-systèmes couplés et de leur interface.** Ainsi le choix du modèle de turbulence en faisceau n'est pas sans incidence sur les écoulements et donc sur les chargements thermohydrauliques pariétaux estimés.

Ces chargements constituent « la moitié » de l'interface fluide structure dans les calculs couplés vibratoires, l'autre partie étant constituée par les déplacements vibratoires de la paroi

du solide induits par ces chargements.

On s'intéresse ici aux seuls chargements, à la modélisation de la turbulence en faisceau et à son effet sur la modélisation des données à l'interface. Les effets inverses du couplage avec la structure sur les chargements sont abordés dans le chapitre III consacré aux couplages.

### 2.2. Ecoulements en faisceaux

La modélisation de la turbulence adoptée repose sur l'approche L.E.S. développée et validée sur plusieurs cas académiques. Elle a été appliquée à des configurations de type piquages industriels dans le cadre de projets[13], pour des études d'acoustique, de thermique (Benhamadouche et al. 2003, Liang et Papadakis 2004, Péniguel et al. 2003), de jets pariétaux (Addad et al. 2003) et de faisceaux de tubes sous écoulements transverses (Benhamadouche et Laurence 2003, Benhamadouche et al. 2002, 2004, 2005, Longatte et al. 2003).

Dans le domaine des faisceaux de tubes, on considère ici le cas des écoulements turbulents monophasiques transverses dans différentes configurations de faisceaux, à pas carrés, rectangulaires ou quinconces, pour plusieurs pas réduits. Pour la représentation des faisceaux, on est amené à simuler des cellules de faisceaux périodiques, en utilisant des conditions aux limites adaptées où sont imposées les valeurs des débits entrant et sortant de la cellule périodique, en tenant compte de la direction axiale, transverse ou oblique des écoulements. Pour la simulation des régimes d'écoulements turbulents, les configurations traitées sont tridimensionnelles (Figure 5).

Les validations ont été réalisées en considérant plusieurs des tailles de cellules périodiques en fonction du nombre de tubes pleins modélisés et de la position des conditions aux limites par rapport aux tubes (Figure 6).

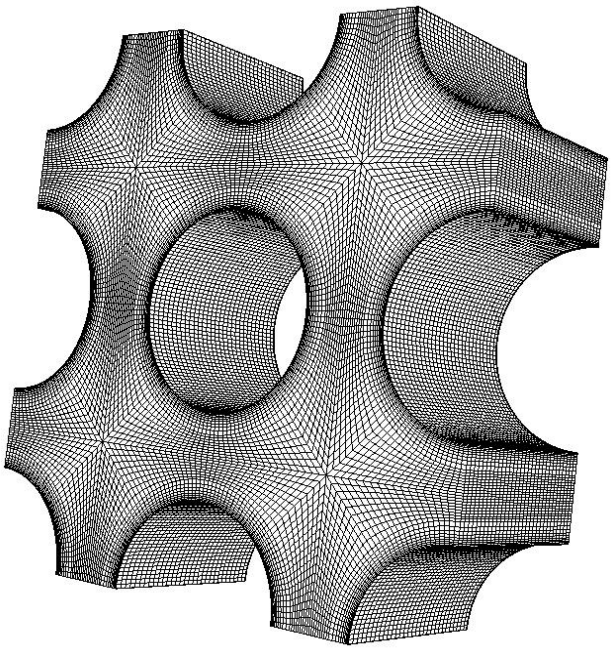

*Figure 5 : Exemple de maillage tridimensionnel pour la simulation des écoulements transverses dans un faisceau de tubes périodique à pas carré droit ou quinconce.*

[13] Projets NATIFS, EMOTHIF et JUPITER

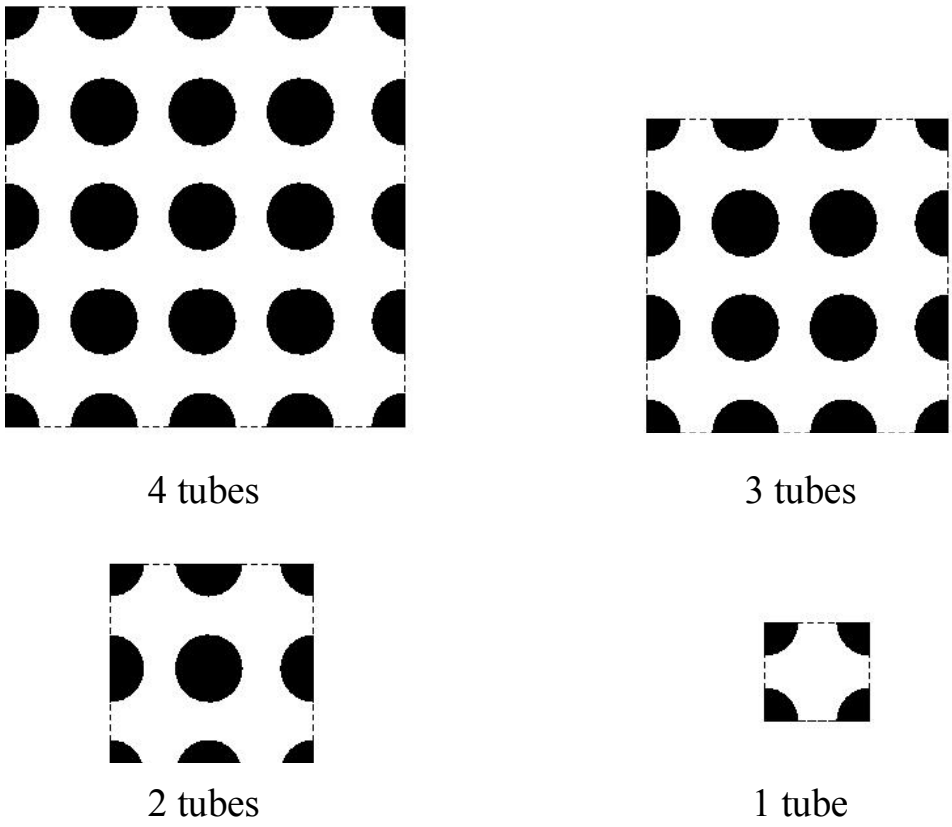


*Figure 6 : Exemples de cellules périodiques utilisées pour les calculs en faisceaux avec 1, 2, 3 ou 4 tubes pleins dans chaque direction transversale.*

L'hydraulique en faisceau a été validée sur une configuration à pas carré avec un angle d'attaque de 45° (Benhamadouche et Laurence 2003). Les résultats ont été comparés à des données de référence disponibles, obtenues par L.E.S. (Rollet-Miet 1997), par D.N.S.[14] (Moulinec et al. 2001) et expérimentalement (Simonin et Barcouda 1988). Dans la configuration considérée, le nombre de Reynolds basé sur le diamètre des tubes et la vitesse débitante amont est égale à *9000*. Des conditions aux limites de périodicité ont été imposées dans les trois directions de l'espace, le débit étant imposé. Le modèle de Smagorinsky constant (Benhamadouche et Laurence 2003) a été choisi suite aux conclusions de Rollet-Miet (1997) concernant les modèles de sous-maille dans le cas des faisceaux de tubes, les modèles dynamiques n'apportant pas de modifications majeures sur les résultats. Plusieurs maillages ont été utilisés pour tester la sensibilité des simulations au raffinement de maillage. Les simulations L.E.S. 3D ont donné des résultats très satisfaisants, y compris en utilisant une cellule périodique minimale (Figure 7), comme en D.N.S, Rij-ε 3D et contrairement à la L.E.S. 2D.

[14] Direct Numerical Simulation

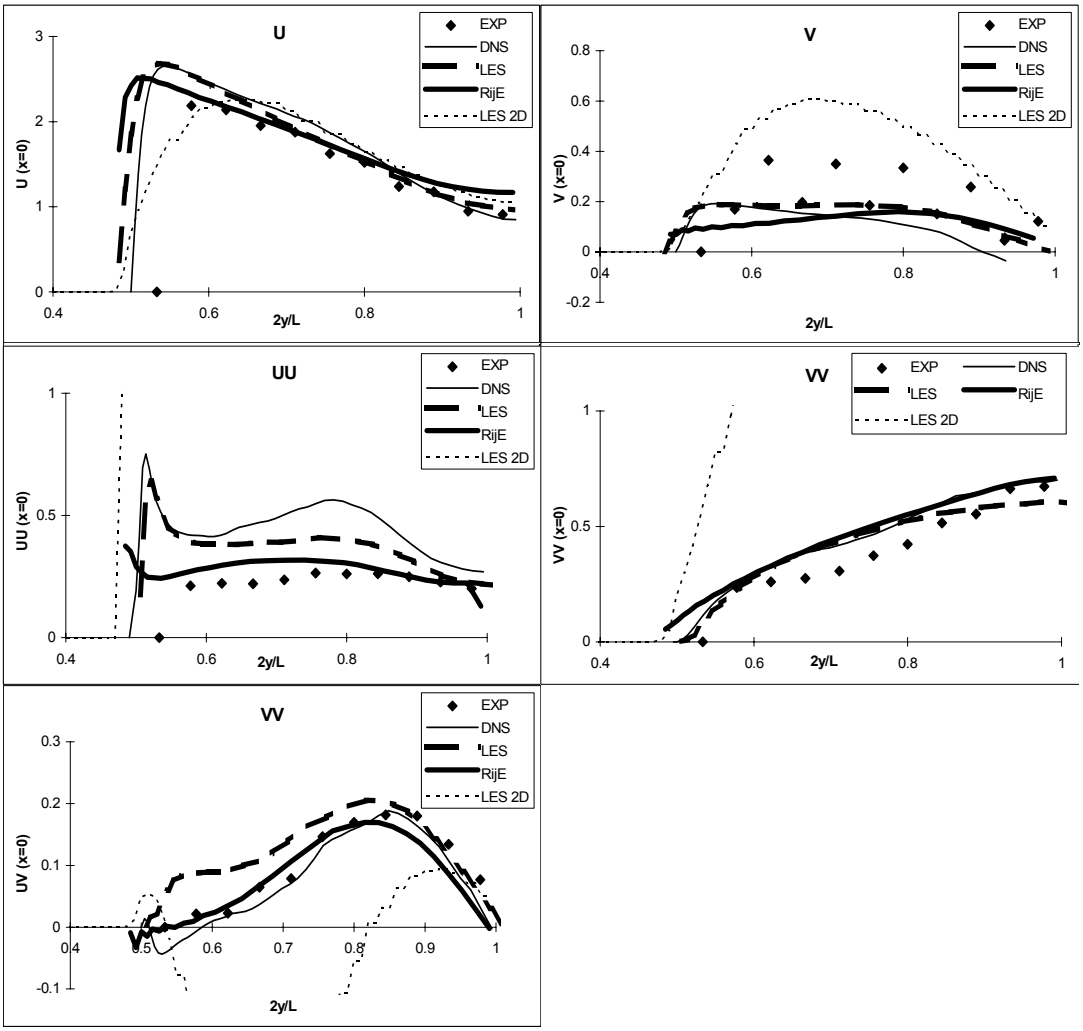


*Figure 7 : Champs de vitesses et moments associés dans un faisceau quinconce de pas réduit 1.47 estimés par D.N.S, par L.E.S. 3D (Benhamadouche and Laurence 2003), avec un modèle Rij-ε 3D, par L.E.S. 2D et expérimentalement par Simonin et Barcouda (1988).*

### 2.3. Modélisation des chargements pariétaux

Outre la connaissance de l'hydraulique, les principales données qui présentent un intérêt majeur pour l'étude des vibrations induites par écoulements sont les chargements pariétaux au niveau des tubes. Ils sont caractérisés en partie par les coefficients de portance et traînée $C_L, C_D$ et les variances associées $\sqrt{\left(C_L'\right)^2}, \sqrt{\left(C_D'\right)^2}$ au cours d'un écoulement instationnaire.

La L.E.S. 3D a été utilisée pour estimer les écoulements et les chargements en faisceaux à pas carrés et rectangulaires avec un angle d'attaque de *0°* (Figure 8). On observe le développement d'un écoulement symétrique pour un pas carré réduit *1.75*, ce qui donne un coefficient moyen de portance nul comme prévu par Chen (1987) sur la base d'observations expérimentales pour la gamme de nombres de Reynolds considérée (de l'ordre de *70000*, Annexe 2). Avec un faisceau rectangulaire de pas réduits *1.44* et *2*, on obtient également un écoulement symétrique.

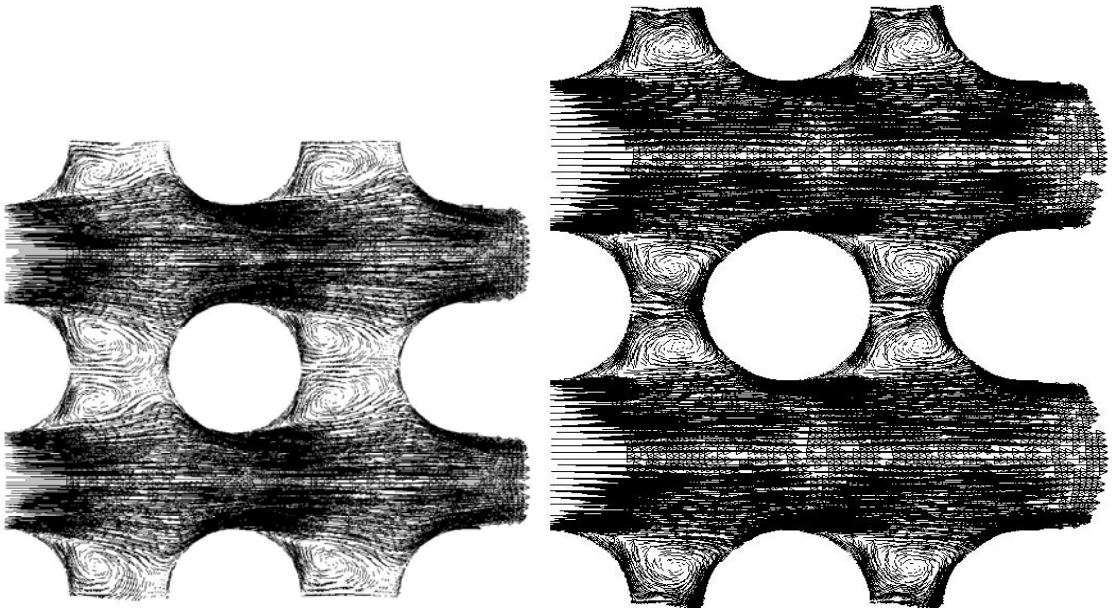

*Figure 8 : Champ de vitesse moyen pour une cellule de faisceau périodique à 2 tubes avec une longueur égale à un diamètre dans la direction longitudinale, pour un faisceau à pas carré de pas réduit 1.75 (à gauche) et un faisceau rectangulaire de pas réduits 1.44 et 2 (à droite).*

On compare dans le Tableau 1 les coefficients de portance, traînée et les valeurs RMS associées aux données expérimentales de Chen (1987). Toutes les grandeurs sont exprimées sur la base des vitesses inter-tubes. Les données expérimentales sont relatives à un tube situé en milieu de faisceau tel qu'il est modélisé numériquement avec des conditions aux limites de périodicité en faisceau de tubes fixes.

Numériquement on obtient un bon comportement qualitatif : la variance du coefficient de portance est plus grande que celle du coefficient de traînée dans des proportions raisonnables par rapport aux données expérimentales. La variance du coefficient de traînée est très proche des valeurs expérimentales. Le coefficient de portance est légèrement surestimé mais il est du bon ordre de grandeur (Benhamadouche et Laurence 2003).

Des études complémentaires ont montré l'importance des effets 3D sur la portance fluctuante. Pour les quantifier, on a vérifié l'amélioration engendrée par une plus grande longueur d'extrusion du maillage dans la direction longitudinale. Plusieurs simulations à pas carré réduit *1 .75* ont été réalisées avec différentes longueurs d'extrusion. On a montré que pour un faisceau carré à pas *1.75*, une longueur d'extrusion de *2.5* diamètres correspond à une longueur seuil au-delà de laquelle les effets tridimensionnels sur la portance sont quasi-asymptotiques (Benhamadouche et Laurence 2003). En-deçà de cette longueur d'extrusion, la valeur de la portance ne peut pas être considérée comme convergée.

Des résultats complémentaires sont reportés dans Benhamadouche et Laurence (2003) mettant en évidence l'importance du choix du modèle de sous-maille, l'effet des tailles de cellules périodiques, l'impact des conditions aux limites périodiques, des lois de parois au niveau des cylindres et la validation des chargements en écoulements à bas et hauts Reynolds pour différentes géométries de faisceaux.

| Pas réduit *1.75* | Calcul *1 diamètre* | Calcul *2 diamètres* | Calcul *2,5 diamètres* | Mesure |
|---|---|---|---|---|
| $\sqrt{(C'_L)^2}$ | *0,41* | *0,29* | *0,25* | *0,08 – 0,10* |
| $\sqrt{(C'_D)^2}$ | *0,13* | *0,07* | *0,06* | *0,04 – 0,06* |
| $C_L$ | *-0,04* | *-0,02* | *0,0009* | - |
| $C_D$ | *0,35* | *0,33* | *0,26* | - |

*Tableau 1 : Comparaisons calculs mesures (Chen 1987) des portance, traînée et variances associées pour un faisceau de pas carré réduit 1.75, une longueur égale à 1, 2 et 2.5 diamètres dans la direction longitudinale pour un nombre de Reynolds de 20000.*

Des travaux complémentaires sont envisagés pour spécifier les modèles de turbulence à utiliser dans le cadre des futurs calculs couplés de vibrations induites par écoulements en faisceaux de tubes mobiles et disposer des chargements thermohydrauliques pariétaux représentatifs de la réalité. Cette phase passera par des validations calculs / mesures sur la base de données expérimentales obtenues sur des maquettes de faisceaux de tubes et fournissant à la fois des résultats de mesures thermohydrauliques (par des techniques de PIV 3 composantes) et vibratoires (avec des jauges de contraintes ou par vibro-laser).

## Annexe 2 : Découplage fluide structure en faisceaux

**Longatte, E.**, Bendjeddou, Z., Souli, M. (2003). Application of DNS and LES to prediction of tube flow-induced vibrations. *DLES 5 Workshop*, Munich.

# APPLICATION OF DNS AND LES TO PREDICTION OF TUBE FLOW-INDUCED VIBRATIONS

Elisabeth Longatte, Zaky Bendjeddou
*EDF Research & Development Division,*
*Fluid Mechanics and Heat Transfer Department, Chatou, France*
elisabeth.longatte@edf.fr,zaky.bendjeddou@edf.fr

Mhamed Souli
*Lille University, Mechanical Engineering Department,*
*Villeneuve d'Ascq, France*
mhamed.souli@univ-lille1.fr

**Abstract** In many industrial applications, mechanical structures like rod cluster control assembly, fuel assembly and heat exchanger tube bundles are subjected to complex flows causing possible vibrations and damage. Fluid forces can be split into two parts : turbulent forces not affected much by structure motion and fluid-elastic forces coupled with tube motion and responsible for possible dynamic instability development leading to possible short term failures through high amplitude vibrations. Most classical fluid force identification methods rely on structure response experimental measurements associated with extensive data processing. Owing to recent improvements in Computational Fluid Dynamics, hydraulics force identification is now practicable in the presence of industrial configurations. The present paper is devoted to the numerical simulation of flow-induced vibrations of tubes and tube bundles submitted to single-phase turbulent flows. Large Eddy Simulation or Direct Numerical Simulation with or without code coupling are applied to the prediction of turbulent or fluid-elastic forces responsible for tube vibrations in the presence or not of strong coupling effects.

**Keywords:** LES, turbulence, code coupling, ALE, fluid structure interactions, flow-induced vibrations, tube bundles

## 1. Introduction

Numerical simulation of fluid structure interactions and particularly of tube flow-induced vibrations is investigated in the present paper. The purpose is to predict numerically tube bundle vibrations generated by single-phase cross flows by using Computational Fluid Dynamics (CFD) codes involving specific numerical methods for multi-physic problems. As far as flow-induced vibrations are concerned, the purpose is to estimate thermo-hydraulics force effects on structure motion and in the same time to account for possible coupling between tube motion and part of fluid forces, so-called fluid-elastic forces, in order to predict possible dynamic instabilities enabling short term failures through high magnitude vibrations. These simulations are now reachable in configurations involving basic geometry thanks to recent improvements in CFD.

Fluid forces acting on mechanical structures can usually be split into two parts: structure motion independent forces generated by flow turbulence patterns, fluid-elastic forces responsible for possible dynamic instability development and induced by a real coupling between flow and structure motion. Tube motion independent forces generated by near-wall pressure fluctuations can be computed numerically by using CFD because they are not affected by structure pattern and dynamic motion effects. It is possible to assume that tube walls are rigid and turbulent force calculation only requires a near-wall unsteady field computation performed on a fixed non-moving mesh. Numerical simulation of fluid-elastic effects requires a real coupling between mechanical models and CFD calculations accounting for wall motion effects on flow patterns and conversely. Such a calculation is still impracticable for industrial purposes through lack of sufficient numerical resources but simplified configurations can be tested.

The present paper provides an overview of three physical problems involving flow-induced vibrations in tube bundles that can be solved by using CFD codes. Specific turbulence models like Large Eddy Simulation (LES) are used, methods for moving boundaries are required like Arbitrary Lagrange Euler formulation (ALE) and numerical scheme adapted to multi-physics problems and code coupling are presented. The first part is related to the study of tube vibrations generated by turbulence in the presence of weak fluid-elastic coupling effects. In the second part LES is applied to identification of flow fields in tube bundles in the presence of cross flows. Finally numerical simulations of flow-induced vibrations in tube bundles in cross flows using ALE and code coupling are presented in the last section and results are discussed in terms of tube vibration frequency according to available experimental data.

# 2. Identification of turbulent force spectra using LES

## 2.1 Physical problem

When fluid-elastic effects are reduced to added mass and damping effects, there is no strong flow structure coupling and structure motion effects acting on turbulent flow patterns can be neglected. It is then possible to perform thermo-hydraulics and mechanics calculations separately to study flow-induced vibrations (Longatte et al. 2001, Moreno et al. 2000). Turbulent force spectrum and time record can be simulated on a non-moving computational domain with a fixed structure by using Large Eddy Simulation (LES) and they are introduced as inlet data into the mechanical calculation providing the structure vibratory response. This computational process was applied to the prediction of a single tube dynamic response generated by a turbulent mainly axial flow in a non-confined area. The test case corresponds to a configuration previously studied experimentally at EDF by Granger and Perotin (1997). A tube is submitted to a turbulent three-dimensional flow crossing a perforated plate located just above the rod and generating mainly axially high turbulent fluctuations near the tube. Eddies are generated along the rod and finally the fluid is evacuated by a lateral outlet. The square test section size (260 mm) is large in front of the tube diameter (15 mm) and confinement effects may be neglected. Hence fluid-elastic effects are restricted to added mass and damping effects due to the fluid that can be deduced from experimental prediction. The computational process is described below.

## 2.2 Numerical methods

As structure motion does not affect turbulent fluid forces, fluid and structure calculations are performed separately. First fluid computation involving LES is performed with a rigid solid non-moving tube and provides unsteady flow fields. Near-wall fluid forces on the tube are estimated in terms of power spectral density and a modal spectral mechanical calculation is carried out to compute the tube dynamic response. Fluid force magnitude and spectrum calculation requires near-wall refined turbulence modelling in order to capture unsteady pressure fluctuations. LES are becoming more and more important in research industrial applications, especially when accurate near-wall unsteady field estimates are required. In the present paper a Large Eddy Simulation is performed in order to compute turbulent force spectra and mean values distributed along the rod. The Smagorinsky model was applied to the

simulation of turbulence in plane duct for instance and good results were obtained. However this modelling features disadvantages. For example it does not account for wall effects on the subgrid scale turbulent stresses unless a specific damping function is applied to reduce the Smagorinsky constant near the wall. A suitable Van Driest function was used by Moin (1982) in order to improve the numerical scheme behaviour. Other models tending to be more efficient in the presence of near-wall turbulence were developed (Bardina 1989, Germano 1992).

In the present article the Smagorinsky modelling is used to predict turbulent forces acting on a rod submitted to an axial flow with $C_s = 0.065$. Possible errors induced by the Smagorinsky modelling can be compensated by sufficient mesh refinement near the wall. Further studies will be carried out in order to compare the results obtained by using other techniques. A dynamic model will be considered by adjusting the constant of the subgrid scale model as a function of space and time.

## 2.3 Numerical results

Main numerical results deduced from LES and from mechanics calculation are presented below. Turbulent forces are expressed in terms of spectra and numerical solutions are validated by using comparisons with available experimental data. Then tube dynamic response deduced from numerical force estimates are compared to experimental measurements in terms of physical stress. Numerical fluid forces are compared to experimental data in Figure 1 in terms of power spectral density. They feature the expected patterns in terms of broadband, slope and magnitude. Finally the tube mechanical response resulting from previously identified forces is in good agreement with experimental measures. These results tend to show that LES provides reasonable estimates of fluid force spectra in the presence of complex geometry configurations embedded in turbulent flows. Accurate information is reachable about flow patterns responsible for structure flow-induced vibrations. Practical application to tube bundle vibration study is considered below.

# 3. Identification of flow fields in tube bundles using LES

## 3.1 Physical problem

In the presence of high fluid-elastic effects, when tubes are subjected to cross flows for example, LES performed on a fixed non moving mesh may also provide interesting information about spectra, lift and drag coefficients in tube bundles. Fluid forces acting on a staggered tube

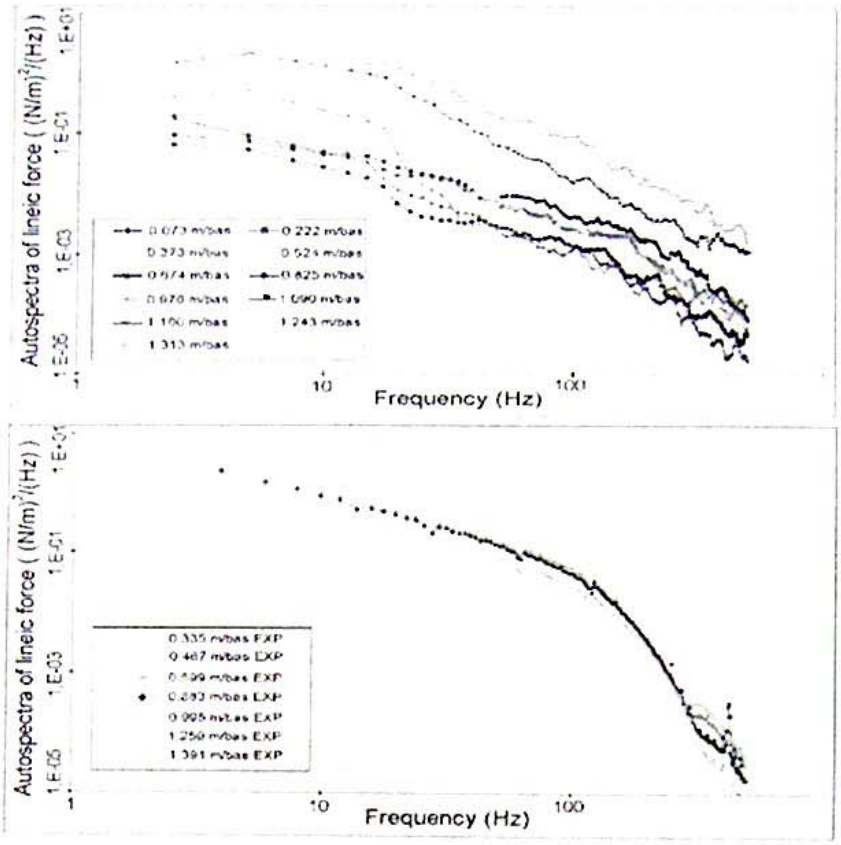


*Figure 1. Near-wall fluid force power spectral density along a tube in turbulent flow estimated numerically with LES (upper) and experimentally with an inverse method (lower).*

array in cross flows were identified by using a 3D LES. Numerical results were compared to solutions provided by DNS, 2D, 3D Rij-$\varepsilon$ modelling and experimental data in terms of mean velocity and Reynolds tensor (Benhamadouche and Laurence 2002). Results tended to show that 3D LES provides realistic flow patterns around the tube for further study of vibrations.

## 3.2 Numerical methods

In what follows LES are carried out in the presence of fixed in-line tube bundles in cross flow without structure motion in order to validate thermo-hydraulics fields. Calculations are carried out in reduced tube bundle cells including periodic conditions in order to reduce CPU time. The purpose is to estimate fluid forces acting on a fixed tube located in the middle tube of an array of fixed tubes. Solutions are estimated in terms of drag and lift mean and root mean square values.

6

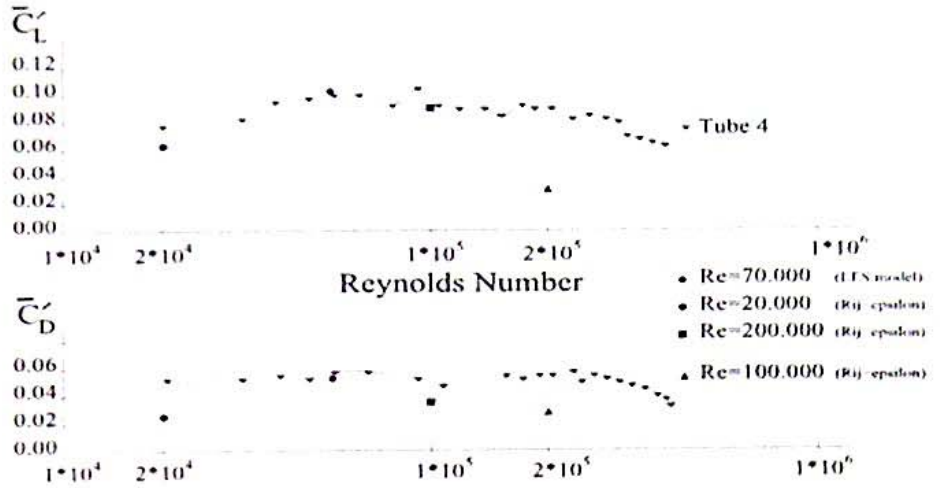


*Figure 2. Comparison between numerical simulation (RANS and LES model) and experimental measurement of lift (upper) and drag (lower) root mean square values for a middle tube (tube 4) in an array of fixed tubes submitted to cross flow for different Reynolds number (Chen 1987).*

## 3.3 Numerical results

A part of numerical results are presented below and compared for several Reynolds numbers to experimental measurements of Chen (1987) for a pitch ratio P/D=1.75 where P designates the pitch diameter and D the tube diameter. A comparison between numerical and experimental values of RMS of drag and lift coefficients is given by Figure 3. The expected tendency is retrieved by numerical solution particularly for small Re number (Chen 1987). For Re=70000 the numerical solution obtained with LES is in good agreement with the experimental solution plotted for tube number 4 located in the middle of tube bundle like in the simulation.

# 4. Identification of fluid-elastic forces in tube bundles using ALE and code coupling

## 4.1 Physical problem

To predict flow structure coupling, a fully computational process for simulation of tube bundle flow-induced vibrations was developed relying on a flow structure code coupling. The methodology consists in solving in the same time thermohydraulics and mechanics problems by using an Arbitrary Euler Lagrange (ALE) formulation for the fluid computation (Souli et al. 2001). The purpose is to take into account the coupling between flow and structure motions in order to be able to capture fluid-elastic effects. The ALE formulation is particularly appropriate in the presence of moving wall boundaries as boundary motion is taken into

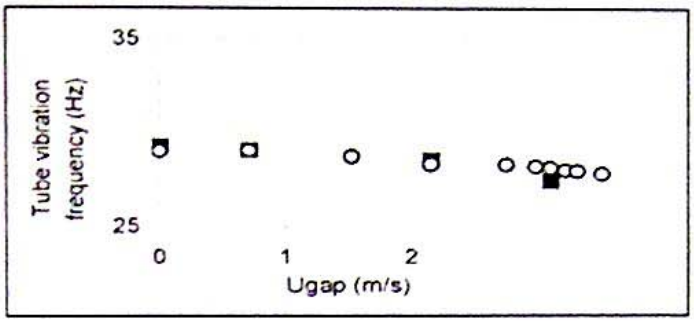


*Figure 3. Tube vibration frequency in flow $f_f$ (Hz) in terms of gap velocity Ugap (m/s) estimated numerically (black points) and experimentally by Granger et al. (1993) (white points).*

account in the fluid calculation while element shape properties are preserved (Bendjeddou et al. 2002).

## 4.2 Numerical methods

From a numerical point of view there are three steps in the computation : the fluid problem is solved on the computational domain; fluid lift and drag forces acting on the flexible tube are estimated ; then these forces are introduced in the structure problem whose computation provides the tube displacement and velocity used to deform the fluid computational domain. Implicit and explicit code coupling processes were tested.

## 4.3 Numerical results

In the present work this process was applied to the identification of fluid-elastic parameters of a single flexible tube moving in a fixed tube bundle. The fluid calculation is performed on a finite tube bundle cell featuring periodicity. The coupling process previously mentioned was applied to the prediction of tube vibration frequency in still water and in flow. Tube motion is generated by an initial displacement. Numerical results are compared to experimental data of Granger et al. (1993) in terms of tube frequency in fluid at rest and in flow. Results are reported in Figure 3 and a good agreement is observed. Other configurations have been tested and the same tendency was retrieved. Convergences in mesh and time were tested in order to ensure the validity of our results. Further validations are required to build numerical tools for study of tube bundle stability in presence of cross flows (Chen 1987, Price and Padoussis 1996).

8

## Conclusion

Numerical results presented in this article illustrate possible applications of CFD to the study of flow-induced vibration problems in tube and tube bundles. Classical approaches are involved in the presence of weak fluid structure coupling. Specific methods using moving meshes are required for the identification of strong flow structure interactions. Further developments are carried out to improve numerical tools and enable the prediction of tube bundle vibration frequency, damping and stiffness in complex configurations.

## Acknowledgments

Authors would like to express their sincere thanks to MM. Caruso, Archambeau, Benhamadouche and Adobes for their helpful contribution in the present work.

## References

Bardina J., Ferziger J.H., Reynolds W.C., (1989), *Improved subgrid-scale models for Large Eddy Simulation*, Rept TF-19Dept Mech. Eng. Stanford CA.

Benhamadouche S., Laurence D., (2002), *LES, coarse LES and transient RANS comparisons on the flow across a tube bundle*, Engineering Turbulence Modeling and Measurements conference 5, Elsevier.

Bendjeddou Z., Longatte E, Souli M., (2002), *Numerical simulation of tube bundle vibrations in cross flows*, FSI, AE&FIV+N conference, proceedings, New Orleans.

Chen S.S., (1987), *Flow-induced vibration of circular cylindrical structures*, Hemisphere Publishing Corporation.

Germano M., (1992), *Turbulence, the filtering approach*, J. Fluid Mech., 238, 325-336.

Granger S., Perotin L. (1997),*An inverse method for the identification of a distributed random excitation acting on a vibrating structure: Part 2: Flow-induced vibration application*, ASME Fluid-Structure Interactions, Dallas.

Granger S., Campistron R., Lebret J., (1993), *Motion-dependent excitation mechanisms in square in -line tube bundle subject to water cross-flow : an experimental modal analysis*, J. Fluid. Struc., 7, 521-550.

Longatte E., Laurence D., Barr F., Ledac P., (2001), *Application of Large Eddy Simulation to a flow-induced vibration problem*, ASME PVP, Conference on Flow-Induced Vibrations, Atlanta.

Moin P., KIM J., (1982), *Numerical investigation of turbulent channel flow*, J. Fluid Mech., 118, 341-377.

Moreno M.M., De Langre E., Le Quere P., (2000), *A large eddy simulation of the turbulent forcing spectrum induced by axial flow on a rod*, Conference on flow-induced vibrations 7, Lucerne.

Price S.J., Paidoussis N., (1986), *A single-flexible-cylinder analysis for the fluidelastic instability of an array of flexible cylinders in cross-flow*, J. Sound Vib., 108, 193-199.

Souli M., Zolesio J.P. (2001), *Arbitrary Lagrangian-Eulerian and free surface methods in fluid mechanics*, Comput. Methods Appl. Mech. Engrg., 2758.

# 3. Exemple de l'aéroacoustique en zone de mélange

## 3.1. Découplage fluide fluide

Le propre de l'aéroacoustique est de faire intervenir deux disciplines : la mécanique des fluides et l'acoustique, deux disciplines en général découplées, vu l'écart entre les ordres de grandeurs des vitesses caractéristiques des fluides des deux sous-systèmes : vitesse d'écoulement d'une part, célérité du son d'autre part. La propagation acoustique étant un phénomène essentiellement linéaire, il est usuel d'utiliser un opérateur linéarisé pour la modéliser. La résolution des EEL[15] permet en général de traiter la propagation acoustique indépendamment des sources qui l'ont générées. Les termes sources acoustiques préalablement identifiées peuvent être placés au second membre des EEL et jouer le rôle de générateurs de bruit (Béchara et al. 1994, Bailly 1994, Bailly et al. 1994, Longatte et al. 1998, Bastin 1997). C'est la raison pour laquelle cette formulation est souvent préférée aux approches classiques issues de l'analogie de Lighthill, en présence d'écoulements et de structures de géométries complexes, au voisinage des sources de bruit, l'extension du tenseur de Lighthill en milieu confiné n'étant pas aisé (Van Herpe 1993).

Toutefois, en présence de non linéarités d'écoulements, la formulation linéarisée ne permet pas de représenter les couplages fluide acoustique, puisque les termes de convection ne sont représentés que partiellement. En particulier elle est inapte à décrire la propagation de bruit en présence de gradients d'écoulement moyen puisque les non linéarités d'écoulement sont mal convectées par le propagateur. Le recours à une formulation alternative est nécessaire.

Cette difficulté propre au domaine de l'aéroacoustique illustre parfaitement le fait qu'**une modélisation physique adaptée en configuration découplée peut devenir impropre en configuration couplée**. Le choix des modélisations des sous-systèmes couplés n'est donc pas anodin. Pour la modélisation de la propagation acoustique, un opérateur non linéaire doit être préféré à un opérateur linéaire dès lors que l'on a couplage avec la turbulence. L'exemple présenté ci-dessous illustre cette problématique. Il met en évidence l'impact du choix du propagateur sur la représentativité du modèle physique. Les sous-systèmes considérés sont d'une part l'écoulement turbulent, d'autre part le son, et l'interface entre les deux systèmes, considérés ici comme découplés, est modélisée par des termes sources qui représentent le bruit généré par la turbulence.

## 3.2. Développement des instabilités

L'étude porte sur la modélisation du développement des instabilités d'une couche de mélange (Figure 9, Annexe 3). Parmi les opérateurs de propagation testés, deux systèmes d'équations ont été retenus pour les comparaisons : d'une part l'opérateur linéarisé EEL, d'autre part l'opérateur semi-linéarisé EESL[16] comprenant une partie des termes du second ordre après linéarisation des équations d'Euler. La convection des instabilités de la couche de mélange obtenue avec ces deux types d'opérateurs est comparée sur la Figure 10. La non prise en compte des termes non linéaires conduit à une divergence du calcul puisque les non linéarités de l'écoulement ne sont pas modélisées. Seul un opérateur non linéaire (partiel ou complet) est valide et permet de reproduire la physique dans ce cas (Figure 11) alors que l'opérateur de propagation acoustique linéaire usuel ne convient pas.

[15] Equations d'Euler Linéarisées

[16] Equations d'Euler semi-linéarisées

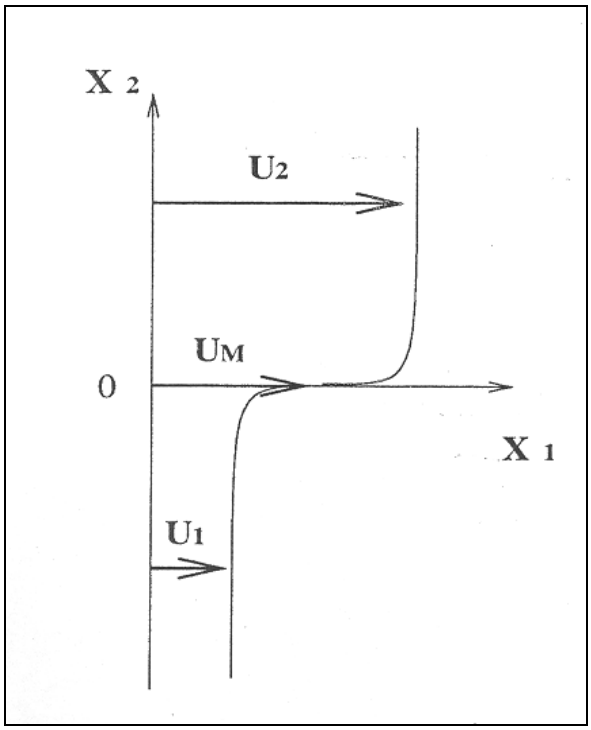


*Figure 9 : Exemple de profil moyen de vitesse d'une couche cisaillée en tanh générée par des écoulements de vitesses différentes de part et d'autre d'une lame mince.*

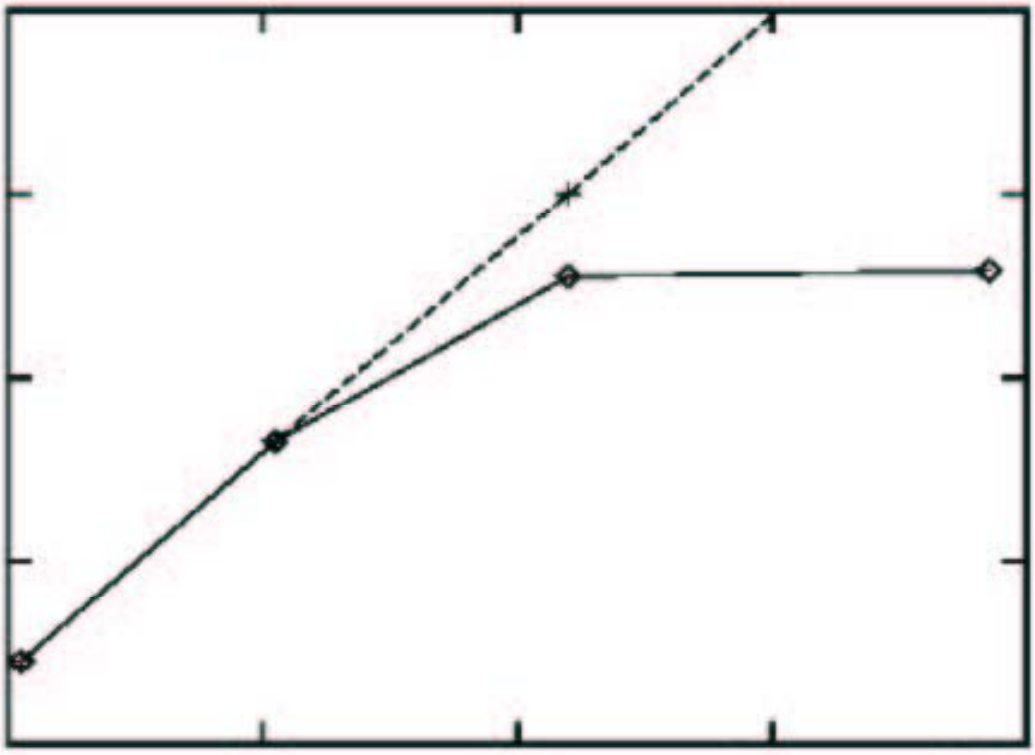

*Figure 10 : Prévision de l'écoulement d'une couche cisaillée avec un opérateur de propagation linéaire (trait pointillé) et non linéaire (trait plein) : valeur des maxima de la vitesse sur l'axe longitudinal de la couche en échelle logarithmique.*

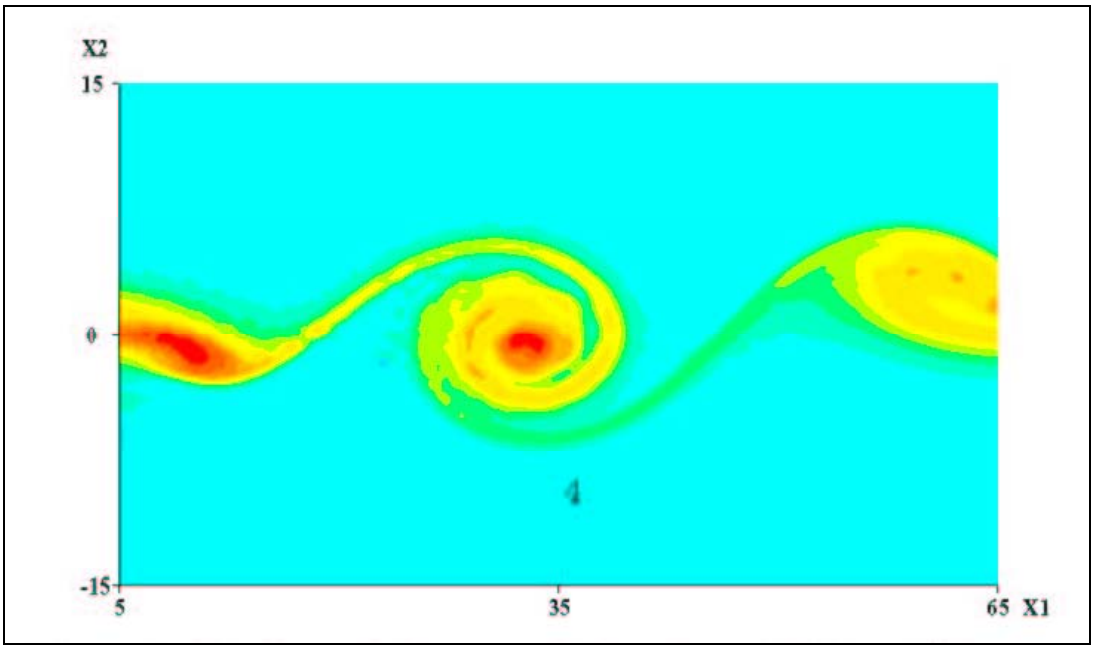


*Figure 11 : Développement de la couche de mélange obtenu avec l'opérateur de propagation non linéaire : champ de vorticité.*

### 3.3. Modélisation de l'interface

Cet exemple apporte un éclairage sur les choix des modélisations adoptées actuellement dans le domaine de l'aéroacoustique. Parmi toutes les approches possibles (Figure 12), l'intérêt des méthodes L.E.S. compressible est mis en évidence (Bogey et al. 2002, Bogey et al. 2003).

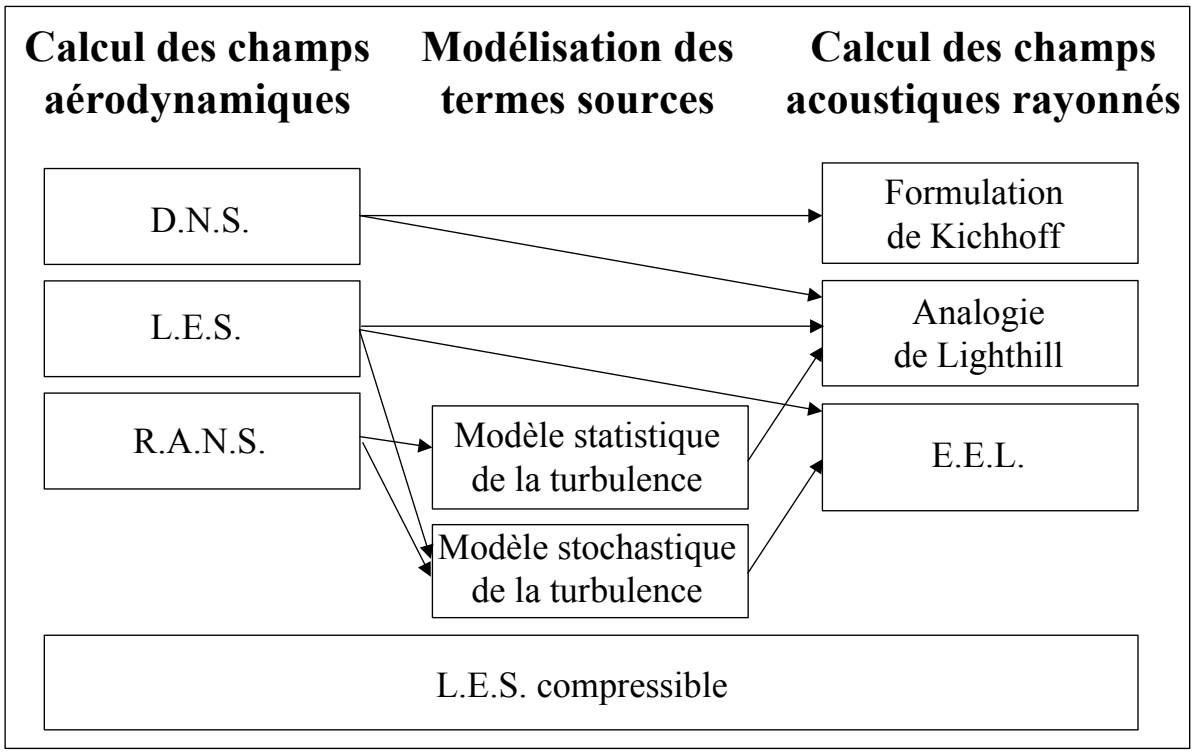


*Figure 12 : Méthodes utilisées en aéroacoustique.*

## Annexe 3 : Découplage turbulence acoustique en zone de mélange

Longatte E., Lafon P., Candel S. (2001). Linear and non linear development of instabilities in a shear layer. *7th AIAA/CEAS Aeroacoustics Conference,* Maastricht.

AIAA 2001-2164

# LINEAR AND NON LINEAR DEVELOPMENT OF INSTABILITIES IN SHEAR LAYERS

E. Longatte[†], P. Lafon[‡]
Département Acoustique et Mécanique Vibratoire,
Electricité de France,
1, Avenue du Général de Gaulle, 92141 Clamart Cedex, France,

S. Candel[§]
Laboratoire EM2C, CNRS, Ecole Centrale Paris
92295 Châtenay-Malabry Cedex, France

**Abstract**

New aeroacoustic noise prediction methods rely on the computation of linearized Euler equations (LEE) associated with source terms. The process may be described as follows : aerodynamic mean fields are deduced from the time-averaged Navier-Stokes equations associated with a closure scheme ensured for example by a k-$\epsilon$ turbulence modelling ; the source terms resulting from turbulent fluctuation effects are calculated separately ; these terms are finally incorporated into the linearized propagation equations providing the acoustic field.

While the LEE are known to bear convective modes, the difficulty associated with the growth of this mode in an inflexional shear flow profile has not been adressed explicitely. This issue is considered in this article. It is first shown that a small flow perturbation, solution of the Rayleigh equation, when used as input to the LEE, will grow exponentially. In order to avoid this unwanted behaviour, a new semi-linearized wave operator including non linear terms is built. This ensures stability and in this way acoustic flow interactions may be correctly described. The SLEE set features finite amplitude perturbations.

## Introduction

In the framework of Lighthill's theory, standard aeroacoustic noise prediction methods rely on an analogy featuring a propagation equation associated with source terms (Lighthill 1952, 1954). These formulations require time-average or unsteady aerodynamic computation (k-$\epsilon$, LES or DNS), they provide acoustic far-fields but they do not account for all acoustic flow interactions. More complex wave operators were derived to improve these prediction methods in the presence of complex free flows (Lilley 1972, Mani 1976). However their application to confined configurations is not straightforward because it requires the determination of near-wall adapted Green's functions (Van Herpe et al. 1995). Also most of these approaches rely on third order equations which are not convenient for numerical purposes.

In this context new aeroacoustic noise prediction methods were developed. They rely on the linearized Euler equations associated with convenient acoustic source terms (Béchara et al. 1994, Bailly et al. 1996, 2000). There are three steps in the calculation : (1) Aerodynamic mean fields are deduced from the time-averaged Navier-Stokes equations associated with a closure scheme ; (2) Turbulent noise generation is modeled by acoustic source terms ; (3) These source terms are incorporated into the linearized Euler equations. Their solution provides the acoustic field.

This modelling is convenient for the prediction of noise generated by turbulent flows. However it is known that Euler equations bear both acoustic and vortical modes and in the presence of inflexional shear profiles, aerodynamic unstable modes will be generated. The difficulty associated with this behaviour has been underestimated. There are at least two possibilities to cope with this problem : (1) One may suppress the mean gradient term which gives rise to the unstable mode of the LEE. The LEE are slightly "degraded" but the unstable mode do not develop in the flow field. This method is not considered



[†]Research Engineer
[‡]Research Scientist, Member AIAA
[§]Professor, Member AIAA

here (Longatte 1998). (2) One may include non linear terms on the right hand side of the LEE. This will limit the unstable mode amplitude and the acoustic field will remain computable. This second technique is investigated in this article. In the first section we show that in a parallel shear layer a small perturbation input to the LEE grows exponentially. To avoid this unstable growth, a semi-linearized wave operator including non linear terms is built. It is presented in the second section. The last section illustrates the application of the semi-linearized operator to the prediction of non linear instability development in a shear layer. The method effectively saturates the perturbation amplitude. Numerical results are in good agreement with analytical and experimental data. It is then possible to conclude that the semi-linearized operator can be useful in the computation of acoustic fields propagating in the presence of shear flows.

## 1. Linear development of unstable modes in shear layers

It is convenient to first summarize the standard aerodynamic instability theory. The model problem is that of a parallel mean flow described by the following velocity profile :

$$U_o(x_2) = U_M[1 + R_u \tanh(\frac{x_2}{2\delta_\theta})]$$

where $\delta_\theta$ designates the profile depth, $U_M = (U_1 + U_2)/2)$ is the mean velocity and $R_u = (U_2 - U_1)/2U_M$ the velocity rate if $U_1$ and $U_2$ are respectively the bottom and the top flow velocities of the shear layer. This profile was used for example by Michalke (1965). A typical profile is displayed in Fig. 1. The presence of an inflexion point drives the instability development (Rayleigh 1880). We use this profile together with the LEE to investigate the growth of an initially small perturbation. The computational process may be described as follows: (1) Shear layer unstable mode parameters are deduced from the Rayleigh equation; (2) Unstable mode velocity and pressure profiles are identified by solving the linearized Euler equations ; (3) These profiles are finally introduced as upstream conditions in the computational domain and the shear layer development is deduced by solving linearized Euler equations.

### 1.1. Determination of shear layer unstable modes

The standard theory of aerodynamic instability is based on the following splitting :

$$\mathbf{u}(x_1, x_2, t) = \mathbf{u_o}(x_1, x_2) + \mathbf{u'}(x_1, x_2, t)$$

For a parallel shear flow $(\mathbf{U_o(x_1, x_2, t)} = \mathbf{U_o(x_2)e_1}$ if $\mathbf{e_1}$ designates the $x_1$), the perturbation satisfies the

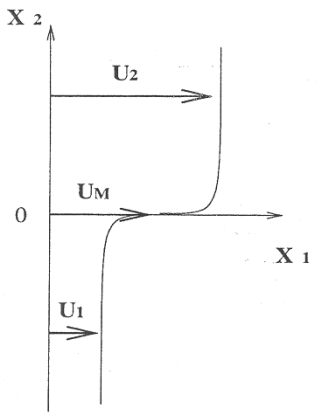


Figure 1: Shear layer mean flow velocity profile : $U_o(x_2) = U_M[1 + R_u \tanh(\frac{x_2}{2\delta_\theta})]$.

classical Rayleigh equation (i.e. the Orr-Sommerfeld equation without viscosity terms) (Rayleigh 1880, Drazin and Reid 1981). This equation may be written as follows:

$$L_\Psi(\mathbf{k}, \omega)[\hat{\Psi}] = 0 \qquad (1)$$

where $\Psi$ designates the stream function of incompressible fluctuations defined by :

$$\hat{u}_1 = \frac{\partial \Psi}{\partial x_2} \quad and \quad \hat{u}_2 = -\frac{\partial \Psi}{\partial x_1}$$

$\mathbf{u}$ is the velocity field, $\mathbf{k}$ the wave number and $\omega$ the fluctuation frequency. The Rayleigh operator $L_\Psi$ is defined by :

$$L_\Psi(\mathbf{k}, \omega) = \left[U_o - \frac{\omega}{k}\right]\left[\frac{d^2}{dx_2^2} - k^2\right] - \frac{d^2 U_o}{dx_2^2}$$

$$+\frac{1}{\rho_o}\frac{d\rho_o}{dx_2}\left[\left[U_o - \frac{\omega}{k}\right]\frac{d}{dx_2} - \frac{dU_o}{dx_2}\right]$$

In presence of a free shear flow, boundary conditions can be set to the Sommerfeld radiation conditions :

$$\left[\frac{d^2}{dx_2^2} - k^2\right]\Psi = 0 \quad \text{for} \quad |x_2| \to \infty$$

Finally the modal problem to be solved may be written as a dispersion relation (Huerre and Monkewitz 1990) :

$$D\left[\omega, \mathbf{k}(\omega)\right] = 0 \qquad (2)$$

According to the spatial theory, unstable modes are defined by the following modal parameters : $\mathbf{k_n}(\omega) =$

$\mathbf{k}_n^r(\omega) + i\mathbf{k}_n^i(\omega)$ solutions of the dispersion relation. Hence incompressible fluctuations are expressed by :

$$\hat{\Psi}_n(x_1, x_2, t) = \Psi(x_2) e^{-k_n^i x_1} e^{i(k_n^r x_1 - \omega t)}$$

with $-k_n^i(\omega)$ the mode growth rate. The phase velocity is given by : $c_p = \omega / k_n^r(\omega)$. For these unstable modes there is at least one frequency featuring a positive growth rate ($k_n^i(\omega) < 0$). This implies that fluctuations grow continuously.

In the presence of a shear layer, parameters $\omega$, $\mathbf{k}(\omega)$ and corresponding eigenfunctions are deduced with the Cebeci and Keller methodology (1977). The dispersion relation is expressed in terms of a first order system discretized with a finite difference scheme and initial conditions are set to known values of $\mathbf{k}(\omega)$ and $\Psi(\omega)$. The unknown solution is splitted into two parts as follows:

$$u_2(x_2) = p(x_2) + jq(x_2)$$
$$\frac{du_2}{dx_2} = r(x_2) + js(x_2)$$

The Rayleigh equation to be solved is written in terms of $u_2$ :

$$\frac{d\mathbf{X}}{dx_2} = \mathbf{M}(x_2; \omega, k)\mathbf{X}(x_2)$$

$$\mathbf{X}(x_2) = [p(x_2), q(x_2), r(x_2), s(x_2)]^t$$

Matrix $\mathbf{M}$ coefficients depend on mean flow fields and also on $k^r$, $k^i$ and $\omega$. The solution is started by using previously found initial conditions for $k^r$, $k^i$ and $\omega$.

Results corresponding to Michalke incompressible shear layer are presented below for $M_o = U_M/c_o = 0.3$ and $R_u = 1$. The frequency corresponding to maximum growth rate is given by :

$$\omega_o \delta_\theta / U_M = 0.207$$

or equivalently :

$$f_o = 0,132 U_M / \delta_\omega$$

with $\delta_\omega = 4\delta_\theta$. Associated mode shapes are displayed in Fig. 2. They are consistent with those obtained analytically and experimentally by Michalke (1965).

### 1.2. Determination of computational domain inlet conditions

Boundary conditions to be introduced at the upstream boundary are deduced from Euler equations expressed as follows :

$$-i(\omega - U_o k_1)\rho_o \hat{u_1} + \frac{dU_o}{dx_2}\hat{u_2} + \frac{c_o^2}{\gamma} i k_1 \hat{\pi} = 0 \quad (3)$$

$$-i(\omega - U_o k_1)\rho_o \hat{u_2} + \frac{c_o^2}{\gamma}\frac{d\hat{\pi}}{dx_2} = 0 \quad (4)$$

$$-i(\omega - U_o k_1)\hat{\pi} + \gamma i k_1 \hat{u_1} + \gamma \frac{d\hat{u_2}}{dx_2} = 0 \quad (5)$$

Velocity and pressure profiles are displayed in Fig. 3. One uses the solution of the Rayleigh equation to get the perturbation to be introduced as inlet into the computational domain.

### 1.3. Shear layer linear development computation

These profiles obtained above are introduced as inlet conditions in the computational domain and linearized Euler equations exhibit the shear layer unstable mode behaviour. Pressure and velocity fields are plotted in Fig 5 and 6. Numerical results are in good agreement with analytical solutions deduced from the theory of instabilities. As expected the modal exponential growth rate is $-k_i$. (Fig. 4). Pressure fields characterizing instability development are plotted in Fig. 7. The convection velocity is about $1,03U_M$ and equals the theoretical phase velocity in the case of an incompressible shear layer. This shows that computed fluctuations deduced from the linearized Euler equations set exactly coincide with the unstable modes of the Rayleigh equation.

The LEE bear convective vortical modes which develop in the presence of inflexional shear flows. According to instability theory these modes grow exponentially. Unless non linear terms are introduced to ensure the system stability, the linear numerical solution may grow continuously and lead to numerical errors. In presence of such phenomenon it is then necessary to account for non linear terms in the wave operator left hand terms. A semi-linearized operator was built to solve this problem.

## 2. Semi-linearized wave operator building

The objective here is to build a semi-linearized wave operator including non linear terms in order to prevent convective unstable modes from developing exponentially.

Non linear phenomena are governed by unsteady Navier-Stokes equations. In two dimensions the conservative system may be written as follows :

$$\frac{\partial \mathbf{q}}{\partial t} + \frac{\partial \mathbf{E}}{\partial x_1} + \frac{\partial \mathbf{F}}{\partial x_2} = \mathbf{S} \quad (6)$$

where $\mathbf{q} = [\rho, \rho u_1, \rho u_2, e]^t$ designates the vector of conservative variables, $\mathbf{E}$, $\mathbf{F}$ the associated flux and $\mathbf{S}$ the terms associated with viscous stress. For non viscous perfect flow $\mathbf{S}$ falls to zero. After linearization the field $\mathbf{q}$ is split into two parts : the mean flow part

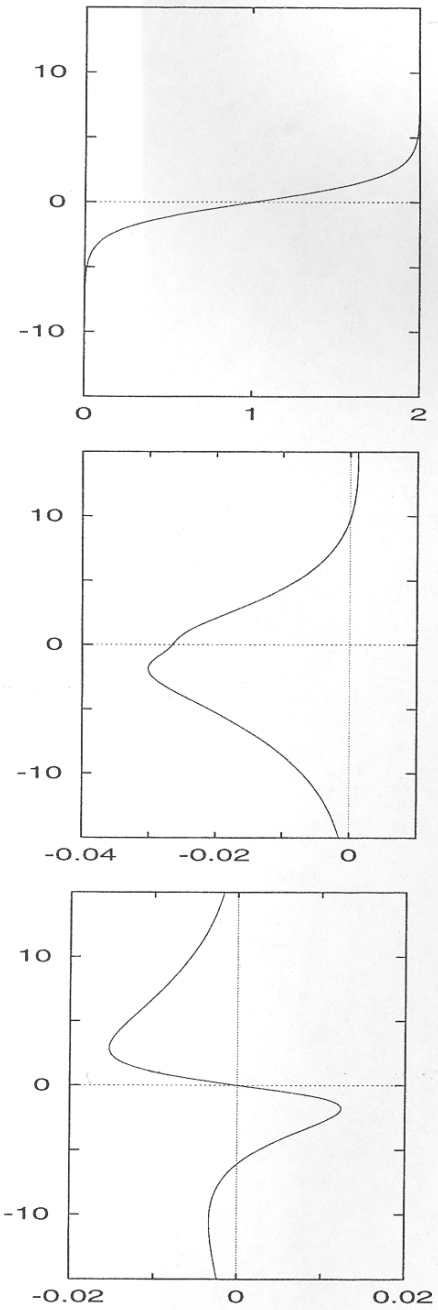


Figure 2: *Top : mean flow velocity profile* $U_o(x_2) = U_M[1 + R_u \tanh(\frac{x_2}{2\delta_\theta})]$. *Middle :* $\Psi$ *real part for the unstable mode. Bottom :* $\Psi$ *imaginary part.*

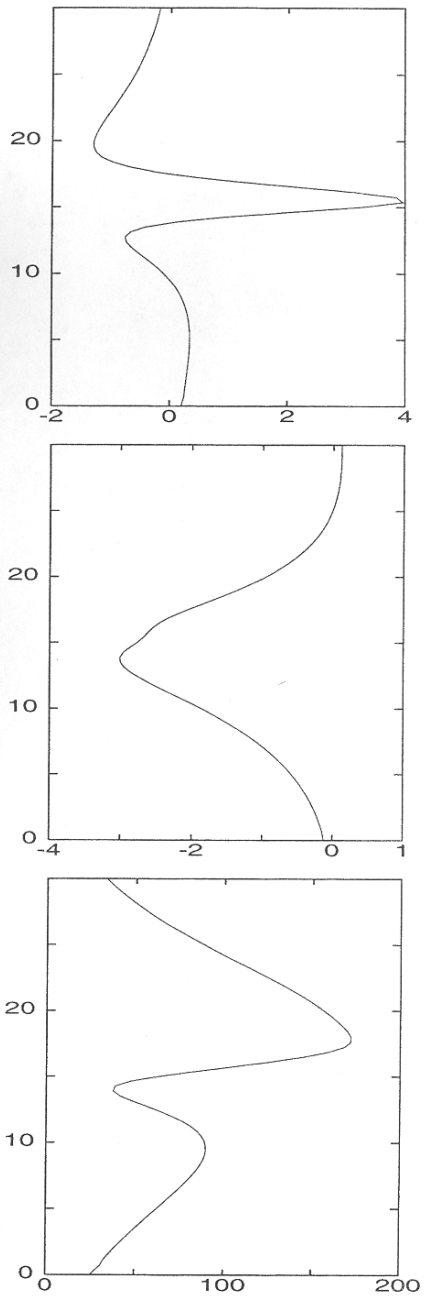


Figure 3: *Top : velocity profile* $u_1' = \frac{\partial \Psi}{\partial x_2}$. *Middle velocity profile* $u_2' = -\frac{\partial \Psi}{\partial x_1}$. *Bottom : pressure profil* $p'$.

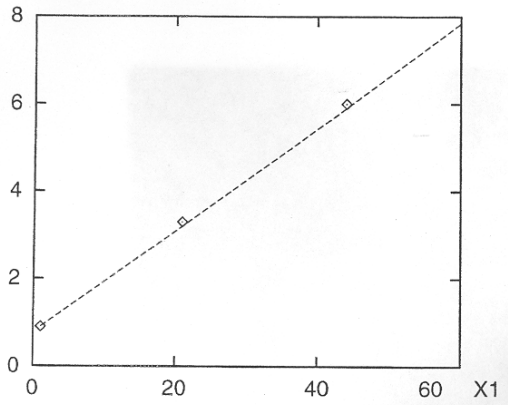


Figure 4: *Maximal values for* $\log(u'_{\max})$ *on axis* $x_2 = 0$. *Numerical values obtained with linearized Euler equations (points). Theoretical exponential growth rate* $-k_i$ *(line).*

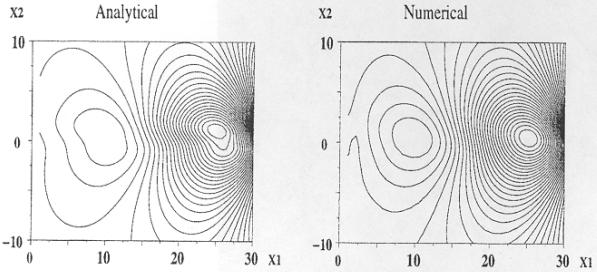


Figure 5: *Linear development of unstable mode. Pressure fields estimated numerically with linearized Euler equations (links) and analytically (rights).*

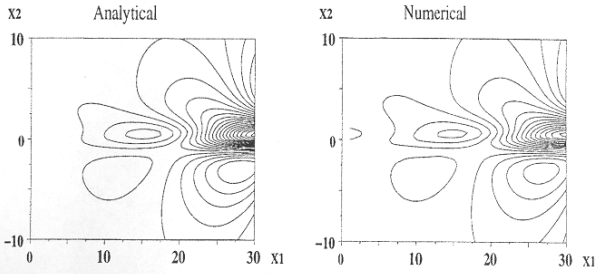


Figure 6: *Linear development of unstable modes. Velocity fields estimated numerically with linearized Euler equations (links) and analytically (rights).*

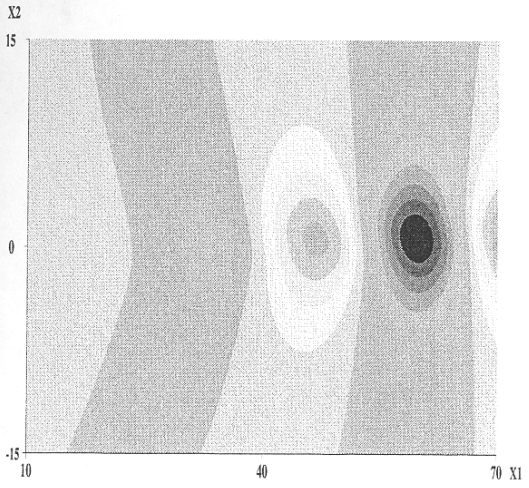


Figure 7: *Linear development of unstable mode. Pressure field estimated numerically.*

$\mathbf{q_o}$ and a perturbation $\mathbf{q}'$ defined by : $\mathbf{q} = \mathbf{q_o} + \mathbf{q}'$. In two dimensions it is possible to express these fields as follows :

$$\mathbf{q_o} = [\rho_o, \rho_o u_{o1}, \rho_o u_{o2}, e_o]^t$$
$$\mathbf{q}' = [\rho', (\rho u_1)', (\rho u_2)', e']^t$$

Instead of neglecting second and third order terms, they are kept in the system to be solved. By convention one denotes :

$$(\rho u_i)' = \rho_o u'_i + \rho' u_{oi} + \rho' u'_i$$

By using equations ( 6), one gets the non linear system to be solved. Conservative equations are given by:

$$\frac{\partial \mathbf{q}'}{\partial t} + \frac{\partial \mathbf{E}'}{\partial x_1} + \frac{\partial \mathbf{F}'}{\partial x_2} + \frac{\partial \mathbf{E}'_\mathbf{n}}{\partial x_1} + \frac{\partial \mathbf{F}'_\mathbf{n}}{\partial x_2} = \mathbf{Q} \quad (7)$$

($\mathbf{E}'$, $\mathbf{F}'$) are associated with linear terms while non linear ones are represented by ($\mathbf{E}'_\mathbf{n}$, $\mathbf{F}'_\mathbf{n}$). Complete expressions are described in the Appendix A. The source term $\mathbf{Q}$ describes convective terms associated with mean fields and also possible viscous terms which are neglected in this case. Here it is set to zero because the problem to be considered involves a steady flow with small perturbations. In presence of an unsteady flow it would be necessary to account for the coupling with aerodynamic mean flow computation. This modelling can easily be extended to three dimensional cases. Numerical methods are developed in Appendix A (Morris 1996).

### 3. Application to shear layer development

In typical shear layers unstable modes grow linearly and after a transient period perturbation amplitudes are of the same order as mean fields which

leads to non linear coupling. In the present section the most unstable mode development is computed by using the afore-mentionned semi-linearized wave operator. Like in the first part we focus our attention on the incompressible shear layer defined in section 2.1. Main results provided by the semi-linearized operator are depicted below. While the linear theory forecasts unstable mode exponential growth, the semi-linearized modelling accounts for non linear coupling leading to a mode saturation (Fig. 8). Pressure and velocity spatial growth estimated linearly and non linearly are represented in Fig. 9. Pressure and vorticity fields are displayed in Fig. 10 and 11 in the plane defined by $(\mathbf{e_1}, \mathbf{e_2})$. The shear layer development is consistent with classical data of Brown and Roshko (1974) and with standard calculations of two dimensional shear layers (Michalke 1984). Non linearities lead to vortex roll up in the shear layer.

In order to explain the mode saturation, one may use a simplified model problem for the temporal evolution of perturbations. In this model the perturbation is represented by :

$$u(\mathbf{x}, t) = f(\mathbf{x})A(t)$$

where the amplitude has the form :

$$A(t) = e^{\omega_i t} e^{-i\omega_r t}$$

$\omega_i$ designates the temporal growing rate. When the Reynolds number $Re$ is smaller than a critical value $Re_c$, $\omega_i > 0$ which ensures the stability of the solution. At higher Reynolds numbers the most unstable mode grows exponentially while other modes decay. According to the linear theory the mode development is desribed by the following relation :

$$\frac{\partial |A|^2}{\partial t} = 2\omega_i |A|^2 \qquad (8)$$

Instabilities may develop when $\omega_i > 0$. A simplified non linear modelling includes a non linear term in relation ( 8). Introduced by Landau (1971) equation ( 8) becomes:

$$\frac{\partial |A|^2}{\partial t} = 2\omega_i |A|^2 - l|A|^4 \qquad (9)$$

with $l$ the Landau constant. According to equation ( 9) mode behaviour depends on the signs of $\omega_i$ and on parameter $l$. By using the variable $|A|^{-2}$, the solution of ( 9) may be obtained in analytical form :

$$|A|^2 = \frac{A_o^2}{\frac{l}{2\omega_i} A_o^2 + \left[1 - \frac{l}{2\omega_i} A_o\right]^2 e^{-2\omega_i t}}$$

If $\omega_i \geq 0$ , with $l > 0$, in the supercritical domain, the perturbation temporal history is deduced from the following relation :

$$\lim_{t \to -\infty} |A| = \lim_{t \to -\infty} |A_o| e^{\omega_i t} = 0 \quad \text{as} \quad A_o = \text{constant}$$

On the other hand one uses the following relation :

$$\lim_{t \to +\infty} |A| = \left[\frac{2\omega_i}{l}\right]^{1/2}$$

Magnitude $|A|$ tends to a finite value independent of $A_o$. Saturation occurs and it is independent of the initial state of the flow.

## Conclusions

Acoustic wave propagation and instability development are both interacting processes. It is now standard to calculate the sound field with the linearized set of Euler equations. Propagation in the mean flow is well described in this way. However there is a hidden difficulty with this approach. The problem arises because the LEE feature unstable modes. This in underlined in this article where it is shown that in the case of a mean shear parallel flow exhibiting an inflexional point an initially small perturbation of the flow obtained as an eigensolution of the Rayleigh equation will grow exponentially in space. As a result the unstable mode amplitude will rapidly exceed the level of the acoustic field and this is of course unacceptable for numerical purposes.

There are at least two ways to deal with this problem : (1) One may suppress the terms responsible for unstable mode development in LEE. In this way one gets "degraded" set of equations and this method is not considered here. (2) One may include non linear terms on the right hand side of LEE in order to limit the unstable mode development. The acoustic field will remain computable. This technique is demonstrated in this artiche and it is shown that it works. Propagation in the mean flow is well described in this way. Aerodynamic unstable mode development can be reduced and numerical problems can be avoided.

## References

[1] Bailly, C., Lafon, P., Candel, S. (1996) Computation of Noise Generation and Propagation for Free and Confined Turbulent Flows. *AIAA-96-1732.*

[2] Bailly, C., Juvé, D. (2000) Noise Computation Using Source Terms in the Linearized Euler Equations. *AIAA-2001-2047.*

[3] Béchara, W., Lafon, P., Candel, S. (1994) Stochastic approach to noise modelling for free turbulent flows. *AIAA J.* **97** (5), 1-14.

[4] Brown, G.L., Roshko, A. (1974) On density effects and large structure in turbulent mixing layers. *J. Fluid Mech.* **64** (4), 775-816.

[5] Cecebi, T.H., Keller, H.B. (1977) Stability calculations for a rotating disk. *AGARD, CP 224* **7**.

[6] Drazin, P.G., Reid, W.H. (1981) Hydrodynamic stability. *Cambridge University Press.*

[7] Huerre, P., Monkewitz, P.A. (1990) Local and global instabilities in spatially developinf flows. *Annu. Rev. Fluid Mech.* **22**, 473-537.

[8] Landau, L., Lifchitz, E. (1971) Physique theorique VI Mecanique des fluides. *Ed. Librairie du Globe*, Ed MIR.

[9] Lighthill, M.J. (1952) On sound generated aerodynamically - I. General theory. *Proceedings of the Royal Society of London*, **A211**, 1107, 564-587.

[10] Lighthill, M.J. (1954) On sound generated aerodynamically - II. Turbulence as a source of sound. *Proceedings of the Royal Society of London*, **A222**, 1148, 1-32.

[11] Lilley, G.M. (1972) The generation and radiation of supersonic jet noise. Vol. IV - Theory of turbulence generated jet noise, noise radiation from upstream sources and combustion noise. Part II: Generation of sound in a mixing region. *Air Force Aero Propulsion Laboratory*, AFAPL-TR-72-53.

[12] Longatte, E. (1998) Modélisation de la génération et de la propagation du bruit au sein des écoulements turbulents confinés. *Ph.D. Dissertation.* Ecole Centrale Paris.

[13] Mani, R. (1976) The influence of jet flow on jet noise. Part I. The noise of unheated jets *J. Fluid Mech.* **73**(4), 753-778.

[14] Michalke, A. (1965) On spatially growing disturbances in an inviscid shear layer. *J. Fluid Mech.* **23**(3), 521-544.

[15] Michalke, A. (1984) Survey on jet instability theory. *Prog. Aerospace Sci.***21**, 159-199.

[16] Morris, P.J., Bangalore, A., Long, L.N. (1996) A parallel three-dimensional computational aeroacoustic method using non linear disturbance equations. *AIAA J.***96**, 1728.

[17] Rayleigh, Lord (1880) On the stability or instability of certain fluid motions. *Proc. London Math. Soc.* **A**(214), 57-70.

[18] Tam, C.K.W., Webb, J.C. (1993) Dispersion -Relation-Preserving Finite Difference Schemes for Computational Acoustics. *Journal of Computational Physics*, **107**, 262-281.

[19] Van Herpe, F., Crighton, D.G., Lafon, P. (1995) Noise generation by turbulent flow in a duct obstructed by a diaphragm. *16 th Aeroacoustics Conference, AIAA Paper*, 95-035, June 12-15, Munich, Germany.

### Appendix A

In two dimensional cases Euler equations may be written in a non conservative form as follows:

$$\frac{\partial \mathbf{U}}{\partial t} + \frac{\partial \mathbf{E_1^L}}{\partial x_1} + \frac{\partial \mathbf{E_2^L}}{\partial x_2} + \frac{\partial \mathbf{E_1^{NL}}}{\partial x_1} + \frac{\partial \mathbf{E_2^{NL}}}{\partial x_2}$$

$$+F_1^L + F_2^L = \mathbf{S} \qquad (10)$$

where $\mathbf{U}$ designates a vector associated with conservative variables:

$$\mathbf{U} = [\rho', \rho_o u_1', \rho_o u_2', p']^t$$

Linear terms are defined by:

$$\mathbf{E_1^L} = \begin{bmatrix} \rho_o u_1' + \rho' u_{o1} \\ \rho_o u_1' u_{o1} + p' \\ \rho_o u_2' u_{o1} \\ u_{o1} p' + \gamma p_o u_1' \end{bmatrix}$$

$$\mathbf{E_2^L} = \begin{bmatrix} \rho_o u_2' + \rho' u_{o2} \\ \rho_o u_1' u_{o2} + p' \\ \rho_o u_2' u_{o2} \\ u_{o2} p' + \gamma p_o u_2' \end{bmatrix}$$

$$\mathbf{F_1^L} = \begin{bmatrix} 0 \\ (\rho_o u_1' + \rho' u_{o1}) \frac{\partial u_{o1}}{\partial x_1} \\ (\rho_o u_1' + \rho' u_{o1}) \frac{\partial u_{o2}}{\partial x_1} \\ (\gamma - 1)(p' \frac{\partial u_{o1}}{\partial x_1} - u_1' \frac{\partial p_o}{\partial x_1} \end{bmatrix}$$

$$\mathbf{F_2^L} = \begin{bmatrix} 0 \\ (\rho_o u_2' + \rho' u_{o2}) \frac{\partial u_{o1}}{\partial x_2} \\ (\rho_o u_2' + \rho' u_{o2}) \frac{\partial u_{o2}}{\partial x_2} \\ (\gamma - 1)(p' \frac{\partial u_{o2}}{\partial x_2} - u_2' \frac{\partial p_o}{\partial x_2} \end{bmatrix}$$

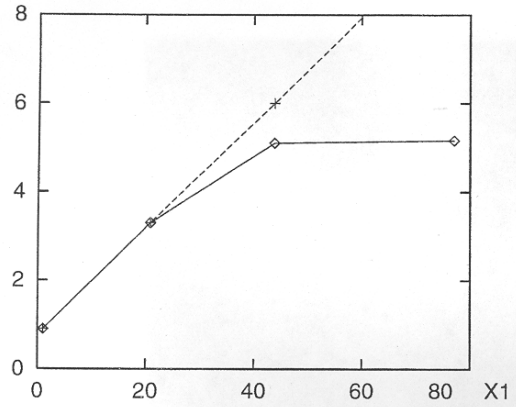


Figure 8: *Velocity maxiam values* $\log(U_{\max})$ *sur l'axe* $x_2 = 0$. *Linear computation (points) and non linear computation (lines).*

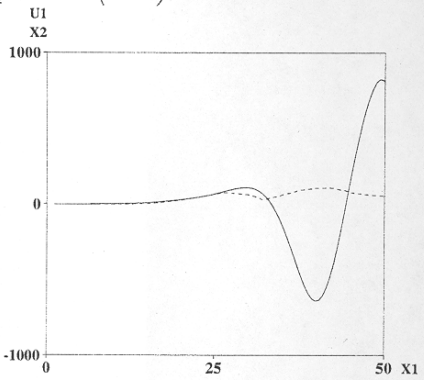


Figure 9: *Spatial development of instabilities on axis* $x_2 = 0$ *computed with LEE (lines) and with SLEE (points). Velocity* $u'_1$.

Non linear terms are given by:

$$\mathbf{E_1^{NL}} = \begin{bmatrix} \rho' u'_1 \\ \rho_o u_1'^2 + 2\rho' u'_1 u_{o1} + \rho' u_1'^2 \\ \rho_o u'_1 u'_2 + \rho' u'_1 u_{o2} + \rho' u'_2 u_{o1} + \rho' u'_1 u'_2 \\ u'_1 p' \end{bmatrix}$$

$$\mathbf{E_2^{NL}} = \begin{bmatrix} \rho' u'_2 \\ \rho_o u'_1 u'_2 + \rho' u'_1 u_{o2} + \rho' u'_2 u_{o1} + \rho' u'_1 u'_2 \\ \rho_o u_2'^2 + 2\rho' u'_2 u_{o2} + \rho' u_2'^2 \\ u'_2 p' \end{bmatrix}$$

A finite difference method due to Tam and Webb (1993) is used with a fourth order Runge Kutta time stepping scheme. Specific techniques relying on characteristic methods are used for the treatment of boundary conditions. These relations can be extended to three dimensional cases.

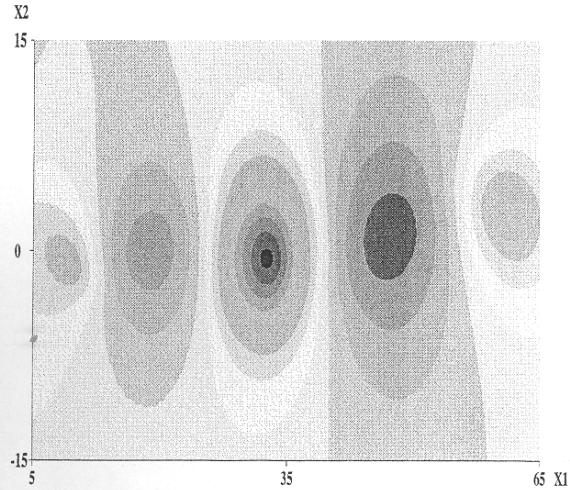


Figure 10: *Shear layer non linear development. Pressure field computed with semi-linearized Euler equations.*

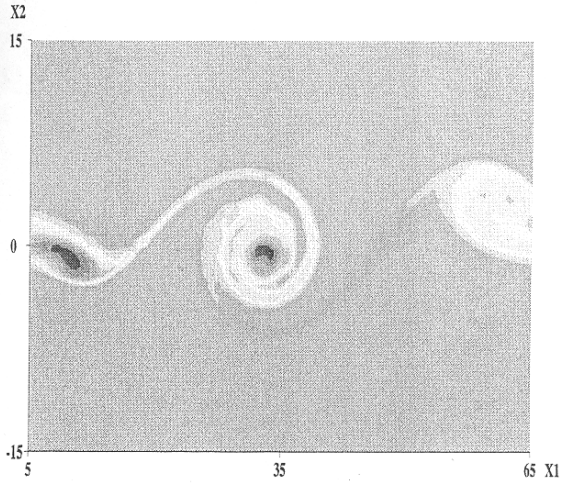


Figure 11: *Shear layer non linear development. Vorticity computed with semi-linearized Euler equations.*

# CHAPITRE II

# -

# CHAINAGE FLUIDE STRUCTURE

# CHAPITRE II - CHAINAGE FLUIDE STRUCTURE

## 1. Chaînage fluide structure

### 1.1. Du découplage au chaînage

Lorsque l'on aborde un problème de couplage fluide structure, il existe deux cas où l'on peut envisager une procédure de chaînage pour la simulation : le cas où la physique est effectivement chaînée, ce qui revient en première approximation à considérer que l'on a découplage fréquentiel entre les physiques fluide et structure, la vitesse réduite du problème couplé étant soit très faible, soit très grande devant l'unité ; le cas où le couplage est faible voire contrôlable et que son effet peut être modélisé à partir de méthodes déterministes (Figure 13).

La simulation chaînée doit donc remplir les deux fonctions suivantes : (1) d'une part **modéliser l'interface chaînée entre les deux sous-systèmes**, c'est-à-dire modéliser l'effet de l'une des deux physiques sur la seconde, (2) d'autre part **être représentative des configurations de couplage faible**, ce qui peut nécessiter des adaptations au niveau des modélisations propres aux sous-systèmes chaînés. Les trois exemples présentés ci-dessous relèvent successivement des domaines des vibrations de structure induites par écoulement (Annexe 4), de l'aéroacoustique (Annexes 5 et 6) et de la dynamique rapide (Annexe 7). Ils illustrent quelques techniques de chaînage possibles et en révèlent les limites lorsque les hypothèses de couplage faible sont mises en défaut.

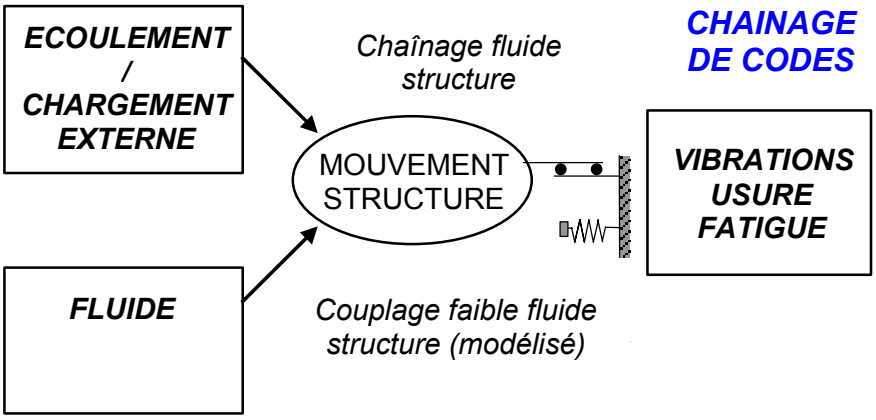


*Figure 13 : Configuration de type chaînage fluide structure simulée par chaînage de codes fluide et structure (les effets de couplage faible induits par la présence du fluide étant modélisés).*

### 1.2. Modélisation tronquée de l'interface

Dans les exemples ci-dessous, les résultats montrent la pertinence d'une approche chaînée lorsque la physique s'y prête, c'est-à-dire en cas de découplage fréquentiel. L'interface entre les sous-systèmes fluide et structure est alors unidirectionnelle, du sous-système impactant vers le sous-système impacté et elle peut être réalisée par différentes approches (chargements, termes sources de seconds membres) dès lors qu'elle assure le transfert d'informations requis entre les deux sous-systèmes, en général un transfert d'énergie.

### 1.3. Modélisations tronquées des physiques chaînées

Néanmoins, dans les trois exemples, on met en évidence l'impact d'une procédure de chaînage sur les choix des modélisations des physiques chaînées, l'hypothèse de couplage faible devant être satisfaite. On fait alors apparaître les limites du chaînage pour des problèmes de couplage fort.

## 2. Exemple des vibrations induites par la turbulence

### 2.1. Chaînage fluide structure

Dans le domaine des interactions fluide structure en faisceaux, on convient d'appeler configuration de « couplage faible » toute configuration dans laquelle les effets de couplages forts fluide-élastiques sont négligeables ; seuls les effets dits de « masse » et d'« amortissement » ajoutés par le fluide sont significatifs et les effets d'« amortissement » et de « raideur » ajoutés par l'écoulement sont négligeables. Dans le cas contraire, on est en présence d'une configuration dite de couplage « fort ». On adopte cette convention, en distinguant couplages « faibles » et « forts ».

Un couplage fort est caractérisé par une dépendance de la fréquence et l'amortissement de la structure vibrante vis-à-vis de la vitesse d'écoulement. En cas d'indépendance, les effets du mouvement de la structure sur l'écoulement sont négligeables. On est alors en présence d'un couplage faible fluide structure avec chaînage écoulement structure en présence d'un écoulement turbulent. Il peut être modélisé par un chaînage fluide structure, sous réserve que les effets de couplage faible induits par le fluide soient introduits sous la forme de données d'entrée du calcul structure. Pour ce faire, on peut utiliser un recalage des caractéristiques de la structure en présence de fluide par rapport à des données expérimentales par exemple.

L'objectif de cette partie est de montrer la faisabilité d'un calcul chaîné fluide structure appliqué à la prévision des vibrations d'une structure filaire sous l'effet d'un écoulement turbulent, dans une configuration semi-industrielle, en l'absence de couplages forts. Un chaînage de codes est mis en œuvre et appliquée à la simulation d'un dispositif expérimental doté de données expérimentales pour la validation des résultats numériques.

### 2.2. Modélisation tronquée de l'interface

Le chaînage consiste à estimer les chargements thermohydrauliques instationnaires pariétaux avec le code fluide à l'aide d'un modèle de turbulence de type L.E.S. 3D sur la structure fixe (Benhamadouche et Laurence 2003, Rollet-Miet 1997). La réponse vibratoire de la structure induite par ces chargements est ensuite estimée avec le code structure. Pour une structure filaire, le calcul mécanique peut reposer sur une approche fréquentielle sur base modale. Les données transférées du code fluide au code structure sont alors les matrices interspectrales des excitations thermohydrauliques estimées le long du tube. Pour recaler les effets de couplages faibles, les coefficients de masse et d'amortissement ajoutés par le fluide sont déduits des données expérimentales et introduits sous forme de données d'entrée du calcul structure. La détermination numérique de ces coefficients de couplage faible nécessite de recourir à la méthodologie de couplage fort qui fait l'objet du chapitre III suivant.

La configuration envisagée est constituée d'un tube flexible soumis à un écoulement turbulent d'incidence axiale dans un environnement peu confiné (Figure 14, Annexe 4). Elle correspond à un dispositif dont l'étude expérimentale a été réalisée par Granger et Perotin (1997).

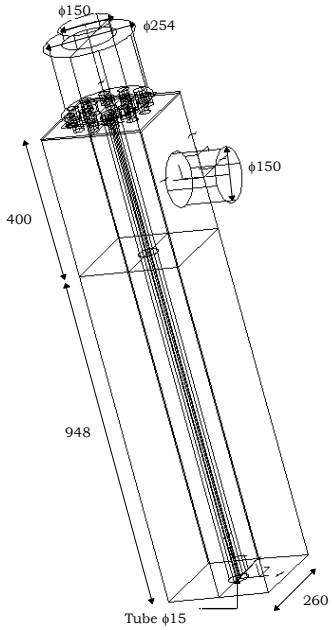


*Figure 14 : Représentation schématique de la configuration comprenant un tube, dans une enceinte non confinée, soumis à un écoulement turbulent d'incidence axiale, issu d'une tuyauterie située en partie haute, traversant une plaque perforée génératrice de turbulence et évacué par une sortie latérale.*

Le maillage utilisé pour le calcul L.E.S. ne présente pas de non conformités (Figure 15). Les champs de vitesse d'écoulements sont comparés aux données expérimentales obtenues par vélocimétrie laser sur maquette (Figure 16). Les spectres d'excitations estimés numériquement sont comparés à ceux identifiés par méthode inverse à partir de mesures vibratoires (Granger et Perotin 1997). Les autospectres des chargements sont reportés sur la Figure 17. Ils sont du même ordre de grandeur en terme de niveaux, de spectres et de distribution spatiale (Longatte et al. 2001).

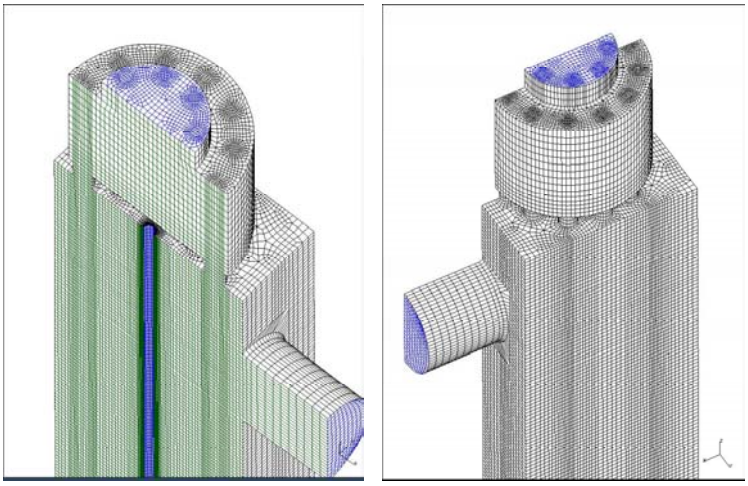

*Figure 15 : Représentation par parties du maillage du domaine fluide de la configuration (maillage conforme comprenant environ 1 million d'éléments).*

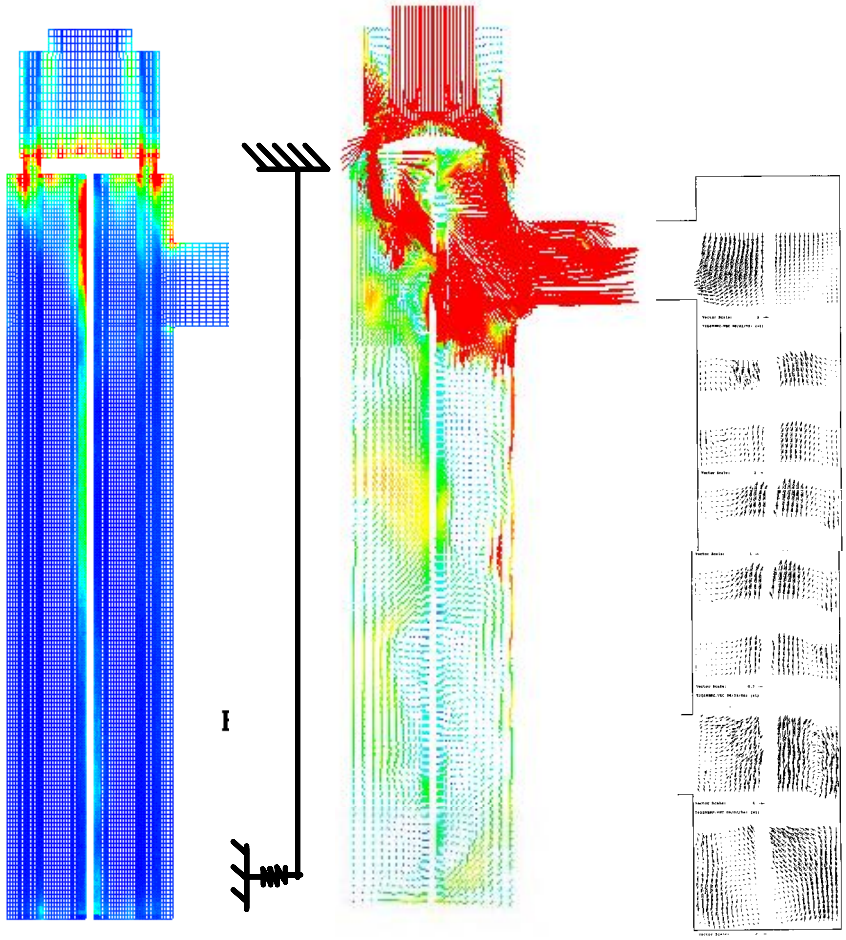

*Figure 16 : Distribution de l'énergie turbulente (à gauche), champs de vitesses autour du tube estimés numériquement par L.E.S (au milieu) et expérimentalement par vélocimétrie laser (à droite).*

### 2.3. Couplage faible fluide structure

Les chargements thermohydrauliques identifiés numériquement par L.E.S. ayant un contenu énergétique correct, les réponses vibratoires du tube calculées avec le code structure sous l'effet de ces chargements sont du bon ordre de grandeur par rapport aux observations expérimentales de Granger et Perotin (1997). Des calculs ont été réalisés aussi bien en régime linéaire qu'en régime non linéaire (Longatte et al. 2001). Le tube est encastré en partie haute.

En linéaire, il est supporté par des ressorts souples en partie basse. La Figure 18 établit une comparaison calculs / mesures des déplacements obtenus. Les résultats sont du même ordre en terme de contraintes et de déplacements généralisés. En non linéaire, le tube est supporté en partie basse par des butées à chocs (Figure 19). Le nombre de chocs par seconde du tube a pu être retrouvé (*72* chocs numériquement et *67* expérimentalement) pour un jeu de butée de $10^{-4}$ *m* (Tableau 2).

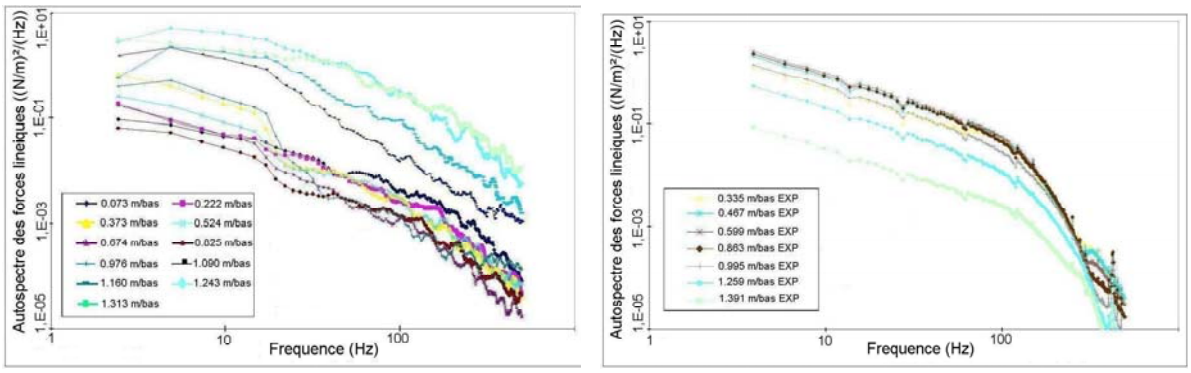


*Figure 17 : Comparaison des autospectres d'excitations exercées sur le tube estimées numériquement par L.E.S. (à gauche) et identifiées expérimentalement sur maquette par méthode inverse (à droite) par Granger et Perotin (1997).*

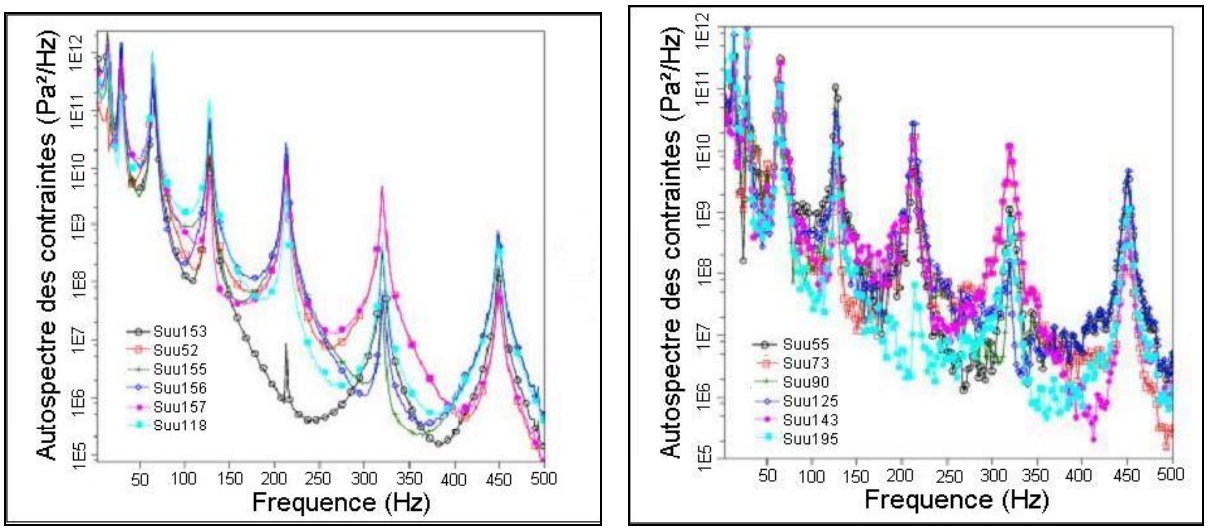


*Figure 18 : Comparaison des réponses généralisées du tube obtenues à partir des chargements estimés numériquement par L.E.S. (à gauche) et expérimentalement sur maquette (à droite).*

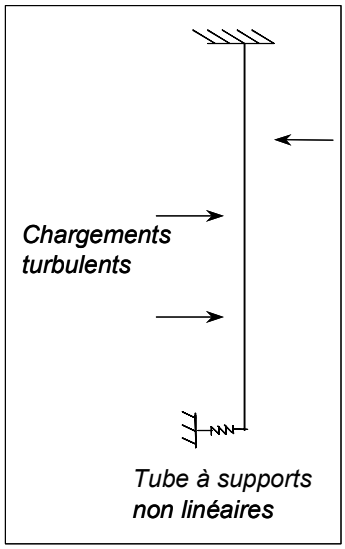


*Figure 19 : Représentation du tube soumis à une excitation turbulente, encastré en haut et supporté non linéairement par une butée à chocs en bas.*

| | Calcul | Expérience |
|---|---|---|
| Nombre de chocs par seconde (-) | 105 | 122 ± 49 |
| Durée moyenne de choc (ms) | 1.09 | 0.97 ± 0.1 |
| RMS de force d'impact (N) | 39.8 | 36.2 ± 0.4 |
| RMS de force de frottement (N) | 14 .1 | 11.3 ± 0.7 |
| RMS de déplacement (mm) | 0.71 | 0.70 ± 0.1 |
| Puissance d'usure (mW) | 207 | 153 ± 91 |

*Tableau 2 : Comparaison calculs mesures du comportement vibratoire du tube supporté non linéairement avec un jeu de butée à chocs de $10^{-4}$m.*

La faisabilité d'un calcul chaîné fluide structure appliqué à la prévision de la réponse vibratoire d'un tube sous écoulement turbulent en l'absence de couplages forts fluide-élastiques a été démontrée. Cette démarche est adaptée à l'étude locale des composants, notamment pour l'identification des spectres d'excitations turbulentes exercées sur les grappes de commande et les crayons combustibles et en partie basse des tubes de générateurs de vapeur en monophasique.

## Annexe 4 : Calcul modal des vibrations induites par la turbulence

Longatte, E., Laurence, D., Barré, F., Ledac, P. (2001). Application of Large Eddy Simulation to a flow-induced vibration problem. *PVP Conference,* Atlanta.

PVP-Vol. 420-2, Flow-Induced Vibration — 2001
Volume 2: Axial Flow, Piping Systems, Other Topics
ASME 2001

# APPLICATION OF LARGE EDDY SIMULATION TO A FLOW INDUCED VIBRATION PROBLEM

**Elisabeth LONGATTE ***
Electricité de France
R&D Division - Fluid Mechanics and Heat Transfer Department
Chatou - France
elisabeth.longatte@edf.fr

**Dominique LAURENCE ***
Electricité de France
R&D Division - Fluid Mechanics and Heat Transfer Department
Chatou - France
dominique.laurence@edf.fr

**François BARRE ***
Commissariat à l'Energie Atomique
Thermohydraulics and Physics Department
Grenoble - France
francois.barre@cea.fr

**Pierre LEDAC ***
Commissariat à l'Energie Atomique
Thermohydraulics and Physics Department
Grenoble - France
triou@alpes.cea.fr

**Adil EL YAMANI ****
Electricité de France
R&D Division - Fluid Mechanics and Heat Transfer Department
Chatou - France

## Abstract

Most classical fluid force identification methods rely on mechanical structure response measurements associated with convenient data processes providing turbulent and fluid-elastic forces responsible for possible vibrations and damage. Owing to recent improvements in Computational Fluid Dynamics, numerical simulations can now be applied to the prediction of flow structure interaction problems in cases of industrial relevance.

The present paper is devoted to the computation of turbulent forces acting on a flexible tube submitted to a complex axial flow by using Large Eddy Simulation. As turbulent forces are independent of structure motion patterns, one may assume that the tube is fixed and the calculation can be performed on a non-moving computational domain. Main numerical results depending on near-wall and small scale turbulence modelling are presented. They are compared to experimental data deduced from measurements carried out on the mock-up that is simulated by the calculation. Numerical estimates are consistent with those obtained experimentally in terms of turbulent excitation amplitudes and spectra. Moreover many physical mechanisms can be explained from the numerical simulation with great accuracy while they are not fully predicted by the experimental method.

It is demonstrated in this article that Large Eddy Simulation is convenient for the treatment of flow structure interaction problems occurring in industrial configurations in the presence of tubes or tube bundles submitted to axial flows. Further developments will be carried out in order to take into account both turbulent and fluid-elastic force effects on flow induced mechanical vibrations.

* Research scientist , ** Research student

## Introduction

In many industrial configurations mechanical structures such as PWR components are submitted to complex flows causing possible vibrations and damage and as far as nuclear security is concerned, it is necessary to prevent wear problems generated by vibratory fatigue. In this context, many experiments are carried out at EDF in order to predict the turbulent forces responsible for possible flow induced vibration problems. These forces can sometimes be directly measured by transducers but with direct approaches it is often difficult to stand between the different physical mechanisms involved when a distributed external loading is considered. On the contrary, indirect experimental prediction methods have shown their ability to provide fluid force estimates. Most of them rely on force density analytical models depending themselves on unknown spectral scaled parameters (Corcos 1963, Blevins 1990, Chen 1987; Lin 1987, Gagnon and Païdoussis 1994, Axisa et al. 1990). They are thus not always reliable, especially in the presence of complex turbulent flows.

That is the reason why a more advanced indirect approach has been developed by EDF since about ten years (Granger and Perotin 1997). It relies on the structure vibratory response measurement and after convenient transfer function calculation and data processing, the method provides an estimate of turbulent excitations acting on dynamic structures. A modal modelling of the mechanical system is used and a spatial orthonormal decomposition of force fields is combined with a regularisation process ensuring the closure system. This approach is efficient and it has been applied to the prediction of turbulent and fluid-elastic forces acting on tubes (Granger and

Perotin 1997) and PWR components like rod cluster control assemblies (Longatte et al. 2000). However this technique often involves high costs because it relies on modelling fitted with experimental data deduced from measurements carried out on specific devices.
In order to reduce these experiments and to be able to study many configurations involving complex flow induced vibration problems, numerical methods are also considered. Owing to recent developments incorporated into Computational Fluid Dynamic (CFD) codes, numerical simulation of flow structure coupling can now be performed for industrial purposes (Moreno et al. 2000). In this article, a Large Eddy Simulation (LES) code is applied to the prediction of turbulent forces acting on a tube submitted to a turbulent axial flow. The full computational method is described in the first section. The second part provides a definition of the test case simulated numerically and in the last section numerical results are discussed and compared to available experimental data. According to the results, Large Eddy Simulation is convenient for the treatment of industrial problems involving flow structure interaction processes.

## 1. Numerical methods

### 1.1 Full computational process

As far as flow induced vibration problems are concerned, available numerical models rely on simplified assumptions making the calculations easier. For example they are often restricted to tubes and shells and it is necessary to use simplified models to describe the real structure geometry which induces a lost of accuracy. Due to CFD code recent improvements it is now possible to simulate numerically part of fluid forces acting on mechanical structures submitted to complex three-dimensional turbulent flows.
Fluid forces acting on mechanical structures can usually be split into two parts :

- structure motion independent forces generated by flow turbulence patterns,
- fluid-elastic forces responsible for possible dynamic instability development and induced by a real coupling between flow and structure motion.

Fluid-elastic effect numerical simulation requires a real coupling between mechanical models and CFD calculations accounting for wall motion effects on flow patterns and conversely. Such a calculation is still impracticable for industrial purposes through lack of sufficient numerical resources. On the contrary turbulent forces generated by near-wall pressure fluctuations can be easier computed numerically because they are not affected by structure pattern and dynamic motion effects. It is possible to assume that tube walls are rigid and turbulent force calculation only requires a near-wall unsteady field computation performed on a fixed non-moving mesh.
In this article we focus our attention on the turbulent forces acting on a rod submitted to a turbulent axial flow. As previously mentioned it is possible to assume that the structure motion does not affect fluid patterns and turbulent forces are deduced from wall pressure fields computed along the rigid tube represented with a non-moving mesh near the wall. The test case corresponds to a configuration previously studied experimentally at EDF by Granger and Perotin (1997). In the present article the purpose is to compare turbulent force numerical estimates to available experimental data expressed in terms of hydrodynamic mean fields, turbulent force magnitudes, root mean square values and spectra.
CFD codes are used to get this information numerically. Force magnitude and spectrum calculation requires near-wall refined turbulence modelling in order to capture unsteady pressure fluctuations responsible for turbulent forces. The most direct numerical approach would consist in using Direct Numerical Simulation (DNS) but in the presence of high Reynolds number problems, the scale rate between the largest and the smallest structure characteristic lengths is increased and a large computational domain size is required to capture significant scale motions. Such a calculation is still impracticable with available computational resources in presence of complex geometry systems.
Reynolds-Averaged Navier-Stokes (RANS) equations are still the most commonly used approach. However Large Eddy Simulations (LES) are becoming more and more important in research industrial applications especially when accurate near-wall unsteady field estimates are required. In the present paper a Large Eddy Simulation is performed in order to compute turbulent force spectra and mean values distributed along the rod. LES results are validated by using comparisons with experimental data and with mean forces deduced from a RANS calculation.

### 1.2 Large Eddy Simulation

Large Eddy Simulation does not feature the DNS previously mentioned disadvantages. It consists in explicitly simulating large-scale turbulent motions by solving three-dimensional time dependent Navier-Stokes equations while modelling the smallest scale motions. The largest structures are generated by mean flow and are inlet condition dependent. On the contrary the smallest scale motions resulting from the Kolmogorov cascade are quite not affected by inlet conditions and their main effect is dissipation; moreover they feature an isotropic behaviour and can be statistically described. According to these properties the principle of LES is to apply a spatial filter to the original Navier-Stokes equations in order to separate large and small scale motions.
The filtering process may be defined as a convolution product as follows :

$$\overline{f}(x) = \int_{\Omega} G_{\overline{\Delta}}(x - x') f(x') dx' \qquad \text{Eq. 1-1}$$

where $\Omega$ designates the computational domain, $G_{\overline{\Delta}}$ the filter function and $\overline{\Delta}$ the filter characteristic length. For a top-hat filter the filtered equations are obtained by averaging over control volumes formed by numerical mesh and a subgrid scale stress $\tau_{SG}$ is produced by this filtering process. This term describes the interaction between resolved large scales and modelled unresolved smaller scales. Assuming the filter length is constant, the filtered equations of motion for an incompressible fluid may be written as follows :

$$\frac{\partial \overline{U_j}}{\partial t}+\frac{\partial \overline{U_i U_j}}{\partial x_j}=-\frac{\partial \overline{p}}{\partial x_i}+\frac{\partial}{\partial x_j}\left[\nu\frac{\partial \overline{U_j}}{\partial x_j}\right]-\frac{\partial \tau_{ij}^{SG}}{\partial x_i} \qquad \text{Eq. 1-2}$$

$$\frac{\partial \overline{U_i}}{\partial x_i}=0$$

with $\tau_{ij}^{SG}=\overline{U_iU_j}-\overline{U_i}\,\overline{U_j}$ the subgrid stress describing the small scale motion effects to be modelled.

Subgrid stress main effects are dissipation. By analogy to molecular diffusion, according to the small scale isotropy pattern, the notion of 'eddy viscosity' $\nu_t$ is currently used to represent energy transfer process. First introduced by Boussinesq to describe small structure dissipation effects, the eddy viscosity was then used by Smagorinsky and Lilly showing that turbulence induces a viscosity increase (Smagorinsky 1963, Lilly 1967). They defined the subgrid stress as follows :

$$\tau_{ij}^{d}=\tau_{ij}^{SG}-\frac{1}{3}\tau_{kk}^{SG}\delta_{ij}=-2\nu_t\overline{S}_{ij}$$

where $\overline{S}_{ij}=\frac{1}{2}\left[\frac{\partial \overline{U_i}}{\partial x_j}+\frac{\partial \overline{U_j}}{\partial x_i}\right]$ designates the deformation rate.

The Smagorinsky modelling relies on the following assumption : $\nu_t=\left(C_s\overline{\Delta}\right)^2\left|\overline{S}\right|$ with $\overline{S}=\sqrt{2\overline{S}_{ij}\overline{S}_{ij}}$ and $C_S$ the Smagorinsky constant. In practice the width $l$ associated with the filter $\overline{\Delta}$ is defined from the grid spacing by : $l=\left|C_s\overline{\Delta}\right|=C_s\left(\Delta x\,\Delta y\,\Delta z\right)^{1/3}$.

If one assumes that the cut-off wave number lies within the Kolmogorov energy cascade, this yields :

$C_s=\frac{1}{\pi}\left(\frac{3}{2}C_k\right)^{-3/4}\approx 0.2$ with $C_k$ the Kolmogorov constant.

Finally the system to be solved is :

$$\frac{\partial \overline{U_j}}{\partial t}+\frac{\partial \overline{U_i}\,\overline{U_j}}{\partial x_j}=-\frac{\partial \overline{p}}{\partial x_i}+\frac{\partial}{\partial x_j}\left[\left(\nu+\nu_t\right)\left[\frac{\partial \overline{U_i}}{\partial x_j}+\frac{\partial \overline{Uj}}{\partial x_i}\right]\right] \qquad \text{Eq. 1-3}$$

$$\frac{\partial \overline{U_i}}{\partial x_i}=0$$

The Smagorinsky model was applied to the simulation of turbulence in plane duct for instance and good results were obtained. However this modelling features disadvantages. For example it does not account for wall effects on the subgrid scale turbulent stresses unless a specific damping function is applied to reduce the Smagorinsky constant near the wall. A suitable Van Driest function was used by Moin (1982) in order to improve the numerical scheme behaviour. Other models tending to be more efficient in the presence of near-wall turbulence were developed (Laurence 1985, Bardina 1989, Germano 1992, Rollet-Miet et al. 1999, Lesieur 1998, Barsamian and Hassan 2000).

In the present article the Smagorinsky modelling is used to predict turbulent forces acting on a rod submitted to an axial flow without damping function near the wall and with $C_s\approx 0.1$. Possible errors induced by the Smagorinsky modelling can be compensated by a sufficient mesh refinement near the wall. Further studies will be carried out in order to compare the results obtained by using other techniques. For example a dynamic modelling will be considered by adjusting the constant of the subgrid scale model as a function of space and time (Lesieur 1998).

### 1.3 Numerical scheme

Large Eddy Simulation requests that the numerical scheme satisfies the following conditions (Bieder et al. 1999) :

- the turbulent kinetic energy is dissipated by the subgrid model only. This requires a neither dispersive nor dissipative convection scheme.
- the smallest transported eddies must be correctly captured by the discretization : the implicit filter defined by the grid spacing is the same for both velocity and pressure field computation. The constraint ratio R is used to define the discretization allowing to capture small eddies. It is defined as the rate between degrees of freedom of pressure and of velocity and must be closed to 1/3 in three-dimensional cases.
- the uniqueness of the solution of the pressure field must be satisfied, i.e. the 'inf-sup' condition must be fulfilled which prevents spurious pressure modes from developing.

Due to the complex geometry of the considered industrial application, a discretisation method on tetrahedral cells is used (Rollet-Miet et al. 1995). A Finite Volume Element technique is applied to locally conserve the mass. For a continuous problem a discrete solution is determined in the finite element's space under consideration of the notation of finite volumes. Conservation equations are used in conservative form.

The element is characterised as P1-non-conforming/P1-iso-P1-bubble. In this discretisation on overlapping co-volumes, the velocity nodes as well as the principal scalar unknowns like temperature are discretised in the centre of faces whereas the pressure unknowns are located on both the centre of gravity and the vertices of a tetrahedral mesh (Figure 1).

The requirement that convection schemes introduce only low numerical diffusion and dispersion is fulfilled only by centred schemes. An alternating procedure is used for the space scheme using a two step Predictor-Corrector time marching scheme (Bieder et al. 1999).

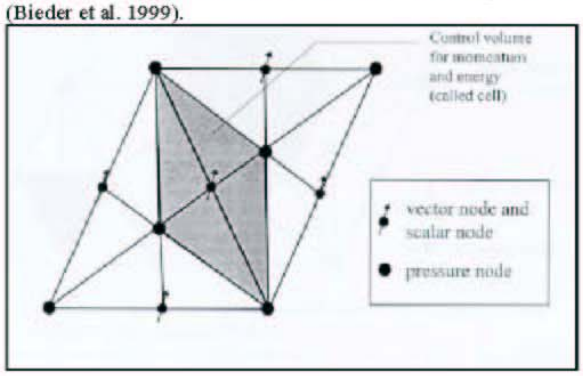


***Figure 1 : P1-non-conforming/P1--iso-P1-bubble element in 2D : pressure nodes in element corners and in the middle of element faces ; velocity nodes in the middle of element faces.***

Concerning wall boundary conditions a standard logarithmic

law is applied.

## 2. Test case presentation

The purpose is to simulate numerically turbulent force magnitudes and spectra along a straight tube submitted to a complex three-dimensional turbulent water flow. The simulated configuration corresponds to a real experimental device previously studied by Granger and Perotin (1997) who used an experimental inverse approach to predict turbulent forces acting on the rod.
After a test case presentation, main results are expressed in terms of hydrodynamic mean fields, turbulent force magnitudes and spectra and compared to available experimental data.

### 2.1 Configuration

The configuration is described in Figure 2. A tube is submitted to a turbulent three-dimensional axial flow crossing a perforated plate located just above the rod and generating high turbulent fluctuations near the tube. Eddies are generated along the rod and finally the fluid is evacuated by a lateral outlet. The square test section size (260 mm) is large in front of the tube diameter (15 mm) and confinement effects may be neglected. Moreover the flow is mostly axial along the tube and transverse flows are not significant. Hence fluidelastic effects are restricted to added mass effects due to the fluid and coupling effects may be neglected. The structure motion does not affect turbulent fluid forces. That is the reason why in the computation the tube is assumed to be a rigid solid non-moving tube and the Large Eddy Simulation is performed by using a full fixed non-moving mesh.

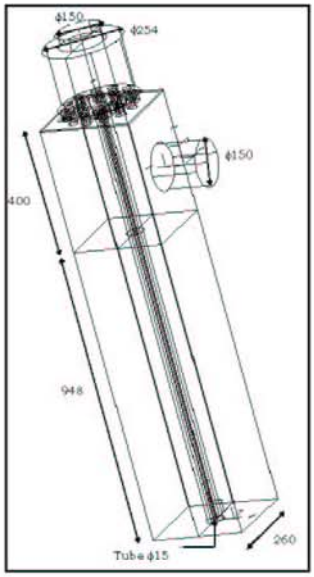


***Figure 2 : Test case geometry : a flexible tube (ϕ 15 mm) submitted to a complex three-dimensional turbulent axial flow. The test section (260 mm × 260 mm) is fitted with water inlet at the top(ϕ 150 mm), the flow is crossing through a perforated plate and evacuated by a lateral outlet (ϕ 150 mm).***

### 2.2 Inlet and outlet conditions

The flow introduced at the top inlet is laminar and a parabolic velocity profile is introduced as follows :

$U_{inlet}(r,\theta,\varphi) = [U_z(r),0,0]$

if the z axis denotes the tube axis oriented downwards. The z axis inlet velocity component is written :

$U_z(r) = 2U_0\left[1-\frac{r^2}{r_0^2}\right]$ with $2r_0$ the tube diameter and $U_0$ chosen to set the total inlet flow rate to 400 m$^3$/h. Turbulent kinetic energy and dissipation are introduced as constants. $K_{inlet}$ is defined by : $K_{inlet} = \frac{3}{2}\left(0{,}02V_{ref}\right)^2$ with $V_{ref}$ the inlet flow velocity and dissipation is deduced from turbulent energy by: $\varepsilon_{inlet} = c_\mu^{3/4}\frac{K_{inlet}^{3/2}}{L}$ with $C_\mu = 0.09$ and L the largest scale motion characteristic length. According to the test section geometry the scale length in this area can be estimated to about 200 mm. In practice the inlet conditions are the following :

$V_{ref}$ $= -6.29\ m.s^{-1}$

$K_{inlet}$ $= 2.37\ 10^{-2}\ kg.m^2.s^{-2}$

$\varepsilon_{inlet}$ $= 2.9\ 10^{-3}\ kg^{3/2}.m^2.s^{-3}$

Free outlet conditions are introduced at the exit and wall conditions on rigid tube and on test section walls.

### 2.3 Computational performances

Large Eddy Simulation is performed with the thermo-hydraulic code PRICELES resulting from a co-operation of the 'Commissariat à l'Energie Atomique' and 'Electricité de France'. The code in C++ is based on an object oriented intrinsically parallel approach and it is especially designated for industrial simulations on non-structured meshes (Bieder et al. 2000). The calculations are performed on a COMPACQ SC232 calculator. As an example with 10 million degrees of freedom and 10 processors the CPU per time step is about 2.8s.
In the considered case the mesh used for the calculation is represented in Figure 3. The full mesh includes about 45000 P1 nodes and 200000 elements. The mesh is refined near the tube rigid wall and the number of elements attached to the rod equals 40. The rate between the smallest and the largest element is about 15. According to the configuration geometry and to hydraulics parameters, the flow is expected to have reached a mean state or quasi-mean state after about 15 s. Hence near-wall force spectra must be computed over a period of about 15s.
The time step changes automatically during the calculation and it is of about $10^{-5}$s. The CFL condition is fulfilled as follows : $\frac{U_{max}\Delta t}{\Delta x_{min}} \approx 1$ where $\Delta x_{min}$ designated the smallest element size ($\Delta x_{min} \sim 3mm$) and $U_{max}$ is the maximal velocity value in the perforated plate ($U_{max} \sim 7.86\ m.s^{-1}$).

*Figure 3 : Wall mesh extracted from the full mesh used for LES: ~45000 P1 nodes, ~200000 elements, near-wall refinement near the tube with 40 wall elements per tube section.*

## 3. Numerical results

Main numerical results deduced from Large Eddy Simulation are presented below. Turbulent forces are expressed in terms of magnitudes, root mean square values and spectra and numerical solutions are validated by using comparisons with available experimental data.

### 3.1 Hydrodynamic mean fields

Hydrodynamic velocity mean fields deduced from a time-averaged Large Eddy Simulation are plotted in Figure 4 in the vertical lateral outlet symmetry plane (plane equation : x=0) and in the orthogonal plane (plane equation : y=0). Just below the perforated plate the fluid is evacuated as an organised jet and three main eddies are generated along the tube : two in the middle of the tube and a small one near the test section bottom. These numerical results are consistent with those obtained experimentally. Velocity fields measured on the EDF experimental set-up are plotted in planes x=0 and y=0 in Figure 5. For lack of visibility trough the mock-up lateral faces, velocity fields deduced from experiments involving laser techniques are partially represented. Main flow patterns obtained experimentally are predicted numerically, especially the jet located near the transverse outlet and the eddy development near the test section bottom. Moreover in this area the flow features the expected patterns in terms of eddy characteristic length and rotation direction.
According to this comparison, Large Eddy Simulation provides a suitable representation of main mean flow patterns around the tube.

### 3.2 Turbulent force magnitudes

Turbulent forces acting on the tube are then deduced from unsteady near-wall pressure fluctuations. They can be expressed in terms of mean force magnitudes and root mean square values. RMS computed numerically along the rod in both planes x=0 and y=0 are plotted in Figure 6. They can be compared to experimental data plotted on the same figure in two planes called x1=0 and y1=0. These planes are not necessarily the same as planes x=0 and y=0 because strain gauges are located in the tube and experimentally it is not possible to chose the vibration measurement location. That is the reason why numerical and experimental results are not exactly similar in terms of magnitude but they are of the same order. Moreover they are in good agreement in terms of force distribution along the tube. As expected, magnitude maximal values are located just below the perforated plate near the transverse outlet. In the middle of the test section the tube is quite not affected by turbulence. At the bottom, the eddy development previously identified numerically and experimentally induces significant pressure fluctuations near the tube and this is the reason why turbulent force RMS values increase at a distance of about 1.3m from the top plate.

However significant discrepancies between numerical and experimental solutions appear in the vicinity of the transverse outlet. The solution computed numerically features three maximal values located just below the perforated plate, at a distance of about 0.2 m and 0.4 m from the plate while the experimental solution features only one maximal value at about 0 .4 m from the top plate. In order to interpret these results, it is interesting to link force maximum locations to turbulent kinetic energy peaks. Mean

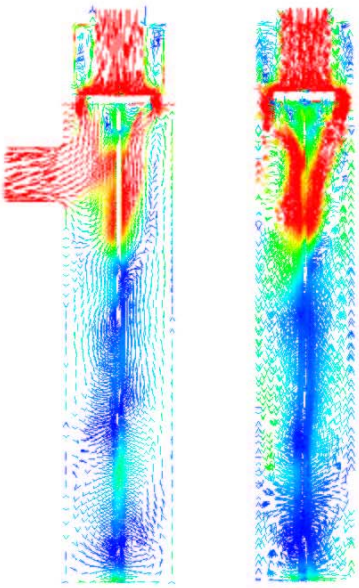

*Figure 4 : Velocity mean fields deduced from a time-averaged LES for t = 15 s in the outlet symmetry plane x=0 (left) and in the orthogonal plane y=0 (right). Minimal value : 0 m/s (blue colour), artificial maximal value represented on the graphic: 3,3 m/s (red colour).*

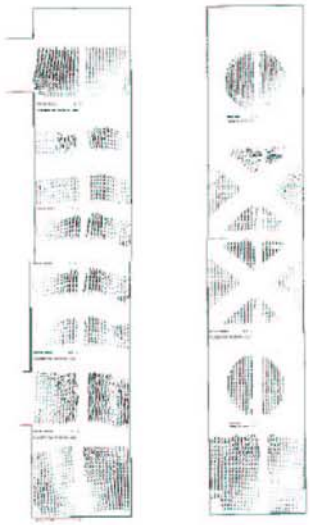

*Figure 5 : Velocity man fields deduced from experiments involving laser techniques and carried out on EDF mock-up in the outlet symmetry plane x=0 (left) and in the orthogonal plane y=0 (right).*

kinetic turbulent energy computed numerically is presented in Figure 7 in both planes x=0 and y=0. Turbulent energy responsible for fluid forces acting on the rod features three peaks located just below the perforated plate in the vicinity of the lateral outlet. As the turbulent energy is directly responsible for the turbulent forces acting along the tube its behaviour explains the RMS distribution obtained numerically in Figure 6.

Numerical simulation provides thus more accurate force RMS and magnitude estimates than the experimental inverse approach. The experimental approach relies on specific assumptions and can not totally predict the real force distribution. It relies on rod vibratory response measurements, a modal analysis of the structure in flow is performed and the system is described by convenient transfer functions. Finally fluid forces responsible for tube motion are deduced from response measurements associated with convenient data processing. As the tube is fixed in the perforated plate, the dynamic motion of the tube necessarily falls to zero near the top plate. Hence turbulent forces acting just below the plate can not be identified by the experimental approach. Moreover experimentally the turbulent energy distribution is coarsely interpolated between the measurement locations and it can not be captured with accuracy.

Large Eddy Simulation does not feature these disadvantages and provides detailed numerical estimates of turbulent forces.

### 3.3 Turbulent force spectra

Finally unsteady pressure fields computed numerically along the tube are used to estimate turbulent force spectra. Associated spectral density functions are plotted in Figure 8 at different locations from the perforated plate. A periodogram including about 10 domains is applied for the spectrum computation and results can be compared to experimental data plotted on the same figure. Numerical spectra are consistent with those obtained experimentally in terms of density magnitude, turbulent energy distribution and spectral content. According to the results, the most significant excitations are located in the vicinity of the transverse outlet. Force spectra feature a realistic behaviour as they are broad-band and slowly decreasing with a factor 100 over the band [0-100 Hz]. Further calculations will be performed in order to improve the accuracy and the spectral resolution of the numerical solution by increasing the physical duration computed numerically.

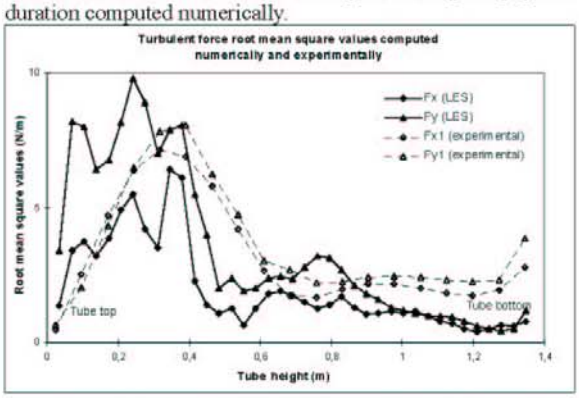


*Figure 6 : Turbulent force root mean square values along the tube (N/m) : Fx and Fy components computed numerically (lines) and experimentally by Granger and Perotin (points).*

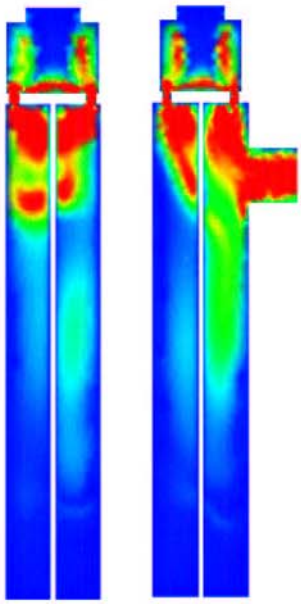

*Figure 7 : Mean kinetic turbulent energy deduced from a time-averaged LES for t=15s in the outlet symmetry plane (right) and in the orthogonal plane (left). Turbulent energy maximal values located near the transverse outlet. Minimal value : 0 kgm²/s² (blue colour), artificial maximal value represented on the graphic: 2,1 kgm²/s² (red colour).*

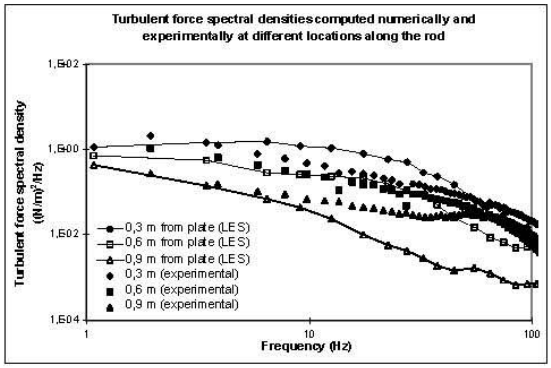


***Figure 8 : Turbulent force spectra ((N/m)²/Hz) computed numerically (lines) and experimentally (points) at three different locations along the tube at 0.3m, 0.6m and 0.9m from the plate.***

Finally Large Eddy Simulation is convenient for the prediction of near-wall turbulent force magnitudes and spectra in presence of complex configurations involving real three-dimensional turbulent flows.

## Conclusions

A flow induced vibration prediction numerical method is presented in this paper. Large Eddy Simulation is applied to the computation of turbulent forces acting on a tube submitted to a complex three-dimensional turbulent axial flow.

According to the results, Large Eddy Simulation is convenient for the treatment of complex problems involving flow induced vibrations in industrial configurations. Numerical results are consistent with experimental predictions in terms of turbulent force magnitude, distribution and spectra. Moreover numerical simulation provides more detailed estimates than classical experimental approaches relying on local dynamic response measurements. Turbulent energy distribution effects are described with accuracy and new phenomena can be identified and interpreted while they could not be observed experimentally because classical experimental identification methods may rely on coarse interpolation processes between measurement locations and may generate a lost of information.

In terms of efficiency the numerical simulation features another advantage. Classical methods rely on convenient models fitted with experimental data and for each component to be studied, it is necessary to build a specific set-up providing a realistic representation of the flow structure coupling system which often generates high costs and long delays of treatments. On the contrary Large Eddy Simulation codes are efficient providing quickly more detailed information than classical CFD codes. Their applications go far beyond the fluid dynamics field. Concerning flow induced vibration problems new developments will be carried out in order to provide a full predictive numerical tool allowing the prediction of both turbulent and fluid-elastic forces in presence of tubes and tube bundles submitted to turbulent complex axial or transverse flows.

## Acknowledgements

Authors would like to express their sincere thanks to their co-workers Mr Ulrich BIEDER and Mr Tobias BUCHAL for their significant contribution in the present study.

## References

AXISA F., ANTUNES J., VILLARD B., 1990, 'Random excitation of heat exchanger tubes by cross-flow', *J. Fluid . Struct.*, Vol. 4, 321-342.

BARDINA J., FERZIGER J.H., REYNOLDS W.C., 1989, 'Improved subgrid-scale models for Large Eddy Simulation', Rept TF-19Dept Mech. Eng. Stanford CA.

BARSAMIAN H.R., HASSAN Y.A., 2000,'New approaches of wall models for large eddy simulation in complex geometries', *7th conference on flow-induced vibrations,* Lucerne, June 19-22.

BIEDER U., EMONOT P., LAURENCE D., 1999, 'PRICELES : summary of the numerical scheme', *CEA, SMTH/LATA/98/50.*

BIEDER U., CALVIN C., EMONOT P., 2000, 'PRICELES : an object oriented code for industrial LES', *8th Annual Conférence of the CFD Society of Canada,* Montréal, June 11-13.

BLEVINS R.D., 1990, 'Flow induced vibration', *2eme ed. Van Nostrand Reinhold.*

CHEN S.S., 1987, 'Flow induced vibration of circular cylindrical structures', *Hemisphere Publiching Corporation.*

CORCOS G.M., 1963, 'Resolution of pressure in turbulence', *J. Acoust. Soc. Am.,* Vol. 35, 192-199.

GAGNON J.O., PAÏDOUSSIS M.P., 1990, 'Fluid coupling characteristic and vibration of cylinder clusters in axial flow. Part 1: Theory', *J. Fluid Struct..,* Vol. 8, 257-291.

GERMANO M., 1992, 'Turbulence ; the filtering approach', *J. Fluid Mech., Vol. 238, 325-336.*

GRANGER S., PEROTIN L., 1997, 'An inverse method for the identification of a distributed random excitation acting on a vibrating structure: Part 1: Theory', *ASME Fluid-Structure Interactions.*

GRANGER S., PEROTIN L. 1997, 'An inverse method for the identification of a distributed random excitation acting on a vibrating structure: Part 2: Flow-induced vibration application', *ASME Fluid-Structure Interactions.*

LAURENCE D., 1985, 'Direct and Large Eddy Simulation of turbulence', *Euromech Colloquium*, Vol. 199, 147-160.

LESIEUR M., 1998, 'Turbulence in fluids', *Kluwers, Third Edition.*

LILLY D.K., 1967, 'The representation of small scale turbulence in numerical simulation experiments', *Ed. H.H. Goldstin, editor,* Vol. 320-1951, 195-210.

LIN W.H., 1987, 'Response of a circular rod to an axial turbulent flow', *ASME, Flow-induced Vibration PVP,* Vol. 122.

LONGATTE E., NHILI R., WEISS T., 2000, 'Prediction of flow induced vibrations of drive line assembly', *ASME PVP 2000,* Seattle, July 23-27.

MOIN P., KIM J., 1982, 'Numerical investigation of

turbulent channel flow', *J. Fluid Mech.*, Vol. 118, 341-377.

MORENO M.M., DE LANGRE E., LE QUERE P., 2000, 'A large eddy simulation of the turbulent forcing spectrum induced by axial flow on a rod', *7th conference on flow-induced vibrations,* Lucerne, June 19-22.

ROLLET-MIET P., LAURENCE D., NITROSSO B., 1995, 'Large Eddy Simulation with unstructured grids and finite elements', *10th Symposium on Turbulent Shear Flows.*

ROLLET-MIET P., LAURENCE D., FERZIGER J., 1999, 'LES and RANS of turbulent flow in tube bundles', *Int. J. Heat & Fluid Flow*, Vol. 20 (3), 241-254.

SMAGORINSKY A., 1963, 'General circulation experiment with the primitive equation : the basic experiment', *Monthly Wheather Review 91*, Vol. 99 (3), 99-164.

8

# 3. Exemple de chaînage en aéroacoustique

## 3.1. Chaînage fluide fluide

L'étude présentée a pour objet le calcul du bruit rayonné par la turbulence en aval d'un obstacle dans un conduit (Annexes 5 et 6). Basée sur le principe selon lequel les deux physiques mises en jeu, la génération de bruit par la turbulence et la propagation acoustique dans le conduit, sont découplées, la méthodologie utilisée consiste à chaîner le calcul de turbulence et le calcul de propagation, le transfert d'informations entre les deux étapes étant assuré par le biais de termes sources bien choisis. Pour la phase de propagation acoustique, il apparaît pertinent d'adopter un opérateur d'Euler Semi-Linéarisé (E.E.S.L.) avec des termes de viscosité supplémentaires, ou à défaut, un opérateur d'Euler Linéarisé Tronqué (E.E.L.T.) sans terme de convection, de façon à éviter la convection des instabilités susceptibles de se développer en présence d'un écoulement turbulent conformément aux conclusions de l'étude réalisée avec une formulation découplée. La procédure de chaînage est décrite ci-dessous (Figure 20).

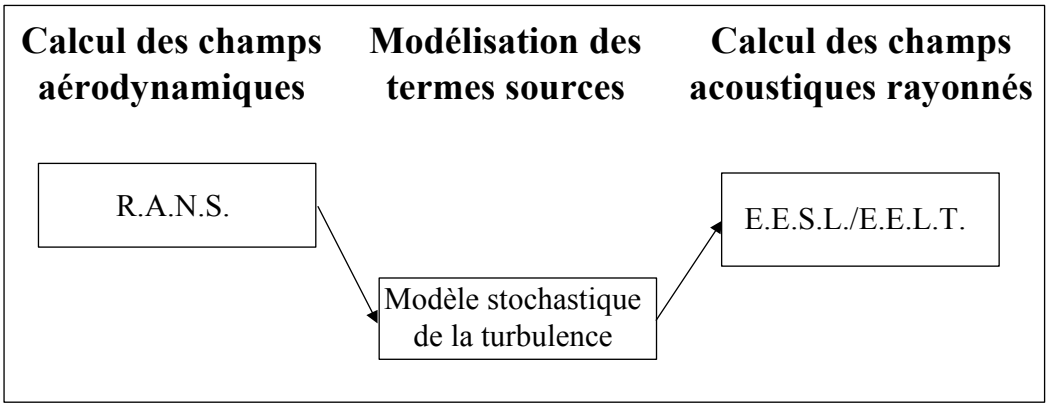


*Figure 20 : Procédure de chaînage possible pour l'aéroacoustique : modélisation de la turbulence, des sources acoustiques induites puis du bruit rayonné.*

## 3.2. Interface de chaînage

Les termes sources sont conçus pour jouer le rôle d'interface entre le calcul de turbulence et le calcul de propagation acoustique. Ils doivent traduire les effets de la turbulence sur la génération de bruit, en particulier les instationnarités de la turbulence, et donc le spectre d'énergie turbulente potentiellement source de bruit. Plusieurs techniques sont possibles pour leur construction. Un calcul L.E.S. est envisageable pour déduire l'expression des sources acoustiques du calcul de turbulence (Crouzet et al. 2002). On propose ici une méthode alternative qui consiste à réaliser un calcul fluide stationnaire, à générer des sources acoustiques synthétiques instationnaires (Annexe 5) et à les introduire au second membre de l'équation de propagation pour le calcul du bruit rayonné (Annexe 6). Il s'agit du modèle dit S.N.G.R.[17]. Il est basé sur une phase d'identification préalable de la localisation des sources à partir de l'analyse des champs moyens qui fournissent la localisation des maxima d'énergie turbulente assimilés aux maxima des sources acoustiques (Figure 21). Les sources sont alors obtenues à partir de champs de turbulence « synthétique » générés à partir du champ moyen calculé et des caractéristiques escomptées de la turbulence dans la zone des sources (Figure 22).

[17] S.N.G.R. Stochastic Noise Generation and Radiation

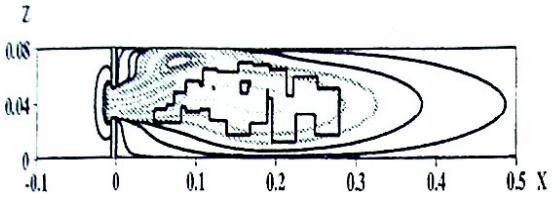


*Figure 21 : Localisation de l'interface de chaînage : identification de la localisation des sources acoustiques induites par la turbulence.*

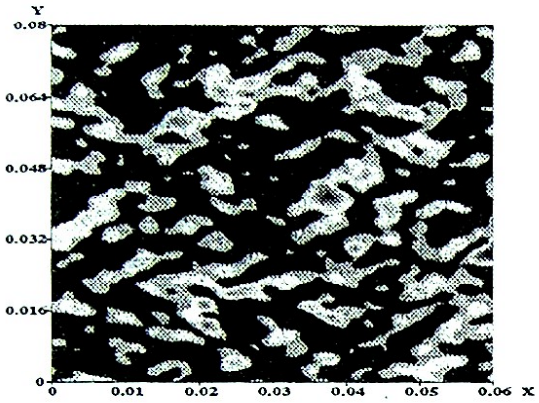


*Figure 22 : Génération de termes sources acoustiques "synthétiques" représentatifs des effets de la turbulence.*

### 3.3. Sources de couplages

Cette méthodologie permet de prédire le bruit rayonné par la turbulence générée dans un environnement confiné encombré (Figure 23). Néanmoins, le choix de l'opérateur de propagation (E.E.L.T.) repose sur l'hypothèse forte selon laquelle la convection peut être négligée dans la propagation, ce qui revient à négliger une partie des phénomènes convectifs. Seul un calcul couplé permettrait d'éviter de telles approximations qui peuvent être peu légitimes dans certaines configurations confinées avec retour des ondes acoustiques et impact sur les sources elles-mêmes (cas d'une cavité, Gloerfelt et al. 2006). Une méthodologie basée sur la L.E.S. compressible est alors recommandée (Bogey et al. 2003).

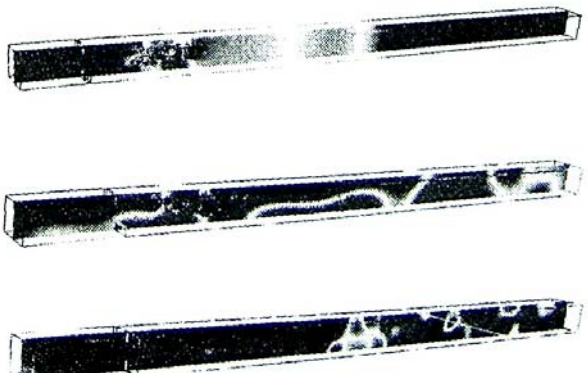

*Figure 23 : Propagation des ondes acoustiques dans un conduit en aval d'un obstacle pour 3 vitesses de l'écoulement amont.*

## Annexe 5 : Génération de bruit par la turbulence

**Longatte, E**., Lafon, P. and Candel, S. (1998). Computation of noise generation by turbulence in internal flows. *4th AIAA/CEAS Aeroacoustics Conference*, Toulouse.

## Annexe 6 : Propagation du bruit généré par la turbulence

**Longatte, E.**, Lafon, P. and Candel, S. (1997). Acoustic wave propagation in two dimensional sheared ducted flows. *18th AIAA Aeroacoustics Conference*, Atlanta.

# COMPUTATION OF NOISE GENERATION BY TURBULENCE IN INTERNAL FLOWS*

E. Longatte† P. Lafon‡
Département Acoustique et Mécanique Vibratoire,
Electricité de France,
1, Avenue du Général de Gaulle, 92141 Clamart Cedex, France,

S. Candel§
Laboratoire EM2C, CNRS, Ecole Centrale Paris
92295 Châtenay-Malabry Cedex, France

## Abstract

Stochastic modelling techniques are currently used to deal with various problems in turbulence. These methods are explored in this article with as objective the computation of the solution of aeroacoustic noise problems.

The principle may be described as follows. The mean flow field is first deduced from a RANS calculation associated with a turbulence closure scheme like the $k-\epsilon$ model. Next, a space-time turbulent field is synthetized stochastically, providing the local turbulent fluctuations and the associated noise sources. The radiated sound field is then calculated numerically.

The present article is structured around the three following points. The aeroacoustic calculation is presented in the first part. The stochastic model of turbulence is described in the second part. The last section is devoted to computational methods and to numerical results related to noise generation by diaphragms placed in ducted flows. Three-dimensional numerical results are compared with experimental data in terms of acoustic levels. Results of calculations are in good agreement with predictions.

## Introduction

In the framework of Lighthill's theory, standard aeroacoustic noise prediction methods rely on an analogy featuring a propagation equation associated with source terms. These formulations require time average or unsteady aerodynamic computation ($k-\epsilon$, LES or DNS) and provide acoustic far-fields. They do not account for all acoustic/mean flow interactions. More complex wave operators were derived to describe these interactions allowing extensions to prediction of noise generated by complex free flows. However, application to confined configurations is not straightforward because it requires the determination of adapted Green's functions. Also, most of these methods rely on third order equations, which is not convenient for numerical purposes. Furthermore, propagation equations bear acoustic disturbances and also convective modes, vorticity and entropy waves.

The stochastic approach used in this article does not feature some weaknesses of the afore-mentioned modellings. It is based on the computation of Euler equations describing the propagation and including acoustic source terms associated with turbulence. Propagation equations are linearized (or semi-linearized) around a mean field deduced from a time average aerodynamic calculation. Noise sources are expressed in terms of a turbulent velocity field provided by a Stochastic Noise Generation and Radiation (SNGR) model. Finally, acoustic fields are deduced from Euler equations associated with the previously computed mean and turbulent fields.

In this article, we describe this method and its applications to three-dimensional confined configurations. The first section is devoted to preliminary aerodynamic computations. In the second part, the stochastic model of turbulence and the synthesis of acoustic source terms are presented. Finally, numerical methods are described and some results related to noise generation by a diaphragm placed in ducted flows are discussed.


†Research Student
‡Research Scientist, Member AIAA
§Professor, Member AIAA

## I. Formulation of the method

Recent progress in numerical methods has allowed a transition from standard noise prediction methods relying on the Lighthill analogy[6] to more direct approaches involving simultaneous computations of aerodynamic and acoustic fields by using turbulence models ($k-\epsilon$) or simulation methods (LES, DNS). However, in presence of complex configurations, the last methods imply high computational costs with regard to the available numerical resources. According to the non dispersive and non dissipative patterns of acoustic disturbances and also to the different size orders of aerodynamic and acoustic fields, it is still useful to separate acoustic source region where turbulent disturbances develop, from the wave propagation domain where acoustic fluctuations take place. As standard integral formulations requires the calculation of Green's functions depending on the geometry, they are not easy to handle from a numerical point of view in the presence of duct walls and obstacles.

It is then more suitable to consider that the flow field is a superposition of three contributions (mean, turbulent and acoustic components) and write:

$$p = p_o + p_t + p_a$$

$$\mathbf{u} = \mathbf{u_o} + \mathbf{u_a} + \mathbf{u_t}$$

Acoustic fluctuations $p_a$, $\mathbf{u_a}$ may be neglected in the source domain whereas turbulent disturbances $p_t$, $\mathbf{u_t}$ vanish in the far field. Noise generated by turbulence is then computed in three steps:

- The first step corresponds to the preliminary time average Navier-Stokes computation associated with a $k-\epsilon$ turbulence model providing mean flow field characteristics. As we are interested in noise generated by subsonic flows with high Reynolds numbers, equations of motion are written as follows:

$$\nabla.\mathbf{u_o} = 0 \qquad (1)$$

$$\rho_o(\mathbf{u_o}.\nabla)\mathbf{u_o} = -\nabla p + \mu\nabla^2\mathbf{u_o} + \nabla.\mathbf{R} \qquad (2)$$

  where $\mathbf{R}$ designates the Reynolds stresses defined as the second-order velocity correlations by $R_{ij} = -\rho_o\overline{u_{ti}u_{tj}}$. Equation (2) is solved provided that the Reynolds tensor can be expressed in terms of mean flow values. This closure problem is solved by introducing a turbulence model. The $k-\epsilon$ model expresses $R_{ij}$ in terms of mean gradients and turbulent viscosity whose computation depends on the turbulent kinetic energy $k$ and the dissipation $\epsilon$.

- The second step is devoted to the determination of acoustic source terms associated with turbulent disturbances. This computation requires the synthesis of time-dependent aerodynamic disturbances not provided by the time average Navier-Stokes calculation. Thus, the turbulent field is deduced from a stochastic model of turbulence (SNGR) involving statistical laws and characteristic properties of turbulence[2] deduced from Kolmogorov theory. The method is described in the next section.

- Finally, radiated acoustic fields are deduced from Euler equations after linearization around the previously computed mean flow and the introduction of acoustic sources. The system to be solved is written under the assumption that acoustic disturbances are small in comparison with aerodynamic fields. The fluid is isentropic and adiabatic. Acoustic pressure and density are related by the relation: $p_a = c_o^2\rho_a$. This yields:

$$\frac{\partial p_a}{\partial t} + (\mathbf{u_o}.\nabla)p_a + (\mathbf{u_a}.\nabla)p_o + \gamma p_o(\nabla.\mathbf{u_a}) + \gamma p_a(\nabla.\mathbf{u_o}) = 0 \qquad (3)$$

$$\frac{\partial \mathbf{u_a}}{\partial t} + (\mathbf{u_o}.\nabla)\mathbf{u_a} + (\mathbf{u_a}.\nabla)\mathbf{u_o} + \frac{1}{\rho_o}\nabla p_a - \frac{\rho_a}{\rho_o^2}\nabla p_o = \mathbf{S} \qquad (4)$$

  $\mathbf{S}$ designates the acoustic source term and is defined by: $S_i = -u_{tj}\dfrac{\partial u_{ti}}{\partial x_j}$. It is associated with second order turbulent disturbances and may be identified as the source noise so called self-noise.[9] The source term is deduced from the stochastic model of turbulence described below.

## II. Stochastic model of turbulence

In what follows, we describe the Stochastic Noise Generation and Radiation model of turbulence (SNGR). There are three steps in the computation: first, the building of a space stochastic turbulent velocity field, then the introduction of the turbulence time dependence, finally, the calculation of acoustic source terms.

### Spatial stochastic velocity field

If one assumes the turbulence is homogeneous, isotropic and frozen, the three-dimensional turbulent velocity field may be considered as a sum of Fourier modes in the frequency domain.[4] At each location, this yields:

$$\mathbf{u_t}(\mathbf{x}) = \int \tilde{\mathbf{u}}_\mathbf{t}(\mathbf{k})e^{i\mathbf{k}.\mathbf{x}}d\mathbf{k} \qquad (5)$$

where $\mathbf{k}$ is the wave vector. After a discretization using $N$ Fourier modes, this relation gives:

$$\mathbf{u_t}(\mathbf{x}) = 2\sum_{n=1}^{N} \tilde{u}_{tn}\cos(\mathbf{k}_n.\mathbf{x} + \Psi_n)\sigma_n \qquad (6)$$

where $\tilde{u}_{tn}$, $\Psi_n$ and $\sigma_n$ are respectively the magnitude, the phase and the direction of the $n^{th}$ mode associated with the wave vector $\mathbf{k}_n$. Furthermore, the turbulent field is incompressible and must satisfy the following condition:

$$\nabla.\mathbf{u_t} = -2\sum_{n=1}^{N} \tilde{u}_n\sin(\mathbf{k}_n.\mathbf{x} + \Psi_n)\mathbf{k}_n.\sigma_n = 0 \qquad (7)$$

Hence, $\mathbf{k}_n$ and $\sigma_n$ are linked by the following relation: $\mathbf{k_n}.\sigma_\mathbf{n} = 0$. Isotropic and homogeneous patterns of this field are ensured by the equiprobability of density functions associated with the coordinates of $\mathbf{k}_n$ and $\sigma_n$ that are initialized as random variables. If $(k_n, \theta_n, \Phi_n)$ designate the spherical coordinates of $\mathbf{k_n}$ (Fig. 1), they are linked by the relation:

$$p(\mathbf{k}_n)d\mathbf{k}_n = \frac{dS}{2\pi k_n^2}$$

where $p$ corresponds to the probability density function. Hence:

$$\frac{k_n \sin\theta_n d\theta_n k_n d\Phi_n}{2\pi k_n^2} = p(\theta_n)d\theta_n p(\phi_n)d\phi_n \qquad (8)$$

We take: $p(\theta_n) = 1/2$, $p(\phi_n) = 1/\pi$ with $0 < \theta_n < \pi$ and $0 < \phi < \pi$. The coordinates of $\sigma_n$ are deduced from relation (7).

Finally, one has to compute the magnitude $\tilde{u}_{tn}$ of each Fourier mode. According to relation (6), the statistical mean of the velocity square is related to the turbulent kinetic energy by:

$$k = \frac{1}{2}\overline{u^2} = \sum_{n=1}^{N} \tilde{u_n}^2 \qquad (9)$$

An homogeneous isotropic turbulence is characterized by a three-dimensional spectrum $E(\mathbf{k})$ which is related to mean turbulent energy and dissipation by:

$$k = \int_0^\infty E(\mathbf{k})d\mathbf{k} \qquad (10)$$

$$\epsilon = 2\nu\int_0^\infty \mathbf{k}^2 E(\mathbf{k})d\mathbf{k} \qquad (11)$$

Hence, the magnitude of each mode $\tilde{u}_n$ is given by: $\tilde{u}_{tn} = [E(k_n)\Delta k_n]^{1/2}$. A modified Von Karman spectrum may be used to represent $E(k)$ whose expression is:

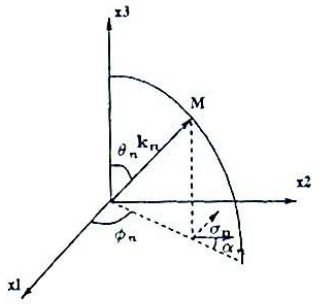


Figure 1: *Notations.*

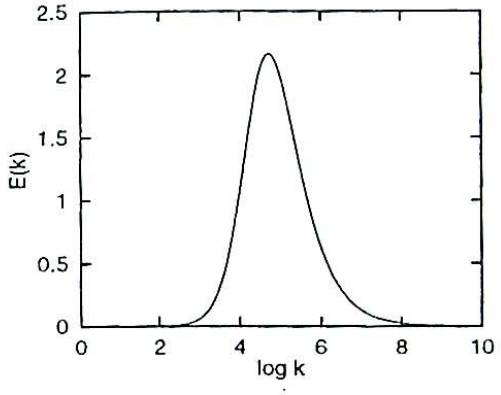


Figure 2: *Von Karman spectrum.*

$$E(\mathrm{k}) = \alpha\frac{\overline{u^2}}{k_e}\frac{(k/k_e)^4}{[1+(k/k_e)^2]^{17/6}}e^{-2(k/k_\nu)^2} \qquad (12)$$

where $\alpha$ and $k_e$ are deduced from relations (10) and (11), the spectrum reaching its maximum for $k = k_e$ (Fig. 2). The Kolmogorov wave number $k_\nu$ is defined by $\mathrm{k}_\nu = (\epsilon/\nu^3)^{1/4}$ and corresponds to the smallest turbulent structures ensuring viscous dissipation. As the discretization implies a finite number of Fourier modes, a logarithmic distribution of wave numbers is used in order to refine the discretization of small wave numbers (i.e. of large turbulent eddies) and to get a suitable resolution of wave numbers included into $[k_1, k_N]$ where $k_1 = \mathrm{k}_\nu = (\epsilon/\nu^3)^{1/4}$ is the Kolmogorov wave number and $k_N = k_L = 2\pi/L$ (with $L$ the largest eddy length) corresponds to the large structure wave number.

In order to check the validity of the stochastic field, we study its statistical properties. This is done in Fig. 3 to 5 which display the statistical mean of velocity, velocity square and velocity products computed over 1000 realizations.

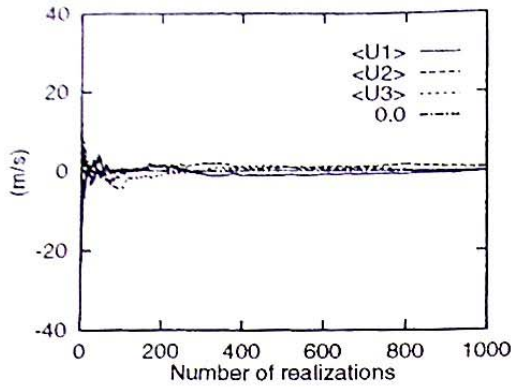


Figure 3: *Statistical mean of velocity* $\overline{u_{ti}}$ *over 1000 realizations.*

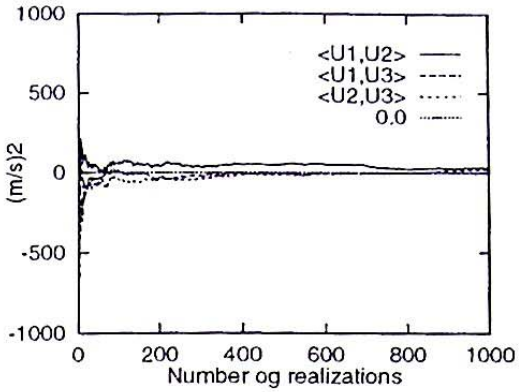


Figure 5: *Statistical mean of velocity product* $\overline{u_{ti}u_{tj}}$ *over 1000 realizations.*

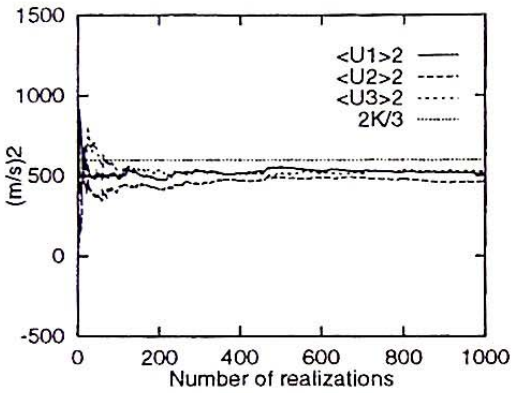


Figure 4: *Statistical mean of velocity square* $\overline{u_{ti}^2}$ *over 1000 realizations.*

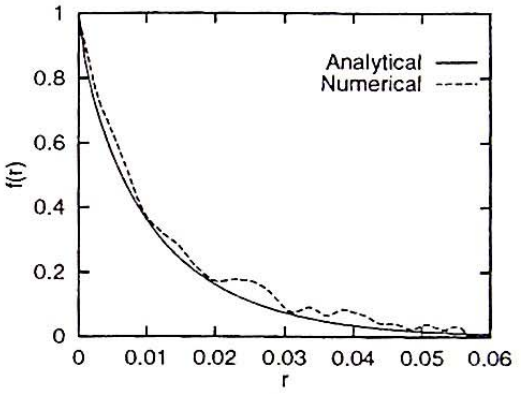


Figure 6: *Longitudinal correlation function* $f(r)$ *evaluated numerically and analytically.*

Numerical and analytical solutions deduced from homogeneous isotropic turbulence properties are compared. One can retrieve the expected turbulence patterns:

$$\overline{u_{ti}} = 0$$

$$\overline{u_{ti}u_{tj}} = \frac{2}{3}k\delta_{ij}$$

Furthermore, one can notice the good agreement between longitudinal, lateral and transverse correlation functions computed numerically and analytically (Fig. 6 to 8).

Turbulence time dependence

The turbulence unsteadiness comes from two processes.

- First, the convection of turbulence by the mean flow $\mathbf{u_o}$. The velocity $\mathbf{u_t}$ is solution of the transport equation:

$$\frac{\partial u_t}{\partial t} + (\mathbf{u_o}.\nabla)\mathbf{u_t} = 0 \qquad (13)$$

Hence, the expression of $u_t$ is given by:

$$\mathbf{u_t}(\mathbf{x},t) = 2\sum_{n=1}^{N} \tilde{u}_n \cos(\mathbf{k_n}.(\mathbf{x} - \mathbf{u_o}t) + \Psi_n)\sigma_\mathbf{n} \qquad (14)$$

- Second, the time dependence of the field governed by the turbulence characteristic frequency must be included. For each mode, we introduce a pulsation $\omega_n$ defined by: $\omega_n = \epsilon^{1/3}k_n^{2/3}$ as small structures contribute to high frequency radiation and conversely. Furthermore, when the wave number $k$ is near $k_e$ (in the region of maximal spectrum), pulsation $\omega_n$ tends

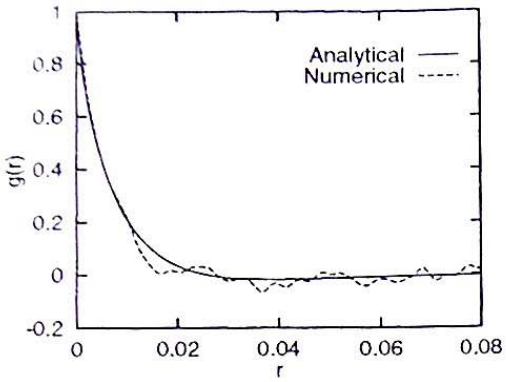


Figure 7: *Lateral correlation function $g(r)$ evaluated numerically and analytically.*

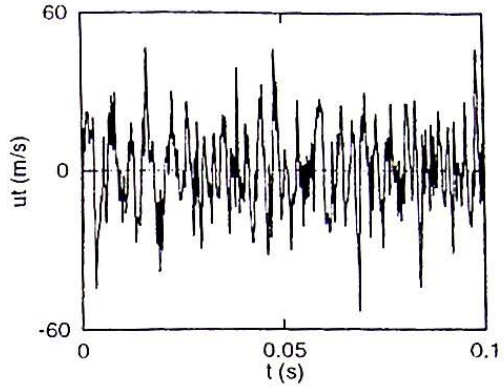


Figure 9: *Time history of $u_{t1}$ at a specific source point.*

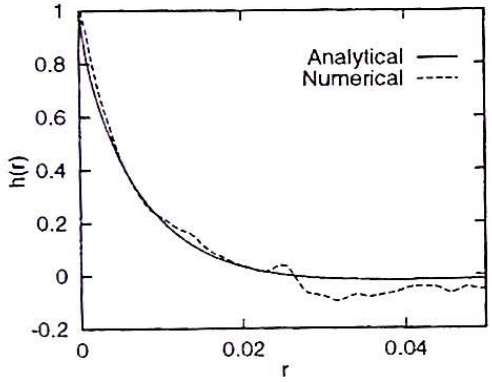


Figure 8: *Transversal correlation function $h(r)$ evaluated numerically and analytically.*

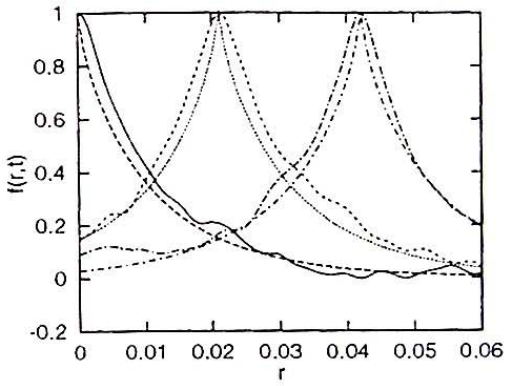


Figure 10: *Convection of longitudinal correlation function $f(r)$ evaluated numerically and analytically.*

to $\alpha 2\pi\epsilon/k$ which is proportional to the characteristic turbulence pulsation.[11] Finally, we take:

$$\mathbf{u_t}(\mathbf{x},t) = 2\sum_{n=1}^{N} \tilde{u}_n \cos(\mathbf{k_n}.(\mathbf{x}-\mathbf{u_o}t)+\Psi_n+\omega_n t)\sigma_\mathbf{n} \tag{15}$$

The time history of the stochastic field at one specific location is given by Fig 9. The convection of the longitudinal correlation function is displayed in Fig. 10.

Acoustic source term building

Numerically, acoustic source terms are identified with regard to their turbulent energy $k$ and it has been shown that their effect may be neglected when $k < 0.3k_{max}$ .

One has to notice that the stochastic field we obtain corresponds to an isotropic homogeneous turbulence. This assumption is not satisfied in complex flows involving high mean shear, particularly, in the presence of obstacles. Hence, we use a splitting of the full acoustic source domain in several subdomains with a size given by the correlation lengths $l_i$ of turbulent large structures defined by:

$$l_i = \frac{\overline{u_{ti}^2}^{3/2}}{\epsilon}$$

with

$$\overline{u_{ti}^2} = -2\nu_t \frac{\partial u_{oi}}{\partial x_i} + \frac{2}{3}k$$

A gaussian smoothing of each subdomain is applied to ensure the continuity in the full domain and a scaling magnitude factor is introduced in order to restore the level of turbulent kinetic energy. The cascade of scales existing in the turbulent flow field is thus correctly described. An example of source domain identification and splitting is displayed in Fig. 11.

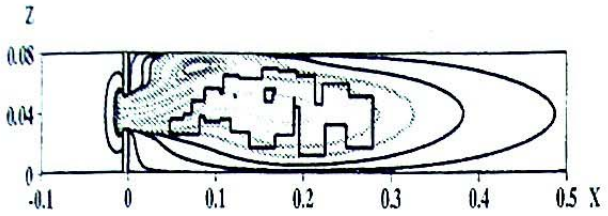


Figure 11: *Source domain identification according to the turbulent energy ($k > 0.3k_{max}$).*

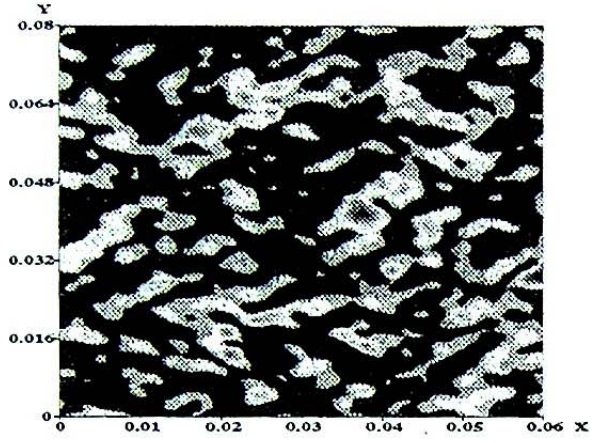


Figure 12: *Source distribution in a plan orthogonal to the $x_3$ direction.*

The term $S_i = -(\mathbf{u_t}.\nabla)\mathbf{u_t}$ is computed at each point of the subdomains. Fig. 12 displays computed source terms in a specific section of a subdomain.

## III. Application to noise radiation prediction

The three-dimensional SNGR model is now applied to the prediction of noise radiation in a confined configuration. In what follows, we first describe numerical methods and we discuss three-dimensional results for the noise generated by a diaphragm placed in rectangular duct flows.

### Numerical methods

The aeroacoustic computation is carried out by solving the linearized Euler system (3 - 4) with the 3D-EOLE code developed by the Department AMV of EDF. The numerical scheme relies on a fourth order Runge Kutta time discretization and an optimized fourth order spatial Dispersion Relation Preserving scheme.[10] A semi-linearized version of the code has been developed in order to account for non linear effects on propagation. Mean fields deduced from a RANS computation involving an irregular near-wall-refined mesh are interpolated on a regular mesh. Duct walls are taken perfectly rigid and an infinite duct length is simulated by using non reflecting conditions. With a total mesh size of $751 \times 33 \times 26$, the full computation requires a memory size of 40 megawords.

The numerical performance of the code has been optimized on a Cray C90 using 8 vector processors and 2 Gbytes of shared memory. This optimization involves vectorization and parallelization. The full computational cost is divided by a factor 15.

It is first worth examining acoustic wave generation and propagation through the diaphragm by assuming that the medium is at rest ($U_o = 0$). One avoid in this way problems induced by interactions with convective modes of oscillation, i.e. by instability waves which may develop in the presence of high mean shear. This assumption is satisfied for subsonic flows. (Specific techniques are required to deal with this problem but are not described in this article).

### Test cases

The geometry of the problem at hand corresponds to an experimental set up allowing validation of numerical simulations. Duct widths are respectively $d = 0.08m$ and $l = 0.1m$. The diaphragm aperture is fixed ($e = 35mm$). The mean flow velocity at the duct inlet $U_o$ takes the three values indicated in the first column of table 1.

Fig. 13 displays the mean turbulent energy provided by the Code ESTET in the three cases.

### Acoustic results

Among the many simulations carried out, we show some typical estimates of sound power level and radiated acoustic fields. Three-dimensional results computed numerically are compared with experimental predictions.[5] Acoustic power levels are displayed in Fig. 14. The level is given in dB (ref. $10^{-12}$ W). Corresponding values are reported in table 1:

| | Acoustic power (dB) | |
|---|---|---|
| | 3D | EXP |
| $u_o$ = 14 m/s | 87.7 | 94 |
| $u_o$ = 32 m/s | 104.2 | 107 |
| $u_o$ = 75 m/s | 122.5 | 120 |

Table 1: *Acoustic powers computed numerically and experimentally.*

Numerical results are closed to those obtained experimentally. On the same figure, we have also plotted the slope of the expected laws which predicts that the acoustic power radiated in presence of a diaphragm placed in a ducted flow is proportional to $U_o^4$.

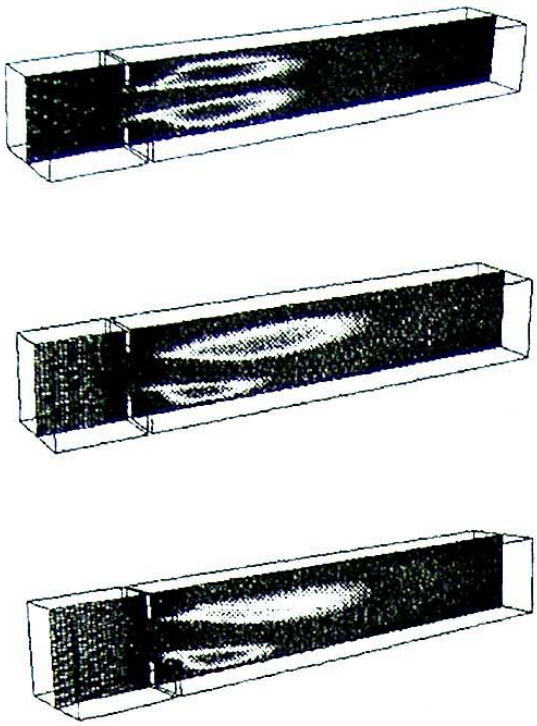

Figure 13: *Mean turbulent energy for $e = 35mm$ with $U_o = 14m/s$ (top), $U_o = 32m/s$ (middle) and $U_o = 75m/s$ (bottom).*

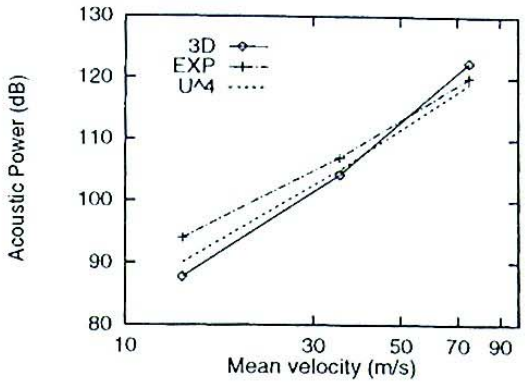


Figure 14: *Acoustic power. Comparison of three-dimensional numerical solution, non-dimensional law and experimental data.*

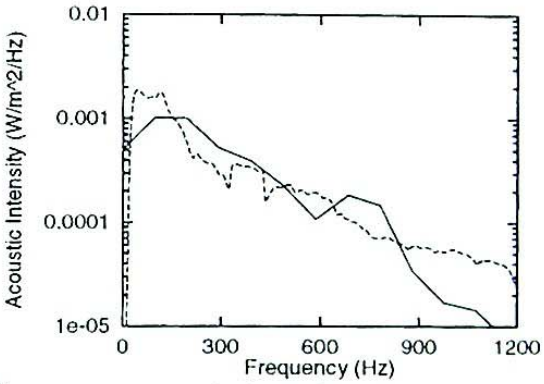


Figure 15: *Acoustic intensity spectrum for $U_o = 14m/s$ computed numerically (solid line) and experimentally (dashed line).*

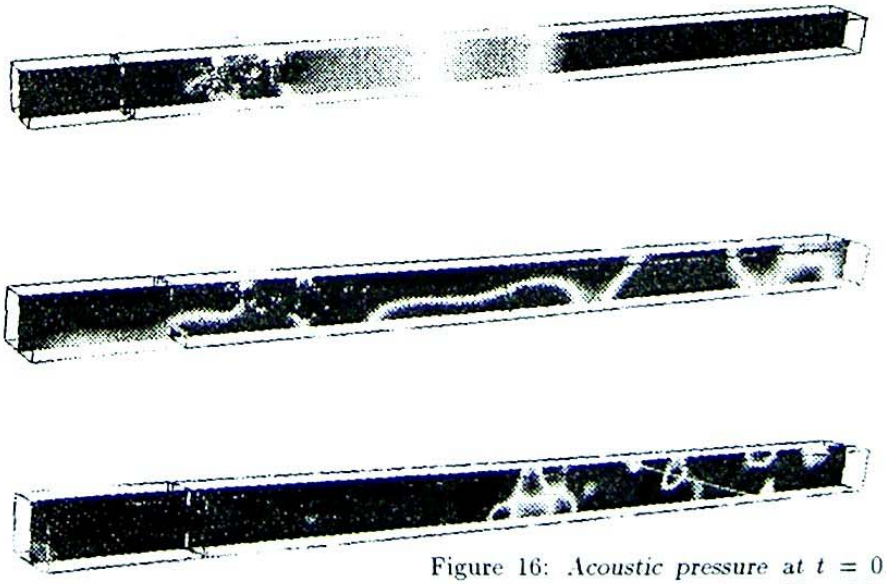

Figure 16: *Acoustic pressure at $t = 0.1s$, for $e = 35mm$ with $U_o = 14m/s$ (top), $U_o = 32m/s$ (middle) and $U_o = 75m/s$ (bottom).*

From this comparison, one may conclude that the three-dimensional numerical predictions feature the expected flow exponant.

Power spectral density of acoustic signal, computed at a point located near the duct exit, is displayed in the case $U_o = 14m/s$ (Fig. 15). This spectrum was calculated by taking a sampling period $\Delta t = 5.\ 10^{-5}$ s, a block size of 2048 points. The data was smoothed with a Hanning window and averaging was carried out over 10 periodograms. The shape of the spectrum compares well with experimental data.

Finally, we display acoustic pressure spatial distribution in the duct at one instant in time ($t = 0.1s$) for the three flow velocities (Fig. 16 ). This figure shows how the wave fronts are progressively formed. The sound field which initially features complicated spatial patterns in the vicinity of the source volume, simplifies at a distance due to the cut-off properties of the duct. The plane mode propagate alone in the first case. Higher modes may develop in the last two cases because higher frequencies are excited by the acoustic sources.

## Conclusions

This article describes a stochastic model of turbulence (SNGR) providing three-dimensional unsteady acoustic sources corresponding to a given turbulent flow. These terms are incorporated in a linearized (or semi-linearized) code to predict noise radiation and propagation. The test cases described in this article indicate that the 3D-SNGR modelling may be used to simulate noise generation in turbulent ducted flows. Numerical estimates are found to be in good agreement with experimental predictions.

Other calculations (not shown here) include non linear terms in the wave operator in order to account for all acoustic/flow interactions occuring during noise generation and propagation. These further developments provide a complete framework for the SNGR modelling.

## References


[1] Bailly, C., Lafon, P., Candel, S. (1996) Computation of Noise Generation and Propagation for Free and Confined Turbulent Flows. *AIAA-96-1732.*

[2] Béchara, W., Lafon, P., Candel, S. (1994) Stochastic approach to noise modelling for free turbulent flows. *AIAA J.* **97** (5), 1-14.

[3] Crighton, D.G. (1975) Basic Principles of aerodynamic noise generation. *Prog. Aerospace Sci.* **16** (1), 31-96.

[4] Kraichnan, R.H. (1970) Diffusion by a random velocity field. *Phys. Fluids*, **13**(1), 22-31.

[5] Lafon, P. (1995) Computation of waves propagation in a complex Flow. *ICASE/LaRC Workshop* (May 95).

[6] Lighthill, M.J. (1952) On sound generated aerodynamically - I. General theory. *Proceedings of the Royal Society of London*, **A211**, 1107, 564-587.

[7] Lighthill, M.J. (1954) On sound generated aerodynamically - II. Turbulence as a source of sound. *Proceedings of the Royal Society of London*, **A222**, 1148, 1-32.

[8] Lilley, G.M. (1972) The generation and radiation of supersonic jet noise. Vol. IV - Theory of turbulence generated jet noise, noise radiation from upstream sources and combustion noise. Part II: Generation of sound in a mixing region. *Air Force Aero Propulsion Laboratory*, AFAPL-TR-72-53.

[9] Mani, R. (1976) The influence of jet flow on jet noise. Part I. The noise of unheated jets *J. Fluid Mech.* **73**(4), 753-778.

[10] Tam, C.K.W., Webb, J.C. (1993) Dispersion -Relation-Preserving Finite Difference Schemes for Computational Acoustics. *Journal of Computational Physics*, **107**, 262-281.

[11] Tennekes, H., Lumley, J.L. (1972) A first course of turbulence. *The MIT Press*, Cambridge.

[12] Van Herpe, F., Crighton, D.G., Lafon, P. (1995) Noise generation by turbulent flow in a duct obstructed by a diaphragm. *16 th Aeroacoustics Conference, AIAA Paper*, 95-035, June 12-15, Munich, Germany.

AIAA JOURNAL
Vol. 38, No. 3, March 2000

# Computation of Acoustic Propagation in Two-Dimensional Sheared Ducted Flows

Elisabeth Longatte* and Philippe Lafon†
*Electricité de France, 92141 Clamart Cedex, France*
and
Sébastien Candel‡
*École Centrale Paris, 92295 Châtenay-Malabry Cedex, France*

**Most aeroacoustic noise-prediction methods rely on an acoustic analogy featuring a propagation equation associated with source terms. These models were mainly applied to computation of acoustic far fields radiated by simple free flows like jets. The assumption is made in many formulations that the radiated acoustic field is not perturbed by the shear flow giving rise to the noise sources. These acoustic analogies thus do not provide a full description of acoustic/flow interactions. The Lilley equation was introduced to account, to a certain extent, for mean shear effects on propagation. More recently, this problem has been treated by making use of the linearized Euler equations, which are more flexible and more adequate for numerical simulations. As several types of modes are supported by the Euler equations, problems linked to their coupling have to be considered. It is then necessary to investigate acoustic field computations in complex flows. Our aim in the present article is to validate the wave operator associated with linearized Euler equations. Numerical tests deal with propagation in two-dimensional sheared ducted flows. Results are compared with other solutions deduced from analytical developments and direct numerical simulations. This study shows that the linearized Euler operator may be used to account for mean effects on wave propagation in the presence of sheared ducted flows. Processes that are specifically considered are 1) convection effects on axial disturbances, 2) refraction effects on oblique wave generation, and 3) source radiation effects on propagation in sheared flows.**

## Nomenclature

| | |
|---|---|
| $c_0$ | = sound velocity |
| $d$ | = duct width |
| $L$ | = duct length |
| $M$ | = Mach number |
| $M_0$ | = duct centerline Mach number |
| $p'$, $p_a$, $p_b$ | = acoustic pressure, acoustic plane mode, acoustic oblique mode |
| $p_0$ | = mean pressure |
| $t$, $t'$ | = reduced and dimensional times |
| $u'$, $v'$ | = acoustic velocity disturbances |
| $u_0$, $v_0$ | = mean velocity |
| $x$, $y$, $x'$, $y'$ | = reduced and dimensional space coordinates |
| $\Omega$, $\omega'$ | = reduced and dimensional angular frequencies |

## I. Introduction

COMPUTATIONAL aeroacoustics (CAA) is a relatively new discipline combining acoustics and computational fluid dynamics (CFD). Whereas CFD methods are often used to solve spatial (time-independent) problems, CAA adds the temporal dimension requiring greater computational resources. Recent numerical developments have allowed gains in efficiency, and many difficulties have been overcome. Standard acoustic theories were primarily linear, assuming that perturbations were monochromatic, and most studies used uniform mean velocity, temperature, and sound speed profiles. These restrictions are not needed anymore. However, some problems remain that are related to acoustic source-term identification, to possible coupling between unstable modes and acoustic waves and to nonlinear interaction processes. In the following, we confine our attention to mean shear effects on acoustic wave propagation.

Most formulations of aeroacoustic problems feature a wave equation associated with source terms. In the framework of Lighthill's analogy, the propagation is described by a standard wave equation in a medium at rest, the second spatial derivative of the aerodynamic stress tensor providing acoustic source terms. This leads to an integral formulation of the sound field expressed in terms of the free-space Green's function corresponding to the wave operator. This analogy is well suited to free space radiation problems; nevertheless, it cannot account precisely for mean flow effects in complex cases. Furthermore, in confined configurations this method may involve numerical difficulties as it requires an adaptation of Green's functions to the specific geometry. It is then more appropriate to use the Euler equations to deal with acoustic/flow interactions.[1] The problem may be treated in three steps:

1) The mean flow is first determined (numerically) by solving the time-average Navier–Stokes equations associated with a turbulence closure scheme like the $k$–$\epsilon$ model.

2) Acoustic source terms related to the turbulent fluctuations are then synthesized by stochastic techniques.[2]

3) Finally, the source terms are incorporated in the right-hand side of the linearized Euler equations (LEE), which are solved in space and time.

The work of Goldstein shows that the linearized Euler system is equivalent to the Lilley's equation when the flow is simply stratified.[3] Now, both formulations, LEE and Lilley's equation, support acoustic and convective (vortical) disturbances. Clearly there is a possibility of coupling between these types of modes, and it is then logical to inquire whether the LEE properly account for acoustic mean/flow interactions including convection and refraction effects.

The present paper deals with this issue in the case of confined flows. To allow simple interpretations, the geometry of the problem has been simplified to the extreme. The purpose here is to understand propagation processes and related energy transfer. The cases under test are chosen to emphasize situations involving exchanges between mean quantities and acoustic modes. They concern

Presented as Paper 97-1631 at the AIAA/CEAS 3rd Aeroacoustics Conference, Atlanta, GA, 12–14 May 1997; received 13 August 1998; revision received 13 August 1999; accepted for publication 16 August 1999. 

*Research Student, Département Acoustique et Mécanique Vibratoire, 1, Avenue du Général de Gaulle.
†Research Scientist, Département Acoustique et Mécanique Vibratoire, 1, Avenue du Général de Gaulle. Member AIAA.
‡Professor, Laboratoire EM2C, Centre National de la Recherche Scientifique. Member AIAA.

interactions between monochromatic acoustic waves and fully developed subsonic mean flow profiles.

Acoustic wave propagation in confined sheared flow was first studied by Pridmore-Brown,[4] who introduced and solved a second-order linearized equation:

$$\frac{1}{c_0^2}\frac{\partial^2 p'}{\partial t'^2} = (1-M^2)\frac{\partial^2 p'}{\partial x'^2} + \frac{\partial^2 p'}{\partial y'^2} - \frac{2M}{c_0}\frac{\partial^2 p'}{\partial t' \partial x'} + 2\rho_0 c_0 \frac{dM}{dy'}\frac{\partial v'}{\partial x'} \tag{1}$$

where $x'$ and $y'$ designate dimensional space coordinates and $t'$ the real time, using conventions of Wang and Kassoy.[5] This equation governs propagation in a flow characterized by a mean Mach number $M = U/c$ and a density $\rho_0$. The fluid is stratified in the $y$ direction, and the flow is adiabatic. Pressure perturbations are isentropic and related to density perturbations by $p' = c^2\rho'$. Equation (1) features the velocity fluctuation $v'$, which is itself related to the pressure by the linearized momentum equation. It is solved by semianalytical techniques, and modal solutions are sought of the form

$$p(x', y', t') = F(\kappa, y')\exp[i(\kappa k_0 x' - \omega t')]$$

where $F$ designates cross-stream eigenfunctions; $\kappa = c_0/v_{ph}$ is the corresponding eigenvalue, and the reference wave number is defined as $k_0 = \omega_0/c$. These solutions take into account changes of axial wave number induced by convection and refraction in the presence of nonuniform mean flow. They feature the expected patterns describing downstream and upstream propagation as well as acoustic intensity distribution through the duct. They were thoroughly studied by Munger and Gladwell[6] and by Hersch and Catton,[7] among many others. However, these studies rely on restrictive assumptions and cannot predict the temporal evolution of an initial disturbance towards a modal form. Source radiation and refraction effects on oblique wave generation cannot be treated in this framework. More recently, Wang and Kassoy[5] proposed new analytical developments and interpretations taking into account transient responses and resonant conditions. Perturbation procedures were carried out for solving initial boundary-value problems and describing processes associated with acoustic generation and propagation. Using direct numerical simulation (DNS) (with the full Navier–Stokes equations), Mu and Mahalingam[8] provided original numerical solutions in agreement with experimental predictions and theoretical developments.

In this paper, we confirm these results by using another approach relying on the computation of LEE. After a brief formulation of the problem and a description of numerical methods and test cases, we discuss results of calculations by using qualitative and quantitative comparisons of numerical and analytical solutions.

## II. Problem Formulation

### A. Model Problem

We solve the LEE associated with a known subsonic mean flow, at high Reynolds number, which ensures that viscosity effects can be neglected. The system to be solved can be written as follows[9]:

$$\frac{\partial p'}{\partial t} + (u_0\cdot\nabla)p' + (u'\cdot\nabla)p_0 + \gamma p_0(\nabla\cdot u') + \gamma p'(\nabla\cdot u_0) = 0 \tag{2}$$

$$\frac{\partial u'}{\partial t} + (u_0\cdot\nabla)u' + (u'\cdot\nabla)u_0 + \frac{1}{\rho_0}\nabla p' - \frac{p'}{\rho_0^2 c_0^2}\nabla p_0 = S \tag{3}$$

where $u'$, $p'$ are dimensional quantities describing flow disturbances. $S_u$ and $S_v$ correspond to acoustic source terms associated with flow turbulence. These terms are not included here as we focus our attention on wave propagation. Mean pressure and velocity are designated as $p_0$, $u_0$, and $v_0$. To deal with propagation in sheared ducted flows, we consider a two-dimensional geometry (Fig. 1), assuming that the mean velocity profile is parallel, taking $v_0 = 0$ and $u_0(x, y) = U(y)$ with

$$U(y) = 4M_0 y(1-y)$$

The reduced spatial coordinate $y$ is defined by $y = y'/d$, where $d$ is the duct width. The duct aspect ratio is defined by $\alpha = d/L$; in what follows, we take $M_0 = 0.08$ and $\alpha = 5$. Duct walls are perfectly rigid, whereas nonreflecting conditions and artificial damping are imposed at the outlet to avoid spurious reflections and simulate infinite duct length. It is interesting to compare the frequency $f$ of monochromatic disturbances imposed at the inlet to the cutoff frequencies of the duct without mean flow: $f_m^c = mc/2d$. The $m$th mode is propagative if $f > f_m^c$. When the Mach number $M_0$ is not too large, this condition will be approximately satisfied. To allow comparisons with previous work, we use the reduced angular frequency $\Omega = \omega' d/c$, which may be related to $f$ and to the first mode cutoff frequency by $\Omega = \pi f/f_1^c$.

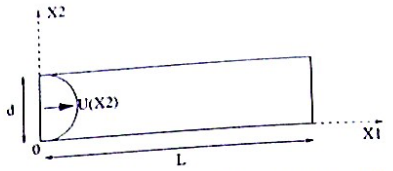


**Fig. 1 Mean flow profile $U(y)$. Inlet disturbances are imposed in section $x = 0$, and nonreflecting conditions in section $x = L$.**

### B. Numerical Methods

The solution of the problem may be obtained by integrating a system of equations that can be cast in the compact form:

$$\frac{\partial W}{\partial t} + A\cdot\frac{\partial W}{\partial X} + B\cdot W + C = 0 \tag{4}$$

with $W = [p', u', v']^t$ and matrices $A$, $B$, and $C$ easily deduced from Eqs. (2) and (3). Two general classes of numerical schemes may be used to deal with this system:

1) The first class relies on a weak formulation of linear equations. The key point of this method is that, in contrast with classical finite element methods, test functions are time dependent and evolve along the characteristic paths. Using splitting techniques, equations are solved in each direction of propagation. One-dimensional problems are then treated in space and time. This approach was implemented a few years ago at Electricité de France (EDF), and applications to aeroacoustic problems were thoroughly discussed by Esposito[10] and Béchara et al.[1] The method features reduced levels of dissipation and dispersion. It requires, however, relatively large computational resources for the treatment of three-dimensional configurations.

2) Other numerical schemes were developed and have become standard in CAA. They are based on finite difference dispersion relation preserving schemes (DRP) devised by Tam and Webb.[11] We use in this study one such sixth-order scheme associated with a fourth-order Runge–Kutta temporal procedure. A strong characteristic method with three-point stencil is used for the treatment of boundaries, and an absorbing domain is introduced together with nonreflecting outflow conditions. The Courant–Friedrichs–Lewy (CFL) criterion must be satisfied to obtain a proper solution, and at least seven grid points are needed per wavelength.

Both schemes are now implemented in the Eole code developed by EDF. Results of both methods are in excellent agreement.

### C. Nature of Inlet Disturbances

We study the propagation of monochromatic disturbances through mean ducted flows to exhibit acoustic/flow interactions. The nature of inlet disturbances is chosen to show as clearly as possible convection, refraction, and source effects on propagation. To check our results, we use a comparison with analytical solutions of Wang and Kassoy[5] and with results of DNS obtained by Mu and Mahalingam.[8] Two kinds of harmonic disturbances are introduced (Fig. 2):

1) In the first case we impose a nonplane source to exhibit generation of oblique waves induced simultaneously by sources and refraction. The plane and the first transverse acoustic modes of the duct without flow are introduced with the same magnitude orders. Inlet conditions are given by

$$u'(y, t) = \epsilon U(y)\sin(\pi y)\sin(t) \qquad \text{with} \qquad U(y) = 4M_0 y(1-y) \tag{5}$$

where $\epsilon$ is the disturbance magnitude and $t$ a reduced time defined by $t = t'\omega'$. This perturbation is somewhat artificial, but this input incorporating the shear-layer profile allows direct comparison of our results with those of Mu and Mahalingam.[8]

2) In the second case we impose the plane mode alone to emphasize refraction effects. Inlet conditions are then specified as

$$u'(y, t) = \epsilon M_0 \sin(t) \tag{6}$$

We note $A(y)$ as the disturbance magnitude, $y$ dependent in the first case, uniform in the second one. Using both inlet conditions, our aim is to study mean shear effects on propagation, which implies an identification of acoustic propagating modes. Hence, to interpret our results, we decompose the numerical acoustic pressure $p'$ into its main components, the plane mode $p_a$ and the first transverse modes $p_b$:

$$p' = p_a + p_b + o(p_b)$$

These components are obtained numerically after Fourier transformation and spatial filtering. This allows direct comparisons with analytical expressions given by Wang and Kassoy in Ref. 5. Their theoretical solutions are built as follows. Linearized hyperbolic equations are written in a strained system of coordinates:

$$\bar{x} = \frac{x}{1 + M\tilde{U}_0} \qquad \text{with} \qquad \tilde{U}_0 = \int_0^1 U(y)\,dy$$

The system is solved by means of a Laplace transform and provides analytical expressions of first- and second-order acoustic pressures designated as $p_1$ and $p_2$ (Ref. 5). However, this method suffers from a lack of generality because it relies on asymptotic appoaches. For this reason only simplified configurations can be considered analytically:

1) When the inlet disturbance magnitude $A$ is $y$ dependent, as in expression (5), the analytical treatment assumes that the mean flow is uniform. In this case expressions of $p'$, $p_a$, and $p_b$ describe the propagation of plane and nonplane modes introduced at the inlet. However, the analytical solution assumes that the flow acts as a bulk and includes only convection effects through the variable $\bar{x}$. Hence, source effects on generation of oblique waves are taken into account, but direct shear effects like refraction are not described.

2) In contrast, when $A$ is constant, as in expression (6), the mean flow is not necessarily uniform, and $p'$ may be written as $p' = p_a + p_b$, with the following decomposition: $p_a = p_1 + Mp_{2a}$ and $p_b = Mp_{2b} + \mathcal{O}(Mp_{2b})$. The axial mode $p_a$ is decomposed into $p_1$ describing convection effects on axial propagation and $Mp_{2a}$ associated with refraction effects induced by mean shear on axial propagation. The higher-order term $Mp_{2b}$ is the superposition of nonplane components of pressure. In this case the computation of the second-order pressure $p_2 = p_{2a} + p_{2b}$ includes refraction effects by shear on axial wave propagation. In the analytical solution, second-order phenomena such as refraction effects on oblique waves are excluded.

Using these formulations, we show next that numerical solutions deduced from LEE and analytical results are in good agreement. Small quantitative differences come from the fact that analytical solutions cannot simultaneously take into account refraction and source effects on oblique wave generation. Qualitative interpretations may be given to understand all mechanisms involved.

To check the results, we also use another comparison (not shown here) with numerical calculations of Mu and Mahalingam[8] based on DNS. Good agreement is found except in the boundary-layer region. This comes from the fact that direct simulations are based on the Navier–Stokes equations, and the corresponding acoustic velocity field falls to zero near the wall. As our solutions are deduced from linearized Euler equations, the acoustic velocity does not vanish near the wall.

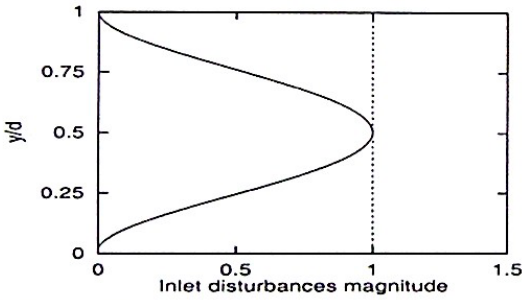


**Fig. 2 Nature of inlet disturbances: ——, two first modes, and - - - -, plane mode.**

## III. Numerical Results and Comments

Many configurations have been tested by selecting different parameters, Mach number, ducted mean flow profile, frequency, magnitude, and nature of inlet disturbances. We here show results obtained for three different frequencies situated next and above the first cutoff frequency of the duct and near the second cutoff frequency. For the reduced frequency we successively take $\Omega = 2$, 8, and $2\pi$. In each case solutions are evaluated numerically and analytically. Acoustic pressure time history, spatial distribution, and spectral contributions deduced from spatial spectral filtering are displayed in selected cases.

### A. Below the First Cutoff Frequency

For a reduced frequency $\Omega = 2$ below the first cutoff frequency $f_1^c$ of the duct without flow, the plane mode is dominant. Figure 3

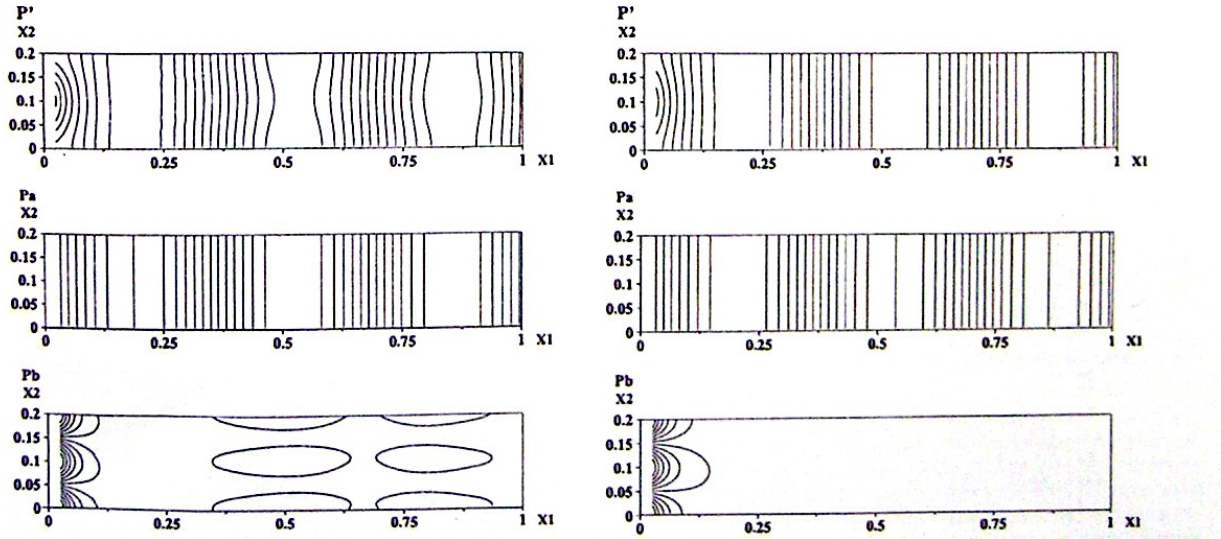


**Fig. 3 Components of acoustic first modes evaluated numerically (left) and analytically (right): full solution (top), plane mode $p_a$ (middle), and nonplane mode $p_b$ (bottom) for $\Omega = 2$, with two modes at the inlet.**

displays a modal distribution of acoustic pressure components when the first two modes are excited at the inlet. Acoustic waves are nearly axial, and the first transverse mode $p_b$ computed analytically decreases quickly and becomes negligible at a sufficient distance from the inlet. In this case the analytical solution describes axial wave propagation but does not include refraction effects. In contrast, the numerical solution features the second-order mode caused by refraction of axial waves, and this mode is still present at a distance from the inlet.

When the plane mode is introduced alone at the inlet for this frequency, the plane mode $p_a$ propagates through the duct without distorsion. Numerical and analytical solutions are in good agreement as shown by the time records of pressure (Fig. 4). As already mentioned, the analytical formulation used in this case takes simultaneously into account propagation of the plane mode introduced at the inlet and small refraction effects induced by shear. Hence, the analytical solution describes the same processes as the numerical one, except for second-order interactions, that is to say, refraction of oblique waves. According to these results, these processes may be neglected at this frequency.

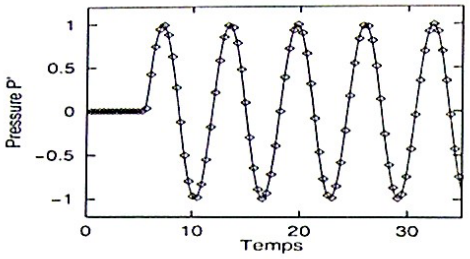


**Fig. 4 Acoustic pressure time history evaluated numerically (——) and analytically (- - - -) at centerline for $\Omega = 2$ and at $x = \lambda$ with the plane mode at the inlet.**

### B. Above the First Cutoff Frequency

For $\Omega = 8$, just above the first cutoff frequency corresponding to the tranverse mode $m = 2$, oblique waves can propagate. With two modes at the inlet, the following processes take place: 1) oblique wave generation by refraction of downstream propagating waves caused by mean shear and 2) oblique wave generation caused by the structure imposed at the inflow. Figure 5 exhibits time histories of total acoustic pressure evaluated numerically and analytically at the wall and at centerline in section $x = \lambda$. This may be compared to Fig. 5 of Mu and Mahalingam.[8] In both results pressure histories differ at the wall and at the centerline indicating that the second tranverse mode develops. Modal distributions of pressure components $p'$, $p_a$, and $p_b$ are given in the spatial domain (Fig. 6) and along the centerline (Fig. 7). One can deduce the following qualitative informations about mode patterns. The plane mode $p_a$ is not affected by refraction, and its magnitude is of the same order as in the case $\Omega = 2$, whereas the second-order pressure $p_b$ supports all refraction effects and is of the same order as the plane mode in contrast with the case $\Omega = 2$. Here, the first two modes introduced at the inlet propagate downstream without attenuation. Whereas numerical and analytical plane modes are strictly similar, second-order pressures differ when the distance of propagation is greater than one wavelength. As refraction by shear is the only process neglected by the analytical computation of $p_b$, one may conclude that refraction by shear induces oblique wave generation.

Turning now to the downstream propagation of the plane mode introduced alone at the inlet for $\Omega = 8$, one observes new patterns. Time histories of acoustic pressure and of its main components are given in Fig. 8. Like in the case $\Omega = 2$, the plane mode is not affected by refraction, which appears only in the second-order pressure $p_b$. However, the magnitude of $p_b$ is smaller than in the preceding case with two modes at the inlet. If one compares the results obtained for different values of the Mach number on the centerline, one can notice that $p_b$ has a magnitude of order $\mathcal{O}(M)$ as expected by analytical developments of Wang and Kassoy.[5]

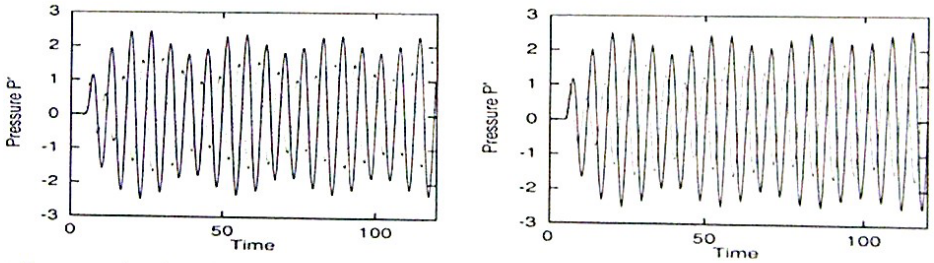


**Fig. 5 Time history of pressure $p'$ evaluated numerically (left) and analytically (right) at centerline (- - - -) and at wall (——) for $\Omega = 8$ and at $x = \lambda$ with two modes at the inlet.**

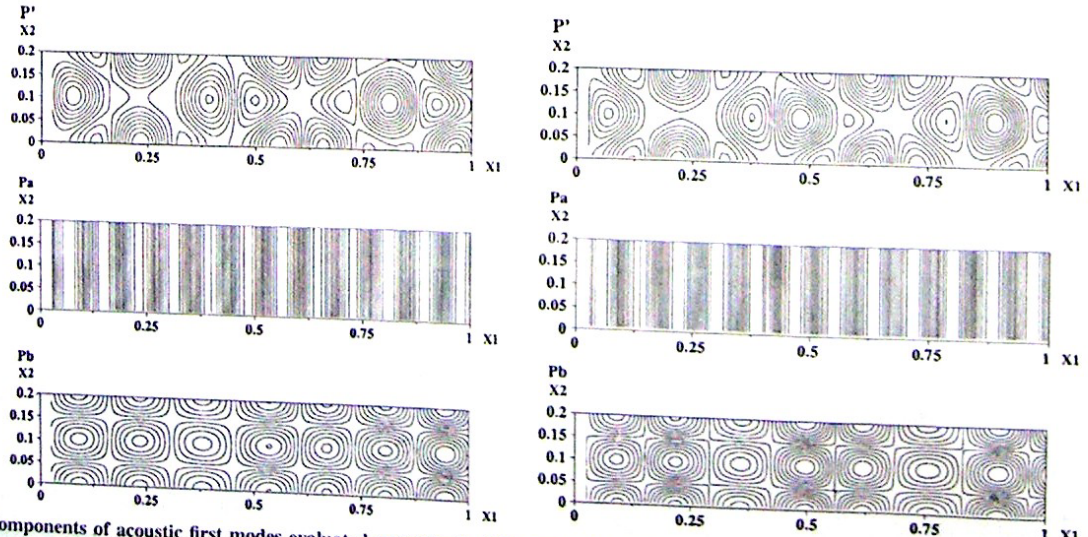


**Fig. 6 Components of acoustic first modes evaluated numerically (left) and analytically (right): full solution (top), plane mode $p_a$ (middle), and nonplane mode $p_b$ (bottom) for $\Omega = 8$ with two modes at the inlet.**

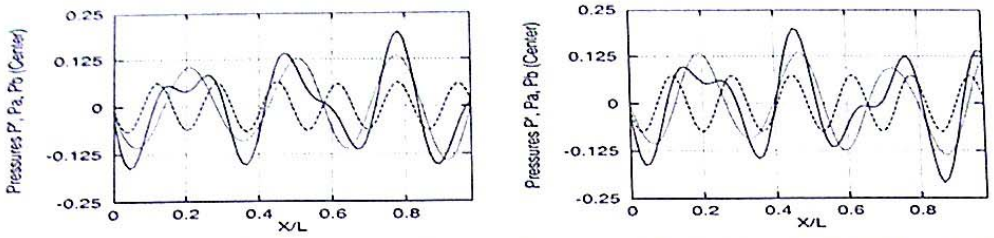


Fig. 7 Spatial propagation of pressures $p'$ (——), $p_a$ (· · · ·), and $p_b$ (- - - -) evaluated numerically (left) and analytically (right) for $\Omega = 8$ at centerline with two modes at the inlet.

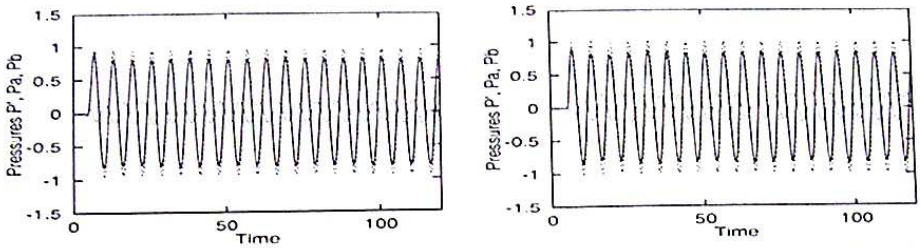


Fig. 8 Time history of pressures $p'$ (——), $p_a$ (· · · ·), and $p_b$ (- - - -) evaluated numerically (left) and analytically (right) for $\Omega = 8$ at $x = \lambda$ with plane mode at the inlet.

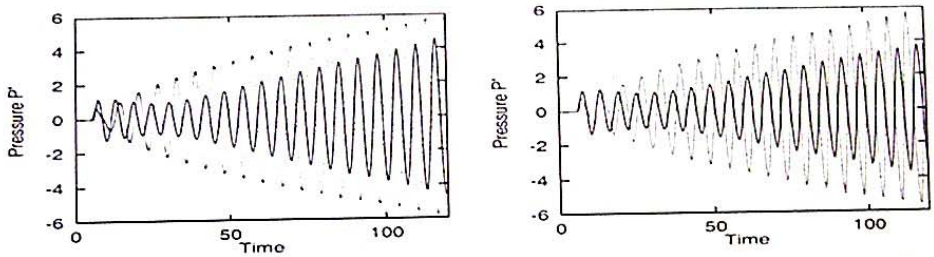


Fig. 9 Time history of pressure $p'$ evaluated numerically (left) and analytically (right) at centerline (- - - -) and at wall (——) for $\Omega = 2\pi$ and at $x = \lambda$ with two modes at the inlet.

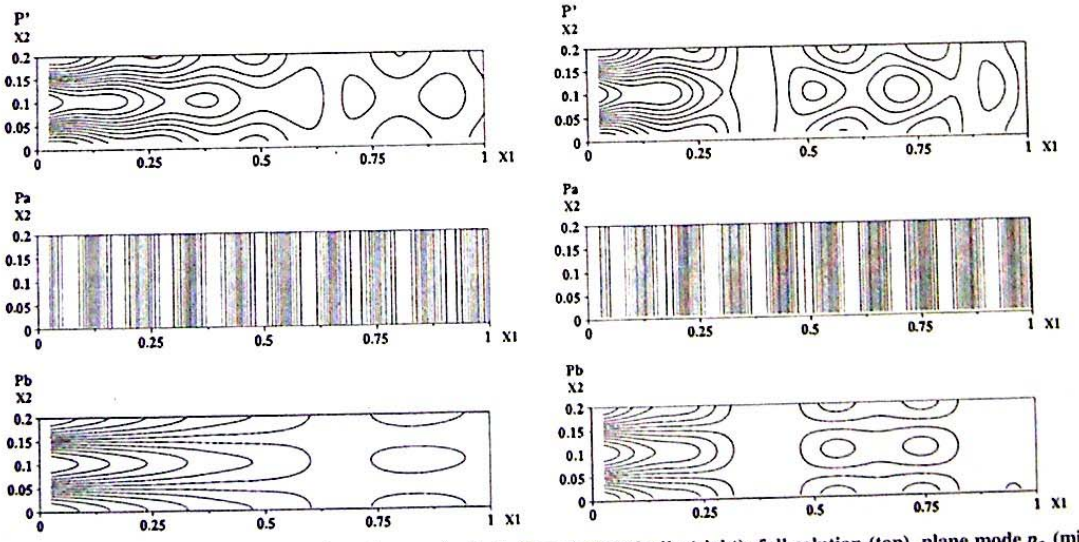


Fig. 10 Components of acoustic first modes evaluated numerically (left) and analytically (right): full solution (top), plane mode $p_a$ (middle), and nonplane mode $p_b$ (bottom) for $\Omega = 2\pi$ with two modes at the inlet.

### C. Near the Second Cutoff Frequency

The last case corresponds to the reduced frequency $\Omega = 2\pi$ close to the second cutoff frequency of the duct without flow $f_2^c$ corresponding to the second tranverse mode $m = 2$. Figure 9 displays the time history of pressure evaluated numerically and analytically in section $x = \lambda$; modal distributions are given in Fig. 10. The plane mode does not feature a resonant behavior, whereas the second-order pressure $p_b$ is nearly resonant. The magnitude of $p_b$ at a given location is modulated in time indicating that energy transfers occur from the boundary layer toward the duct center and conversely. These processes can be explained by interactions between axial waves and nearly transverse modes that are excited at resonant frequencies. Like in the case $\Omega = 8$, the two modes introduced at the inlet propagate without attenuation.

In the case of plane mode excitation for $\Omega = 2\pi$, the plane mode propagates without distorsion, whereas the second-order mode $p_b$

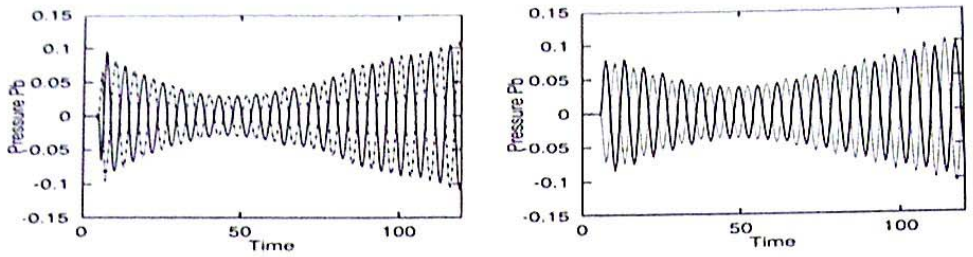


**Fig. 11 Time history of pressure $p_b$ evaluated numerically (left) and analytically (right) with $M = 0.08$ for $\Omega = 2\pi$ at $x = \lambda$ at centerline (- - - -) and at wall (——) with the plane mode at the inlet.**

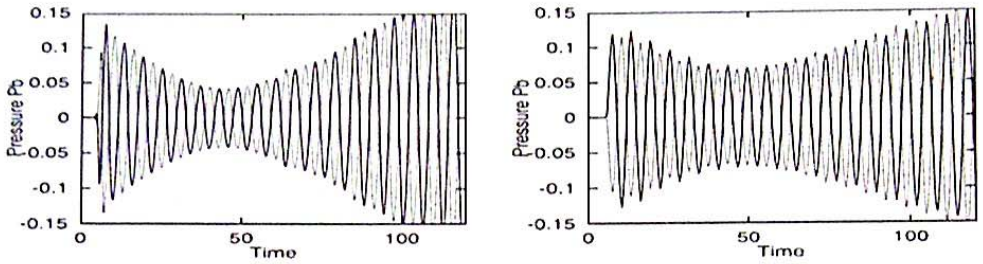


**Fig. 12 Time history of pressure $p_b$ evaluated numerically (left) and analytically (right) with $M = 0.12$ for $\Omega = 2\pi$ at $x = \lambda$ at centerline (- - - -) and at wall (——) with the plane mode at the inlet.**

is nearly resonant. As expected in this case, the magnitude of $p_b$ is much smaller than that of $p$ and $p_a$. If one compares the results for different Mach number values (Fig. 11 for $M = 0.08$ and Fig. 12 for $M = 0.12$), one finds that numerical and analytical solutions are in good agreement over a long period. However, for $M = 0.12$ a difference arises beyond $t \sim 70$. According to Wang and Kassoy,[5] under resonant conditions $p_b$ is of magnitude of order $\mathcal{O}(M)$ until $t$ is of order of $\mathcal{O}(M^{-2})$. For large times the theoretical solution is invalid. Hence, numerical results are in good agreement with theoretical solutions, at least until the theoretical solution breaks down.

## IV. Conclusions

The wave operator associated with LEE can be used to describe the propagation of acoustic disturbances through sheared ducted flows. Results are in good agreement with analytical theories and numerical solutions deduced from direct simulation. The LEE suitably describe mean shear effects on the distribution of acoustic intensity in ducts. Other calculations not shown here indicate that opposite effects of convection and refraction on downstream and upstream propagating waves are well calculated. Refraction effects on propagation and oblique wave generation are included. Effects of initial inlet distribution, frequency, and magnitude on transverse mode generation are displayed through modal decompositions. Transitions that may occur between propagating modes at resonant frequencies are well observed. Except for the acoustic boundary layer that is not included in our inviscid treatment and has to be explicitely introduced, all processes associated with acoustic propagation are well modeled.

This study provides a validation of acoustic fields computed in confined configurations. This is a first step in the analysis of coupling occuring between flows and waves originating from embedded noise sources. Acoustic-flow interactions may be significant as some vortical convective structures are supported by LEE and can develop or act on acoustic propagation when the velocity profile is unstable. Such cases will be developed in further studies related to noise generation by turbulence and relying on stochastic synthesis of acoustic source terms.

## References

[1]Béchara, W., Bailly, C., Lafon, P., and Candel, S. M., "Stochastic Approach to Noise Modeling for Free Turbulent Flows," *AIAA Journal*, Vol. 32, No. 3, 1994, pp. 455–463.

[2]Bailly, C., Lafon, P., and Candel, S., "A Stochastic Approach to Compute Noise Generation and Radiation of Turbulent Flows," AIAA Paper 95-092, June 1995.

[3]Colonius, T., Moin, P., and Lele, S. K., "Direct Computation of Aerodynamic Sound," Stanford Univ., Rept. TF-65, Stanford, CA, June 1995.

[4]Pridmore-Brown, D. C., "Sound Propagation in a Fluid Flowing Through an Attenuating Duct," *Journal of Fluid Mechanics*, Vol. 4, 1958, pp. 393–406.

[5]Wang, M., and Kassoy, D. R., "Transient Acoustic Processes in a Low-Mach-Number Shear Flow," *Journal of Fluid Mechanics*, Vol. 238, 1992, pp. 509–536.

[6]Munger, P., and Gladwell, G. M. L., "Acoustic Wave Propagation in a Sheared Fluid Contained in a Duct," *Journal of Sound and Vibration*, Vol. 9, No. 1, 1969, pp. 28–48.

[7]Hersch, A. S., and Catton, I., "Effect of Shear Flow on Sound Propagation in Rectangular Ducts," *Journal of the Acoustical Society of America*, Vol. 50, No. 3, 1971, pp. 992–1003.

[8]Mu, S., and Mahalingam, S., "Direct Numerical Simulation of Acoustic/Shear Flow Interactions in Two-Dimensional Ducts," *AIAA Journal*, Vol. 34, No. 2, 1996, pp. 237–243.

[9]Lafon, P., "Computation of Waves Propagation in a Complex Flow," *ICASE/LaRC Workshop on Benchmark Problems in Computational Aeroacoustics*, Inst. for Computer Applications in Science and Engineering, Hampton, VA, 1995, pp. 125–129.

[10]Esposito, P., "A New Numerical Method for Wave Propagation in a Complex Flow," *Numerical Methods in Laminar and Turbulent Flow*, Vol. 5, edited by C. Taylor, W. G. Habashi, and M. M. Hafez, Pineridge, Swansea, Wales, U.K., 1987, pp. 1315–1326.

[11]Tam, C. K. W., and Webb, J. C., "Dispersion-Relation-Preserving Finite Difference Schemes for Computational Acoustics," *Journal of Computational Physics*, Vol. 107, No. 2, 1993, pp. 262–281.

P. J. Morris
*Associate Editor*

# 4. De la quasi-statique à la dynamique rapide

## 4.1. Exemple de problématique de dynamique rapide

La problématique considérée ici concerne la simulation du mouvement d'un composant assimilable à une poutre en première approximation et soumis à des sollicitations mécaniques et thermohydrauliques dans son mouvement : il s'agit de la chute d'une grappe de contrôle, constituant l'un des principaux organes de sûreté d'un réacteur (Figure 24). La chute de grappe est provoquée par une seule force motrice : le poids de la grappe et elle est freinée par des forces de frottement mécaniques et thermohydrauliques. Compte tenu des échelles de temps caractéristiques de la chute de grappe, on peut considérer qu'elle relève quasiment du domaine de la dynamique rapide. Sa simulation numérique requiert à la fois la modélisation de la dynamique et des chargements thermohydrauliques qui impactent sa cinétique. Une simulation couplée fluide structure de toute la course de la grappe étant actuellement hors de portée (quelques mètres en une seconde), la méthodologie mise en œuvre repose sur une procédure de couplage quasi-statique. Pour ce type de problématique, on montre que c'est suffisant dans des conditions de fonctionnement de référence (Andriambololona et al. 2005, Annexe 7).

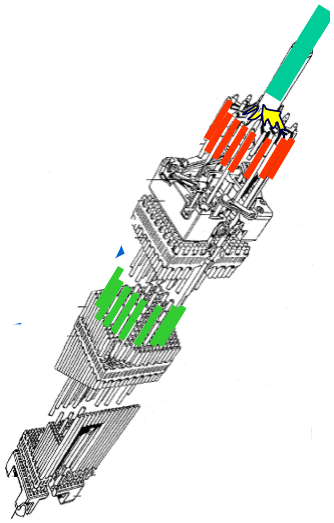

*Figure 24 : Représentation d'une grappe de commande insérée dans un assemblage combustible.*

## 4.2. Approximation quasi-statique

La méthodologie consiste à modéliser la chute de la grappe sous l'effet de son poids propre au moyen d'un modèle de dynamique de poutre et à introduire les chargements thermohydrauliques sous forme de forces extérieures quasi-statiques. Ces chargements ont estimés au moyen de modèles simplifiés et sont réactualisés à chaque itération pour prendre en compte leur dépendance vis-à-vis de la cinématique de la grappe. Il s'agit d'un couplage fluide structure dans la mesure où l'influence des chargements sur la dynamique est pris en compte et inversement les chargements sont réactualisés en fonction de la position et de la cinétique de la grappe. Le couplage mis en œuvre est complètement explicite, sans aucun test de convergence à chaque itération. Néanmoins on peut dire qu'il s'agit d'une approximation quasi-statique puisque les chargements sont estimés à partir des vitesses d'écoulements locales, en négligeant les modifications d'écoulements induites par le mouvement de la grappe.

### 4.3. Du chaînage quasi-statique au couplage

Cette méthodologie a permis de retrouver le comportement de la grappe tel qu'il a été mesuré sur un dispositif expérimental (Figure 25). Néanmoins elle ne permet pas la simulation de phénomènes locaux qui peuvent être générés par les écoulements au voisinage de la grappe et sont susceptibles de modifier sensiblement la cinétique de chute de la grappe en la ralentissant ou en l'accélérant temporairement. A titre d'exemple, si l'on souhaite examiner l'influence de la forme de la pointe des crayons de la grappe de commande en partie basse, il est nécessaire d'envisager une procédure de couplage fort en prenant en compte l'influence des écoulements locaux au voisinage des crayons et en estimant avec précision les chargements induits exercés sur le composant dans son mouvement. Tout l'intérêt des méthodes de couplages fluide structure est là encore mis en évidence.

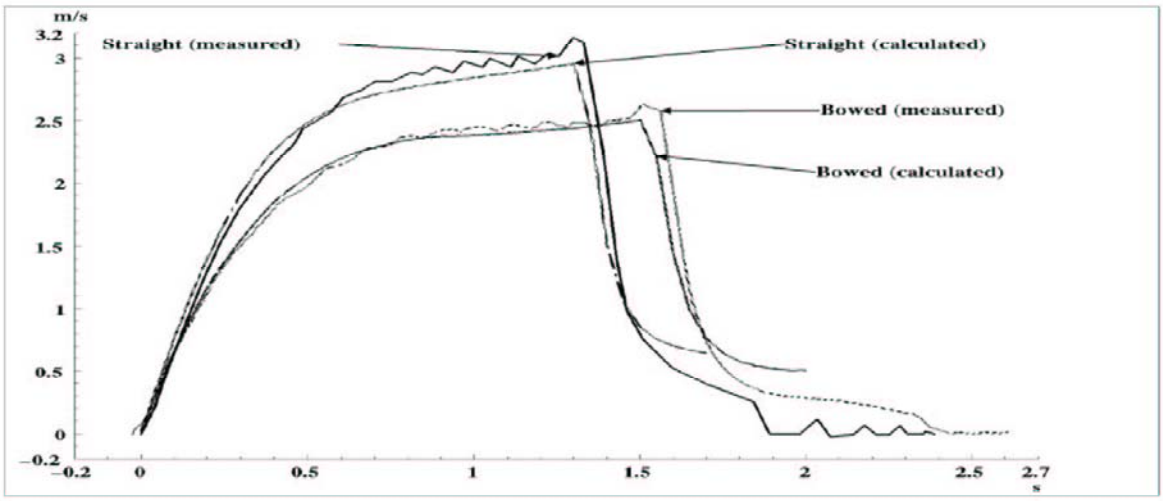


*Figure 25 : Comparaison des cinétiques de chute de grappe calculées et mesurées pour une grappe s'insérant dans un canal droit et dans un canal déformé.*

## Annexe 7 : Modélisation quasi-statique d'une dynamique rapide

Andriambololona, H., Bosselut, D., **Longatte, E.** (2005). Insertion of a slim structure into a channel : simulation and parametric analysis. *EURODYN*, Paris.

# Insertion of a slim structure into a channel - Simulations and parametric analysis

H. Andriambololona, D. Bosselut & E. Longatte
*EDF R&D, France*

ABSTRACT: We present in this paper a methodology about the calculation of the insertion of a slim beam into a cylindrical guide. The problem is the study of the drop of a rod cluster into the core of a nuclear plant. This one is needed to suppress the neutronic activity. A numerical model is elaborated in which many loads are taken into account : fluid load, gravity and friction force between the beam and the guide. The numerical results are compared to experimental measurements obtained from a full-scale structure. A parametric analysis is performed. This study shows clearly that the friction force cannot be neglected when the guide is bowed. Finally, the model can help the decider to make his choice amongst different rod cluster/fuel assembly systems.

## 1 INTRODUCTION

In a nuclear pressurised water reactor, control rod assemblies are used to control the neutronic activity of the core. The control rod passes through a guide (fuel assembly guide tube) with an inner diameter slightly higher than the outer diameter of the rod. High pressurised water flows in this guide. When the control rod is in its withdrawn position, the activity of the core is maximum. When it is in an inserted position, the activity of the core vanishes.

The measurements of the rod drop time are commonly used before each reactor start up. It may be prevented if it exceeds a limit value, which is assessed by safety requirements. It assures the effectiveness of the control system.

In addition, the measurement of the insertion resistant forces is an indication of the defection of the control rod cluster/guide tube component. It determines the optimal component and can justify the interest of a technical evolution.

In this paper, a methodology for the calculation of the mechanical comportment of the system rod cluster/guide is presented.

## 2 NUMERICAL MODELLING

The particularity of this system is its dimension. The length of the control rod is about 4 m with an outer diameter about 10 mm. It has to move in a guide with an inner diameter slightly higher than the outer diameter of the rod. This rod is guided by a mechanism system guide, a discontinuous guide, a continuous guide and a thimble guide (fuel assembly guide tube). At the beginning of the life of the fuel assembly, this one is practically straight, so the friction between the rod and the guide can be neglected. The only reaction force is the hydraulic load. When the fuel assembly has been submitted to external loadings, it may have a permanent deflexion. Figure 1 shows a schematic of the rod cluster/guide system.

In this study, we consider a bowed fuel assembly with an imposed lateral displacement of the guide. The lateral displacement of the mid of the guide is equal to 30 mm. We mention that it is very little compared to the length of the fuel assembly, which is about 4 m.

A three dimensional numerical model of the system control rod cluster/guide was carried out with a finite element approach with Code_Aster. The control rod cluster is modelled with Euler Bernoulli beam elements (850 elements) and the guide with Kirchoff plate elements (550 elements). So we have a model with 13500 degrees of freedom.

The displacement of the control rod is large (3.8 m) and supposed to be in plane vertical movement. The control rod is submitted to hydraulic and mechanical loads. Hydraulic loads consist of Archimedes forces and forces induced by pressure losses, viscous friction, fluid pressure and lift force. Mechanical loads are gravity, contact and friction forces.

### 2.1 *Hydraulic load*

The hydraulic loads are assessed by considering a weak fluid structure coupling. They are deduced from the Bernoulli relation and the conservation laws in the annular fluid domain between the control rod and the guide. This methodology is applied at each singularity and along the guide.

A complete description of the hydraulic loads is made in Longatte (2003). The flexion of the rod is not taken into account in the calculation of the fluid load. We assume that the fluid is viscous and incompressible.

Hydraulic characteristics are identified at each singularity of the system. They are located in three distinct zones : in the control rod drive mechanism, in the inner part of the control rod assembly and in the guide thimble (fuel assembly guide tube).

The hydraulic load is applied to the neutral fibre of the beam element and oriented vertically from the bottom to the top of the structure. They are evaluated at each step of time according to the altitude of the rod.

### 2.2 *Mechanical loads*

The main mechanical loads are gravity and friction forces. The contact between the rod and the guide can be characterised by the unilateral contact relation. It can be formulated as no interpenetration between the two structures. The two structures cannot pull on each other and either they press on each other or they are separated.

The adhesion is not taken into account. A Coulomb friction law (without regularisation) is used for the mathematical representation of the friction, which stipulates that the tangential force depends only on the normal force. And the tangential force cannot exceed a limit value.

The friction force between the beam and the plate is a vertical force applied directly at the neutral fibre of the beam. We neglected the bending moment due to the radius of the beam which is very weak.

The choice of the normal direction for the evaluation of the gap between the two structures is very important. Here, the direction of the normal is chosen as the normal to the plate element.

### 2.3 *Numerical resolution*

A finite element method is used to simulate the rod cluster behaviour. The deflection of the guide is obtained numerically by imposing a lateral displacement at the mid of the fuel assembly.

The resolution of the differential equation of the movement is regularized by using the implicit integration Hilber–Hugues–Taylor (HHT) method explained in Aufaure (1995). This regularization reduces the high frequency effect due to the nonlinearity of the system.

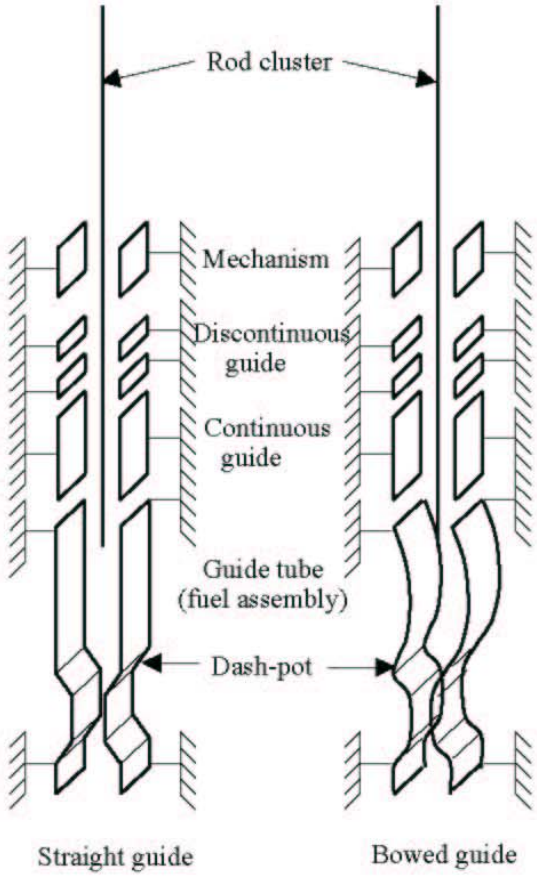


Figure 1 : schematic view of the numerical model.

The contact and friction problems are solved by using the standard lagrangian contact method. The formulation of this method can be seen in Tardieu (2003)

Two types of numerical simulations are realized : the insertion and the drop of the rod. Experimental measurements are done with a full-scale structure for the validation of the model. The description of the measurement conditions and the results obtained are described in Collard (1998).

## 3 INSERTION OF THE ROD INTO THE GUIDE

The insertion test underlines the presence of a bowed guide. The vertical displacement of the rod is imposed to be 1 m per minute. A none zero friction force indicates that the guide is not straight. In this insertion test, the fluid force is not taken into account. The loads correspond only to the mechanical forces.

The Coulomb friction coefficient of the numerical model is tuned to the measurement test. The friction coefficient of Coulomb identified is 0.6.

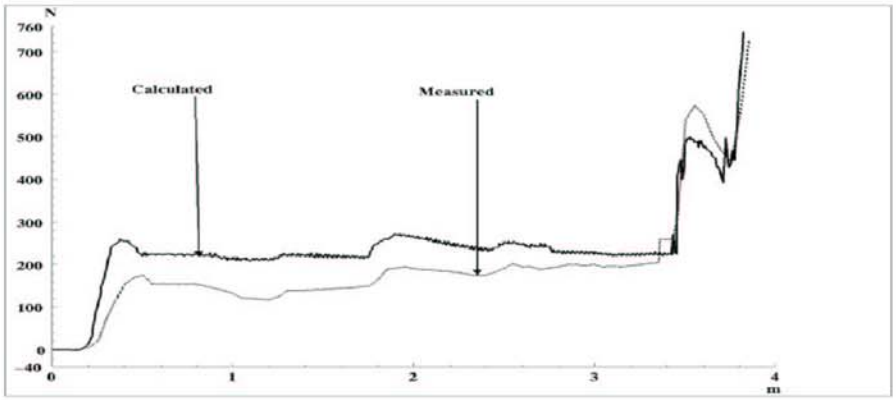


Figure 2 : Comparison of calculated and measured friction forces according to the vertical displacement of the rod.

This insertion force analysis reveals that the force resistance depends closely on the deflexion of the guide.

Figure 2 shows the comparison of the calculated and the measured force resistance for an insertion of a rod with a 30 mm bowed guide. The aspect of the estimated force is in relation to the measured one.

## 4 ROD DROP TIME CALCULATION

To qualify a rod cluster and the associated fuel assembly, a rod drop test must be performed before each start up. The duration of the drop of a rod cluster must be less than a critical value assessed by safety requirement.

The drop time is calculated by considering hydraulic and mechanical loads.

Figure 3 shows the comparison of estimated and measured kinematics of the rod drop for a straight and a bowed guide.

The configuration presented here corresponds to a flow rate of the fluid of 284 m3/h at a temperature of 50 °C.

The effect of the hydraulic load is more important than the effect of the mechanical forces.

If we only consider the gravity force, the velocity increases according to the time. It shows that the fluid load is so important that it can oppose to the vertical velocity of the rod. We can also see that if the guide is bowed, the friction force between the rod and the guide cannot be neglected (figure 2).

The critical time of the rod drop is the duration of the drop (from the withdrawn position to the passage of the bottom of the rod in front of the dash-pot). One has to measure or evaluate precisely the duration of the drop $t_d$ and the corresponding velocity $v_d$ (velocity of the rod when it passes in front of the dashpot). The value of $v_d$ is an indication of overpressure at the dash-pot and thus of the behaviour of the component.

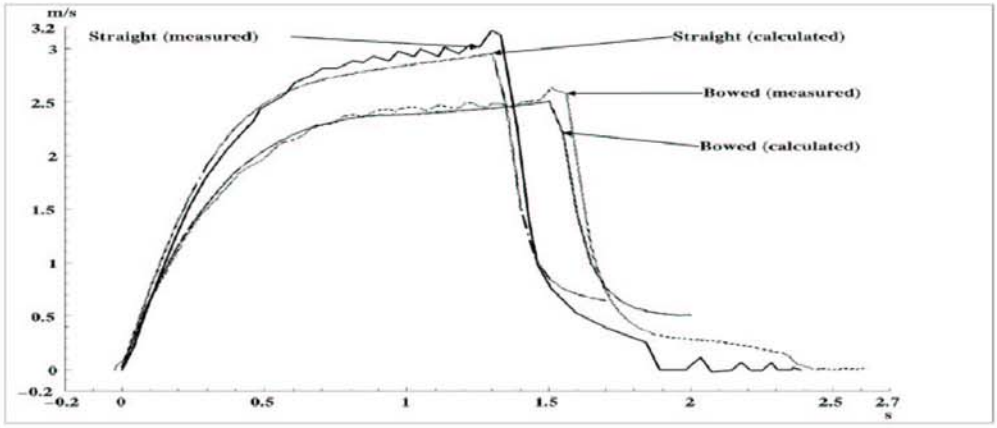


Figure 3 : Comparison of calculated and measured cinematic of the rod drop for a straight and a bowed guide.

## 5 PARAMETRIC ANALYSIS

To identify the most pertinent parameter for the calculation of the kinematics of the rod drop, parametric analyses are performed. The effect of a variation of some parameters of the model were studied. We study respectively the effect of hydraulic parameters and the effect of a variation of the coefficient of friction of Coulomb.

### 5.1 *Effect of hydraulic parameters*

The effect on the rod drop time of some hydraulic parameters is evaluated : flow rate, fluid density, cinematic viscosity, singular pressure losses, and linear pressure loss.

For a straight guide, $t_d$ is estimated numerically at 1.33 s and the corresponding velocity $v_d$ is 2.95 m/s.

The choice of the variation of each parameter corresponds to the uncertainty usually evaluated in experiments during the identification process.

| Parameter and its variation | Relative variation of $t_d$ (%) | Relative variation of $v_d$ (%) |
|---|---|---|
| Fluid density (10 %) | 6 | 7 |
| Singular pressure loss (20 %) | 4 | 2.5 |
| Linear pressure loss (20 %) | 0.5 | 0.2 |
| Flow rate (5%) | 2 | 1.2 |
| Cinematic viscosity (20%) | 0.5 | 0.2 |

Table 1 : Relative variation of rod drop time according to numerical parameters variation.

This calculation shows that the fluid density is the most important parameter for the assessement of the rod drop time. Accuracy on this parameter is required for a correct estimation of the rod drop time.

### 5.2 *Effect of the friction coefficient*

The effect of the friction coefficient during the drop is analysed in the configuration of a bowed guide. Figure 4 shows the vertical velocity of the rod according to the altitude. It shows that the effect of the friction cannot be neglected if the guide is bowed. This figure also shows that the effect of an uncertainty on the friction coefficient of Coulomb is relatively weak if compared to the effect of the deflection of the guide.

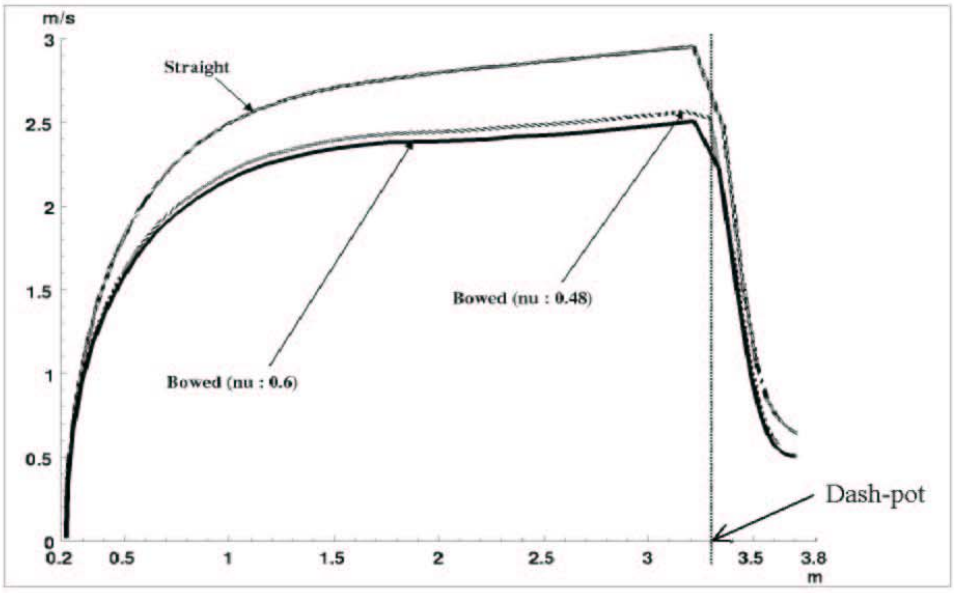


Figure 4 : velocity of the rod according to the altitude. The effect of uncertainty on the friction coefficient is relatively weak compared to the effect of the deflection of the guide.

## 6 CONCLUSION

We present in this paper a method for the calculation of control rod drop time. The numerical model was obtained by tuning the Coulomb friction coefficient from a full scale experimental measurements. Hydraulic loads and friction are taken into account.

The model we used allows to evaluate the uncertainty of some parameters. The drop time model shows the importance of the distributed loads such as the fluid density and the flow rate.

The friction force cannot be neglected when the guide is bowed.

The numerical model created here can then estimate the effect of an hypothetical deflection of the fuel assembly.

Localisation of a geometrical default of a guide can be suggested by analysing the velocity of the drop of the rod or by analysing the reaction force during an insertion simulation according to the altitude of the rod.

## REFERENCES

Aufaure M.. 1995. *Algorithme non linéaire dynamique du Code_Aster*. Manual reference Code_Aster R5.05.05-A.

Collard B. *Compte rendu des essais Cigare 900 MWE*. 1998. Technical note DEC SECA/LHC 98/016.

Longatte Lacazzedieu E., Boyere E. & Vivan L. 2004. *Documentation de référence, documentation de validation, documentation d'utilisation du module de calcul de cinétique de chute de grappe avec Code_Aster*. EDF report HI-86/03/024/A.

Tardieu N. & Massin P. 2003. *Contact – frottement discret en 2D et 3D*. Manual reference Code_Aster R5.03.51-C.

# CHAPITRE III

# -

# COUPLAGE FLUIDE STRUCTURE

# CHAPITRE III - COUPLAGE FLUIDE STRUCTURE

## 1. Couplage fluide structure

### 1.1. Du chaînage au couplage

Tous les exemples illustrés précédemment révèlent les limites des procédures de chaînages de codes fluide structure dès lors que l'on est en présence de couplages physiques. La simulation des physiques couplées est impossible par simple chaînage, sauf à avoir recours à des méthodes simplifiées et des modélisations approchées des interfaces qui comme précédemment peuvent être facilement mises en défaut. **Par couplages, on entend couplages « faibles » ou « forts », c'est-à-dire phénomènes d'action-réaction entre les dynamiques fluide et structure pouvant conduire à des modifications du comportement propre de la structure**. Lorsque le fluide est initialement au repos et dans l'hypothèse des petits mouvements, on parle de couplages faibles et les chargements exercés par le fluide sont appelés « forces fluide structure » ; en présence d'écoulement, dès lors que les couplages peuvent induire des non conservatismes au sein de chaque sous-système, il s'agit de couplages forts et les forces de couplage sont dites « fluide-élastiques ».

### 1.2. Couplages faibles et forts

On s'intéresse dans ce chapitre à des configurations de couplages «faibles » ou « forts » avec ou sans écoulement permanent (Figure 26).

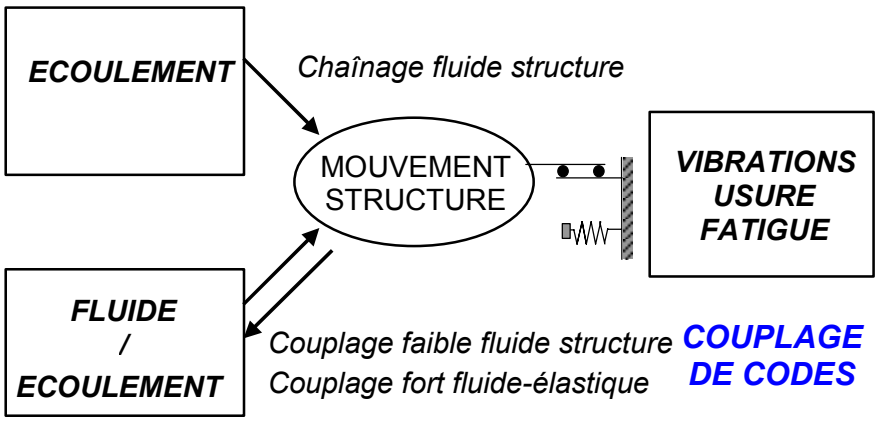


*Figure 26 : Configuration de type couplage faible ou fort simulée par couplage de codes fluide et structure.*

L'objectif est de montrer la faisabilité d'une simulation numérique de couplages pouvant induire des non-conservatismes voire des instabilités au sein de chacun des deux sous-systèmes couplés. Les exemples cités sont issus du domaine des vibrations de structures induites par écoulements pour lesquels les non-conservatismes peuvent se traduire par des effets d'inertie (Figure 27-a), d'amortissement (Figure 27-b) et/ou de raideur induits par couplage. On s'intéresse tout particulièrement aux deux premiers effets, avec ou sans écoulements permanents, les derniers ayant fait l'objet de nombreuses études numériques par ailleurs, notamment dans le domaine de l'aéroélasticité (Figure 27-c).

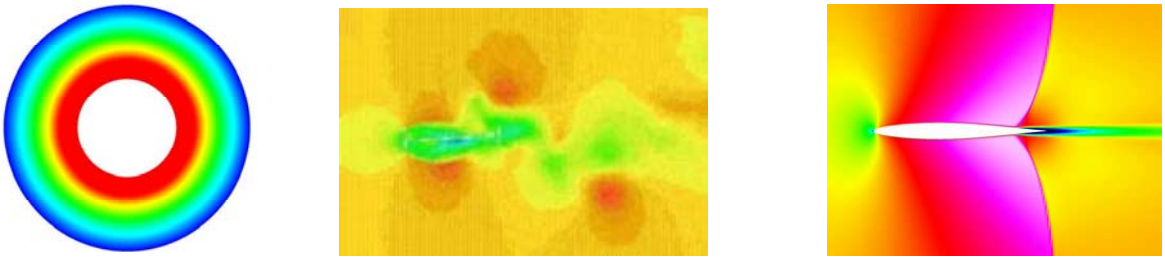

*(a)* *(b)* *(c)*

*Figure 27 : Exemple d'effets induits par couplage fluide structure : (a) effet d'inertie induit par le fluide au voisinage d'une structure, (b) effet d'amortissement induit par un écoulement siège d'instationnarités générées par couplage, (c) effet de raideur induit par apparition d'une instabilité statique.*

### 1.3. Simulation numérique des couplages

Par opposition aux techniques de chaînage, la simulation des couplages requiert la modélisation complète de l'interface fluide structure, soit, dans le domaine des vibrations induites par écoulements, la modélisation à chaque instant à la fois des chargements thermohydrauliques pariétaux et des mouvements de la structure. Pour ce faire, deux types d'approches sont envisageables suivant que les systèmes d'équations fluide et structure sont résolus conjointement dans un même système global par une procédure dite « monolithique » (Morand et Ohayon 1995) ou consécutivement, alternativement à chaque pas de temps (ou de fréquence en spectral), par une procédure dite « partitionnée » qui consiste à transférer les données à l'interface entre les deux solveurs (Piperno et Fahrat).

En vertu de la propriété selon laquelle « **tout système couplé dont l'énergie est conservée à l'interface est stable** » (Piperno et Fahrat), il conviendrait d'adopter systématiquement une procédure monolithique qui, par construction, assure la conservation de l'énergie à l'interface et est inconditionnellement stable. C'est la stratégie utilisée par exemple en interactions fluide structure tant que les non linéarités du fluide n'interviennent pas dans le couplage. Ainsi la plupart des codes de dynamique des structures intègrent des formulations spécifiques pour la prise en compte d'interfaces avec un fluide s'il peut être représenté par des champs scalaires (pressions, potentiels) solutions d'un système global fluide structure (Morand et Ohayon 1995). Des exemples de calculs de coefficients de masses et d'amortissements ajoutés un fluide par une procédure monolithique pour une structure immergée dans un milieu fluide visqueux ou non visqueux sont disponibles en Annexe 11.

Cette démarche n'est toutefois pas envisageable en présence de fortes non linéarités fluide et/ou structure, les méthodes numériques requises pour les calculs fluide et structure étant en général distinctes, rendant la plupart des programmes de développements de codes multi-physiques monolithiques irréalistes à l'échelle industrielle à ce jour. D'où l'usage de plus en plus répandu de procédures partitionnées pour la simulation de couplages multi-physiques, et tout particulièrement des couplages fluide structure. C'est dans ce contexte que le coupleur *Cosmethyc*[18], objet de ces travaux, a été développé. Il réalise le couplage en mode temporel entre les codes de thermohydraulique et de mécanique développés à EDF R&D. Il est néanmoins connectable à tout code fluide et/ou structure mettant en œuvre des méthodes numériques similaires.

[18] COSMETHYC COupleur pour la Simulation MEcanique et ThermohYdrauliQUE

Le présent chapitre est consacré à la présentation des principes généraux de *Cosmethyc* autant qu'il illustre quelques premières utilisations de l'outil mettant en évidence son intérêt sur les plans physiques, scientifiques et industriels (Annexes 8 à 11). Les travaux en cours, perspectives, alternatives et possibilités d'extensions de ces travaux sont abordés dans le chapitre suivant.

# 2. Coupleur fluide structure

## 2.1. Modélisation des sous-systèmes

Le coupleur comprend d'une part les composants couplés : les solveurs fluide et structure, d'autre part les opérateurs de couplage : en temps et en espace.

### 2.1.1. Formulation A.L.E. en thermohydraulique

En présence de couplages, les écoulements fluides locaux sont impactés par les mouvements de la structure. La présence de l'interface fluide structure mobile doit donc être prise en compte au niveau du calcul fluide et des modifications doivent être apportées au solveur fluide. Parmi les approches possibles, on peut citer les méthodes P.M.D.F. (ou méthodes de transpiration) consistent à gérer le couplage uniquement au niveau des conditions aux limites à l'interface. Ainsi le calcul fluide est réalisé sur un domaine fixe au cours du temps et les conditions aux limites sont modifiées pour prendre en compte le déplacement de la structure grâce à un développement limité de celui-ci autour de sa position initiale (Le Tallec et al. 1996). Cette classe de méthodes est efficace (Renou 1998) mais son champ d'application est restreint au le cadre des petits déplacements. Une autre approche possible consiste à modifier la formulation eulérienne usuelle mise en œuvre en thermohydraulique et à réaliser un calcul sur maillage mobile en utilisant une formulation mixte Lagrange Euler (A.L.E.) basée sur l'introduction d'un référentiel de calcul, dit arbitraire, distinct du référentiel eulérien du calcul fluide sur domaine fixe, et relié au référentiel lagrangien attaché à la structure mobile par le biais d'une matrice de changement de base évoluant dans le temps (Hugues et al. 1981, Donea 1982, Souli 2000, Souli et al. 2000, 2001, Longatte et al. 2003, Thomas et Lombard 1979). Avec cette formulation les équations fluide sont décrites dans un référentiel arbitraire qui coïncide avec le référentiel eulérien loin de l'interface et avec le référentiel lagrangien au voisinage de l'interface (Figure 28, Annexe 8).

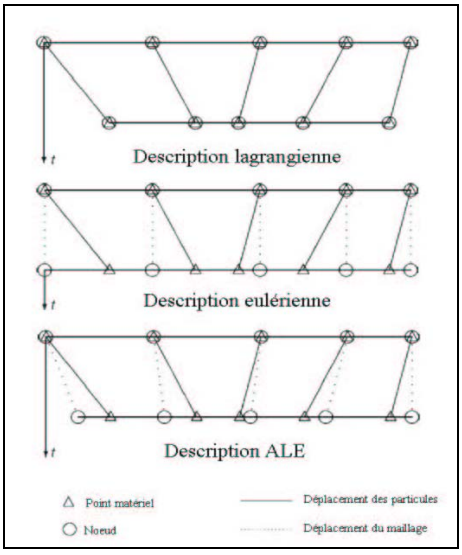


*Figure 28 : Principe de la gestion de maillage déformable avec une formulation A.L.E.*

Au premier ordre et pour un fluide incompressible, seules les équations de quantité de mouvement doivent être modifiées, les termes de convection devant prendre en compte la contribution de la vitesse du maillage intervenant dans le référentiel arbitraire, l'équation de conservation de la masse restant inchangée (Guimet 1998).

La mise à jour de la grille de calcul étant liée aux mouvements de la structure au niveau des nœuds de l'interface et arbitraire pour les nœuds internes, plusieurs méthodes peuvent être mises en œuvre pour déformer le maillage au cours du temps, la principale contrainte étant de préserver la qualité du maillage et de garantir un raffinement suffisant proche des parois de l'interface. La technique généralement la plus utilisée est la résolution d'une équation de diffusion appliquée aux déplacements de la grille, avec introduction éventuelle d'une viscosité locale de maillage pour assurer un contrôle des déformations de maillages. L'intérêt de cette viscosité a été mis en évidence dans le cas des faisceaux de tubes pour limiter les déformations de mailles au voisinage de l'interface mobile (Figure 29). Le seuil d'amplitude des déformations de maillages admissibles a été identifié sur des cas tests analytiques, notamment sur le cas d'un écoulement de Poiseuille traité avec et sans déformation de maillage. Un cas de validation de référence a été défini, il porte sur la prévision des fluctuations de pression induites par un mouvement harmonique de piston (Figure 30 et Figure 31). La méthode A.L.E. de type Laplacien est efficace mais présente l'inconvénient d'induire un coût significatif du fait de la résolution du système linéaire associé pour chacun des composantes du déplacement de la grille. D'autres approches ont été envisagées, comme une méthode de recherche des adjacents applicable dans le cadre des maillages conformes structurés hexaédriques (Figure 32) (Annexe 9).

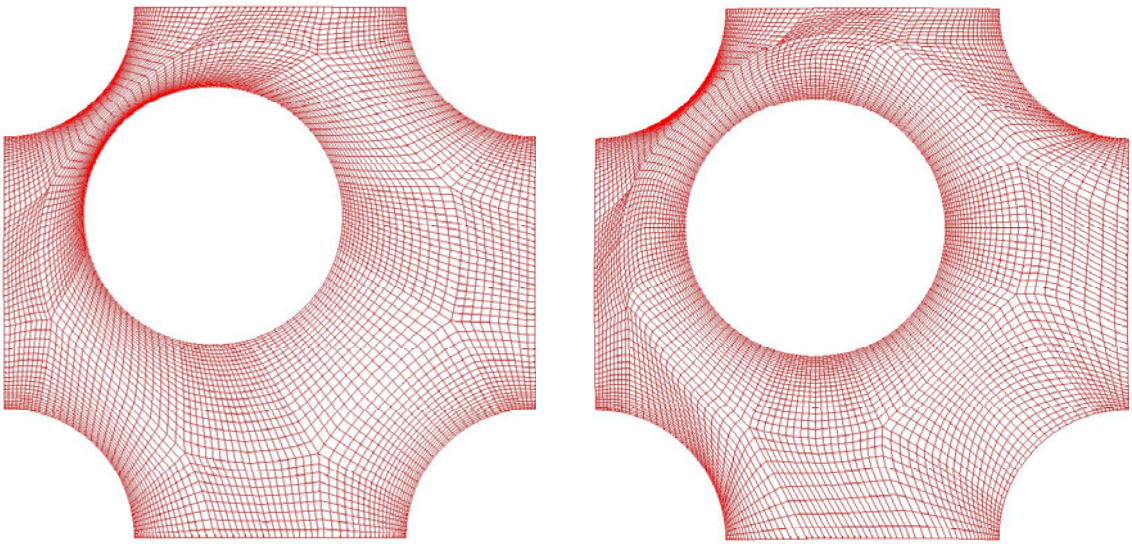

*Figure 29 : Déplacement du maillage avec une viscosité de maillage constante (à gauche) et variable (à droite) par une méthode A.L.E. de type Laplacien.*

### 2.1.2. Modèle mécanique et couplage

Du point de vue mécanique, aucune spécificité propre au couplage avec le calcul fluide n'est introduite au niveau du solveur structure. L'équation locale de conservation de la quantité de mouvement est résolue avec un formalisme lagrangien et les lois de comportement propres à la structure restent inchangées. L'interface fluide structure intervient par le biais des conditions aux limites sur les chargements surfaciques imposés par le fluide.

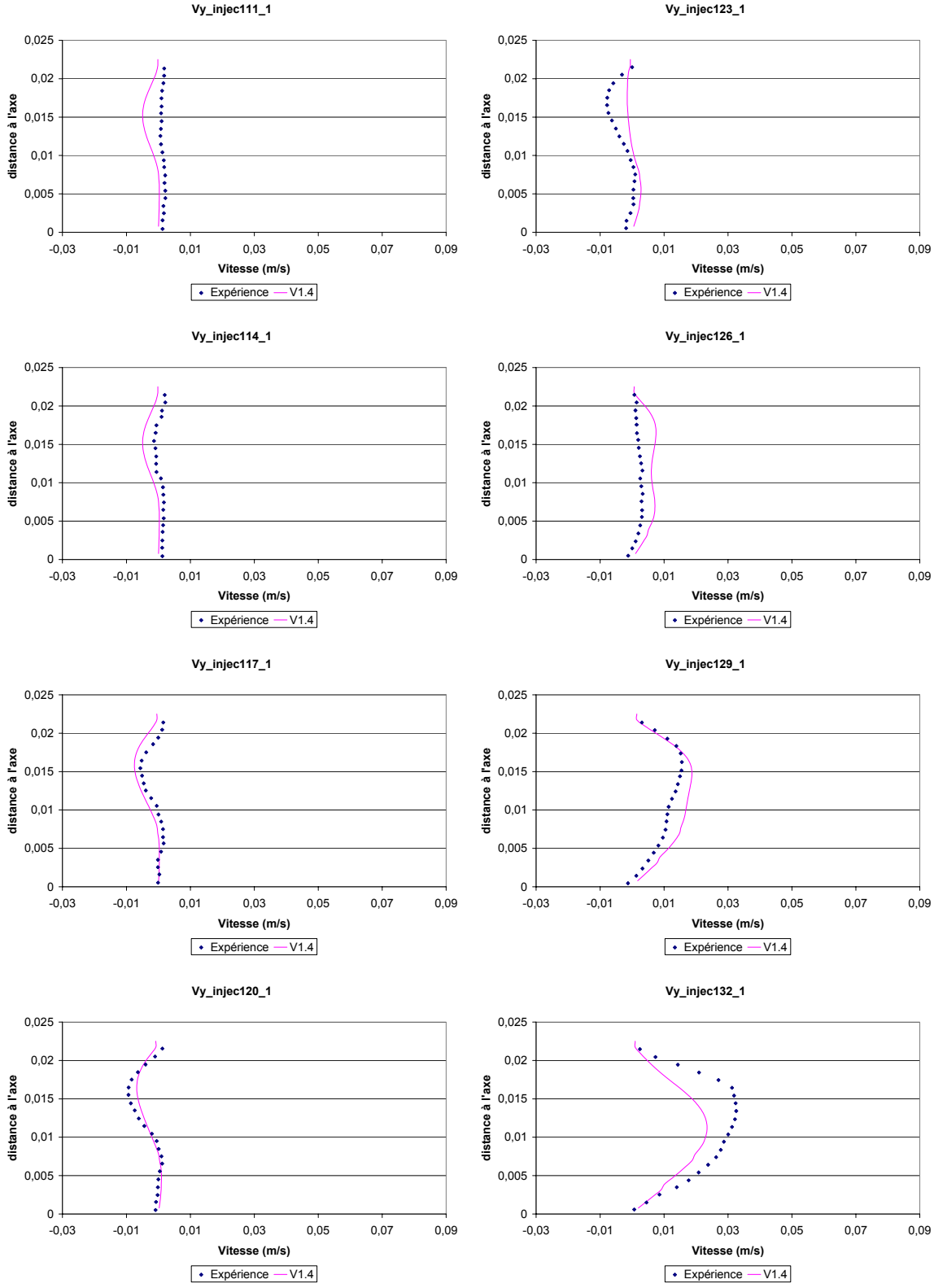


*Figure 30 : Exemples de vitesses radiales instantanées d'un fluide lors de la phase d'injection d'un piston de mouvement harmonique en configuration axisymétrique. Comparaison des valeurs numériques obtenues avec une formulation A.L.E. de type Laplacien et des données expérimentales mesurées.*

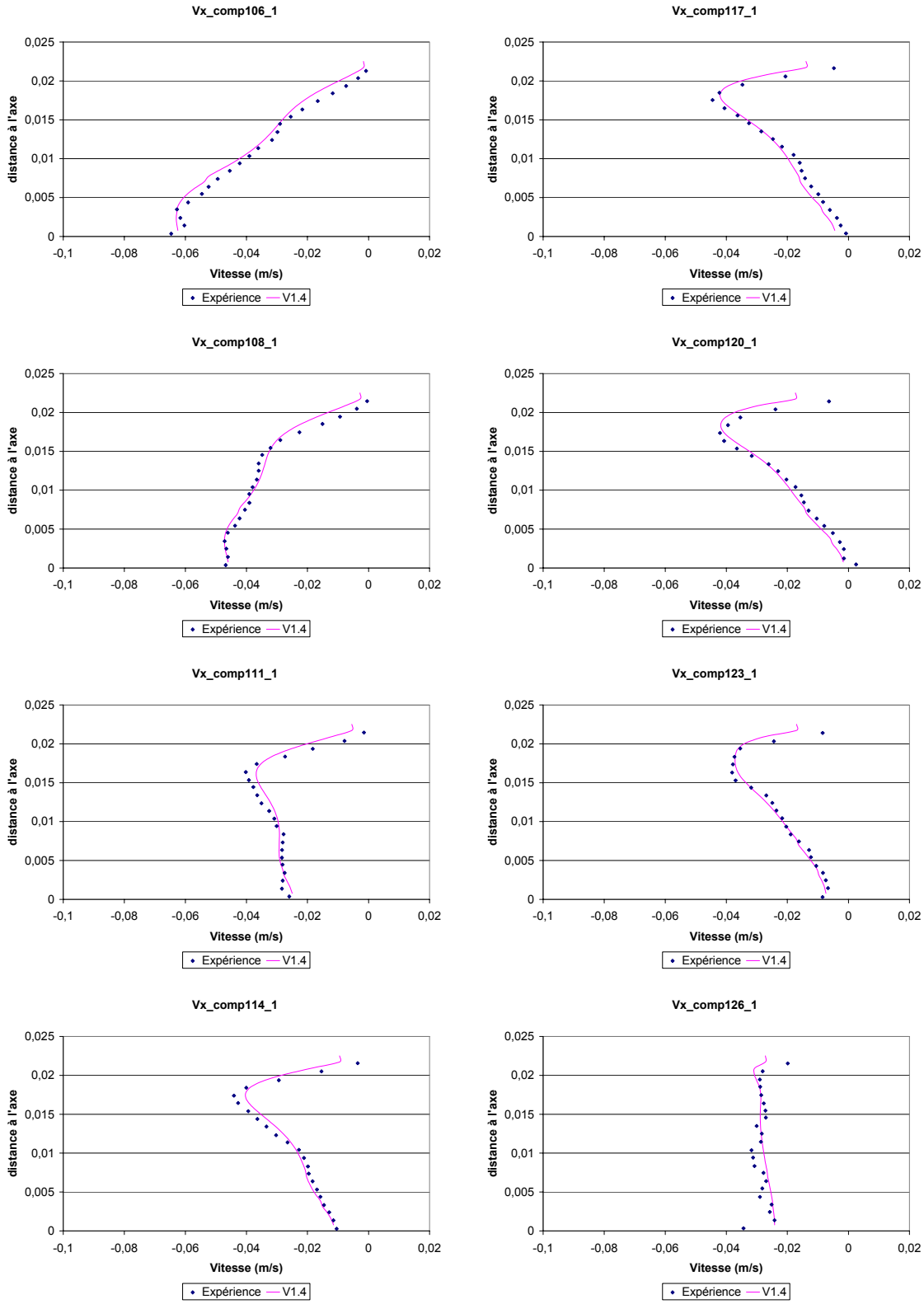


*Figure 31 : Exemples de vitesses axiales instantanées d'un fluide lors de la phase de compression d'un piston de mouvement harmonique en configuration axisymétrique. Comparaison des valeurs numériques obtenues avec une formulation A.L.E. de type Laplacien et des données expérimentales mesurées.*

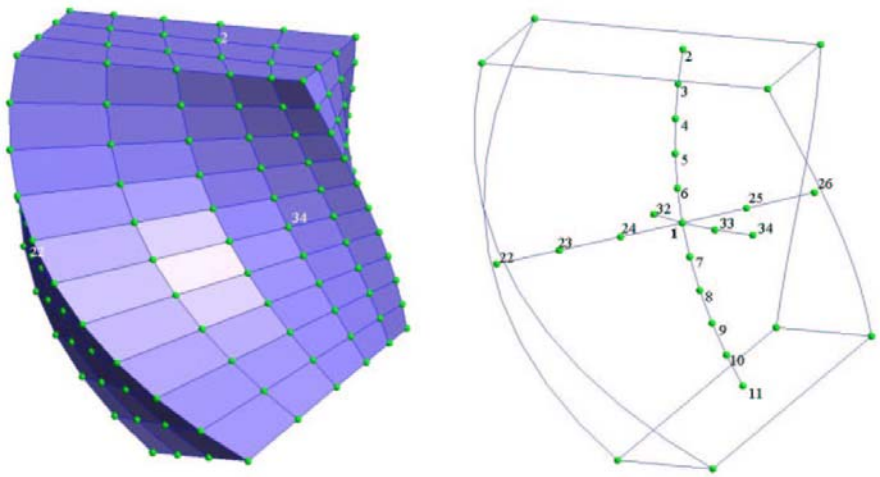


*Figure 32 : Exemple de recherche de connectivité entre nœuds par la méthode des adjacents.*

### 2.1.3. Interface fluide structure

Dans le cadre des méthodes partitionnées, une procédure itérative assure le couplage des calculs fluide et structure. Les solveurs étant à itérations en temps, un superviseur pilote le couplage temporel avec la gestion des schémas d'avancée en temps (Figure 33). Des convertisseurs assurent les transferts de données échangées entre solveurs, ce qui comprend mises en données, éventuelles projections et interpolations grilles à grilles (Figure 34). Le solveur structure reçoit les chargements thermohydrauliques pariétaux qui s'exercent sur la structure et renvoie au calculateur fluide les déplacements de l'interface qui en découlent. Les codes fluide et structure fonctionnent en parallèle ou en séquentiel et échangent les informations à chaque pas de temps. Les transferts de données sont assurés au moyen d'un formalisme de supervision gérant les appels et entrées/sorties des codes via des formats de données directement en mémoire. L'outil est intégrable et destiné à terme à être intégré au sein d'une plateforme généraliste de couplages multi-physiques basée sur des procédures partitionnées, appelée *Salomé* et co-développée par EDF R&D dans le cadre de partenariats multiples.

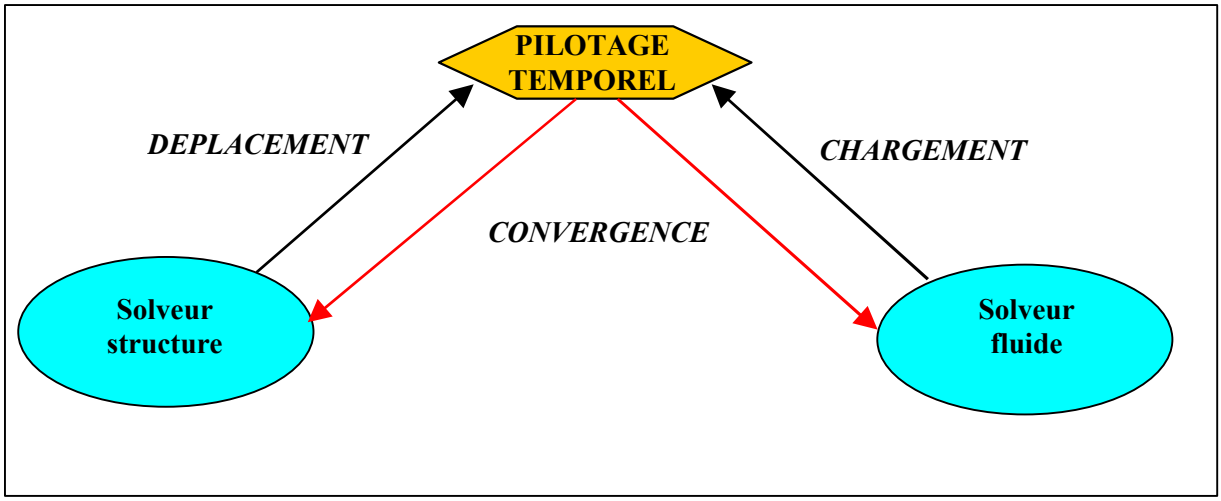


*Figure 33 :Principe du pilotage du couplage temporel dans Cosmethyc.*

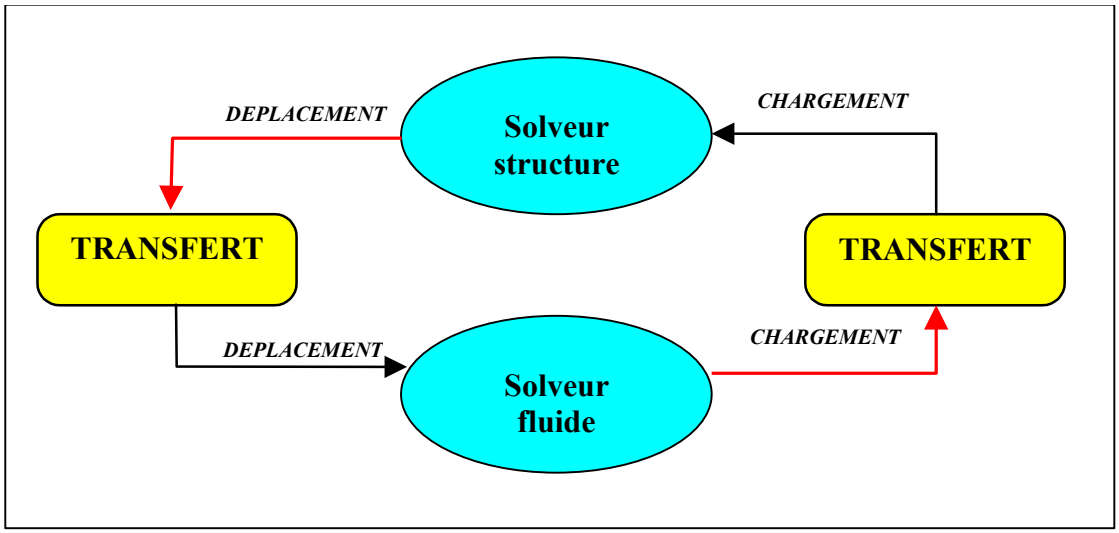


*Figure 34 :Principe du pilotage des transferts de données spatiales entre solveurs dans Cosmethyc.*

## 2.2. Couplage en temps

### 2.2.1. Couplages quasi-statique et dynamique

L'avancée en temps est gérée par le biais d'un pilote de l'algorithme de couplage qui supporte a minima :

- une procédure de couplage quasi-statique, c'est-à-dire une suite de calculs chaînés fluide structure et structure fluide, qui peut être activée pour la résolution de certains problèmes spécifiques - comme calculer la solution statique d'un problème couplé ou accélérer le processus de convergence de l'initialisation d'un calcul couplé transitoire (Figure 35).
- un algorithme de couplage dynamique qui consiste à calculer la réponse transitoire de la structure en tenant compte du chargement mécanique, thermohydraulique et des éventuels mouvements imposés. Un cycle de calcul fait intervenir à chaque pas de temps tour à tour le solveur fluide et le solveur structure. Le pilote contrôle la convergence et l'avancée en temps, c'est-à-dire le passage aux itérations ou sous-itérations suivantes (Figure 36).

### 2.2.2. Schémas de calcul

Le couplage est de type partitionné, c'est-à-dire qu'il s'agit d'un couplage de codes externe, dit couplage « faible » par opposition aux techniques de couplage « fort » qui font intervenir des procédures monolithiques intégrées dans un seul code de calcul. Plusieurs schémas de couplage « faibles » peuvent être utilisés, explicites, synchrones, asynchrones, semi-implicites (Longatte et al. 2004, Abouri et al. 2003, Piperno et Farhat 2001, 1995, 1997, Piperno 1997, Farhat et al 1995, 1997, Farhat et Lesoinne 1993). Le couplage peut être en partie implicite avec une convergence assurée par le biais d'une méthode de prédiction-correction sur les chargements fluide ou les déplacements structure et un algorithme de type point fixe (Piperno et Farhat 2001, 1995, Piperno 1997) et possibilité d'utiliser une méthode de Newton-Raphson pour accélérer le processus (Abouri 2003, Abouri et al. 2003).

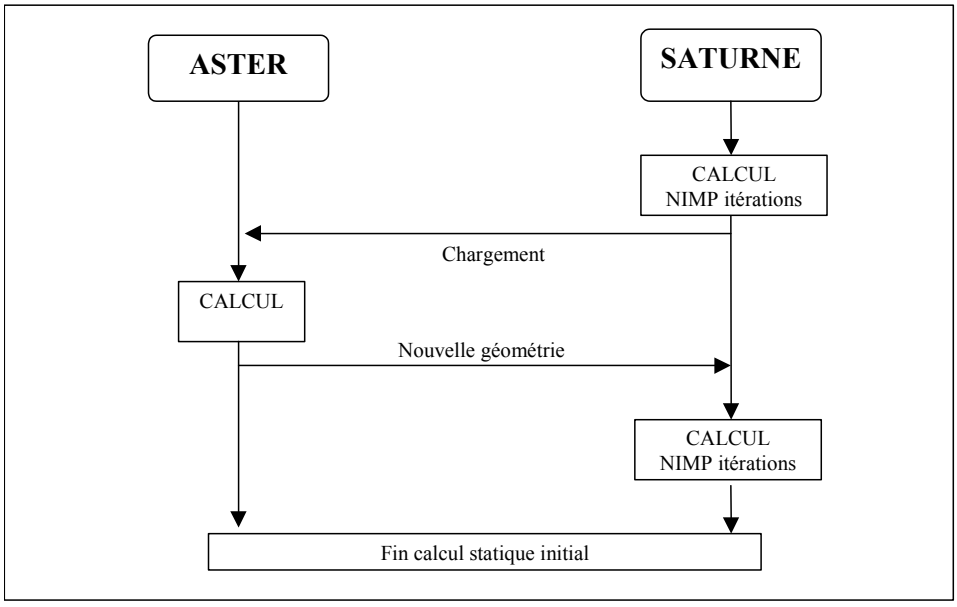


*Figure 35 : Procédure de couplage quasi-statique.*

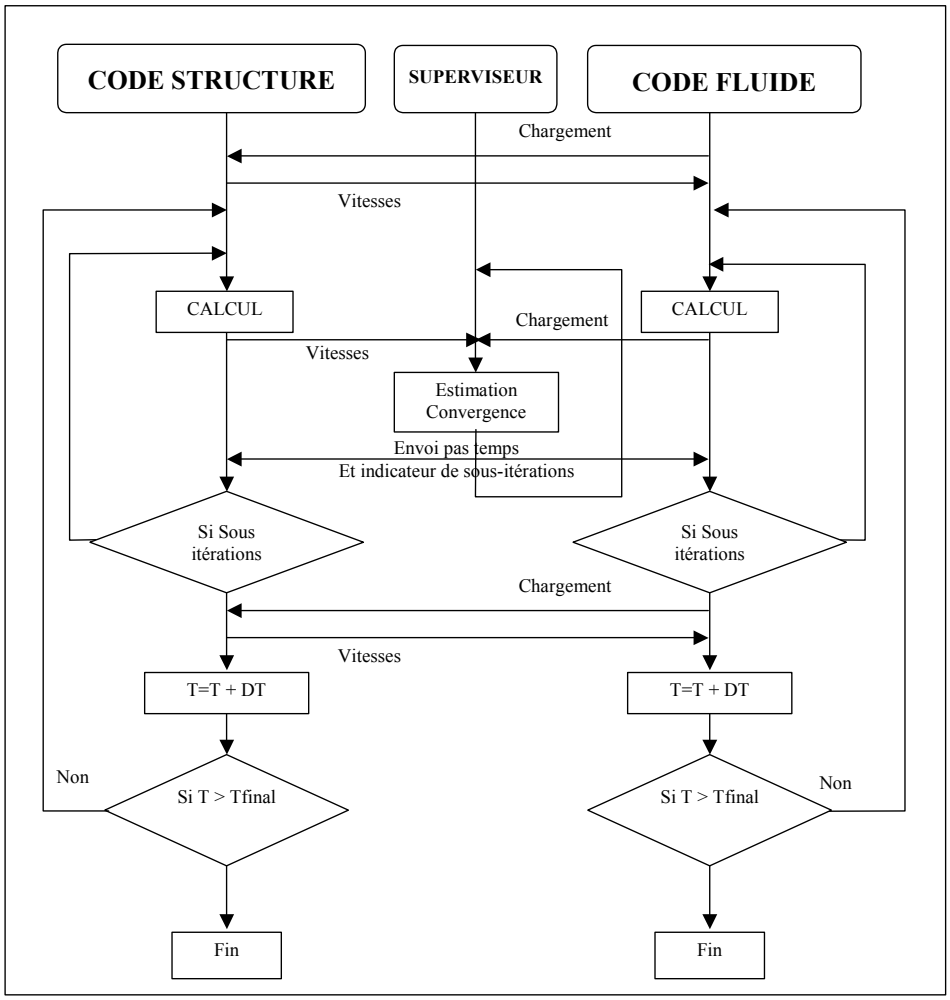


*Figure 36 : Procédure de couplage dynamique.*

Ci-dessous un exemple de schéma possible par sous-cyclage :

Le principe consiste à sous-itérer sur chaque pas de temps jusqu'à ce que la précision sur la prédiction de l'interface soit satisfaisante, moyennant le choix de critères pertinents. Soit un état fluide et un état structure donnés au temps *n*. La sous-itération *k* du pas de temps *n+1* est réalisée de la façon suivante :

- Prédiction du déplacement de l'interface (c'est-à-dire des conditions aux limites sur le déplacement de la grille de calcul fluide à la sous-itération *k* du temps *n+1*) à partir des valeurs du déplacement et de la vitesse calculées par le solveur structure à la sous-itération *k-1* de l'itération *n+1*.
- Résolution des équations fluide à la sous-itération courante à partir des grandeurs structure à la sous-itération courante, des grandeurs fluide à l'itération *n* précédente et des conditions aux limites à l'interface fluide prédite précédemment.
- Calcul des efforts fluides à appliquer à la structure.
- Résolution des équations structure à la sous-itération courante à partir des chargements précédents et des grandeurs structure obtenues à l'itération *n.*
- Test de convergence sur le déplacement entre les sous-itérations *k* et *k-1* de l'itération *n+1*.
- Passage à l'itération *n+2* en cas de convergence, sinon passage à la sous-itération *k+1* de l'itération *n+1*.

#### 2.2.3. Conservation d'énergie

Les performances de différents schémas de calcul (explicite synchrone, explicite asynchrone et implicite avec sous-cyclage) ont été comparées en terme de conservation d'énergie à l'interface sur des configurations simples (Longatte et al. 2005, Bendjeddou 2005, Annexe 10).

On considère deux masses ponctuelles en air non amorties couplées par un ressort (Figure 37). Il s'agit d'un système couplé 0D-0D dans lequel l'une des deux structures représente un fluide et l'autre une structure ponctuelle. Les erreurs entre les solutions numériques et analytiques sont comparées dans le Tableau 3 pour différents schémas de calcul. On compare la fréquence des structures ainsi que l'amortissement numérique induit par les schémas de couplage. Le schéma implicite avec sous-itérations fluide fournit le résultat le plus proche de la solution analytique et génère très peu d'amortissement numérique. Avec l'algorithme explicite asynchrone, l'amortissement numérique est légèrement plus fort mais reste constant dans le temps. En revanche le schéma explicite synchrone génère un amortissement numérique croissant dans le temps.

*Figure 37 : Configuration de type masses ponctuelles en air non amorties couplées par un ressort.*

| Ordre de grandeur de l'erreur calcul / théorie (-) | En fréquence | En amortissement |
|---|---|---|

| | | |
|---|---|---|
| *Couplage faible partitionné explicite synchrone* | *0.0* | *$8.0\ 10^{-4}$* |
| *Couplage faible partitionné explicite asynchrone* | *0.0* | *$7.0\ 10^{-6}$* |
| *Couplage faible partitionné implicite* | *0.0* | *$9.0\ 10^{-12}$* |
| *Couplage fort monolithique* | *0.0* | *$7.0\ 10^{-12}$* |
| *Solution analytique* | *0.0* | *0.00* |

*Tableau 3 : Comparaison des fréquences et amortissements des masses ponctuelles non amorties couplées par un ressort obtenus par couplages faibles partitionnés explicite synchrone, explicite asynchrone, implicite, par couplage fort monolithique et analytiquement.*

Le même exercice peut être fait avec des configurations 1D et 2D, par exemple avec des tubes et des faisceaux de tubes. Ci-dessous, on choisit une configuration simplifiée comprenant un cylindre flexible non amorti inséré dans un tube guide rigide fixe en l'absence d'écoulement permanent pour laquelle on dispose d'une solution analytique de référence pour certaines gammes de nombres de Stokes (Chen 1987, Figure 38). Les coefficients de masse et d'amortissement ajoutés par le fluide obtenus avec les différents schémas de couplage sont comparés aux valeurs analytiques et aux solutions obtenues par couplage fort monolithique dans le Tableau 4. On retrouve les conclusions précédentes. Les schémas explicite asynchrone et implicite avec sous itérations fluide sont plus conservatif qu'un schéma explicite synchrone et permettent de reproduire le comportement du système couplé fluide structure avec un bon niveau de fiabilité.

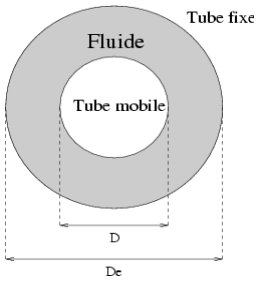


*Figure 38 : Configuration de type cylindres coaxiaux.*

| Ordre de grandeur de l'erreur calcul / théorie (-) | En fréquence | En amortissement |
|---|---|---|
| *Couplage faible partitionné explicite synchrone* | *0.0* | *0.033* |
| *Couplage faible partitionné explicite asynchrone* | *0.0* | *0.022* |
| *Couplage faible partitionné implicite* | *0.0* | *0.003* |
| *Couplage fort monolithique* | *0.0* | *0.001* |
| *Solution analytique* | *0.0* | *0.00* |

*Tableau 4 : Comparaison des masses et amortissements en configuration cylindres coaxiaux pour un tube mobile non amorti obtenus par couplages faibles partitionnés explicite synchrone, explicite asynchrone, implicite, par couplage fort monolothique et analytiquement (Chen 1987).*

## 2.3. Couplage en espace

### 2.3.1. Projections

Le couplage en espace comprend la mise en données des conditions aux limites liées à l'interface pour chaque code couplé. Les opérations à réaliser portent sur les données communes aux deux milieux à l'interface, à savoir :

- les efforts exercés par le fluide sur la structure calculés aux points de discrétisation de l'interface du milieu fluide à transmettre aux points de discrétisation de l'interface structure.
- les déplacements de la structure estimés aux points de discrétisation de son interface et à transmettre aux points de discrétisation de l'interface fluide.

On entend par points de discrétisation les entités géométriques où les équations sont résolues par les solveurs. Pour un modèle structure de type éléments finis, ces entités désignent les nœuds du maillage ; pour un modèle fluide en volumes finis, les points de discrétisation peuvent être les centres des mailles (Huvelin et al. 2006).

Les transferts de données entre grilles incluent : des conversions de données, des projections d'un maillage sur un autre (Figure 39), des condensations 3D-1D ou 2D-1D en cas de non homogénéité des dimensions entre les modélisations fluide et structure utilisées.

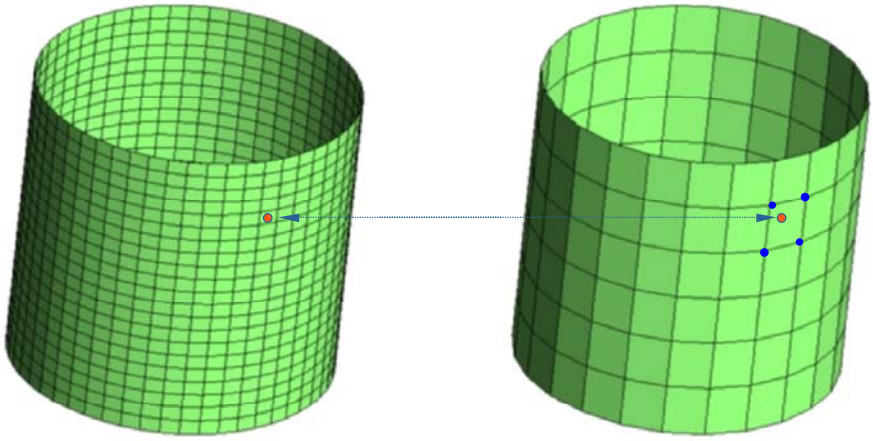

*Figure 39 : Projection de données d'une grille à une autre.*

### 2.3.2. Interpolations

Parmi les méthodes de projection de données entre maillages à l'interface, on peut citer :

- les algorithmes basés sur les multiplicateurs le Lagrange, optimaux mais sources de surcoûts en cas de raffinements de maillages importants
- les algorithmes utilisant des interpolations consistantes, très répandus et assurant, sous certaines conditions, les conditions d'équilibre à l'interface (Farhat et al. 1998, Piperno et al. 1995, Maman et Farhat 1995). Les fonctions d'interpolation étant choisies, les grandeurs, respectivement les chargements et les déplacements, sont identifiées aux points de l'interface d'un sous-système à partir des valeurs calculées aux points de discrétisation de l'interface du sous-système antagoniste.

Cette dernière technique est adaptée au cas des interfaces jointes, c'est-à-dire lorsque les interfaces fluide et structure coïncident avec l'interface physique (Figure 40-a) mais requiert le recours à des techniques de projection spécifiques en cas d'interfaces disjointes (Figure 40-b). Dans le cadre des formulations maître-esclave, l'utilisation de méthodes de projection basée sur les normales aux faces des éléments maître d'interface est usuelle (Figure 41-a), avec recours localement à des méthodes alternatives en cas d'impossibilité (changement de norme, utilisation des distances entre points de discrétisation, changement de maître, Figure 41-b).

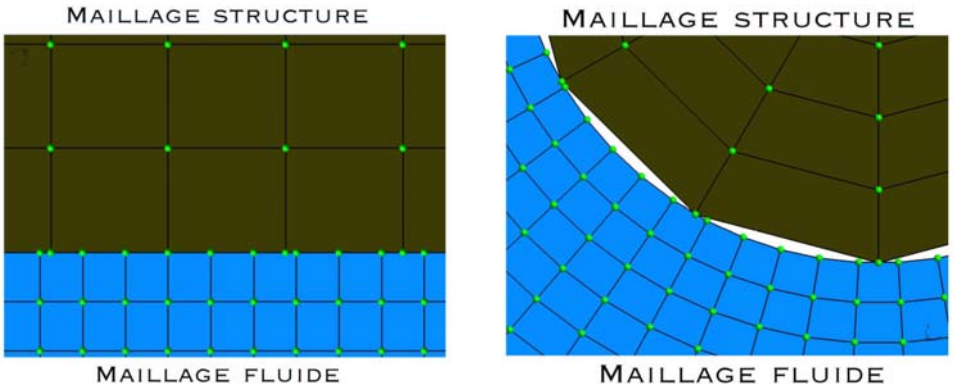


*(a)* *(b)*

*Figure 40 : (a) Exemple d'interface jointe entre maillages fluide et structure. (b) Exemple d'interface disjointe entre maillages fluide et structure.*

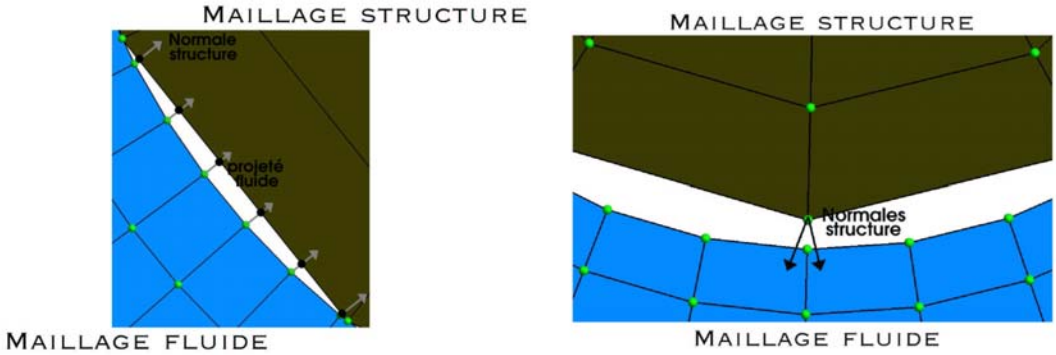


*(a)* *(b)*

*Figure 41 : (a) Méthode de projection basée sur le calcul des normales des faces maître à l'interface dans le cas où la structure est considérée comme maître. (b) Exemple de non unicité du projeté par la méthode des normales dans le cas où la structure est considérée comme maître.*

### 2.3.3. Equilibre à l'interface

La principale contrainte induite par la résolution de problèmes de couplages fluide structure étant de préserver l'équilibre entre grandeurs calculées et grandeurs transférées en amont et en aval de l'interface, plusieurs méthodes de transfert de données ont été testées dans *Cosmethyc*, l'objectif étant d'obtenir une classification des méthodes en terme de conservation d'énergie à l'interface en fonction de la nature du problème considéré (en particulier en fonction du rapport entre les niveaux de raffinement de maillages fluide et structure à l'interface, en fonction des formulations mises en œuvre dans les solveurs fluide et structure, éléments finis ou volumes finis, P1-P0/Q0 ou P1-P1/Q1). Les exemples présentés ci-dessous sont basés sur

une méthode d'interpolation avec projection par la méthode des normales, avec structure maître et moyennage par blocs des données pour la conversion 3D-1D ou 2D-1D en cas d'utilisation d'un modèle mécanique de poutre filaire.

## 3. Exemples en interactions fluide structure

Les exemples illustrés ci-dessous relèvent du domaine des vibrations de structures induites par écoulements et ont pour objet l'identification numérique des effets d'inertie et d'amortissement induit par un fluide sur une structure vibrante. La structure est une poutre représentée par un modèle filaire, elle est immergée au sein d'un fluide initialement au repos et perturbe son environnement par ses vibrations libres. Les résultats numériques obtenus avec *Cosmethyc* sont comparés à des solutions numériques, analytiques ou expérimentales disponibles (Longatte et al. 2005, 2006, Annexe 11).

### 3.1. Cylindres coaxiaux

On simule le comportement vibratoire d'un tube rigide mobile inséré dans un tube guide fixe en présence d'un fluide au repos (Figure 42) et au vu du signal de déplacement du tube dans ce milieu, on identifie les coefficients de masses et d'amortissements ajoutés par le fluide (Figure 43 et Figure 44) dans différentes configurations dépendant de la géométrie et du nombre de Stokes, le fluide pouvant être visqueux ou non visqueux. On obtient un bon accord entre les solutions numériques et théoriques (Chen et al. 1976).

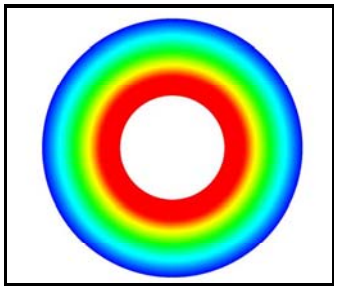

*Figure 42 : Module du déplacement du maillage pour une configuration cylindres coaxiaux en fluide au repos, tube interne mobile libre et tube externe fixe.*

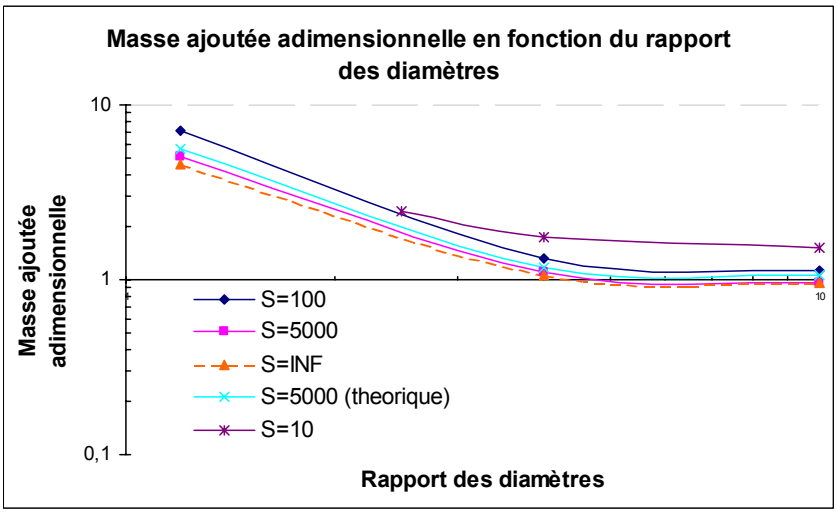


*Figure 43 : Masse ajoutée en fonction du rapport des diamètres des tubes coaxiaux pour différents nombres de Stokes en fluide visqueux (10, 100, 5000) et non visqueux (infini). Comparaison entre les solutions numériques et analytiques (Chen et al. 1976).*

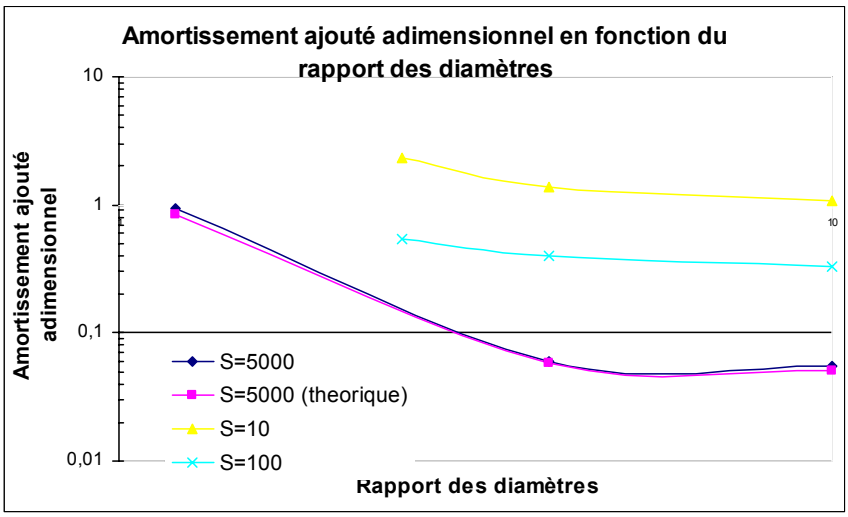


*Figure 44 : Amortissement ajouté en fonction du rapport des diamètres des tubes coaxiaux pour différents nombres de Stokes en fluide visqueux (10, 100, 5000). Comparaison entre les solutions numériques et analytiques (Chen et al. 1976, 1977).*

### 3.2. Cylindres excentrés

On procède de même pour identifier les coefficients de masses et d'amortissements ajoutés par un fluide au repos pour une configuration avec cylindres excentrés (Figure 45) et pour différentes géométries, on compare les résultats obtenus avec *Cosmethyc* à ceux fournis par une procédure de couplage monolithique éléments finis structure, éléments finis fluide (Figure 46, Chen et al. 1976) . Les résultats sont du même ordre de grandeur (Annexe 11).

### 3.3. Faisceaux de tubes

Cette configuration présente un intérêt industriel pour les études vibratoires des composants constitués de faisceaux de tubes. Ces derniers étant en général de grande taille, les faisceaux peuvent être assimilés à des assemblages infinis de rangées de tubes de sorte qu'en première approximation, on peut considérer que la géométrie des faisceaux est périodique suivant la direction transverse aux tubes. Cette hypothèse est d'autant plus utile qu'elle permet de réduire la taille du domaine de calcul fluide en introduisant une cellule de faisceau de tubes périodique, la simulation d'un domaine de calcul complet étant généralement hors de portée, surtout à grands nombres de Reynolds, dans les conditions de fonctionnement industriel. L'identification du motif élémentaire a été réalisée en fluide au repos. Un exemple de calcul des coefficients de masses et d'amortissements ajoutés en faisceau en fluide au repos est fourni (Figure 47) et les résultats numériques sont comparés aux solutions analytiques de Rogers et al. (1994) basées sur une équivalence configuration faisceau – configuration tubes coaxiaux bien choisie (Tableau 5). Les résultats sont en accord (Annexe 11).

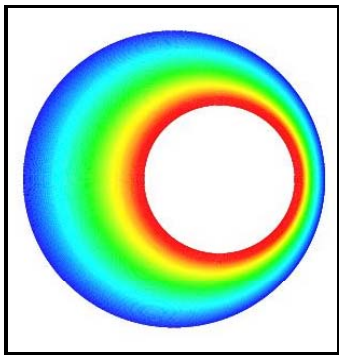

*Figure 45 : Module du déplacement du maillage pour une configuration cylindres coaxiaux excentrés en fluide au repos, tube interne mobile libre et tube externe fixe.*

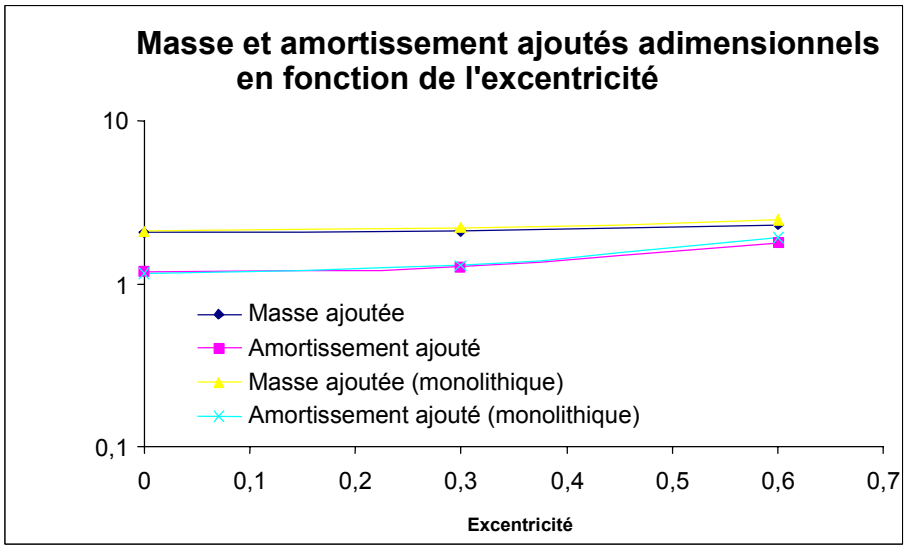


*Figure 46 : Masse et amortissement ajoutés en fonction de l'excentricité. Comparaison entre la solution numérique obtenue avec Cosmethyc et par couplage monolithique (Chen et al. 1976, Yang et Moran 1979).*

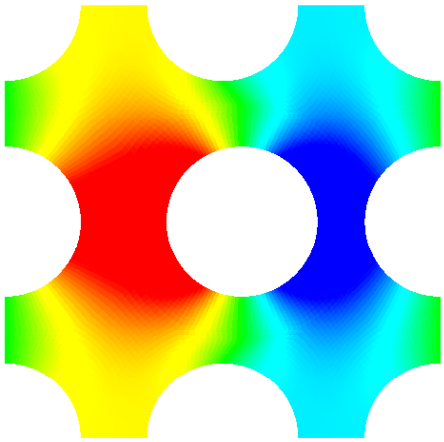

*Figure 47 : Cellule périodique de faisceau de tubes en fluide au repos. Tube central plein mobile libre, tubes coupés fixes.*

| | Masse ajoutée (-) | Amortissement ajouté (-) |
|---|---|---|
| *Numérique (Cosmethyc)* | *1.077* | *721.8* |
| *Analytique (Rogers et al. 1994)* | *1.074* | *723.4* |

*Tableau 5 : Comparaison des masses et amortissements ajoutés par le fluide pour un faisceau de tubes de pas réduit 1.44 et un nombre de Stokes de l'ordre de 1500.*

# 4. Exemples de couplages fluide-élastiques

On cite ci-dessous deux exemples de simulation d'effet de couplage fluide-élastique avec *Cosmethyc*, c'est-à-dire de couplage fluide structure non conservatif : le cas dit du tuyau d'arrosage et le cas du faisceau de tubes soumis à un écoulement transverse. Dans les deux cas, le départ en instabilité de la structure est générée par l'apport d'amortissement négatif à la structure sous l'effet du couplage entre l'écoulement et l'un des modes de vibration de la structure. Pour ces différentes configurations, l'identification de la vitesse réduite correspondant au seuil critique de départ en instabilité de la structure en accord avec les prévisions analytiques ou expérimentales disponibles témoigne du caractère prédictif de l'outil *Cosmethyc*. En particulier, l'identification fiable de l'amortissement renseigne sur l'aptitude des méthodes de couplage mises en œuvre pour assurer la conservation de l'énergie au niveau de l'interface fluide structure aussi bien pour l'avancée en temps que pour les transferts de données entre solveurs (Huvelin et al. 2006).

## 4.1. Tuyau d'arrosage

La configuration est représentative d'un cylindre flexible contenant un fluide visqueux en écoulement (Figure 48). Parmi toutes les solutions numériques et analytiques disponibles pour ce type de configurations, dans différentes conditions de géométrie et d'écoulement et pour différents paramètres comme le rapport de masses entre fluide et structure, on présente une configuration avec cylindre d'extrémités encastrée-libre pour laquelle sont disponibles des solutions analytiques dont une basée sur une analogie avec un cylindre immergé dans un fluide en écoulement (Païdoussis) et des solutions numériques obtenues avec une méthode de transpiration (Renou 1998, Fernandez-Varela 2001) valable en petits déplacements (Annexe 9).

Au vu du signal de déplacement du tube (Figure 49), on obtient avec *Cosmethyc* une bonne identification de la fréquence (Figure 50) et de l'amortissement (Figure 51) des vibrations du tube pour différentes vitesses d'écoulement ce qui permet une identification correcte de la vitesse critique de départ en instabilité, c'est-à-dire de la vitesse réduite pour laquelle l'amortissement de la structure s'annule et devient négatif (Figure 51).

## 4.2. Faisceaux de tubes

L'identification de la vitesse critique d'un faisceau de tubes avec *Cosmethyc* est illustrée sur la Figure 52. Ces résultats ouvrent la voie à de nombreuses applications industrielles de l'outil, a minima dans le domaine des vibrations et des couplages fluide structure (Schäfer et al. 2001, 2005, Sigrist et al. 2004, Fischer et al. 2003, Abouri et al. 2003).

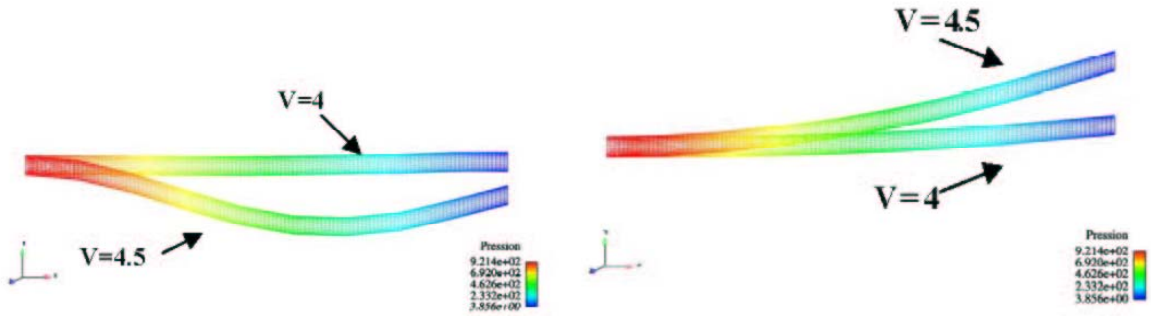


*Figure 48 : Configuration de type cylindre flexible contenant un fluide en écoulement à différentes vitesses. Déformées du tube pour un vitesse réduite en-deçà de la vitesse critique de départ en instabilité (à gauche), au-delà (à droite).*

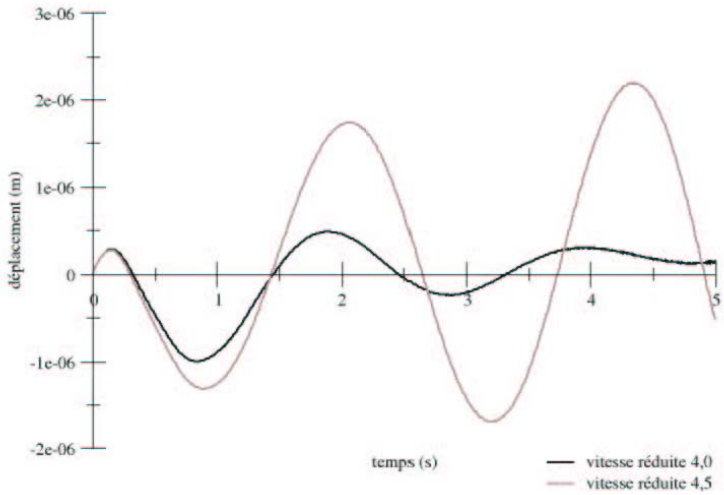


*Figure 49 : Signal de déplacement d'un point de la structure flexible pour deux valeurs de la vitesse réduite en-deçà et au-delà de la vitesse critique de départ en instabilité.*

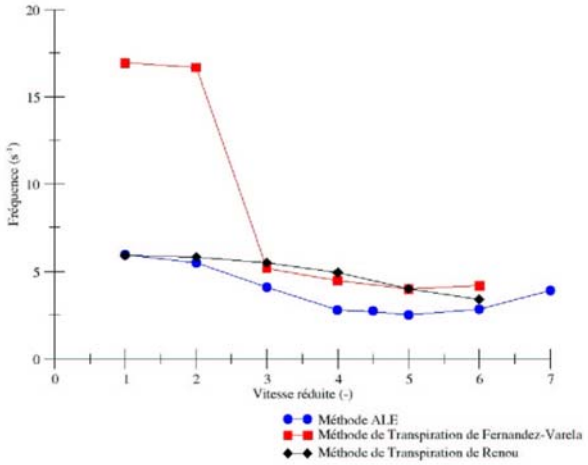


*Figure 50 : Fréquence des vibrations du cylindre en fonction de la vitesse réduite estimée avec Cosmethyc et avec une méthode de transpiration (Renou 1998, Fernandez Varela 2001).*

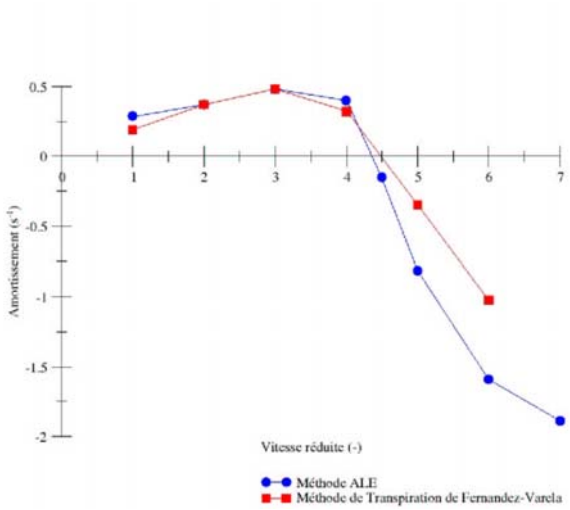


*Figure 51 : Amortissement des vibrations du cylindre en fonction de la vitesse réduite estimée avec Cosmethyc et avec une méthode de transpiration (Fernandez Varela 2001).*

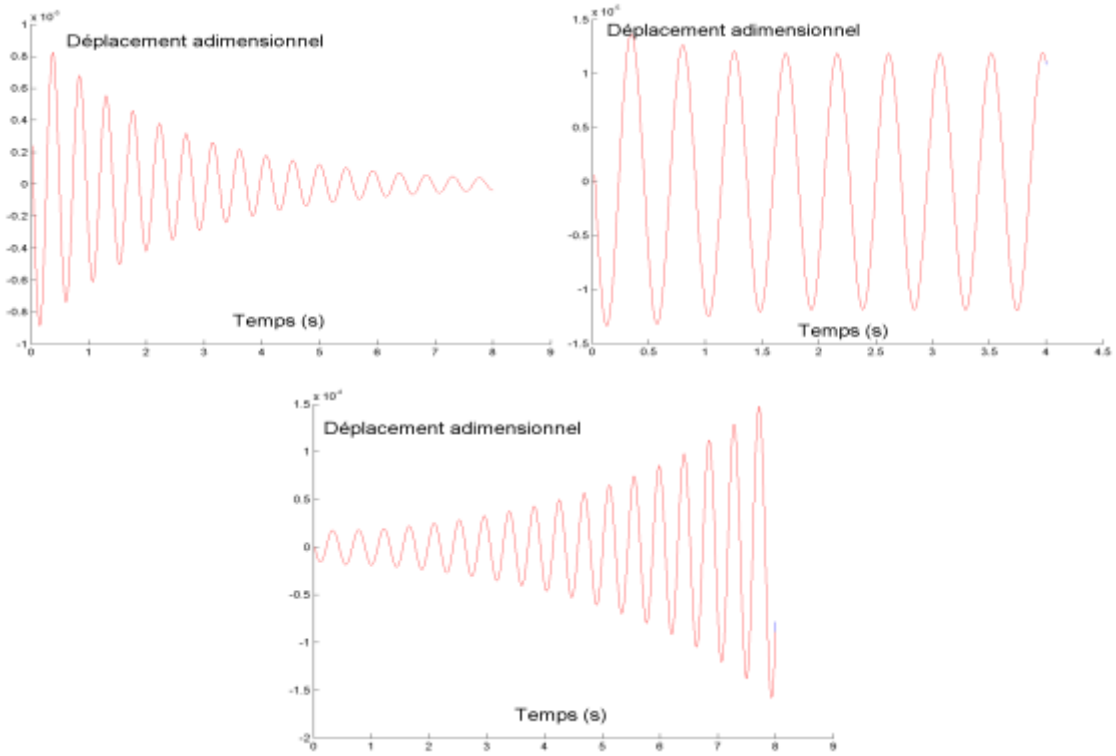


*Figure 52 : Identification de la vitesse critique de départ en instabilité d'un tube dans un faisceau de tubes soumis à un écoulement transverse. Signal de déplacement du tube pour une vitesse réduite inférieure (en haut à gauche), égale (en haut à droite) et supérieure (en bas) à la vitesse critique.*

## Annexe 8 : Coupleur fluide structure

**Longatte, E.**, Bendjeddou, Z., Souli, M. (2003). Methods for numerical study of tube bundle vibrations in cross flows. *Journal of Fluids and Structures, 18, 513-528*.

## Annexe 9 : Simulation de couplages forts

Huvelin, F., **Longatte, E.**, Verreman, V., Souli, M. (2006). Numerical simulation of dynamic instability for a pipe conveying fluid. *PVP Conference*, Vancouver.

## Annexe 10 : Propriétés du couplage

**Longatte, E.**, Bendjeddou, Z., Verreman, V., Souli, M. (2005). Explicit and implicit code coupling schemes in fluid structure interaction. *PVP Conference*, Denver.

## Annexe 11 : Couplages forts en faisceaux de tubes

**Longatte, E.**, Verreman, V., Bendjeddou, Z., Souli, M. (2005). Comparison of strong and partitioned fluid structure code coupling methods. *PVP Conference*, Denver.

ELSEVIER

Journal of Fluids and Structures 18 (2003) 513–528

JOURNAL OF FLUIDS AND STRUCTURES

www.elsevier.nl/locate/jnlabr/yjfls

# Methods for numerical study of tube bundle vibrations in cross-flows

E. Longatte[a,*], Z. Bendjeddou[b], M. Souli[b]

[a] *Fluid Mechanics and Heat Transfer Department, EDF-R&D Division, 6 Quai Watier, Chatou 78400, France*
[b] *Mechanical Engineering Department, University of Lille, 1 Boulevard Paul Langevin, Lille 59655, France*

Received 14 March 2003; accepted 18 August 2003

**Abstract**

In many industrial applications, mechanical structures like heat exchanger tube bundles are subjected to complex flows causing possible vibrations and damage. Part of fluid forces are coupled with tube motion and the so-called fluid-elastic forces can affect the structure dynamic behaviour generating possible instabilities and leading to possible short term failures through high amplitude vibrations. Most classical fluid force identification methods rely on structure response experimental measurements associated with convenient data processes. Owing to recent improvements in Computational Fluid Dynamics, numerical simulation of flow-induced vibrations is now practicable for industrial purposes. The present paper is devoted to the numerical identification of fluid-elastic effects affecting tube bundle motion in presence of fluid at rest and one-phase cross-flows. What is the numerical process? When fluid-elastic effects are not significant and are restricted to added mass effects, there is no strong coupling between structure and fluid motions. The structure displacement is not supposed to affect flow patterns. Thus it is possible to solve flow and structure problems separately by using a fixed nonmoving mesh for the fluid dynamic computation. Power spectral density and time record of lift and drag forces acting on tube bundles can be computed numerically by using an unsteady fluid computation involving for example a large Eddy simulation. Fluid force spectra or time record can then be introduced as inlet conditions into the structure code providing the tube dynamic response generated by flow. Such a computation is not possible in presence of strong flow structure coupling. When fluid-elastic effects cannot be neglected, in presence of tube bundles subjected to cross-flows for example, a coupling between flow and structure computations is required. Appropriate numerical methods are investigated in the present work. The purpose is to be able to provide a numerical estimate of the critical flow velocity for the threshold of fluid-elastic instability of tube bundle without experimental investigation. The methodology consists in simulating in the same time thermohydraulics and mechanics problems by using an arbitrary Lagrange Euler (ALE) formulation for the fluid computation. A fully coupled numerical approach is suggested and applied to the numerical prediction of the vibration frequency of a flexible tube belonging to a fixed tube bundle in fluid at rest or in flow. Numerical results turn out to be consistent with available experimental data obtained in the same configuration. This work is a first step in the definition of a computational process for the full numerical prediction of tube bundle vibrations induced by flows.


## 1. Introduction

In many industrial configurations, mechanical structures such as PWR components are subjected to complex flows causing possible vibrations and damage and as far as nuclear security is concerned, it is necessary to prevent wear

*Corresponding author.
*E-mail addresses:* elisabeth.longatte@edf.fr (E. Longatte), mhamed.souli@univ-lillel.fr (M. Souli).

0889-9746/$ - see front matter © 2003 Elsevier Ltd. All rights reserved.
doi:10.1016/j.jfluidstructs.2003.08.010

**Nomenclature**

| | |
|---|---|
| $C_f$ | added damping in flow per unit length (N s/m$^2$) |
| $C_s$ | structural damping per unit length (N s/m$^2$) |
| $C_w$ | added damping in still water per unit length (N s/m$^2$) |
| $\overline{\overline{D}}$ | fluid deformation tensor (s$^{-1}$) |
| $D_e$ | tube outer diameter (m) |
| $D_o$ | tube outer diameter in test facility (m) |
| $D_i$ | tube inner diameter (m) |
| $f$ | tube frequency (Hz) |
| $f_o$ | forced tube frequency (Hz) |
| $f_f$ | fluid-elastic force per unit length (N/m) |
| $f_t$ | turbulent force per unit length (N/m) |
| $K_s$ | structural stiffness per unit length (N/m$^2$) |
| $K_f$ | added stiffness in flow per unit length (N/m$^2$) |
| $\overline{\overline{I}}$ | identity tensor (dimensionless) |
| $L$ | tube length (m) |
| $M_a$ | added mass per unit length (kg/m) |
| $M_s$ | structural mass per unit length (kg/m) |
| $P$ | pitch in square tube bundle (m) |
| $\overline{\overline{R}}$ | Reynolds stress tensor (N m/kg) |
| St | Stokes number (dimensionless) |
| $x$ | tube displacement (m) |
| $x_o$ | forced tube displacement (m) |
| $U$ | pitch flow velocity (m/s) |
| $\xi_a$ | tube damping ratio in still air (%) |
| $\xi_e$ | tube damping ratio in still water (%) |
| $\xi_f$ | tube damping ratio in flow (%) |
| $\overline{\overline{\sigma_f}}$ | fluid stress tensor (N/m$^2$) |
| $\overline{\overline{\sigma_s}}$ | structure stress tensor (N/m$^2$) |
| $\omega$ | "in flow" circular frequency $\omega = 2\pi f$ (rad/s) |
| $\omega_d$ | forced frequency in still water (rad/s) |
| $\omega_w$ | circular frequency in still water (rad/s) |
| $\omega_a$ | circular frequency in still air (rad/s) |

problems generated by vibration fatigue. In this context, many experiments are carried out at EDF in order to predict turbulent and fluid-elastic forces responsible for possible flow-induced vibration problems. These forces can sometimes be directly measured by transducers but with direct approaches it is often difficult to stand between the different physical mechanisms involved when a distributed external loading is considered. On the contrary, indirect experimental prediction methods have shown their ability to provide fluid force estimates. Most of them rely on force density analytical models depending themselves on unknown spectral scaled parameters (Corcos, 1963; Gagnon and Païdoussis, 1994; Axisa et al., 1990). They are thus not always reliable, especially in the presence of complex turbulent flows. An advanced indirect approach has also been developed by EDF since about 15 years (Granger and Perotin, 1997a, b). It relies on structural vibration response measurement. After convenient transfer function calculation and data processing, the method provides an estimate of fluid excitations acting on dynamic structures. A modal modelling of the mechanical system is used and a spatial orthonormal decomposition of force fields is combined with a regularization process ensuring the closure system. This approach is efficient and it has been applied to the prediction of turbulent and fluid-elastic forces acting on tubes (Granger and Perotin, 1997a, b) and on PWR components like rod cluster control assemblies (Longatte et al., 2000) and heat exchanger tube bundles (Adobes et al., 2001). However, this technique often involves high costs because it relies on modelling fitted with experimental data deduced from measurements carried out on specific devices. As far as tube bundle vibrations in cross-flows are concerned, it is also possible to use a semi-analytical quasi-unsteady modelling fitted with experimental, numerical or analytical data and providing tube response expressed in terms of drag and lift force coefficients (Granger and Païdoussis, 1995; Granger and Gay, 1996). However, this modelling does not describe all physical phenomena involved by flow-induced vibrations.

In order to reduce experiments and to be able to study many configurations involving complex flow-induced vibration problems, numerical methods are also considered. Owing to recent developments incorporated into Computational Fluid Dynamic (CFD) codes, numerical simulation of flow structure coupling is investigated. There are three cases to be considered, as follows.

(i) In presence of fluid at rest, without flow, mass and damping terms added by fluid can be identified numerically by using a moving mesh formulation for the fluid computation. An Arbitrary Lagrange Euler (ALE) formulation is required (Souli et al., 1999; Souli, 2000, 2001; Souli and Zolesio, 2001) and structure motion is introduced in the fluid calculation as a moving boundary conditions.

(ii) In presence of turbulent flows, when turbulent forces are the most significant and fluid-elastic effects are reduced to added mass and damping effects, structural motion effects acting on turbulent flow patterns can be neglected. It is then possible to perform thermohydraulics and mechanics calculations separately (Benhamadouche and Laurence, 2002). Turbulent force spectrum and time record can be simulated by using large Eddy simulation (LES) and introduced as inlet conditions into the mechanical calculation providing the structure vibration response. LES has already been applied to the numerical prediction of turbulent loading acting on tubes subjected to turbulent mainly axial flows without confinement and numerical results turned out to be in good agreement with available analytical or experimental data (Moreno et al., 2000; Longatte et al., 2001).

(iii) Finally, in presence of flow with high fluid-elastic effects, it is necessary to use a specific numerical method. The configuration we are interested in is a flexible tube moving in a fixed tube bundle submitted to cross-flows (Fig. 1). The methodology consists in simulating in the same time thermohydraulics and mechanics problems by using an ALE formulation (Bendjeddou et al., 2002; Longatte et al., 2002). The purpose is to take into account the coupling between flow and structural motions. The fluid computational domain is distorted at each time step of the process to account for tube motion and associated strains and conversely fluid forces acting on structure walls are used to compute wall displacements.

The second configuration is not investigated here (Longatte et al., 2001). The present work is devoted to the study of the first and the third cases, i.e. to the identification of fluid-elastic parameters of tubes in fluid at rest and in cross-flows. The main objectives and methods are specified in the first section. The second part is devoted to the presentation of ALE formulations and of their application to the prediction of fluid-elastic parameters of tubes in fluid at rest. In the third part, the main flow-structure coupling processes are discussed and some results related to tube flow-induced vibrations are presented. According to the comparisons between numerical results and available experimental data, it is demonstrated that a full numerical simulation of tube bundle vibrations in cross-flows is now reachable.

## 2. Objectives

### 2.1. Physical problem

In nuclear power plants heat exchanger tube bundles carrying primary fluid are subjected to cross-flows of secondary fluid. External fluid forces may generate high magnitude vibrations of tubular structures causing possible dramatic damages in terms of nuclear safety. Vibrations result from four kinds of fluctuations (Pettigrew and Taylor, 2002a, b;

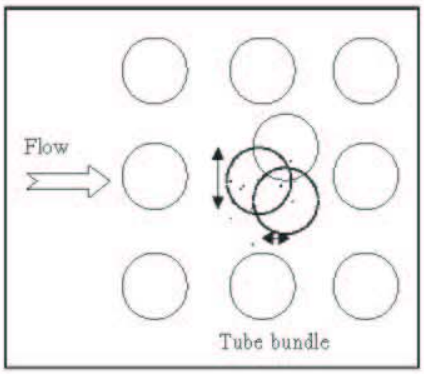


Fig. 1. Lift and drag force effects on a flexible tube belonging to a fixed tube bundle in cross-flow.

Chen, 1987; Price and Païdoussis, 1989): (i) random fluctuations generated by turbulence in fluid at large Reynolds numbers; (ii) fluctuations induced by structure-flow motion coupling due to fluid-elastic effects; (iii) resonance with flow periodicity due to vortex shedding; and (iv) possible acoustic excitation.

Fluid-elastic forces and resonance with flow periodicity resulting from this coupling can affect the structural dynamical behaviour, causing possible instabilities and leading to possible short term failures through high magnitude vibrations. For industrial concerns, it is necessary to be able to predict these fluid-elastic forces and their effects on tube bundle dynamic stability. In the present work we focus our attention on this kind of fluid forces.

Flow-structure interaction induces energy exchange between flow and structural motions and, up to a critical flow velocity, the flow-structure system may become unstable and high magnitude structure displacements occur. Fig. 2 features a typical response showing tube motion amplitude and cross-flow velocity.

Fluid-elastic instability development has been widely studied experimentally and many experiments were carried out to identify critical flow velocity in many different configurations. Experimental data resulting from these studies gave rise to available reference instability maps providing critical velocity thresholds in terms of tube bundle characteristic parameters. The purpose of the present work is to build a numerical method to retrieve numerically the laws between tube bundle parameters and critical flow velocity.

### 2.2. *Fluid-elastic parameters definition*

We are interested in the study of vibrations of a flexible tube belonging to a regular fixed tube bundle subjected to a fluid coupling, with or without flow. This configuration is defined by known parameters describing the system geometry and hydraulics (Adobes et al., 2001). For each configuration to be studied, for a given parameter gather, fluid-elastic forces may affect tube motion. As we will see below, fluid-elastic effects can be expressed and measured in terms of fluid-elastic parameters. These coefficients were previously identified experimentally in many different configurations (Chen, 1986; Price and Païdoussis, 1986). The purpose here is to show how to estimate numerically these fluid-elastic parameters.

Geometric parameters characterizing a regular tube bundle are the following: tube external and internal diameters $D = D_e$ and $D_i$; tube gap $P$; tube row angle $\theta$; and tube bundle length $L$. From a mechanical point of view, the flexible tube motion is characterized by: tube mass $M_s$; tube stiffness $K_s$; tube damping $C_s$; and mass of the tube internal fluid $M_f$. In presence of one vibration mode, which may be a double one, and is denoted $s$, the equation of motion of the tube without fluid can be written as follows:

$$M_s\ddot{x} + C_s\dot{x} + K_s x = 0, \tag{1}$$

or equivalently,

$$\ddot{x} + 2\xi_s\omega_s\dot{x} + \omega_s^2 x = 0, \tag{2}$$

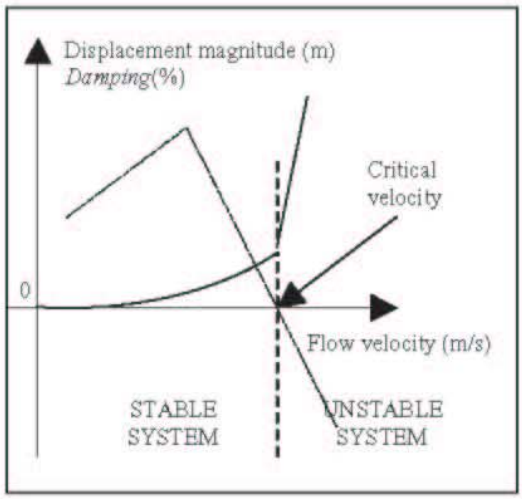


Fig. 2. Critical flow velocity generating structure instability development.

where $\omega_s$ and $\xi_s$ designate pulsation and damping coefficients of the tube alone defined by

$$K_s = M_s\omega_s^2 \tag{3}$$

and

$$C_s = 2M_s\omega_s\xi_s. \tag{4}$$

Concerning the hydraulics parameters, the flow is supposed to cross-perpendicularly the tube bundle and the axial component is zero. The flow is totally defined by its Reynolds number,

$$\mathrm{Re} = \frac{\rho D U}{\mu},$$

where $U = U_{\mathrm{gap}} = [P/(P-D)]U_\infty$ designates the gap velocity, $U_\infty$ the inlet flow velocity before crossing the tube bundle and $\mu$ the fluid dynamic viscosity. Concerning the structural motion in the fluid at rest, the apparent mode mass and damping are affected by added mass effects (represented by $M_a$), by internal fluid mass effects (represented by $M_i$) and by fluid viscosity (represented by $C_v$) . The equation of motion becomes

$$(M_s + M_a + M_i)\ddot{x} + (C_s + C_v)\dot{x} + K_s x = 0, \tag{5}$$

or

$$\ddot{x} + 2\xi_e\omega_e\dot{x} + \omega_e^2 x = 0, \tag{6}$$

where $\omega_e$ and $\xi_e$ designate the pulsation and damping coefficients of the tube in fluid at rest. Then one can use the following identification:

$$K_s = M_s\omega_s^2 = (M_s + M_a + M_i)\omega_e^2.$$

This yields

$$M_a = M_s\left(\frac{\omega_s^2}{\omega_e^2} - 1\right) - M_i, \tag{7}$$

$$C_v = 2(M_s + M_a + M_i)\omega_e\xi_e - C_s. \tag{8}$$

If one knows the structural parameters in air, mass and damping terms added by the fluid are totally expressed in terms of tube frequency and damping in fluid at rest.

In presence of flow, stiffness and damping terms are affected as follows:

$$(M_s + M_a + M_i)\ddot{x} + (C_s + C_f + C_v)\dot{x} + (K_s + K_f)x = F_t, \tag{9}$$

with $F_t$ designating fluid forces independent on structure motion. Equivalently one gets

$$\ddot{x} + 2\xi_f\omega_f\dot{x} + \omega_f^2 x = 0, \tag{10}$$

and after identification

$$(K_s + K_f) = (M_s + M_a + M_i)\omega_f^2,$$

$$(C_s + C_f + C_v) = 2\zeta_f\omega_f(M_s + M_a + M_i).$$

Finally, the stiffness and damping terms added by flow are given by

$$K_f = (M_s + M_a + M_i)\omega_f^2 - M_s\omega_s^2,$$

$$C_f + C_v = 2\omega_f\xi_f(M_s + M_i + M_a) - 2M_s\omega_s\xi_s.$$

They can be expressed in terms of tube frequency and damping in air and in flow as follows:

$$K_f = M_s\omega_s^2\left(\frac{\omega_f^2}{\omega_e^2} - 1\right), \tag{11}$$

$$C_f + C_v = 2M_s\left(\omega_f\xi_f\frac{\omega_s^2}{\omega_e^2} - \omega_s\xi_s\right). \tag{12}$$

From a practical point of view, the critical flow velocity is reached when a structure dynamic instability develops. That is the reason why it is important to be able to control these parameters. The fluid-elastic parameters $M_a$, $C_f$, $C_v$ and $K_f$ can be identified experimentally after measurement of tube frequency and damping in air, in fluid at rest and in

flow. The purpose of the present work is to introduce a method for the numerical evaluation of these parameters. This requires specific techniques (i) to perform the fluid computation, (ii) to perform the structural calculation, (iii) and finally to make the data-exchange possible between the two calculations by using a convenient moving boundary condition or an appropriate code coupling process. The computational process is described below.

### 2.3. Computational process

In continuum mechanics one can describe fluid motion with two classical formulations: (a) An Eulerian formulation: one focuses as his attention on a particular volume in space. This volume is fixed with respect to a laboratory frame, and one consider the fluid as it passes through the fixed volume. The fluid is continuously renewed inside the domain and a convective term is introduced in the basic equations of motion to express the material time derivative in the reference configuration; (b) A Lagrangian formulation: one identifies and follows a particular region of fluid. The volume of fluid changes in shape while the total mass remains constant. The computational domain mesh moves with the particle flow velocity and this may lead to an element entanglement. This formulation is not convenient in presence of high magnitude motions.

For problems involving moving wall boundaries, it is necessary to have a middle formulation following the boundary motion and preserving the element shape in the same time. An ALE formulation has been introduced to ensure these capabilities. Finite element ALE formulation for incompressible viscous flows has been introduced by Hughes et al. (1981), Liu and Huerta (1988), Belyschko et al. (1982), and the finite difference formulation by Noh (1964) and Hirt et al. (1974). The purpose of the ALE algorithm is to enable the computational mesh to remain regular even in presence of high magnitude structure displacements (Benson, 1989).

In the present work, an ALE formulation is used to study numerically the vibrations of a tube in fluid at rest and a tube in cross-flow. From a numerical point of view there are two cases to be considered:

(i) the tube motion can be introduced as a moving boundary condition and the fluid problem is solved by using an ALE formulation involving a time-dependent computational domain; or

(ii) a flow-structure code coupling is required to account for interactions between fluid and structure problems. At each time step, the fluid problem is solved on the reactualized computational domain and fluid forces acting on the flexible tube are estimated. These forces are then introduced as inlet conditions in the right-hand side of mechanical equation (1) providing tube displacement and velocity, the tube velocity is used to deform the computational mesh and to estimate the new problem geometry at each iteration.

Both cases are considered below. In each case, numerical methods are described and results are discussed. Finally, one gets a full computational process, making it possible to identify numerically all fluid-elastic parameters characterizing tube bundle vibrations in cross-flows.

## 3. Numerical methods

### 3.1. ALE formulation

The ALE formulation was previously used to solve defence problem and nowadays its application was extended to free surface problems, high velocity impact, offshore structures, multi-physics problems. It has also medical applications like modelling of blood vessel deformation. There are two ways to solve ALE equations: the first one which is used here corresponds of an Eulerian viewpoint, the fully coupled equations are solved in one step; this approach can only handle with one-phase flows; the second method described by Souli et al. (1999, 2000) is a split method: it uses two steps to solve ALE equations: (i) a Lagrangian step in which the mesh moves with material velocity, and (ii) an advection step where the mesh moves from its material position to its arbitrary position. This method is better to model two-phase flows for explosion modelling for instance.

Here the ALE method is investigated to evaluate numerically the fluid-elastic parameters of a flexible tube in tube bundle in fluid at rest or in flow. In the framework of Arbitrary Lagrangian Eulerian formulations the fluid dynamic problem is solved as follows. One defines three domains in space and associated mappings from one domain to another (Fig. 3). The first one is called the material domain $\Omega_m$ and follows the fluid particle motion $X$ (Lagrangian formulation). The second domain called spatial domain $\Omega_x$ is fixed and occupies fixed positions in space $x$ (Eulerian formulation). It is convenient to rely the Eulerian and Lagrangian space reference coordinates, respectively, $x$ and $X$ as follows:

$$x = x(X, t),$$

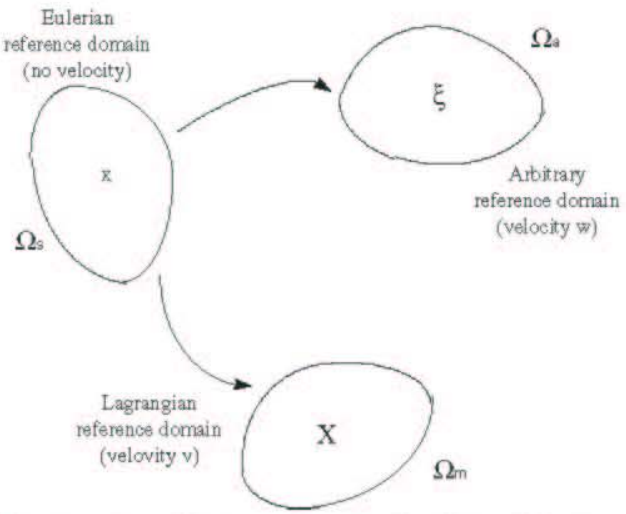


Fig. 3. Representation of Eulerian, Lagrangian and arbitrary reference domains $\Omega_e$, $\Omega_m$ and $\Omega_a$ whose velocities are, respectively 0, $v$ and $w$.

$$\left.\frac{\partial x}{\partial t}\right|_X = v(X,t) = v(x,t), \tag{13}$$

with $v$ the material velocity. Moreover, the material time derivative of a physical property $\phi$ is given by

$$\frac{\partial \phi}{\partial t} = \left.\frac{\partial \phi(X,t)}{\partial t}\right|_X = \left.\frac{\partial \phi(x,t)}{\partial t}\right|_x + \left.\frac{\partial \phi(x,t)}{\partial x_i}\right|_t v_i(x_i,t). \tag{14}$$

Finally, a third domain is introduced, called the arbitrary domain $\Omega_a$, with an arbitrary motion different from the material domain motion. In the fixed spatial domain $\Omega_e$, the arbitrary domain may be described by coordinates $\xi$ expressed as follows:

$$x = x(\xi,t), \tag{15}$$

$$\left.\frac{\partial x}{\partial t}\right|_\xi = w(\xi,t) = w(x,t),$$

with the following time derivative expression:

$$\left.\frac{\partial \phi(\xi,t)}{\partial t}\right|_\xi = \left.\frac{\partial \phi(x,t)}{\partial t}\right|_x + \left.\frac{\partial \phi(x,t)}{\partial x_i}\right|_t w_i(x_i,t). \tag{16}$$

In presence of structural wall motion, it is then useful to choose the arbitrary domain $\Omega_a$ according to the moving structure boundaries. In this way, $\xi$ and $\omega$ designate location and velocity of the domain $\Omega_a$. Thus, the governing equations in $\Omega_a$ are deduced from the ALE formulation. If one assumes the fluid is incompressible, the mass, momentum and energy conservation equations are formulated as follows:

$$\mathrm{div}_x(v) = 0, \tag{17}$$

$$\rho\left\{\left.\frac{\partial v}{\partial t}\right|_\xi + (v-w)\,\mathrm{grad}_x(v)\right\} = -\mathrm{grad}_x(p) + \mathrm{div}_x(\mu\,\mathrm{grad}_x(v)) - \rho\mathrm{div}_x(R),$$

$$\rho\left\{\left.\frac{\partial R_{ij}}{\partial t}\right|_\xi + (v-w)\,\mathrm{grad}_x(R_{ij})\right\} = -P_{ij} + \rho\Phi_{ij} - d_{ij} - \rho\varepsilon_{ij},$$

$$\rho\left\{\left.\frac{\partial \varepsilon}{\partial t}\right|_\xi + (v-w)\,\mathrm{grad}_x(\varepsilon)\right\} = \rho C_{\varepsilon 1}\frac{\varepsilon}{k}P - \rho C_{\varepsilon 2}\frac{\varepsilon^2}{k} + \mathrm{div}_x(B(\mathrm{grad}_x(\varepsilon)).$$

Here $R$ describes the Reynolds tensor defined by

$$R_{ij} = \overline{v_i' v_j'}.$$

In the framework of turbulence statistical approaches, each physical field $\phi$ can be split into two components: a mean part $\bar{\phi}$ and a fluctuating part $\phi'$; i.e.,

$$\phi = \bar{\phi} + \phi'.$$

In order to solve this problem it is necessary to introduce the mapping from one domain to the others. The relation between Eulerian $x$ and Arbitrary Lagrangian $\xi$ coordinates is ensured by

$$J = J(\xi, t) = \left| \frac{\partial x_i}{\partial \xi_j} \right| \quad \text{with} \quad J = Id \text{ due to the first-order discretization.}$$

Finally, all fields are expressed in terms of $J$ in $\Omega_a$ and at each time step the solution is projected in the new spatial domain $\Omega_s$. The point is that it is necessary to compute the velocity $w$ or the displacement $x$ of the arbitrary domain. A first-order approximation consists in relying velocity and displacement by

$$\xi_j^{n+1} = \xi_j^n + w_j^n \Delta t,$$

with $\Delta t$ the time step, $\xi_j^n$ and $\xi_j^{n+1}$ the displacement of $\Omega_a$ at time steps $n$ and $n+1$, and $w_j^n$ the velocity at time step $n$.

In order to compute displacement, the domain $\Omega_a$ is represented as a continuum domain. The difficulty in the ALE formulation is to choose an appropriate arbitrary velocity in order to avoid element entanglement. There are many algorithms to get this velocity (Souli et al., 1999; Soli, 2000). In the general case, the mesh is considered as an elastic body and its distortion is solution of a classical "mechanical problem". A stress tensor is defined for the mesh and this tensor can be a linear or nonlinear function of displacement or velocity.

In this computation the mesh domain corresponds to an incompressible fluid, it has thus a constant volume and the stress tensor is chosen as a linear function of velocity. For instance one can assume that the mesh is the most distorted near moving boundaries and the distortion propagates through the full domain, falling to zero far from the

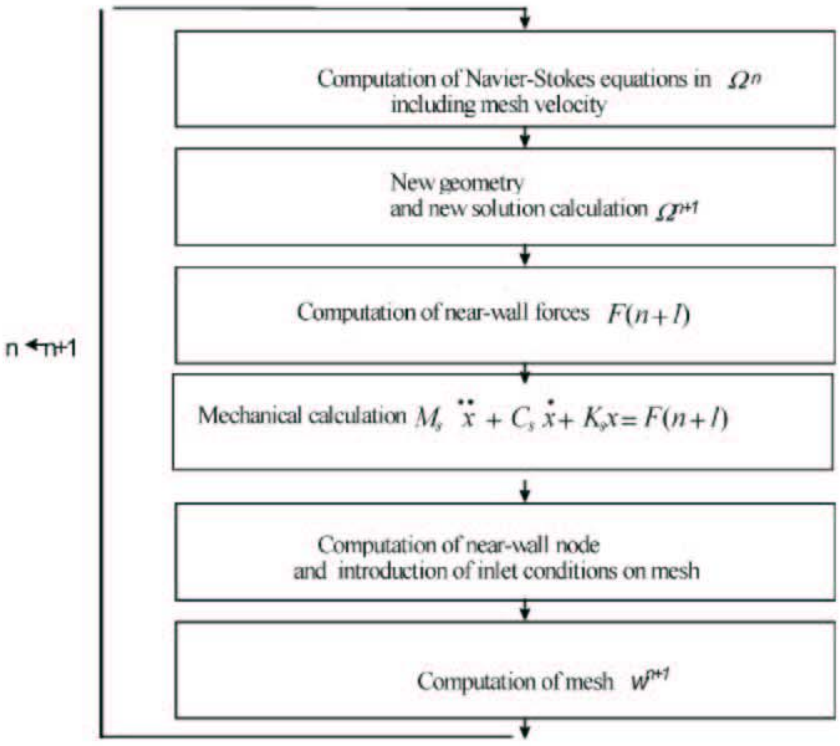


Fig. 4. Computational process for flow and structure motion coupling.

boundaries. This process can be described by a classical diffusion equation for $w$ or $\xi$ in $\Omega_a$:

$$\mathrm{div}(\lambda\,\mathrm{grad}\,w) = 0 \tag{18}$$

associated with convenient boundary conditions as displacements are known on moving and nonmoving arbitrary domain boundaries. $\lambda$ designates a specific viscosity to be defined. In the present work one puts $\lambda = 1$ far from the moving boundary and $\lambda = 10^6$ near the tube to keep the mesh distortion homogeneous near moving walls.

Moreover, the fluid dynamic code used in the present work relies on a finite volume formulation with nonstructured meshes. Hence physical mean fields are computed on element volumes and normal gradients are estimated on each volume boundary. In the case of a nonstructured mesh, gradients may be rebuilt. Here meshes are cell-centred and fields are explicitly expressed in volume centres and in face centres. Finally, a semi-implicit method for pressure linked equations (SIMPLE algorithm) is used and one solves a linear system by using an iterative method, like the preconditioned conjugate gradient for pressure and Jacobi or Gauss–Seidel method for velocity. The mechanical equation is solved by using a second order centred scheme or a Newmark scheme. The mesh velocity $w$ is also cell-centred and the velocity of each node is explained as a simple average of velocities cells including this node.

### 3.2. *Fluid force modelling*

The structure response is directly generated by near-wall fluid forces. At each time step of the fluid calculation, lift and drag forces acting on the flexible tube and responsible for its motion are estimated. These forces are expressed in terms of the stress tensor $\overline{\overline{\sigma}}$ by

$$\vec{F} = \vec{T}S, \tag{19}$$

where $S$ designates the wall surface and $\vec{T}$ is defined by

$$\vec{T} = \overline{\overline{\sigma}} \cdot \vec{n}, \tag{20}$$

with $\vec{n}$ the unitary normal vector of the structure wall. According to the Stokes approximation, the stress tensor expression is given by

$$\overline{\overline{\sigma}} = -p\overline{\overline{I}} + 2\mu\overline{\overline{D}} \quad \text{for laminar flows,}$$

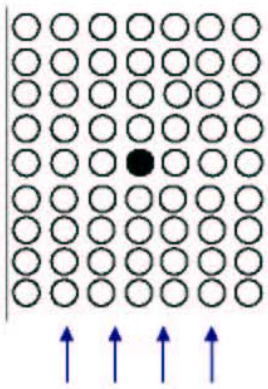

Fig. 5. Experimental set-up section: in-line tube bundle including $7 \times 9$ fixed tubes except the middle tube that is moving in presence of cross-flow.

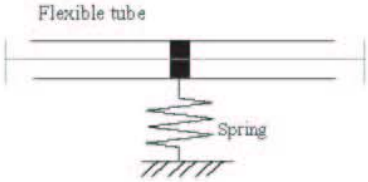


Fig. 6. Supporting process of the middle flexible moving tube.

Table 1
Flexible tube characteristic parameters

| | |
|---|---|
| Tube modal mass $M_s$ (kg) | 0.223 |
| Internal fluid modal mass $M_i$ (kg) | 0.061 |
| Tube length $L$ (m) | 0.250 |
| Tube external diameter $D_e$ (m) | 0.022 |
| Tube modal stiffness $K_s$ (N/m) | 13185 |
| Tube modal damping $\xi_s$ (%) | 0.13 |

Table 2
Flexible tube characteristic parameters

| | |
|---|---|
| Tube vibration frequency $f_t$ (Hz) | 38.7 |

$\overline{\overline{\sigma}} = -p\overline{\overline{I}} + 2\mu\overline{\overline{D}} - \rho\overline{\overline{R}}$ with a Reynolds stress-model for turbulent flows.

The vortex shedding frequency is characterized by the Strouhal number: $\mathrm{St} = fD/U$, with $f$ the lift force frequency. Vortex shedding is a well-known phenomenon for a single tube in cross-flow but it is much more complicated for tube bundle and in this case the determination of the Strouhal number is difficult and depends on Reynolds number and tube confinement.

### 3.3. Coupling process

To account for fluid or flow structure coupling it may be necessary to use a code coupling to simulate both physical problems in the same time. The full computational process may be described as follows (Fig. 4). It relies on an ALE formulation for the fluid computation. At each step $n$ of the fluid calculation, Navier–Stokes equations are solved in the fluid computational domain $\Omega^n$ and the system is modified to take into account a mesh velocity in the momentum conservation equation for the convective term. Then the new geometry and the new solution are calculated in domain $\Omega^{n+1}$. Near-wall forces $F^{n+1}$ acting on the moving tube are deduced from stress tensor at step $n+1$. These forces are introduced in the right-hand side of tube motion equations (1). According to Eq. (9), they can be identified to added flow effects as follows:

$$M_s\ddot{x} + C_s\dot{x} + K_s x = F = -(M_a + M_i)\ddot{x} - (C_f + C_v)\dot{x} - K_f x. \tag{21}$$

The mechanical calculation provides displacement $x$ describing tube motion. Tube node velocity is then deduced from near-wall node displacement and it is introduced as inlet conditions on mesh velocity. Finally, the mesh velocity $w^{n+1}$ is computed in the full domain $\Omega^{n+1}$ at step $n+1$ by solving the mesh diffusion equation.

In this way, one takes into account both fluid effects on tube displacements and conversely tube motion effects on fluid patterns. The previously mentioned method relies on a first-order explicit staggered coupling scheme. The main disadvantage of this approach is that the energy conservation equation for the full system is not satisfied because structure or fluid energy is numerically dissipated or created at the fluid–structure boundary.

To avoid this unwanted property another method is also considered. It consists in using other kinds of staggered synchronous or asynchronous schemes minimizing errors on numerical energy dissipation (Piperno and Farhat, 2001). It is also possible to use implicit code coupling process introducing sub-cycling until convergence of fluid calculation at each time step (Hermann and Steindorf, 1999).

## 4. Application

### 4.1. Test case

The previously mentioned numerical methods were used to build a complete numerical tool devoted to the prediction of tube vibrations in fluid at rest and in cross-flows. Numerical simulations were carried out on a specific test case corresponding to an experimental device (Granger et al., 1993). In this configuration many experimental data are available providing tube vibration frequency, damping ratio and r.m.s. vibration in terms of gap velocity. The

Table 1
Flexible tube characteristic parameters

| | |
|---|---|
| Tube modal mass $M_s$ (kg) | 0.223 |
| Internal fluid modal mass $M_i$ (kg) | 0.061 |
| Tube length $L$ (m) | 0.250 |
| Tube external diameter $D_e$ (m) | 0.022 |
| Tube modal stiffness $K_s$ (N/m) | 13185 |
| Tube modal damping $\xi_s$ (%) | 0.13 |

Table 2
Flexible tube characteristic parameters

| | |
|---|---|
| Tube vibration frequency $f_s$ (Hz) | 38.7 |

$\overline{\overline{\sigma}} = -p\overline{\overline{I}} + 2\mu\overline{\overline{D}} - \rho\overline{\overline{R}}$ with a Reynolds stress-model for turbulent flows.

The vortex shedding frequency is characterized by the Strouhal number: $St = fD/U$, with $f$ the lift force frequency. Vortex shedding is a well-known phenomenon for a single tube in cross-flow but it is much more complicated for tube bundle and in this case the determination of the Strouhal number is difficult and depends on Reynolds number and tube confinement.

### 3.3. Coupling process

To account for fluid or flow structure coupling it may be necessary to use a code coupling to simulate both physical problems in the same time. The full computational process may be described as follows (Fig. 4). It relies on an ALE formulation for the fluid computation. At each step $n$ of the fluid calculation, Navier–Stokes equations are solved in the fluid computational domain $\Omega^n$ and the system is modified to take into account a mesh velocity in the momentum conservation equation for the convective term. Then the new geometry and the new solution are calculated in domain $\Omega^{n+1}$. Near-wall forces $F^{n+1}$ acting on the moving tube are deduced from stress tensor at step $n+1$. These forces are introduced in the right-hand side of tube motion equations (1). According to Eq. (9), they can be identified to added flow effects as follows:

$$M_s\ddot{x} + C_s\dot{x} + K_s x = F = -(M_a + M_i)\ddot{x} - (C_f + C_v)\dot{x} - K_f x. \tag{21}$$

The mechanical calculation provides displacement $x$ describing tube motion. Tube node velocity is then deduced from near-wall node displacement and it is introduced as inlet conditions on mesh velocity. Finally, the mesh velocity $w^{n+1}$ is computed in the full domain $\Omega^{n+1}$ at step $n+1$ by solving the mesh diffusion equation.

In this way, one takes into account both fluid effects on tube displacements and conversely tube motion effects on fluid patterns. The previously mentioned method relies on a first-order explicit staggered coupling scheme. The main disadvantage of this approach is that the energy conservation equation for the full system is not satisfied because structure or fluid energy is numerically dissipated or created at the fluid–structure boundary.

To avoid this unwanted property another method is also considered. It consists in using other kinds of staggered synchronous or asynchronous schemes minimizing errors on numerical energy dissipation (Piperno and Farhat, 2001). It is also possible to use implicit code coupling process introducing sub-cycling until convergence of fluid calculation at each time step (Hermann and Steindorf, 1999).

## 4. Application

### 4.1. Test case

The previously mentioned numerical methods were used to build a complete numerical tool devoted to the prediction of tube vibrations in fluid at rest and in cross-flows. Numerical simulations were carried out on a specific test case corresponding to an experimental device (Granger et al., 1993). In this configuration many experimental data are available providing tube vibration frequency, damping ratio and r.m.s. vibration in terms of gap velocity. The

test-section is described in Fig. 5. An in-line tube bundle includes $7 \times 9$ fixed tubes, except the middle tube that is moving under the action of cross-flow. In the cross-direction the bundle is limited by two parallel walls simulating symmetry conditions. The flexible tube support is depicted in Fig. 6. The mockup was so built that the tube can only move in the cross-direction without any deformation. The tube displacement is called $x$ and it is governed by a mechanism whose characteristic parameters are an apparent spring stiffness $K_s$ and an apparent damping ratio $\xi_s$.

The main tube mechanical and geometrical parameters are reported in Table 1. According to these data, the theoretical tube motion frequency without fluid is deduced from Eq. (3), (Table 2).

### 4.2. Computation of tube vibration frequency in still water

The purpose is to evaluate numerically fluid-elastic parameters of a flexible tube in fluid at rest, i.e. added mass and damping terms induced by the fluid: $M_a$ and $C_v$. An ALE formulation is used and there is no fluid–structure coupling, as the structure is supposed not to be affected by the fluid and its motion is imposed.

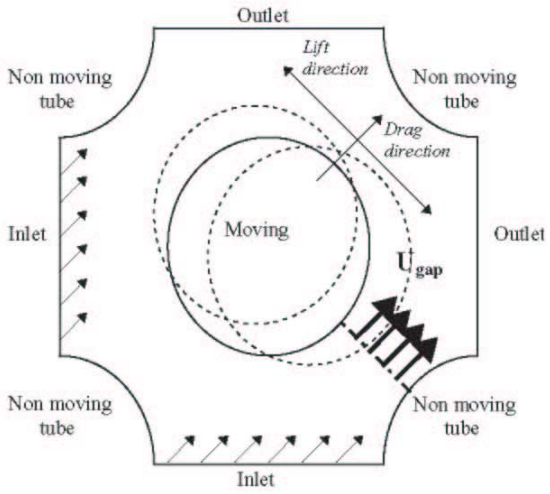


Fig. 7. Fluid computational domain providing a simplified representation of the experimental set-up depicted in Fig. 5. The tube bundle is supposed to be infinite. With periodic inlet and outlet conditions, each flexible tube neighbour is fixed and the tube motion is not expected to affect the other flexible tube motion. Inlet flow rates is introduced to get the convenient gap velocity $U_{gap}$. The tube is expected to move in the drag direction and to oscillate in the lift direction.

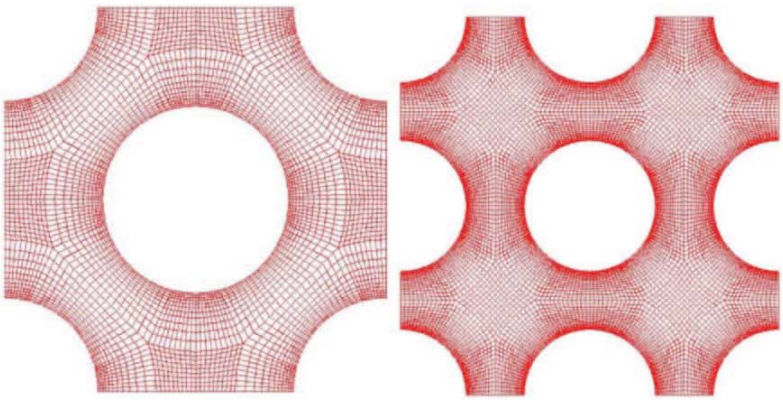

Fig. 8. Fluid computational domain mesh section at time step $n = 0$ in 5-tubes (left) and 9-tubes (right) configurations.

*4.2.1. Fluid computational domain*

Numerical simulation of the previous experiment relies on simplified assumptions making the calculation easier and shorter. The fluid computational domain describing the experimental set-up is represented in Fig. 7. It is restricted to the smallest tube bundle cell featuring periodicity involving 5 or 9 tubes as shown on Fig. 8, showing also the associated meshes. The tube bundle is supposed to be infinite in the lift and drag directions. This assumption is checked if one only considers vibrations of the middle tube in the tube bundle (Fig. 5). The fluid flow is supposed to be two-dimensional (2-D) and each tube is supposed to have infinite length in the length direction.

*4.2.2. Boundary conditions*

The computational domain is limited by periodic inlet and outlet conditions on the flow. In this way each near neighbour of the flexible tube is fixed and interactions between several flexible tubes are neglected. Periodic and free outlet boundary conditions have been tested. To model periodic boundary conditions, periodic cells are added to the real mesh and a term source is defined and introduced in the right-hand side of Navier–Stokes equations to keep a constant flow rate in case of fluid motion. One uses a second-order Newton method to compute the term source (Benhamadouche and Laurence, 2002).

There is no fluid flow, so turbulence effects and added stiffness decrease to null if displacements remain small. Here the fluid motion is only due to structural displacements and one keeps small tube displacements in order to keep laminar flow and neglect the turbulence forces.

Furthermore, the structural motion is supposed to be linear and a modal base is defined to compute displacement. To model correctly the fluid forces, the boundary condition between fluid and structure must be defined properly and precisely. Here the continuity of velocity and normal stress tensor at the fluid–structure interface is satisfied. No wall law is used on the moving boundary.

*4.2.3. Identification of tube vibration frequency in fluid at rest*

The tube motion is introduced as an imposed harmonic boundary condition solution of the homogeneous structure problem. For this calculation a periodic tube motion is imposed as fluid and mesh inlet conditions with a fixed frequency $\omega_d = 2\pi f_d$. At each time step fluid forces acting on the tube are estimated. According to Eq. (5) these forces are expressed in terms of added mass and viscosity damping terms as follows:

$$(M_s + M_l)\ddot{x} + C_s\dot{x} + K_s x = F = -M_a\ddot{x} - C_v\dot{x}. \tag{22}$$

Table 3
Inlet data for the calculations in fluid at rest : tube imposed harmonic frequency $f_d$ (Hz) and tube vibration magnitude $x_o$ (m)

| | Inlet data 9 tubes | Inlet data 5 tubes |
|---|---|---|
| Harmonic frequency $f_d$ (Hz) | 29 | 29 |
| Tube displacement magnitude $x_o$ (m) | $10^{-4}$ | $10^{-4}$ |

Table 4
Numerical results for the calculation in fluid at rest in terms of force magnitudes $F_o$ (N) and phase $\varphi$ between forces and tube displacement

| | Results 9 tubes | Results 5 tubes |
|---|---|---|
| Force magnitude $F_o$ (N) | $2.7 \times 10^{-3}$ | $1.9 \times 10^{-3}$ |
| Force phase $\varphi$(rad) | 0.06 | 0.06 |

Table 5
Comparison between added mass term $M_a$ deduced numerically from Eq. (24) and experimentally from Eq. (7). Good agreement between tube frequency in the fluid at rest deduced from Eq. (5) numerically and experimentally

| | Num. 9 tubes | Num. 5 tubes | Exp. |
|---|---|---|---|
| Added mass $M_a$ (kg) | 0.104 | 0.057 | 0.116 |
| Frequency in fluid at rest $f_s$ (Hz) | 29.3 | 31.3 | 29.0 |

For an harmonic tube motion $x = x_o e^{i\omega_d t}$, fluid forces are also periodic $F = F_o e^{i(\omega_d t+\varphi)}$, with $\varphi$ the phase between fluid forces and tube displacement, and they can be split into two parts:

$$F_o e^{i\varphi} e^{i\omega_d t} = -M_a \ddot{x} - C_v \dot{x} = (M_a \omega_d^2 x_o - i C_v \omega_d x_o) e^{i\omega t}.$$

Then coefficients are given by

$$M_a = \frac{F_o \cos\varphi}{\omega_d^2 x_o}, \tag{23}$$

$$C_v = -\frac{F_o \sin\varphi}{\omega_d x_o}. \tag{24}$$

Accuracy on damping estimate depends on the Stokes number as the phase $\varphi$ decreases with St. High Stokes number configurations requires small time steps. Inlet data used for these calculations are reported in Table 3. Fluid force and tube displacement histories are plotted in Fig. 9. Corresponding force magnitude $F_o$ and phase $\varphi$ are reported in Table 4. They are compared to experimental data deduced from Eqs. (7) and (8). Results are in good agreement. Added mass and viscosity damping terms are of the right order. The tube motion frequency and damping ratio in fluid at rest are finally deduced from Eqs. (5) and (6). Numerical values for $M_a$ and $f_e$ are reported in Table 5 and compared to experimental data. A good agreement is observed. It is interesting to notice that the ALE formulation enables the estimation of added mass effects. The 9-tubes mesh and periodic condition provide better results for added mass and added viscosity than the 5-tube configuration. These results tend to show that the assumption of an infinite tube bundle is not quite validated. Fluid–structure interactions depend on the confinement and in the 5-tube mesh the periodic boundary conditions are not sufficient to describe the effect of fixed tubes located near the moving tube, which tends to underestimate fluid–structure coefficients. Damping ratio is expressed in terms of $\sin\varphi$; hence results are very much dependent on mesh refinement and time step at high Stokes number. Added mass terms are sufficient to estimate vibration frequency characterizing tube motion in fluid at rest.

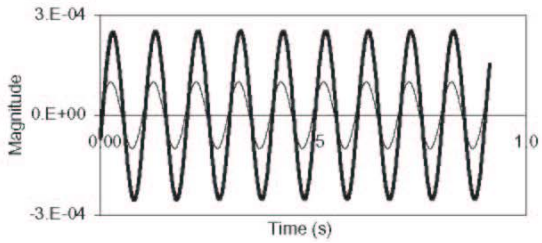


Fig. 9. Fluid force $F$ (heavy line) and tube displacement $x$ (thin line) time history. Estimation of force phase $\varphi$ and force magnitude $F_o$.

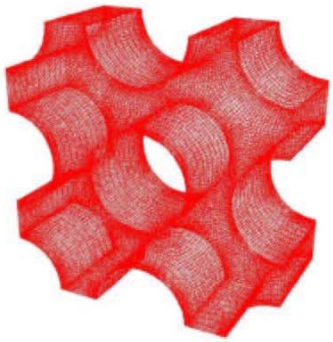

Fig. 10. 3-D mesh of the fluid computational domain at time step $n = 1$ with a 9-tubes configurations.

### 4.3. Simulation of flow-induced vibrations

In what follows, the purpose is to use the ALE method and a coupling with the mechanical calculation previously described in order to simulate the tube behaviour in presence of cross-flows. A first estimation of tube frequency in flow is provided for several gap velocities.

#### 4.3.1. Fluid computation

Inlet flow rates are introduced to get the convenient gap velocity $U_{gap}$. The mechanical modelling is made up such that the tube is expected to deflect in the drag direction and to oscillate in the lift direction, as observed experimentally (Fig. 9). Three-dimensional (3-D) representation of the computational domain mesh used for the calculation is shown in Fig. 10. It is near-wall refined in the region near flexible tube where fluid forces must be estimated with accuracy.

#### 4.3.2. Structure computation

For the coupling with the mechanical calculation, a staggered explicit time scheme is applied. At each time step, the tube motion is reactualized according to the coupling process described in Section 2.3. Tube displacement is solution of Eq. (21) solved by using appropriate numerical scheme. An Euler explicit scheme, a centred second order scheme and a Newmark scheme were compared, and the last one provided the best results in terms of numerical damping reduction.

#### 4.3.3. Identification of tube vibration frequency in flow

Numerical results are described below. They are compared to experimental data obtained with the previously described experimental set-up. Calculations are performed in presence of turbulent flows in order to identify fluid-elastic parameters. Three-dimensional calculations were carried out for different gap velocity values corresponding to a Reynolds number range of 1 to $4 \times 10^4$. Turbulence modelling was introduced to describe the flows. Several models were tested and, for 3-D calculations, it was shown that a $R_{ij} - \varepsilon$ modelling provides good results in terms of drag and lift forces near the tube (Benhamadouche and Laurence, 2002). In the present work a $R_{ij} - \varepsilon$ modelling involving an appropriate near-wall treatment or a DNS was used. In practice fluid-elastic forces are supposed to be independent of turbulence effects and the turbulence model may not affect numerical results in terms of tube vibration frequency.

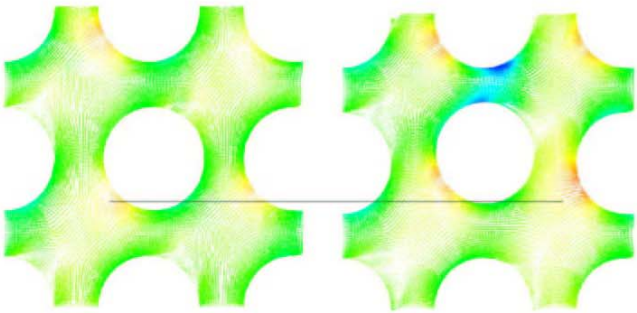

Fig. 11. Velocity fields coloured by pressure at two time steps by numerical simulation involving an ALE formulation and a flow structure coupling process.

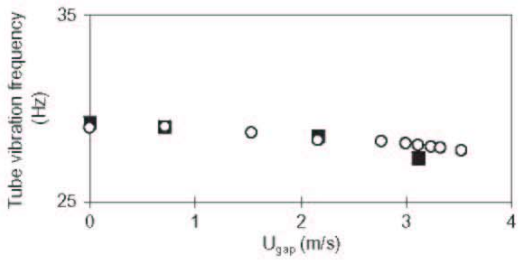


Fig. 12. Tube vibration frequency in flow $f$ (Hz) in terms of gap velocity $U_{gap}$ (m/s) estimated numerically (black points) and experimentally by Granger et al. (1993) (white points).

Table 6
Comparison between tube frequency $f_f$ (Hz) of tube in flow estimated numerically in 2-$D$ and in 3-$D$ and experimentally for several gap velocity values $U_{gap}$

| Frequency in flow $f_f$ (Hz) | Numerical estimates 3-$D$ | Numerical estimates 2-$D$ | Experimental estimates |
|---|---|---|---|
| $U_{gap} = 0$ m/s | | 29.30 | 29.00 |
| $U_{gap} = 0.71$ m/s | 29.06 | 29.85 | 29.05 |
| $U_{gap} = 2.16$ m/s | | 28.57 | 28.32 |
| $U_{gap} = 3.11$ m/s | 27.39 | | 28.09 |

Fig. 11 provides flow fields simulated by using the full computational process for a given flow velocity. The time history of tube displacement induced by flow is illustrated. Finally, in-flow tube vibration frequency estimated numerically and experimentally are reported in Fig. 12 for several gap velocity values. Experimental and numerical results are compared and the expected trend is retrieved. Tube frequency numerical estimate is reasonable. This tends to show that the computational process involved in the present work enables the numerical prediction of flexible tube behaviour in cross-flows.

These first computations provide a first validation of the computational process applied in this article to the numerical prediction of a flexible tube vibrations in a tube bundle in cross-flow.

Results are reported in Table 6 for several gap velocity values. Finally, one can deduce from previous calculations fluid-elastic coefficients by using appropriate data processing.

These computations tend to show that a computational process for the numerical prediction of flexible tube vibrations in cross-flows is now reachable. Required CPU time with VPP5000 is 16/100 000 s per iteration per cell per processor with about 50 000 iterations without ALE until fluid calculation convergence and 15 000 iterations with ALE.

## 5. Conclusion

A flow-induced vibration prediction numerical method is presented in this paper. The fluid problem is solved by using an arbitrary Lagrangian Eulerian (ALE) formulation and a coupling process between fluid and structure computations is involved in order to account for flow structure coupling and fluid-elastic effects. Finally, the approach is applied to the numerical prediction of flexible tube bundle vibration frequency in cross-flows. Numerical results are consistent with experimental predictions and feature the expected tendency.

In the present work, small flow velocities are involved and no instability development is observed. Other simulations will be performed in order to study the tube bundle behaviour below, near and above the critical flow velocity.

This will require a new validation of turbulence modelling in tube bundles. Further developments will be carried out in order to improve the coupling process and the flow modelling in presence of moving boundaries.

## Acknowledgements

The authors want to acknowledge Messrs Caruso, Adobes, Fournier, Archambeau and Benhamadouche for their helpful contribution in the present work.

## References

Adobes, A., Gosse, A., Baratte, C., 2001. Qualification of motion dependent fluid forces coefficients. ASME PVP Conference, Atlanta.

Axisa, F., Antunes, J., Villard, B., 1990. Random excitation of heat exchanger tubes by cross-flow. Journal of Fluids and Structures 4, 321 342.

Belyschko, T., Flanagran, D.F., Kennedy, J.M., 1982. Finite element method with user-controlled meshes for fluid structure interactions. Computational Methods in Applied Mechanics and Engineering 33, 689 723.

Bendjeddou, Z., Longatte, E., Souli, M., 2002. Numerical simulation of tube bundle vibrations in cross flows. ASME PVP Conference on Flow-Induced Vibrations, Vancouver.

Benhamadouche, S., Laurence, D., 2002. LES, coarse LES and transient RANS comparisons on the flow across a tube bundle. In: Engineering Turbulence Modeling and Measurements Conference, Vol. 5. Elsevier, Amsterdam.

Benson, D., 1989. An efficient accurate, simple ale method for non linear finite element programs. Computational Methods in Applied Mechanics and Engineering 33, 689 723.
Chen, S.S., 1986. Flow-induced Vibration of Circular Cylindrical Structures. Hemisphere Publishing Corporation, Washington.
Corcos, G.M., 1963. Resolution of pressure in turbulence. Journal of Acoustic Society of America 35, 192 199.
Gagnon, J.O., Païdoussis, M.P., 1994. Fluid coupling characteristic and vibration of cylinder clusters in axial flow. Part 1: Theory. Journal of Fluids and Structures 8, 257 291.
Granger, S., Campistron, R., Lebret, J., 1993. Motion-dependent excitation mechanisms in square in -line tube bundle subject to water cross-flow: an experimental modal analysis. Journal of Fluids and Structures 7, 521 550.
Granger, S., Paidoussis, N., 1995. An improvement to the quasi-steady model with application to cross-flow-induced vibration of tube arrays. Journal of Fluid Mechanics 320, 163 184.
Granger, S., Gay, N., 1996. An unsteady semi-analytical model for cross-flow induced vibration of the tube bundle: comparison with experiment. In: Bearman, P.W. (Ed.), Flow Induced Vibration. Balkema, Rotterdam, pp. 327-338.
Granger, S., Perotin, L., 1997a. An inverse method for the identification of a distributed random excitation acting on a vibrating structure: Part 1: Theory. ASME Conference on Fluid Structure Interactions. Dallas, TX, USA.
Granger, S., Perotin, L., 1997b. An inverse method for the identification of a distributed random excitation acting on a vibrating structure: Part 2: Flow-induced vibration application. ASME Conference on Fluid Structure Interactions. Dallas, TX, USA.
Hermann, G., Steindorf, J., 1999. Efficient partitioned procedures for the computation of fluid structure interaction on parallel computers. In: Developments in Computational Mechanics High Performance Computing. Civil-Comp Press, Edinburgh, pp. 127 136.
Hirt, C.W., Amsdern, A.A., Cook, H.K., 1974. An arbitrary Eulerian Lagrangian method for all flow speeds. Journal of Computational Physics 14, 229 253.
Hughes, T.J.R., Liu, W.K., Zimmerman, T.K., 1981. Lagrangian eulerian finite elements formulation for viscous flows. Journal of Computational Methods in Applied Mechanics and Engineering 21, 329 349.
Liu, W.K., Huerta, A., 1988. Viscous flows for large free surface motion. Journal of Computational Methods in Applied Mechanics and Engineering 69, 277 324.
Longatte, E., Nhili, R., Weiss, T., 2000. Prediction of flow induced vibrations of drive line assembly. ASME PVP Conference, Seattle, WA, USA.
Longatte, E., Laurence, D., Barré, F., Ledac, P., 2001. Application of large Eddy simulation to a flow-induced vibration problem. ASME PVP Conference on Flow-Induced Vibrations, Atlanta, GA, USA.
Longatte, E., Bendjeddou, Z., Souli, M., 2002. Numerical simulation of tube bundle vibrations in cross flows. ASME IMECE Conference, New Orleans, LA, USA.
Moreno, M.M., De Langre, E., Le Quere, P., 2000. A large eddy simulation of the turbulent forcing spectrum induced by axial flow on a rod. Seventh International Conference on Flow-Induced Vibrations, Lucerne, Switzerland.
Noh, W.F., 1964. A time dependent two space dimensional coupled Eulerian Lagrangian code. In: Fenbach, A.E., Rosenberg (Eds.), Methods for Computational Physics 3, 117 179.
Pettigrew, M.J., Taylor, C.E., 2002a. Vibration analysis of steam generators and heat exchangers: an overview Part I: Flow, damping, fluid-elastic instability, ASME IMECE, Conference on Flow-Induced Vibrations, New Orleans, LA, USA.
Pettigrew, M.J., Taylor, C.E., 2002b. Vibration analysis of steam generators and heat exchangers: an overview Part II: Vibration, response, fretting-wear, guidelines, ASME IMECE, Conference on Flow-Induced Vibrations, New Orleans, LA, USA.
Piperno, S., Farhat, C., 2001. Partitioned procedures for the transient solution of coupled aeroelastic problems, part II: Energy transfer analysis and three-dimensional applications. Journal of Fluids and Structures 3, 61 82.
Price, S.J., Paidoussis, M.P., 1986. A single-flexible-cylinder analysis for the fluidelastic instability of an array of flexible cylinders in cross-flow. Journal of Sound and Vibrations 108, 193 199.
Price, S.J., Paidoussis, N., 1989. The flow-induced response of a single flexible cylinder in an in-line array of rigid cylinders. Journal of Fluids and Structures 3, 61 82.
Souli, M., 2000. ALE and fluid structure interaction capabilities in LS-Dyna, ASME PVP Conference, Seattle.
Souli, M., 2001, Euler Lagrange Formulation for fluid structure interactions problems. ASME PVP Conference, Atlanta, GA, USA.
Souli, M., Zolesio, J.P., 2001. Arbitrary Lagrangian-Eulerian and free surface methods in fluid mechanics, Journal of Computational Methods in Applied Mechanics and Engineering 191, 451 466.
Souli, M., Ouahsine, A., Lewin, L., 1999. Ale formulation for fluid structure interaction problems. Journal of Computational Methods in Applied Mechanics and Engineering 190, 659 675.

**Proceedings of PVP2006-ICPVT-11**
**2006 ASME Pressure Vessels and Piping Division Conference**
**July 23-27, 2006, Vancouver, BC, Canada**

**PVP2006-ICPVT11-93717**

# NUMERICAL SIMULATION OF DYNAMIC INSTABILITY FOR A PIPE CONVEYING FLUID

**Fabien Huvelin, Elisabeth Longatte, Valérie Verreman**
Electricité de France- R&D Division
Fluid Dynamics, Power Generation and Environment Department
6, Quai Watier, 78400 Chatou, France
Email : fabien.huvelin@edf.fr, elisabeth.longatte@edf.fr, valerie.verreman@edf.fr

**M'hamed Souli**
Université des Sciences et Technologies de Lille I
1, Boulevard Paul Langevin, Cité Scientifique, 59655 Lille, France
Email : mhamed.souli@univ-lille1.fr

## ABSTRACT

The present work is devoted to simulation of fluid-structure interaction and flow-induced vibration problems by using a partitioned procedure. A finite element structure solver is coupled with a finite volume fluid solver. A coupling interface has been developed for grid interpolation and scheme coupling control. An alternative mesh motion to a classical ALE formulation is proposed for the fluid computation and the method is validated by means of a test-case involving a pipe conveying fluid.

## NOMENCLATURE

| | |
|---|---|
| $D_s$ | Damping coefficient (-) |
| $dS$ | Area of the fluid structure interface ($m^2$) |
| $e$ | Thickness of the pipe (m) |
| $E$ | Young's modulus (Pa) |
| $\mathbf{F_f}$ | Fluid load acting on the structure (N) |
| $\mathbf{F_v}$ | Viscous forces acting on the structure (N) |
| $I$ | Inertia ($m^4$) |
| $K_s$ | Stiffness coefficient (-) |
| $L$ | Length of the pipe (m) |
| $M_f$ | Fluid mass (kg) |
| $M_s$ | Structure mass (kg) |
| $\mathbf{n}$ | Normal of the fluid structure interface (-) |
| $p$ | Pressure (Pa) |
| $R$ | Radius of the pipe (m) |
| $t$ | Time (s) |
| $\mathbf{u_s}$ | Structure displacement (m) |
| $\dot{\mathbf{u}}_s$ | Structure velocity ($m.s^{-1}$) |
| $\ddot{\mathbf{u}}_s$ | Structure acceleration ($m.s^{-2}$) |
| $\mathbf{v_f}$ | Fluid velocity ($m.s^{-1}$) |
| $\dot{\mathbf{v}}_f$ | Fluid acceleration ($m.s^{-2}$) |
| $\mathbf{V}$ | Reduced fluid velocity (-) |
| $\mathbf{w}$ | Fluid grid velocity ($m.s^{-1}$) |
| $\mathbf{X}$ | Langrangian coordinates (m) |
| $\mathbf{x} = (x,y)$ | Eulerian coordinates (m) |
| $\alpha$ | Parametric coefficient (-) |
| $\beta$ | Damping coefficient ($s^{-1}$) |
| $\lambda$ | Diffusivity coefficient for the ALE method (s) |
| $\mu$ | Dynamic viscosity ($kg.m^{-1}.s^{-1}$) |
| $f$ | Frequency ($s^{-1}$) |
| $\rho_f$ | Fluid density ($kg.m^{-3}$) |
| $\rho_s$ | Structure density ($kg.m^{-3}$) |
| $\overline{\overline{\sigma_f}}$ | Cauchy stress tensor for the fluid ($kg.s^{-2}$) |
| $\overline{\overline{\sigma_s}}$ | Cauchy stress tensor for the structure ($kg.s^{-2}$) |
| $\boldsymbol{\chi}$ | ALE coordinates (m) |

## 1 INTRODUCTION

The natural frequency and damping of a structure can be dramatically modified when it is in contact with a flow. Structure motion is affected by fluid load at the interface between the two domains, and reciprocally the flow is affected by the new position of the structure. Such oscillations can damage structure because instabilities may appear. Thus, for industrial applications, it is important to be able to catch the critical fluid velocity up to which the structure may switch from a stable to an unstable behaviour.

To perform such a multi-physics computation, fluid and structure problems can be solved in single code by means of a monolithic procedure. Monolithic process is a fully implicit method ensuring the energy conservation of the coupled system. However its implementation may be difficult when specific methods are required for both fluid and structure solvers. The linear coupled system is ill conditioned because of the different time scales of fluid and structure. It also may be a long work when very efficient fluid and structure softwares are already available. In a such case a partitioned procedure can be used in order to couple the two codes ([1],[2]). The main disadvantage of this process is that during one time step, fluid and structure computations are staggered in time. The energy conservation of the full coupled system may not be conserved. The coupling scheme must be chosen in order to avoid or to reduce as much as possible numerical dissipation. Another problem is that fluid and structure grids can have different mesh refinements. Thus, at each time step, interpolations must be performed in order to transfer fluid force to structure and structure position to fluid solver ([3], [4]).

The present work is devoted to simulation of fluid structure interaction and flow-induced vibration problems by using such a partitioned procedure. In a first part, the coupling tool is presented with a specific method for fluid grid deformation. In a second part, an application of the method to flexible structure is presented by means of a test case involving a pipe conveying fluid. Numerical results are compared to reference data.

## 2 GOVERNING EQUATIONS

Lets $\Omega_f^n \in R^k$, $k=2$ or 3, denote the domain occupied by the fluid at time $n$, $\Omega_s^n \in R^k$, $k=2$ or 3, denote the domain occupied by the structure at time $n$ and $\Gamma_{sf}^n = \partial\Omega_f^n \cap \partial\Omega_s^n$ denote the interface between the two domains at time $n$ (Fig. 1).

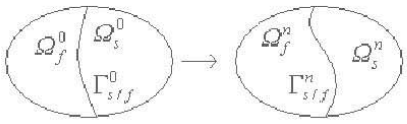


Fig. 1 - *Description of the fluid-structure domain*

The structure dynamic response is governed by the equation of motion :

$$M_s\ddot{\mathbf{u}}_\mathbf{s} + D_s\dot{\mathbf{u}}_\mathbf{s} + K_s\mathbf{u}_\mathbf{s} = \mathbf{F_f}(t) \qquad \text{(Eq. 1)}$$

The fluid load acting on the structure is given by :

$$\mathbf{F_f}(t) = -\int_{\Gamma_{sf}} \overline{\overline{\sigma}}_f \cdot \mathbf{n}\, dS \qquad \text{(Eq. 2)}$$

The fluid is assumed to be an incompressible Newtonian fluid. The equations of the mass and momentum are given by :

$$\begin{cases} \nabla\cdot(\mathbf{v_f}) = 0 \\ \rho_f\dot{\mathbf{v}}_\mathbf{f} + \rho_f\mathbf{v_f}\cdot\nabla\mathbf{v_f} = \nabla\cdot\overline{\overline{\sigma}}_f \end{cases} \qquad \text{(Eq. 3)}$$

with $\overline{\overline{\sigma}}_f = -p\overline{\overline{Id}} + \mu(\nabla\mathbf{v_f} + \nabla\mathbf{v_f}^T)$

The fluid is solved by using an Eulerian formulation, while the structure is discretised by a Lagrangian approach. An ALE method ([5],[6]) has to be applied to the Navier-Stokes equations in order to follow the fluid-structure interface.

When an ALE formulation is used, an arbitrary referential is introduced. The total time derivative of a variable $\varphi$ is described by :

$$\frac{d\varphi(\mathbf{X},t)}{dt} = \frac{\partial\varphi(\boldsymbol{\chi},t)}{\partial t} + (\mathbf{v_f} - \mathbf{w}).\nabla\varphi(\boldsymbol{\chi},t) \qquad \text{(Eq. 4)}$$

where $\mathbf{w}$ denotes the grid velocity of the fluid domain for the numerical simulation.

This velocity allows to have an eulerian formulation near the fixed boundaries when its value is $\mathbf{w}=0$, and a formulation close to the lagrangian formulation near the moving boundaries when its value is $\mathbf{w}=\dot{\mathbf{u}}_s$.

With an ALE formulation, the equations of the mass and momentum become :

$$\begin{cases} \nabla\cdot(\mathbf{v_f}) = 0 \\ \rho_f\dot{\mathbf{v}}_\mathbf{f} + \rho_f(\mathbf{v_f} - \mathbf{w})\cdot\nabla\mathbf{v_f} = \nabla\cdot\overline{\overline{\sigma}}_f \end{cases} \qquad \text{(Eq. 5)}$$

With this formulation, it is necessary to have a remapping of the fluid domain at each time step. A standard method consists in solving a diffusion equation for the grid velocity as follow :

$$\begin{cases} \nabla \cdot (\lambda \nabla \mathbf{w}) = 0 \\ \mathbf{w} = 0 \quad on \quad \partial\Omega_f \setminus \Gamma_{s/f} \\ \mathbf{w} = \dot{\mathbf{u}}_s \quad on \quad \Gamma_{s/f} \end{cases} \qquad \text{(Eq. 6)}$$

$\lambda$ allows one to keep the properties of the mesh near the boundary conditions.

The fluid-structure problem is closed by means of the specific boundary conditions for the fluid and the structure, and by means of the conditions at the interface $\Gamma_{s/f}$, where the boundary conditions are :

$$\begin{cases} \mathbf{v_f} = \mathbf{v_s} \quad on \quad \Gamma_{s/f} \\ \overline{\overline{\sigma_f}}.\mathbf{n} = \overline{\overline{\sigma_s}}.\mathbf{n} \quad on \quad \Gamma_{s/f} \end{cases} \qquad \text{(Eq. 7)}$$

## 3 COMPUTATIONAL PROCESS

The methodology involved here for the numerical simulation is based on a partitioned procedure i.e. a weak code coupling. It can be split, for each time step, into four steps : predicting the structure displacement at the fluid-structure interface, updating the fluid mesh motion thanks to an ALE formulation, solving the fluid problem and computing the fluid force acting on the structure and solving the mechanical problem.

A good prediction of the fluid-structure interface is required in order to ensure energy conservation at the interface. As the structure is flexible, a sub-cycling coupling scheme has been chosen ([2],[3],[7]) (Fig. 2). It allows the fluid and structure interfaces to converge at the same location. For each time step, this algorithm computes sub-cycling until convergence on a criterion based on the velocities and forces at the interface. Each sub-cycling is computed with the value at time step $t^n$ except the position of the fluid mesh which is taken at the previous sub-cycling $t^{n+1,k-1}$, where $t^{n+1,k-1}$ denotes the k-1$^{th}$ iteration during the sub-cycling at time step $t^{n+1}$. This scheme features good properties in terms of energy conservation.

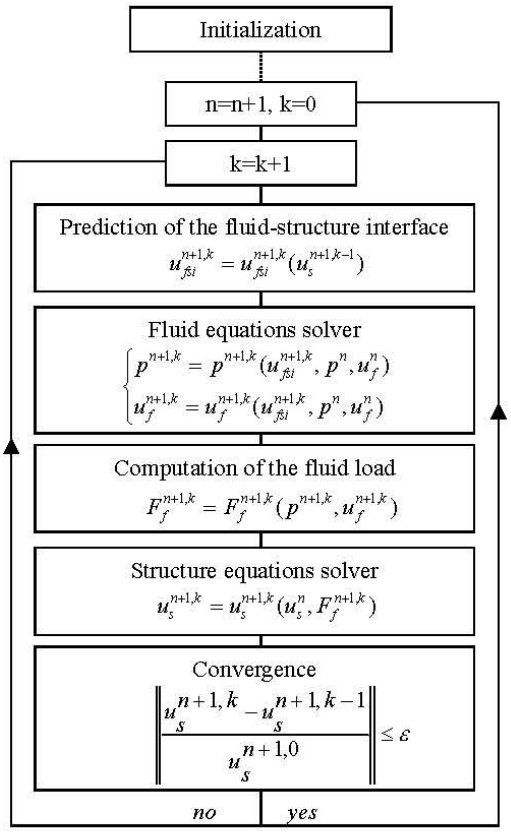


Fig. 2 - *Sub-cycling coupling scheme*

The standard ALE equation for updating the fluid mesh has been explained previously (Eq. 6). It costs CPU time because two or three linear systems have to be solved. The geometric properties of the test case considered below have been used in order to develop another mesh deformation method. One Considers the mesh of the Fig. 3, which is composed of three moving boundaries with nodes numbering from 1 to 14 and one fixed boundary with node numbering from 14 to 16 and node 1.

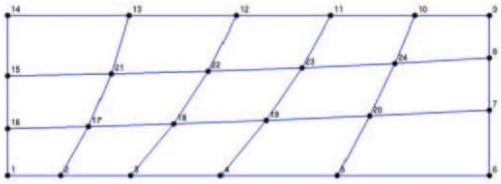

Fig. 3 – *Mesh and node connection for the grid updating*

The displacement values of bottom and top moving boundaries (nodes from 1 to 6 and nodes from 9 to 14) are high enough in order to update the grid. The principle consists in linking each node of the mesh to two nodes of these moving boundaries. For example, node 17 is linked to nodes 2 and 13. Thus, since boundary node displacement are known, the new position of each node can be easily computed :

$$\mathbf{X}_{node} = \alpha \mathbf{X}_{boundary1} + (1-\alpha)\mathbf{X}_{boundary2} \qquad \text{(Eq. 8)}$$

Thanks to the parametric coordinates $\alpha$ , nodes located near moving boundaries move with a value closed to those of the boundary nodes. The properties of the mesh near the boundary conditions are automatically preserved.

With this kind of coupling procedure, the only link between structure and fluid solvers are fluid force acting on the structure on one hand and structure displacement at the interface on the other hand. The mesh refinement at the interface for fluid and structure can be different (Fig. 4). An interpolation based on the finite element method has been developed ([3], [4]) in order to be able to transfer the data between the two domains.

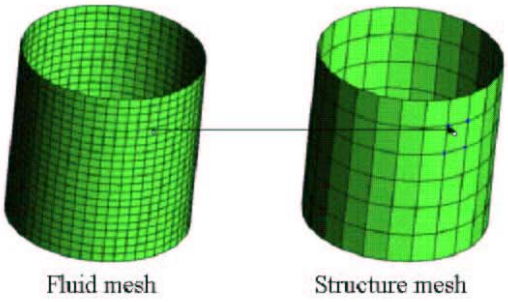


Fig. 4 - *Example of non matching fluid and structure meshes*

## 4 NUMERICAL TEST CASE

In order to apply the methodology to a flexible structure, the test case of a pipe conveying fluid clamped at upstream end and free at the other side is modelled for different inlet fluid velocities. The motion is supposed to be small and lateral. It is shown that for sufficiently large flow velocities the structure is subjected to oscillatory dynamic instabilities. An Analytical model for the solution is available ([8], [9]). The equation of motion is given by :

$$EI\frac{\partial^4 y}{\partial x^4} + M_s v_f^2 \frac{\partial^2 y}{\partial x^2} + 2M_s v_f \frac{\partial^2 y}{\partial x \partial t} + F_v + (M_s + M_f)\frac{\partial^2 y}{\partial t^2} = 0 \qquad \text{(Eq. 9)}$$

Thanks to a decomposition in Taylor's series, the damping coefficients and frequencies of the system can be found. It is shown that the instability appears on the second mode for which the damping coefficient becomes negative.

This test-case has been modelled numerically ([10], [11]) with a fixed fluid grid with transpiration conditions imposed at the fluid-structure interface of the fluid domain. In this work the flow was assumed to be in a 2D channel. The properties of these previous numerical simulations are used here. The physical parameters are as follows :

$$L = 1\ \text{m},\quad R = 2.10^{-2}\ \text{m},\quad e = 4.10^{-4}\ \text{m},$$
$$\rho_s = 3{,}22.10^{6}\ \text{kg.m}^{-3},\quad E = 1.510^{-9}\ \text{N.m}^{-2},$$
$$\rho_f = 1.10^{3}\ \text{kg.m}^{-3},\quad \mu = 5.10^{-2}\ \text{kg.m}^{-1}.\text{s}^{-1}$$

For numerical simulation, the structure domain is discretized with beam elements, while the 2D fluid mesh is discretized with quadrangle elements.

A Poiseuille flow is applied to the fluid and when a fully-developed velocity distribution is reached (Fig. 5), an initial velocity is given to the structure close to the shape of the second mode in order to speed up the convergence (Fig. 6).


Fig. 5 - *Initial pressure and velocity in the pipe*

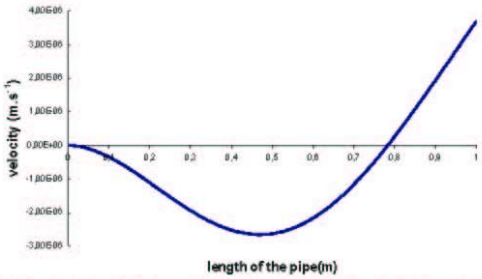


Fig. 6 - *Shape of the second fundamental mode of the structure*

A post-processing of the displacement at the free end of the structure is applied in order to estimate the first frequency numerically by using the following identification :

$$u_s(t) = e^{-\beta t}(A\cos(2\pi ft) + B\sin(2\pi ft)) \qquad \text{(Eq. 10)}$$

Fig. 7 shows the results in the frequency-damping plane for different inlet velocity values. They are compared to the numerical results of [11] based on a transpiration method. In both cases the critical velocity is caught for a value between $v_f = 2.456\,\text{m.s}^{-1}$ $(V = 4)$ and $v_f = 2.763\,\text{m.s}^{-1}$ $(V = 4.5)$ (Fig. 8, Fig. 9, Fig. 10).

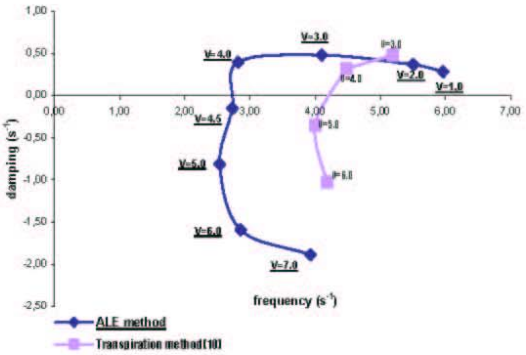


Fig. 7 – *Frequency-damping plane for different inlet velocities*

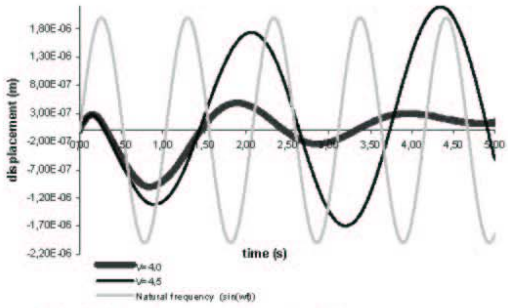


Fig. 8 - *Displacement of the end of the structure*

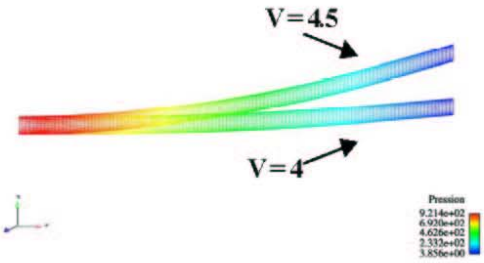


Fig. 9 - *Shape of the structure at time 1.99 s*

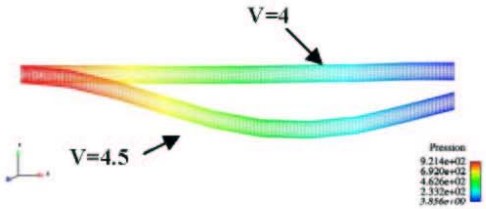


Fig. 10 - *Shape of the structure at time 5.00 s*

For small velocities both methods give results in good agreement. A difference between the results appears for the velocities closed to the critical velocity (Fig. 11, Fig. 12). It seems to disappear for frequencies when flow velocity increases.

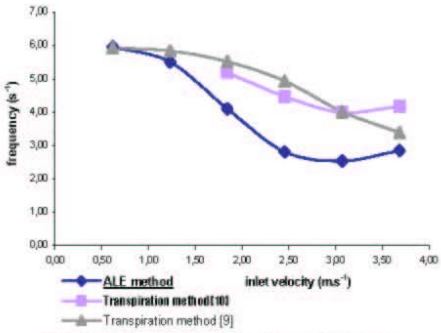


Fig. 11 - *Frequency of the structure response*

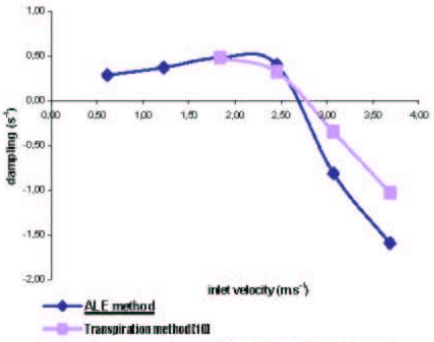


Fig. 12 - *Damping of the structure response*

## 5 CONCLUSION

A partitioned scheme coupling procedure with sub-cycling has been presented. An interface has been built in order to simulate the motion of a flexible structure. A fluid grid deformation method has been proposed.

This approach has been applied to the test case of a pipe conveying fluid. The stable and unstable behavior of the structure for different inlet fluid velocities has been modeled. According to numerical results, the critical fluid velocity up to which the instability of the structure appears has been predicted.

## REFERENCES

[1] C. Farhat, M. Lesoinne, 2000. Two efficient staggered algorithms for the serial and parallel solution of three-dimensional nonlinear transient aeroelastic problems. *Computer methods in applied mechanics and engineering*, 182, pp 499-515.

[2] D. Abouri, A. Parry, A. Hamdouni, 2003. Fluid-rigid body dynamic interaction in complex industrial flow. *Chapter advanced in fluid mechanics : Fluid Structure* interaction II, Wit Press, pp 295-305.

[3] C. Farhat, M. Lesoinne, P. LeTallec, 1998. Load and motion transfer algorithms for fluid/structure interaction problems with non-matching discrete interfaces : Momentum and energy conservation, optimal discretization and application to aeroelasticity. *Computer methods in applied mechanics and engineering*, 157, pp 95-114.

[4] N. Maman, C. Farhat, 1995. Matching fluid and structure meshes for aeroelastic computations : a parallel approach. *Computers & Structures*, vol. 54, No. 4, pp 779-7852.

[5] N. Aquelet, M. Souli, L. Olovsson, 2006. Euler-Lagrange coupling with damping effects : Application to slamming problems. *Computer methods in applied mechanics and engineering*, 195, pp 110-132.

[6] E. Longatte, Z. Bendjeddou, M. Souli, 2003. Methods for numerical study of tube bundle vibrations in cross-flow. *Journal of Fluids and Structure*, 18, pp 513-528.

[7] G.M. Hermann, J. Steindorf, 1999. Efficient partitioned procedures for computation of fluid-structure interaction on parallel computers. Developments in Computational Mechanics with High Performance Computing. *B.H.V., Civil-Comp Press*, Edinburgh, S, pp 127-136.

[8] M. Païdoussis, 1966. Dynamics of flexible slender cylinders in axial flow. *Journal of Fluid Mechanics*, vol. 26, part 4, pp. 717-736.

[9] J.-L. Lopes, M.P. Païdoussis, C. Semler, 2002. Linear and non-linear dynamics of cantilevered cylinders in axial flow. Part 2 : the equations of motion. *Journal of Fluids and Structures*, vol. 16, part 6, pp 715-737.

[10] J.Y. Renou, 1998. Une méthode eulérienne pour le calcul numérique de forces fluides-élastiques. *PhD thesis*, Université Paris VI.

[11] M.A. Fernandez-Varela, 2001. Modèles simplifiés d'interactions fluide-structure. *PhD thesis*, Université Paris IX.

**Proceedings of ASME**
**2005 ASME Pressure Vessels & Piping Division Conference**
**Denver, Colorado, USA, July 17-21, 2005**

**PVP2005-71647**

# EXPLICIT AND IMPLICIT CODE COUPLING SCHEMES IN FLUID STRUCTURE INTERACTION

**Longatte E.**
Electricité de France- R&D Division
Department of Fluid Mechanical and Heat Transfert
6, Quai Watier, 78400 Chatou, France
Email: elisabeth.longatte@edf.fr

**Bendjeddou Z.**
Electricité de France- R&D Division
Department of Fluid Mechanical and Heat Transfert
6, Quai Watier, 78400 Chatou, France
Email: zaky.bendjeddou@edf.fr

**Verreman V.**
Electricité de France- R&D Division
Department of Fluid Mechanical and Heat Transfert
6, Quai Watier, 78400 Chatou, France

**Souli M.**
Université des Sciences et Technologies de Lille I
1, Boulevard Paul Langevin, Cité Scientifique
59655 Lille, France
Email: mhamed.souli@univ-lille1.fr

## ABSTRACT

*In multi-physics numerical computations a good choice of code coupling schemes is required. Several methods are possible like: an explicit synchronous scheme an Euler implicit method and no interpolation on velocity pressure ; an explicit asynchonous scheme using a Crank-Nicholson time integration scheme and interpolation on velocity and pressure ; an implicit scheme using a fixed iterative method. In the present paper these different schemes are compared for application in fluid structure interaction field. In the first part numerical coupling schemes are presented. Then their capability to ensure energy conservation is discussed according to numerical results obtained in analytical test cases. Finally application of coupling process to fluid structure interaction problems is investigated and results are discussed in terms of added mass and damping induced by a fluid for a structure vibrating in fluid at rest.*

**Keywords**: *fluid-structure, code-coupling scheme, energy conservation, added mass, added damping.*

## NOMENCLATURE

| | |
|---|---|
| $M_s$ | Structure mass in air $kg$ |
| $K_s$ | Structure stiffness in air $kg.s^{-2}$ |
| $C_s$ | Structure damping in air $kg.s^{-1}$ |
| $U$ | Tube displacement $m$ |
| $X$ | "Corrected" displacement $m$ |
| $A$ | Displacement amplitude $m$ |
| $\omega$ | Structure circular frequency $H_z$ |
| $P_f$ | Fluid force $kg.m.s^{-2}$ |
| $D$ | Tube diameter $m$ |
| $D_e$ | External tube diameter $m$ |
| $P$ | Longitudinal pitch $m$ |
| $T$ | Transversal pitch $m$ |
| $P/D$ | Tube diameter pitch ratio |
| $M_a$ | Added mass $kg$ |
| $C_a$ | Added damping $kg.s^{-1}$ |
| $\rho$ | Fluid density $kg.m^{-3}$ |
| $L$ | Reference length $m$ |
| $\tilde{M}_a$ | Dimensionless added mass in still water |
| $\tilde{C}_a$ | Dimensionless added damping in still water |
| $F$ | Fluid force $kg.m.s^{-2}$ |
| $F_o$ | Fluid force amplitude $kg.m.s^{-2}$ |

$x_o$ Displacement amplitude $m$
$\phi$ Force and displacement diphase
$St$ Stokes number
$\mu$ Dynamic viscosity of fluid $kg.m^{-1}.s^{-1}$
$\nu$ Kinematic viscosity of fluid $m^2.s^{-1}$
$f_s$ Structure frequency in air at rest $H_z$
$f_e$ Structure frequency in water at rest $H_z$
$L_z$ Reference length $m$

## INTRODUCTION

In order to study structures submitted to crossflows (tube bundle, heat exchanger, panel flutter), fluid and structure equations have to be solved at the same time. There are different ways to accomplish this task. First of all fluid and structure equations can be solved in a single system (monolithic algorithm). This is a strong code coupling scheme between fluid and structure problems ensuring energy conservation of the full fluid structure system. But this code coupling scheme is often hard to setup in industrial applications as it requires significant change in fluid and structure solvers. This difficulty can be overcome by using an explicit code coupling scheme. This type of code coupling is easy to setup and it allows independent evolution for the different numerical solvers. The easiest way for ensuring code coupling is to determine fluid force acting on the structure then to compute the structure displacement and velocity induced by this fluid force and use the structure velocity as boundary condition for the next fluid computation. With this explicit scheme fluid and structure computations are staggered in time and energy conservation is violated. Furthermore this scheme produces or dissipates energy and this leads to a lack of accuracy in numerical results. In order to avoid this difficulty, high order explicit staggered schemes (Farhat et al. 1995, Farhat et Lesoinne 1997, Piperno et Farhat 1997) and implicit schemes (Hermann et Steindorf 1999, LeTallec et Mouro 2001, Mani 2003) using iterative method are introduced.

In the first part, several explicit and implicit code coupling schemes are introduced. In the second part, code coupling schemes are studied in terms of energy conservation. Finally numerical simulations are performed for several test cases and numerical results are compared to analytical or experimental results in configurations involving one-dimensional and two-dimensional cases, non viscous fluid and viscous fluid in concentric cylinders.

## 1 Code coupling scheme

To model fluid structure coupling, different numerical steps are used: computation of fluid force acting on the structure, resolution of mechanical equation, fluid mesh actualisation using an Arbitrary Lagrange Euler (ALE) formulation and structure displacement and velocity as boundary condition for the next fluid computation. In order to set up this coupling, different code coupling schemes can be considered. A first order explicit scheme may produce or dissipate energy. It is necessary not to produce nor dissipate energy in the fluid structure interface in order to avoid numerical damping polluting numerical results. Other code coupling schemes are possible: fully implicit monolithic schemes ensuring energy conservation, implicit schemes using iterative methods (fixed point methods) and high order staggered explicit schemes.

Energy conservation with fluid structure coupling schemes is considered below. Energy variation induced by fluid computation at each time step is expressed by the following equation:

$$\Delta E_f^{n+1} = -P_f^n (X^{n+1} - X^n) \tag{1}$$

where $P_f^n$ designates fluid forces acting on the structure, $X^n$ and $X^{n+1}$ the "corrected" displacement by the code coupling scheme at time $t^n$ and $t^{n+1}$.

The structure displacement is modelled by using a classical mechanical equation:

$$M_s A + C_s V + K_s U = P_s \tag{2}$$

where $A$, $V$ et $U$ designate structure acceleration, velocity and displacement.

This equation is solved with a Newmark algorithm:

$$M_s A^{n+1} + C_s V^{n+1} + K_s U^{n+1} = P_s^{n+1} \tag{3}$$

$$V^{n+1} = V^n + \frac{\Delta t}{2}(A^{n+1} + A^n) \tag{4}$$

$$U^{n+1} = U^n + \frac{\Delta t}{2}(V^{n+1} + V^n) \tag{5}$$

Structure energy is the sum of kinetic and potential energy:

$$E_s = \frac{1}{2} M_s V^2 + \frac{1}{2} K_s U^2 \tag{6}$$

and energy variation induced by structure computation at time $t^n$ and $t^{n+1}$ can be written:

$$\begin{aligned} \Delta E_s^{n+1} &= E_s^{n+1} - E_s^n \\ &= \frac{1}{2} K_s (U_s^{n+1^2} - U_s^{n2}) + \frac{1}{2} M_s (V_s^{n+1^2} - V_s^{n2}) \end{aligned}$$

$$
\begin{aligned}
&= \frac{1}{2}K_s(U_s^{n+1}+U_s^n)(U_s^{n+1}-U_s^n) \\
&+ \frac{1}{2}M_s(V_s^{n+1}+V_s^n)(V_s^{n+1}-V_s^n) \\
&= K_s\Delta t V_s^{n+\frac{1}{2}}U_s^{n+\frac{1}{2}} + M_s\Delta t V_s^{n+\frac{1}{2}}A_s^{n+\frac{1}{2}} \\
&= \Delta t V_s^{n+\frac{1}{2}}(P_s^{n+\frac{1}{2}} - C_s V_s^{n+\frac{1}{2}}) \qquad (7)
\end{aligned}
$$

Finally one gets:

$$
\Delta E_s^{n+1} = (U^{n+1}-U^n)\frac{P_s^{n+1}+P_s^n}{2} - \Delta t V^{n+\frac{1}{2}}C_s V^{n+\frac{1}{2}} \qquad (8)
$$

The energy variation induced by the second term of the equation is due to the structure damping $C_s$ and do not account for code coupling variation energy. To reduce code coupling error, the following relation must be satisfied:

$$
\begin{aligned}
\Delta E_s^{n+1} &= (U^{n+1}-U^n)\frac{P_s^n+P_s^{n+1}}{2} \\
&= -P_f^n(X^{n+1}-X^n) = \Delta E_f^{n+1} \qquad (9)
\end{aligned}
$$

Code coupling schemes are based on this relation and "corrected" displacement $X^n$ and force $P_s^n$ are constructed to minimize energy variation. In the following section, three explicit and implicit code coupling schemes are presented.

### 1.1 Scheme A: Explicit synchronous algorithm

With explicit schemes structure displacement at time $t^{n+1}$ is deduced from fluid mesh at time $t^n$ used for fluid force computation (figure 1).

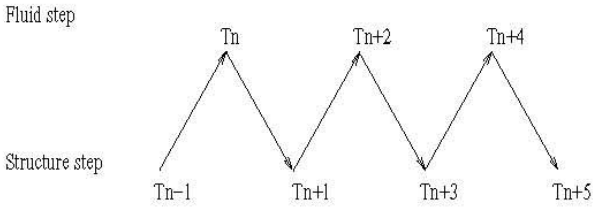


Figure 1. Time progression for a synchronous code coupling scheme

The synchronous scheme gives a prediction of the fluid structure interface position at time $t^{n+1}$ using previous position at times $t^n$ and $t^{n-1}$:

$$
X^{n+1} = U^n + \alpha_0\Delta t\dot{U}^n + \alpha_1\Delta t(\dot{U}^n - \dot{U}^{n-1}) \qquad (10)
$$

where:

$U^n$ designates structure displacement at time $t^n$,
$\dot{U}^n$ and $\dot{U}^{n-1}$ designate structure velocity at time $t^n$ et $t^{n-1}$,
$\Delta t$ the current time step,
$\alpha_0$ and $\alpha_1$ code coupling scheme coefficients.

Structure displacement is known and structure is moving with or without subcycling. Subcycling stabilizes the numerical process. Fluid force acting on the structure is calculated and structure displacement is deduced from the mechanical equation. $\alpha_0$ et $\alpha_1$ are chosen to get high order code coupling scheme. For $\alpha_0 = 1$ and $\alpha_1 = 0.5$ a second order code coupling scheme in time is obtained. A third order code coupling scheme can be obtained by using the following "corrected fluid force" $P_s^n$ expressed in term of the fluid force $P_f^n$ :

$$
P_f^n = \frac{P_s^{n+1}+P_s^n}{2} \qquad (11)
$$

This algorithm is introduced by Farhat et al. (1995, 1997). It gave good results for aeroelactic problems like flow past planel flutter (Piperno et al. 1995, 1997).

### 1.2 Scheme B: Explicit Asynchronous algorithm

With an asynchronous code coupling scheme fluid and structure are not solved at the same time step. Fluid computation is expressed at time $t^{n+\frac{1}{2}}$ and structure computation at time $t^{n+1}$ (figure 2).

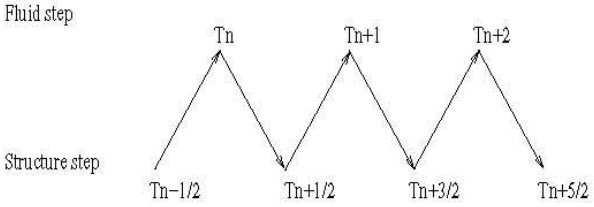


Figure 2. Time progression for a asynchronous code coupling scheme

The following prediction is used for structure displacement:

$$
X^{n+\frac{1}{2}} = U^n + \frac{\Delta t}{2}\dot{U}^n \qquad (12)
$$

Then fluid force are computed at time $t^{n+1}$. This procedure ensures geometry mesh conservation and ensures displacement and

velocity continuity in the fluid structure interface according to the Geometric Conservation Law (CGL, Thomas et Lombard, 1979).

This conservation property is due to the structure solver algorithm (trapezoidal rule):

$$\dot{\omega} = \frac{X^{n+\frac{1}{2}} - X^{n-\frac{1}{2}}}{\Delta t} = \frac{U^n - U^{n-1}}{\Delta t} + \frac{\dot{U}^n - \dot{U}^{n-1}}{2} = \dot{U}^n \quad (13)$$

where $\dot{\omega}$ designates corrected velocity (Piperno, 2001).

### 1.3 Scheme C: Implicit Algorithm

In this section an implicit code coupling scheme using iterative method is presented. This algorithm is based on the work of Hermann et al. (1999), LeTallec and Mouro (2001), Mani (2003) and Abouri et al. (2003).

This algorithm uses convergent explicit predictions of the coupled fluid structure system and a criteria based on fluid force or structure velocity is used to stop the numerical process.

The numerical steps for the implicit algorithm are a reference state at time $t^n$ is defined for fluid (velocity, pressure, mesh) and structure (displacement, velocity, acceleration) and four numerical steps are used:

1. Fluid force computation $(F^{n+1})^k$
2. Prediction of structure displacement $(x^{n+1})^{k+1}$ and velocity $(v^{n+1})^{k+1}$ at time $t^{n+1}$
3. Deformation of the current geometry $(\Omega^{n+1})^k$ and determination of the new geometry $(\Omega^{n+1})^{k+1}$
4. Calculation of the error estimator $E = \frac{|(F^{n+1})^{k+1} - (F^{n+1})^k|}{F^{n+1^0}}$

If the error estimator is lower than a critical value $\varepsilon$ ($E < \varepsilon$) then next time step $t^{n+2}$ is beginning. Otherwise the process restarts from the initial state $t^n$ and the last velocity estimation $(v^{n+1})^k$ is used for the next subcycling of this algorithm. This iterative process is naturally convergent but it could be accelerated by using Richardson method (Abouri et al., 2003) or conjugate gradient method (Daim et al., 2002). In order to conserve the code coupling algorithm property, high numerical time order solver must be used for fluid and structure.

## 2 Energy conservation

To illustrate the property of the three kinds of explicit and implicit code couping schemes, several test cases are considered below.

### 2.1 One-dimensional test case

In this part a one-dimensional coupling case test is considered with two different masses linked by a spring with stiffness and without damping.

Figure 3. One-dimensional case test

The system of coupled mass structures satisfies the following equation:

$$\begin{aligned} M_{s_1}\frac{d^2U_1}{dt^2} + K_sU_1 &= K_sU_2 \\ M_{s_2}\frac{d^2U_2}{dt^2} + K_sU_2 &= K_sU_1 \end{aligned} \quad (14)$$

For this system, an analytical solution is known:

$$\begin{aligned} U_1(t) &= Asin(\omega t) \\ U_2(t) &= -2U_1(t) \end{aligned} \quad (15)$$

where $\omega = \sqrt{3K_{s_1}/M_{s_1}}$ designates the system circular frequency and $A$ the displacement amplitude. Furthermore the following initial conditions are imposed:

$$\begin{aligned} U_2(0) &= -2U_1(0) = 0 \\ \frac{\partial U_1}{\partial t}(0) &= -2\frac{\partial U_2}{\partial t}(0) \end{aligned} \quad (16)$$

The variation of fluid and structure energy respectively $\Delta E_f$ and $\Delta E_s$ are estimated under the assumption that the first equation of the system describes the structure displacement and the second equation the fluid flow. Then the uncorrected fluid force acting on the structure is $P_f^n = K_sU_2^n$. If the explicit synchronous or asynchronous code coupling scheme is chosen, the two following equations have to be satisfied in order to minimize code coupling energy:

$$P_f^n = K_sX_2^n \quad (17)$$

$$P_f^n = \frac{P_s^n + P_s^{n+1}}{2} \quad (18)$$

These extrapolations are not necessary with an implicit code coupling scheme because fluid force is predicted by a serie of subcycling in the fluid computation.

Fluid and structure energy variation are reduced by using scheme B or scheme C (figure 4) and numerical damping is lower with these two schemes (figure 5).

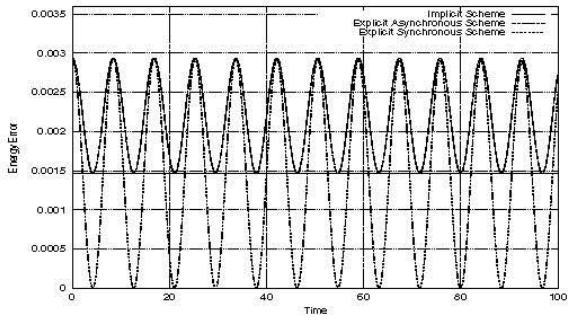


Figure 4. Comparison of the energy variation for three schemes A, B and C.

| Coupling scheme | $f$ (Hz) | $\alpha$ (Hz) |
|---|---|---|
| Explicit synchronous | 0.0593924 | $8.67221.10^{-5}$ |
| Explicit asynchronous | 0.0593934 | $6.97416.10^{-6}$ |
| Implicit | 0.0593965 | $9.0218.10^{-12}$ |
| Analytical solution | 0.05939661 | 0 |

Table 1. Comparison of analytical and numerical solutions obtained for three code coupling explicit synchronous, explicit asynchronous and implicit schemes with a time step $dt = 10^{-2}$ ms , a structure mass $M_s = 2272\ mg$ and a structure stiffness $K_s = 105.48\ mg.ms^{-2}$ and no damping $C_s = 0$.

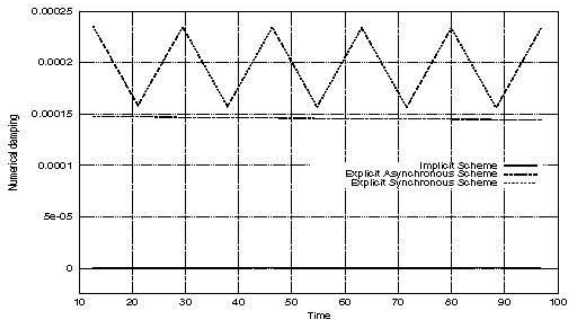


Figure 5. Comparison of numerical damping time evolution for three schemes A, B and C estimated by using tube displacement.

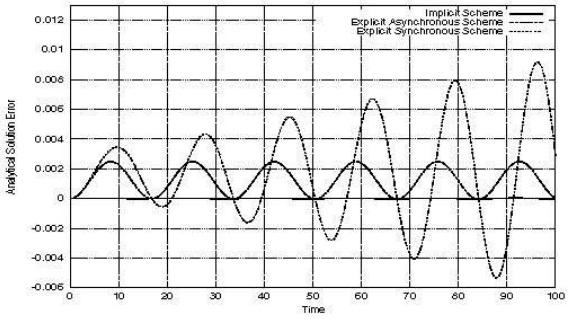


Figure 6. Analytical Error for three code coupling scheme A, B and C.

Furthermore errors between analytical and numerical solutions are compared on figure 6 for the three code coupling schemes A, B and C. Schemes B and C provide the best results and the error increases slowly in time. The explicit synchronous scheme can not satisfy in the same time velocity and displacement continuity and it leads to numerical errors polluting the numerical simulation. To conclude numerical damping created by implicit or explicit asynchronous code coupling schemes is lower than damping generated by explicit synchronous scheme.

### 2.2 Two-dimensional non viscous test case

Fluid structure forces induced by a rigid and undamped moving tube surrounded by a non viscous fluid at rest and a fixed tube is investigated in the present part (cf. figure 7). The purpose is to focuse on the global energy conservation of the fully coupled fluid structure system.

First the analytical solution for high Stokes number is recalled. Then numerical model is presented and finally both analytical and numerical results are compared.

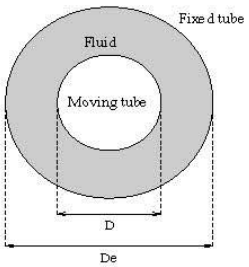


Figure 7. Experimental mockup

**Analytical model** For high Stokes numbers added mass and damping induced by fluid at rest are approached by (Chen, 1987) :

$$M_a = \rho D^2 L \left( \frac{\pi}{4} \frac{1+\left(\frac{D}{D_e}\right)^2}{1-\left(\frac{D}{D_e}\right)^2} + \sqrt{\frac{\pi}{St}} \right) \quad (19)$$

$$C_a = \mu L \left( 2\pi^{\frac{3}{2}} \sqrt{\frac{\rho f D^2}{\mu}} \frac{1+\left(\frac{D}{D_e}\right)^3}{\left(1-\left(\frac{D}{D_e}\right)^2\right)^2} \right) \quad (20)$$

Here the fluid is non viscous (with dynamic viscosity $\mu = 0$) so the associated Stokes number satifies $St = \frac{\rho f D^2}{\mu} = \infty$. The previous system (20) is simplified as follows:

$$M_a \simeq \rho D^2 L \left( \frac{\pi}{4} \frac{1+\left(\frac{D}{D_e}\right)^2}{1-\left(\frac{D}{D_e}\right)^2} \right)$$
$$C_a \simeq 0 \quad (21)$$

Fluid and structure characteristics are given by:

$\rho = 1000\ kg.m^{-3}$ fluid density
$\mu = 0$ dynamic fluid viscosity
$D = 2$ mm tube diameter
$D_e = 2.5 * D = 5$ mm external diameter
$L_z = 1$ mm reference length
$M_s = 5.96\ 10^{-4}$ kg structure mass
$C_s = 0$ structure damping
$f_s = 119.36$ Hz structure damping
$St = \infty$ Stokes number
$A = 1 * 10^{-2}$ mm initial tube displacement amplitude

Analytical added mass and damping for this case test are:

$$M_a = 4.3384.\ 10^{-6}\,\text{kg}$$
$$C_a = 0$$

The expected displacement for a undamped structure in a non viscous fluid are according to the anaytical prediction:

$$x = x_o cos(2\pi f_{water} t)$$

**Numerical model** Tube displacement satifies the classical mechanical equation:

$$M_s \frac{d^2x}{dt^2} + C_s \frac{dx}{dt} + K_s x = F \quad (22)$$

where $M_s$, $C_s$, $K_s$ and $F$ designate respectively structure mass, damping, stiffness and fluid structure force. By analogy with the mechanical equation, fluid structure force $F$ is modelled by this relation:

$$F = -M_a \frac{d^2x}{dt^2} - C_a \frac{dx}{dt} \quad (23)$$

where $M_a, C_a$ are added mass and added damping for fluid at rest. A fluid structure code coupling is used to get these coefficients.

Second time order solvers, Newmark for the structure and Crank-Nicholson for the fluid are used.

Numerical simulation introduces a numerical damping and the tube displacement satisfies this relation:

$$x = x_o\, cos(2\pi f_{water}\, t) e^{\alpha t} \quad (24)$$

where $\alpha$ designates the numerical damping to be identified. In what follows one compares the damping produced by the three coupling schemes previously mentioned.

**Analytical and numerical results** Tube frequency $f_{water}$ and numerical damping $\alpha$ for the three code coupling schemes are given in the next table.

| Code coupling scheme | $f_{water}$ (Hz) | $\alpha$ (Hz) | $M_a$ (kg) |
|---|---|---|---|
| explicit synchronous | 118.92 | 0.03312 | $4.418.\ 10^{-6}$ |
| explicit asynchronous | 118.92 | 0.02285 | $4.418.\ 10^{-6}$ |
| Implicit | 118.92 | 0.003283 | $4.418.\ 10^{-6}$ |
| Analytical solution | 118.93 | 0 | $4.338.\ 10^{-6}$ |

Table 2. Comparison of analytical and numerical results with three code coupling explicit synchronous, explicit asynchronous and implicit schemes using a time step $dt = 10^{-5}$ s .

As in the one-dimensional test case, the numerical damping is reduced with the implicit and explicit asynchronous scheme and each scheme gives a good estimation of tube frequency in fluid at rest. Best results could be obtained by using more fine fluid mesh.

The mechanical energy of the whole fluid structure system is expressed for these different code coupling schemes. This mechanical energy is conserved for non viscous fluid and an undamped structure. The implicit code coupling scheme ensures the best energy conservation (figure 8).

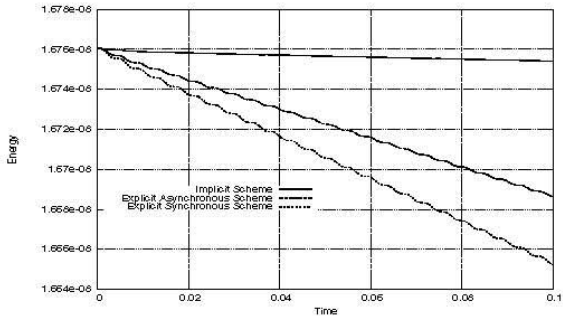


Figure 8. Comparison of fluid structure mechanical energy for three code coupling schemes explicit synchronous, explicit asynchronous and implicit

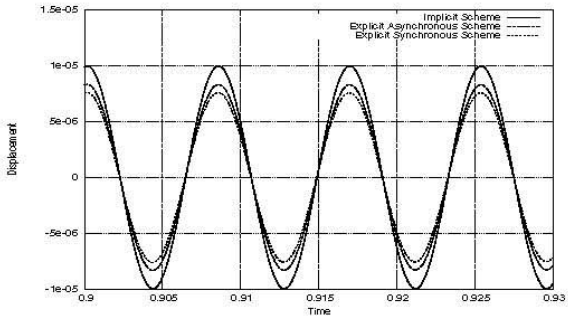


Figure 9. Comparison of structure displacement for three code coupling scheme explicit synchronous, explicit asynchronous and implicit

### 2.3 Two-dimenional viscous test case

Fluid structure forces induced by a rigid moving tube surrounded by a viscous fluid at rest and a fixed tube is modelled (figure 7).

**Analytical model** A complete analytical and experimental study of this case test was made by Chen and al.(1976, 1987), Yeh and Chen (1978) and analytical estimations of added mass and added damping are available. The following notation are recalled:

$D$ tube diameter

$D_e$ external tube diameter

$\gamma = \frac{D}{D_e}$ tube diameter and external tube diameter ratio

$St = \frac{fD^2}{\nu}$ Stokes number

$a$ following determinants ratio

$$a = -\begin{vmatrix} 1 & 1 & F_1(\alpha) & G_1(\alpha) \\ 0 & 1 & \gamma F_1(\beta) & \gamma G_1(\beta) \\ 2 & 2 & \alpha F_0(\alpha) & \alpha G_0(\alpha) \\ 0 & 2 & \alpha F_1(\alpha) & \alpha G_0(\beta) \end{vmatrix} \div \begin{vmatrix} 1 & 1 & F_1(\alpha) & G_1(\alpha) \\ \gamma^2 & 1 & \gamma F_1(\beta) & \gamma G_1(\beta) \\ 0 & 2 & \alpha F_0(\alpha) & \alpha G_0(\alpha) \\ 0 & 2 & \alpha F_1(\alpha) & \alpha G_0(\beta) \end{vmatrix}$$

where $F_n$ and $G_n$ designate 1srt or 2nd kind Bessel functions and $\lambda$, $\alpha$, $\beta$ the following coefficients:

$$\lambda = \sqrt{\frac{-2i\pi St}{D^2}} \quad \alpha = \frac{\lambda D}{2} \quad \beta = \frac{\lambda D_e}{2} \tag{25}$$

Yeh and Chen (1978) give an analytical solution for added mass and damping $\tilde{M}_a$ et $\tilde{C}_a$:

$$\begin{aligned} \tilde{M}_a &= -\frac{\pi}{4} Re(1+2a) \\ \tilde{C}_a &= \frac{\pi^2 St}{2} Im(1+2a) \end{aligned} \tag{26}$$

For high Stokes numbers, added mass and added damping are approached by the formula (Chen 1987):

$$\begin{aligned} \tilde{M}_a &= \frac{\pi}{4} \frac{1+\left(\frac{D}{D_e}\right)^2}{1-\left(\frac{D}{D_e}\right)^2} + \sqrt{\frac{\pi}{St}} \\ \tilde{C}_a &= 2\pi^{\frac{3}{2}} \sqrt{St} \frac{1+\left(\frac{D}{D_e}\right)^3}{\left(1-\left(\frac{D}{D_e}\right)^2\right)^2} \end{aligned} \tag{27}$$

The following characteristics are used for the numerical simulations:

$D$=22 mm tube diameter
$D_e$=2.5*D= 55 mm external tube diameter
$St$=800 Stokes number
A=1.1 mm initial tube displacement amplitude
$\frac{\delta}{D} = \frac{1}{\sqrt{\pi St}} \simeq 0.1994$ Dimensionless boundary layer thickness

Analytical added mass and damping for this case test are (Chen 1987):

$$\begin{aligned} \tilde{M}_a &= 1.1790 \\ \tilde{C}_a &= 497.62 \end{aligned}$$

and for high Stokes number the formula is:

$$\begin{aligned} \tilde{M}_a &= 1.1472 \\ \tilde{C}_a &= 474.98 \end{aligned}$$

Besides there is an empirical law in order to get added mass and damping in a tube bundle using estimations of this coefficient for coaxial cylinders. Rogers (1984) introduces this law:

$$\frac{D}{D_e} = f(\frac{P}{D}) = \left(1.07 + 0.56\frac{P}{D}\right)\frac{P}{D} \tag{28}$$

Dimensional Mass and damping are calculated as follows:

$$M_a = \rho D^2 L \tilde{M}_a$$
$$C_a = \mu L \tilde{C}_a$$

where $\rho$, $\mu$, $D$, $L$ designate respectively fluid density, fluid kinematic viscosity, tube diameter and tube length in the length direction.

**Numerical model** Tube displacement satisfies the classical mechanical equation:

$$M_s\frac{d^2x}{dt^2} + C_s\frac{dx}{dt} + K_s x = F \tag{29}$$

where $M_s$, $C_s$, $K_s$ and $F$ designate respectively structure mass, damping, stiffness and fluid structure force. By analogy with the mechanical equation, fluid structure force $F$ is modelled by this relation:

$$F = -M_a\frac{d^2x}{dt^2} - C_a\frac{dx}{dt} \tag{30}$$

where $M_a$, $C_a$ are added mass and added damping for a fluid at rest.

The numerical fluid structure coupling method introduces code coupling between fluid and structure computation. From an experimental point of view results can be compared to those obtained with a similar experimental corresponding method (Sadok, 1994). This method needs initial conditions (displacement, velocity, force). Here initial structure displacement $x_0$ is chosen to start structure displacement with a fluid initially at rest.

The three code coupling explicit synchronous, explicit asynchronous and implicit schemes are tested. To get accurate results, second time order solver, Newmark for the structure and Crank-Nicholson for the fluid are used. Moreover in the Crank Nicholson scheme, pressure is expressed at time $t^{n+1/2}$ and velocity at time $t^{n+1}$. A linear extrapolation of the pressure at time $t^{n+1}$ is made to compute fluid force acting on the tube:

$$P^{n+1} = \frac{3}{2}P^{n+1/2} - \frac{1}{2}P^{n-1/2} \tag{31}$$

**Results** First, numerical displacement obtained with the three code coupling schemes with the same time step and fluid mesh are compared. Table 3 and figure 10 show that numerical damping induced by coupling is reduced by using explicit asynchronous or implicit code coupling scheme.

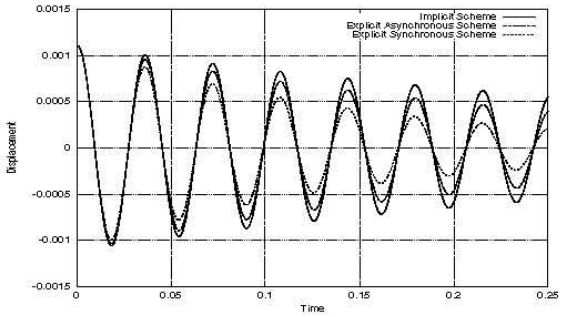


Figure 10. Comparison of structure displacement for different code coupling explicit synchronous, explicit asynchronous and implicit schemes with 896 cells mesh and $5.10^{-4}$ s time step.

| | $\tilde{M}_a$ | $\tilde{C}_a$ |
|---|---|---|
| Analytical results | 1.1790 | 497.2 |
| Synchronous scheme | 1.220 | 1266.63 |
| Asynchronous scheme | 1.218 | 759.32 |
| Implicit scheme | 1.204 | 503.69 |

Table 3. Comparison of different code coupling schemes: explicit synchronous, explicit asynchronous and implicit schemes with 896 cells mesh and $5.10^{-4}$ s time step.

Convergence in time and space for the explicit asynchronous code coupling scheme was tested. Three meshes with different boundary layer refinements were used for space convergence (figure 11) and four time steps were tested for time convergence. As shown in table (4) numerical results are in good agreement with analytical solution with less than 5% error.

Finally the influence of the initial displacement and higher Stokes number have been tested on fluid-structure coefficients. Table (6) shows that there is no significant effect of the initial amplitude on numerical results (less then 1%).

Numerical results for a Stokes number of 14036 are in good agreement with analytical solution (cf. table 7).

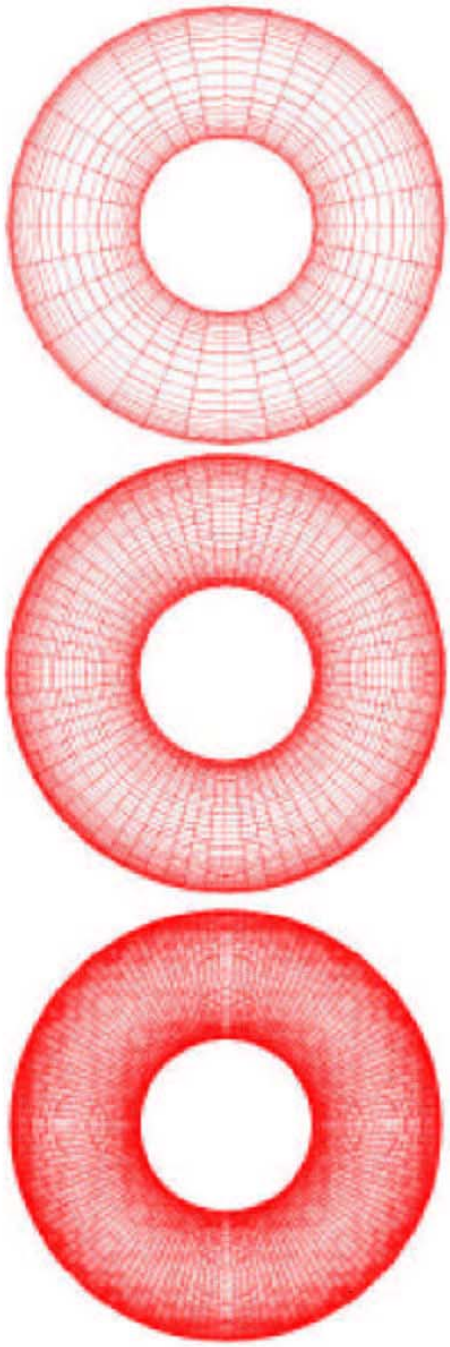

Figure 11. Coarse mesh (896 cells), middle (3712 cells) et fine (16048 cells)

| | coarse mesh | middle mesh | fine mesh |
|---|---|---|---|
| $\tilde{M}_a$ | 1.1944 | 1.1848 | 1.1868 |
| $\tilde{C}_a$ | 495.7 | 497.6 | 501.1 |

Table 4. Convergence in space using a asynchronous scheme and a numerical time step $1.25\,10^{-5}$ s.

| Time step $s$ | $5*10^{-4}$ | $5*10^{-5}$ | $2.5*10^{-5}$ | $1.25*10^{-5}$ |
|---|---|---|---|---|
| $\tilde{M}_a$ | 1.19156 | 1.1878 | 1.1888 | 1.1848 |
| $\tilde{C}_a$ | 738.83 | 513.42 | 500.99 | 497.6 |

Table 5. Time convergence using a asynchronous explicit scheme on a 3712 cells mesh.

| Initial amplitude | 5% | 1% | 0.1% |
|---|---|---|---|
| $\tilde{M}_a$ | 1.1851 | 1.1838 | 1.1838 |
| $\tilde{C}_a$ | 517.09 | 517.85 | 518.53 |

Table 6. Influence of initial tube displacement $x_0$ expressed in percent of tube diameter on fluid-structure coefficient using asynchronous code-coupling scheme with a time step of $5.10^{-5}$ s and 3712 cells mesh.

**Stokes number comparison**

Stokes=800

| | Analytical results | Numerical results |
|---|---|---|
| $\tilde{M}_a$ | 1.1790 | 1.1868 |
| $\tilde{C}_a$ | 497.2 | 501.1 |

Stokes=14036

| | Analytical results | Numerical results |
|---|---|---|
| $\tilde{M}_a$ | 1.1044 | 1.1069 |
| $\tilde{C}_a$ | 1989.6 | 2039.21 |

Table 7. Comparison of analytical and numerical results for two Stokes numbers $St = 800$ and $St = 14036$.

## CONCLUSION

These results allow the validation of numerical code coupling schemes for fluid structure interaction applications, especially for the estimation of added mass and damping by fluid at several Stokes numbers and several configurations. The good properties of numerical implicit schemes and explicit asynchronous schemes were pointed out. The next step will be to apply this tool to further applications.

## ACKNOWLEDGMENT

Authors want to acknowledge MM. Fournier, Archambeau and Benhamadouche for their helpful contribution in the present work.

## REFERENCES

[1] Abouri, D., Parry, A., Hamdouni, A., 2003. Fluid-rigid body dynamic interaction in complex industrial flow. chapter Advances in fluid Mechanics: Fluid Structure interaction II, Wit Press, 295-305.

[2] Chen, S.S., Wambsganss, M.W., Jendrzejczyk, J.A., 1976. Added mass and damping of a vibrating rod in confined viscous fluids. Journal of Applied Mechanics, Transaction of ASME, 43, 325-329.

[3] Chen, S.S., 1987. Flow-Induced Vibration of circular cylindrical structures. Hemisphere publishing corporation.

[4] Daim, F., Eymard, E., Hilhorst, D., Mainguy, M., Masson, R., 2002. A Preconditionned Conjugate Gradient based algorithm for coupling Geomechanical-Reservoir Simulation. Oil & Gas Science and Technology- Rev. IFP, 57, 5, 515-523.

[5] Farhat, C., Lesoinne, M., Maman, N., 1995. Mixed explicit/implicit time integration of coupled aeroelastic problems: three field formulation, geometric conservation and distribution solution, International Journal for Numerical Methods in Fluids. 21, 807-835.

[6] Farhat, C., Lesoinne, M., 1997. Improved Staggered Algorithms for Serial and Parallel Solution of Three-Dimensional Nonlinear Transient Aeroelastic Problems. Center for Aerospace Structures- 97-11, University of Colorado, Boulder, Colorado., AIAA Journal.

[7] Hermann, G.M., Steindorf, J., 1999. Efficient partitioned procedures for computation of fluid-structure interaction on parallel computers. Developments in Computational Mechanics with High Performance Computing, B.H.V, Civil-Comp Press, Edinburgh, S, 127-136.

[8] Le Tallec, P., Mouro, J., 2001. Fluid structure interaction with large structural displacement, Comput. Methods Appl. Mech. Engrg, 190, 3039-3067.

[9] Mani, S., 2003. Truncation error and energy conservation for fluid-structure interactions, Comput. Methods Appl. Mech. Engrg, 192, 4769-4804.

[10] Piperno, S., Farhat, C., Larrouturou, B., 1995. Partitionned procedures for the transient solution of coupled aeroelastic problems. Part I: Model problem, theory and two-dimensional application. Comput.Methods Appl.Mech.Engrg, 124, 79-112.

[11] Piperno, S., Farhat, C., 1997. Design and Evaluation of Staggered Partionned Procedures for Fluid-Structure Interaction Simulations.

[12] Piperno, S., Farhat, C., 2001. Partitioned procedures for the transient solution of coupled aeroelastic problem- Part II: energy transfer analysis and three-dimensional applications. Comput.Methods Appl.Mech.Engrg, 190, 3147-3170.

[13] Rogers, R.J., Taylor, C., Pettigrew, M.J., 1984. Fluid effects on multispan heat exchanger tube vibration. In ASME Pressure Vessel and Piping Conference, San Antonio, Texas.

[14] Thomas, P.D., Lombard, C.K., 1979. Geometric Conservation Law and Its Application to Flow Computations on Moving Grids. AIAA Journal, 17, 1030:1037.

[15] Yeh, T.T., Chen, S.S., 1978. The effect of fluid viscosity on coupled tube/fluid vibration. Journal of Sound and Vibration, 59(3), 453-467.

Proceedings of PVP2005:
2005 ASME Pressure Vessels & Piping Division Conference
Denver, Colorado, USA, July 17 -21, 2005.

PVP-2005-71251

# Comparison of strong and partitioned fluid structure code coupling methods

**Longatte E.** [1]
Electricité de France- R&D Division
Fluid Mechanics and Heat Transfer Department
6, Quai Watier, 78400 Chatou, France
Email: elisabeth.longatte@edf.fr

**Verreman V.** [2]
Electricité de France- R&D Division
Fluid Mechanics and Heat Transfer Department
6, Quai Watier, 78400 Chatou, France

**Bendjeddou Z.** [2]
Electricité de France- R&D Division
Fluid Mechanics and Heat Transfer Department
6, Quai Watier, 78400 Chatou, France
Email: zaky.bendjeddou@edf.fr

**Souli M.** [3]
Université des Sciences et Technologies de Lille I
1, Boulevard Paul Langevin, Cité Scientifique
59655 Lille, France
Email: mhamed.souli@univ -lille1.fr

## ABSTRACT

*As far as flow-induced vibrations are concerned, fluid structure interactions and fluid elastic effects are involved. They may be characterized by parameters like added mass, added damping and added stiffness describing fluid and flow effects on structure motion. From a numerical point of view, identifying these parameters requires numerical simulation of coupled fluid and structure problems. To perform such a multi-physics computation, several numerical methods can be considered involving either a partitioned or a monolithic fluid structure code coupling procedure. Monolithic process is a fully implicit method ensuring the energy conservation of the coupled system. However its implementation may be difficult when specific methods are required for both fluid and structure solvers. The partitioned procedure does not feature the same disadvantage because fluid and structure computations are staggered in time. However a specific attention must be paid to the energy conservation of the full coupled system and one must choose code coupling schemes in order to avoid or to reduce as much as possible numerical dissipation polluting the results.*
*In the present paper, several techniques for fluid structure code coupling are compared. Several configurations are considered and numerical results are discussed in terms of added mass and damping for structures vibrating in fluid at rest. These results contribute to the validation of a full fluid structure code coupling procedure with many possible applications in the fields of fluid structure interactions and flow-induced vibrations.*

## NOMENCLATURE

| | |
|---|---|
| $\delta_s$ | Structure logarithmic decrement in air at rest *[Hz]* |
| $\delta_e$ | Structure logarithmic decrement in water at rest *[Hz]* |
| $\xi_s$ | Structure reduced damping in air at rest *[Hz]* |
| $\xi_e$ | Structure reduced damping in water at rest *[Hz]* |
| $\rho$ | Fluid density *[kg.m$^{-3}$]* |
| $\mu$ | Dynamic viscosity of fluid *[kg.m$^{-1}$.s$^{-2}$]* |
| $\nu$ | Cinematic viscosity of fluid *[m$^{-2}$.s$^{-1}$]* |
| $\omega$ | Circular frequency *[rad.Hz]* |
| $\Delta t$ | Time step *[s]* |
| $A$ | Displacement amplitude *[m]* |
| $C_a$ | Added damping in still water (for concentric tubes) *[kg.s$^{-1}$]* |
| $C_{aa}$ | Dimensionless added damping [-] |
| $C_V$ | Added damping in still water (for eccentric tubes) *[kg.s$^{-1}$]* |
| $C_s$ | Structure damping *[kg.s$^{-1}$]* |
| $D$ | Tube diameter *[m]* |
| $D_e$ | External tube diameter *[m]* |
| $f_s$ | Structure frequency in air at rest *[Hz]* |

[1] Research engineer
[2] Research student
[3] Professor

| | |
|---|---|
| $f_e$ | Structure frequency in water at rest *[Hz]* |
| $F$ | Fluid force *[kg.m.s$^{-2}$]* |
| $F_o$ | Fluid force amplitude *[kg.m.s$^{-2}$]* |
| $K_s$ | Structure stiffness *[kg.s$^{-2}$]* |
| $L$ | Reference length *[m]* |
| $L_z$ | Reference length *[m]* |
| $M_a$ | Added mass in still water *[kg]* |
| $M_{aa}$ | Dimensionless added mass [-] |
| $M_s$ | Structure mass *[kg]* |
| $P$ | Longitudinal pitch *[m]* |
| $P/D$ | Tube diameter pitch ratio *[-]* |
| $P_f$ | Fluid force *[kg.m.s$^{-2}$]* |
| $R_k$ | Reynolds circular number *[-]* |
| $St$ | Stokes number *[-]* |
| $T$ | Transversal pitch *[m]* |
| $u$ | Tube displacement *[m]* |
| $x$ | "Corrected" displacement *[m]* |
| $x_o$ | Displacement amplitude *[m]* |

## INTRODUCTION

Numerical simulation of flow-induced vibrations of mechanical industrial components is investigated here below. The purpose is to suggest a suitable numerical methodology and to validate the tool on few test cases.

The study is divided into three parts : first a presentation of code coupling schemes involved for the identification of fluid-structure parameters is made; then a study on scheme properties is proposed showing and comparing their capability for ensuring energy conservation; finally a validation of the procedure is performed using several test cases whose numerical results are compared to available analytical or experimental solutions. The configurations to be studied are a circular cylinder moving in a concentric annular incompressible non viscous or viscous fluid at rest, an eccentric cylinder moving in a concentric annular incompressible viscous fluid at rest and a rigid tube moving in a fixed square tube array in fluid at rest.

## 1. Theory

### 1.1 Code coupling process

Numerical simulation of fluid structure code coupling is performed in three steps : firstly computation of fluid forces acting on the structure, secondly resolution of mechanical equation and finally actualisation of the fluid domain and the mesh by using an Arbitrary Lagrange Euler (ALE) formulation and by introducing the tube displacement and the velocity as boundary condition for the next time step. Fluid motion equation is solved by using collocated finite volume scheme.

The structure displacement is modelled using a classical mechanical equation :

$$M_s \ddot{u} + C_s \dot{u} + K_s u = P_s \quad (1)$$

where $\ddot{u}$, $\dot{u}$, $u$ and $P_s$ designate respectively structure acceleration, velocity, displacement, fluid force and $M_s$, $C_s$ and $K_s$ structure mass, damping and stiffness. This equation is solved with a second order Newmark algorithm as follows :

$$M_s \ddot{u}^{n+1} + C_s \dot{u}^{n+1} + K_s u^{n+1} = P_s^{n+1} \quad (2)$$

$$\dot{u}^{n+1} = \dot{u}^n + \frac{\Delta t}{2}(\ddot{u}^{n+1} + \ddot{u}^n) \quad (3)$$

$$u^{n+1} = u^n + \frac{\Delta t}{2}(\dot{u}^{n+1} + \dot{u}^n) \quad (4)$$

Predicting structure displacement and velocity at time $t^{n+1}$ requires the computation of fluid forces acting on the structure estimated on the latest geometry called $\Omega^n$ at time $t^n$. To set up this coupling, different code coupling schemes are possible.

### 1.2 Coupling schemes

Three schemes are presented below.

(1) An explicit synchronous code coupling scheme gives a prediction of the fluid structure boundary position at time $t^{n+1}$ using previous position at time $t^n$ and time $t^{n-1}$ as follows :

$$x_{n+1} = u_n + \alpha_0 \Delta t \dot{u}_n + \alpha_1 \Delta t (\dot{u}_n - \dot{u}_{n-1}) \quad (5)$$

where $u^n$ designates tube displacement at time $t^n$, $\dot{u}^n$ and $\dot{u}^{n-1}$ tube velocity at time $t^n$ et $t^{n-1}$. $\Delta t$ is the current time step and $\alpha_0$ and $\alpha_1$ are code coupling coefficients.

With such a formulation the explicit synchronous scheme can not satisfy simultaneously velocity and displacement continuity, violating Geometric Conservation Law (GCL) and thus leading to numerical errors polluting the results. $\alpha_0$ and $\alpha_1$ are chosen so as to get a high order code coupling scheme. For $\alpha_0=1$ and $\alpha_1=1/2$ a second order code coupling scheme in time is obtained. This algorithm was introduced by Farhat et al. (1995, 1997) and gave good results for aeroelastic problems like flow past plane flutter (Piperno et al. 1995).

(2) An explicit asynchronous code coupling scheme ensures that fluid and structure computations are staggered in time. Fluid computation is performed at time $t^{n+1/2}$ while structure computation is performed at time $t^{n+1}$. The following prediction is used for the structure displacement :

$$x^{n+1/2} = u^n + \frac{\Delta t}{2}\dot{u}^n \quad (6)$$

This procedure preserves geometry mesh and ensures displacement and velocity continuity at the fluid structure interface as shown by Thomas and Lombard (1979).

(3) An implicit code coupling scheme using iterative method is also possible. This algorithm is based on the work of Hermann et al. (1999), Le Tallec and Mouro (2001), Piperno and Farhat (2001) and Mani (2003) and Abouri et al. (2003). It uses convergent explicit prediction on the coupled fluid structure system. A criteria based on fluid force or structure velocity is used to stop the numerical process.

Starting with an initial fluid structure state at time $t^0$, the process is made of the following steps :

- Fluid force computation $(F^{n+1})^k$
- Prediction of structure displacement $(x^{n+1})^k$ and structure velocity $(v^{n+1})^k$
- Deformation of the current geometry $(\Omega^{n+1})^k$ and determination of the new geometry $(\Omega^{n+1})^{k+1}$
- Calculation of the error estimator $E$ :

$$E = \frac{\left|(F^{n+1})^{k+1} - (F^{n+1})^k\right|}{F^{n+1\,0}}$$

- If the error estimator is smaller than a critical value ($E < \varepsilon$) the next fluid structure computation at time $t^{n+1}$ is achieved. Otherwise the process restarts from the initial state $t^n$ and the last velocity estimation $(v^{n+1})^k$ is used for the next subcycling of the algorithm.

This iterative process is naturally convergent and it can be accelerated by using a Richardson method (Abouri et al., 2003) or a conjugate gradient method (Daim et al., 2002). In order to keep the code coupling algorithm property, high numerical time order solver must be used for fluid and structure problems.

### 1.3 Fluid structure force identification

In this section numerical identification of fluid structure forces is described. These results are compared to the analytical solution proposed by Chen (1987). The mechanical equation of a structure moving in a fluid at rest can be written :

$$M_s \ddot{X} + C_s \dot{X} + K_s X = F_e + F_t = -M_a \ddot{X} - C_a \dot{X} + F_t \quad (7)$$

with $C_a$ added damping induced by fluid, $M_a$ added mass induced by fluid, $F_e = -M_a \ddot{X} - C_a \dot{X}$ fluid structure force in still water and $F_t$ fluid force independent of structure motion ($F_t \sim 0$ for laminar flows).

The process for numerical identification of fluid structure coefficients is presented in Appendix 1 and relies on convenient data processing. Estimation of added mass and damping in fluid at rest in specific configurations is discussed below. First the properties of coupling schemes are pointed out. Then a validation of the most convenient procedure is proposed with different test cases.

## 2. Scheme properties

Fluid structure interactions for a rigid and undamped moving tube surrounded by a non viscous fluid at rest in a fixed guide tube are investigated below. The configuration is represented in Figure 1. In this test case one focuses his attention on global energy conservation for the fully coupled fluid structure system. The properties of the three previously mentioned coupling schemes are compared. The purpose is to identify the most convenient coupling scheme ensuring energy conservation and good prediction of fluid structure interaction in a physically non dissipative configuration.

### 2.1 Configuration

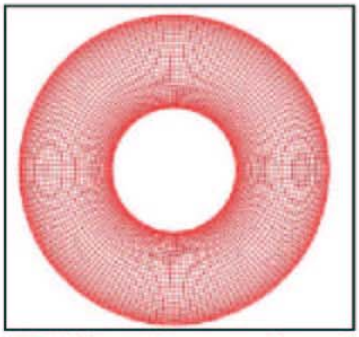

*Figure 1 : Fluid mesh for a concentric moving tube.*

The configuration involves two concentric tubes with an annular fluid at rest. For high Stokes number, added mass and damping induced by fluid at rest are approached by :

$$M_a = \rho D^2 L \left( \frac{\pi}{4} \frac{1 + \left(\frac{D}{D_e}\right)^2}{1 - \left(\frac{D}{D_e}\right)^2} + \sqrt{\frac{\pi}{St}} \right) \quad (8)$$

$$C_a = \mu L \left( 2\pi^{\frac{3}{2}} \sqrt{\frac{\rho f D^2}{\mu}} \frac{1 + \left(\frac{D}{D_e}\right)^3}{\left(1 - \left(\frac{D}{D_e}\right)^2\right)^2} \right) \quad (9)$$

Theory is recalled in Appendix 2.

In the numerical modelling the fluid is non viscous and the associated Stokes number is $St = \frac{\rho f D^2}{\mu} = \infty$.

The previous equations are written :

$$M_a \equiv \rho D^2 L \left( \frac{\pi}{4} \frac{1 + \left(\frac{D}{D_e}\right)^2}{1 - \left(\frac{D}{D_e}\right)^2} \right) \quad (10)$$

$$C_v \equiv 0$$

The empirical law introduced by Rogers et al. (1984) establishes the correspondence between fluid-structure force in tube bundle and fluid-structure force in concentric cylinders by :

$$\frac{D_{eq}}{D} = f\left(\frac{P}{D}\right) = \left(1.07 + 0.56 \frac{P}{D}\right) \frac{P}{D}$$

The test case characteristics are :
$\rho = 1000\ kg.m^{3}$ : fluid density
$\mu = 0$ : fluid dynamic viscosity
$D = 2mm$ : moving tube diameter
$D_e = 2.5*D = 5\ mm$ : external tube diameter
$L_z = 1mm$ : reference length ( z )
$M_s = 5.96\ 10^{-6}\ kg$ : structure mass
$C_s = 0$ : structure damping
$f_s = 119.36\ Hz$ : structure frequency
$ST = \infty$ : Stokes number
$A = 1.0\ 10^{-2}\ mm$ : initial tube displacement amplitude

Analytical added mass and damping in this case are :
$M_a = 5.5238\ 10^{-6}\ kg$
$C_v = 0$
The expected displacement for an undamped structure in a non viscous fluid satisfies the relation :
$x = x_0 \cos(2\pi f_{water} t) e^{\alpha t}$

### 2.2 Numerical results

In what follows one compares tube frequency $f_{water}$ and numerical damping $\alpha$ for the three previously mentioned code coupling schemes (Table 1). Every scheme gives a good estimation of tube frequency in fluid at rest. The numerical damping is smaller with the implicit and explicit asynchronous schemes and it is larger with the explicit synchronous process (Figure 2).

| Coupling schemes | $F_{water}$ (Hz) | $\alpha$ (-) | Ma (Kg) |
|---|---|---|---|
| Explicit synchronous | 118.92 | 0.033 | $4.418*10^{-6}$ |
| Explicit staggered | 118.92 | 0.022 | $4.418*10^{-6}$ |
| Implicit | 118.92 | 0.00032 | $4.418*10^{-6}$ |
| Analytical solution | 118.93 | 0 | $4.338*10^{-6}$ |

*Table 1 : Comparison of analytical and numerical results with the three code coupling schemes explicit synchronous, explicit asynchronous and implicit using the same time step and the same mesh.*

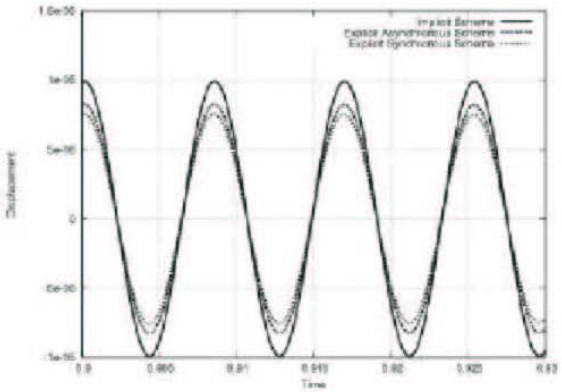


*Figure 2 : Comparison of structure displacement for the three code coupling schemes explicit synchronous, explicit asynchronous and implicit.*

Moreover the mechanical energy of the full coupled fluid structure system is plotted for the different code coupling schemes in Figure 3. The mechanical energy is conserved for a non viscous fluid and an undamped structure. According to the results implicit code coupling scheme ensures the best energy conservation.
The explicit asynchronous scheme provides intermediate results. It is chosen for the next numerical computations presented in this document. The time cost is lower with this scheme than with the implicit scheme involving subcycling in the fluid calculation and the quality of results is acceptable in terms of added mass and damping.

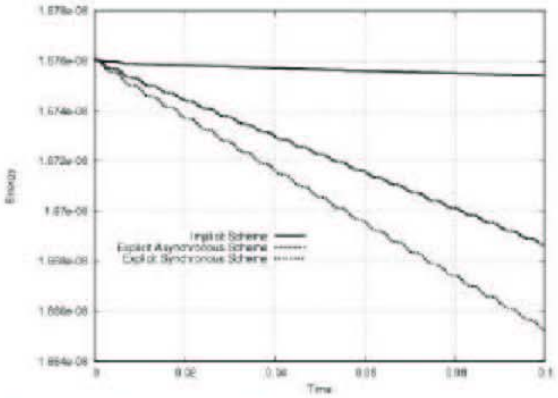


*Figure 3 : Comparison of fluid-structure mechanical energy for the three code coupling schemes explicit synchronous, explicit asynchronous and implicit.*

## 3. Validation

The next part is devoted to the validation of the fluid structure coupling tool using different test cases. The explicit asynchronous scheme is involved with a time step $\Delta t = 10^{-5}$ s.

### 3.1 Concentric tubes

Fluid structure forces induced by a rigid moving tube surrounded by a viscous fluid at rest and a fixed tube is modelled. A complete analytical and experimental study of this configuration is proposed by Chen et al. (1976), Chen (1987) and Yeh and Chen (1978). Analytical estimations of added mass and added damping are available.
The following notation are introduced :
D : moving tube diameter
$D_0$ : fixed tube diameter

$$St = \frac{\omega D^2}{4\nu} : \text{Stokes number}$$

$$\frac{\delta}{D} = \frac{1}{\sqrt{\pi St}} : \text{boundary layer thickness}$$

Different tube diameter ratio values $D_0/D$ are studied for $D_0/D = 1.2, 2.5, 4, 10$ and in each case, different Stokes number values $St$ are considered for $St = 10, 100, 5000, \infty$. To test several Stokes numbers, the dynamic viscosity $\mu$ is modified and a

small dynamic viscosity $\mu=10^{-43}$ is chosen for $St = \infty$. Moreover for all computations, the initial tube displacement is small and chosen so that the flow remains laminar. In each case, a space and a time convergence has been achieved.
The mesh displacement is represented in Figure 4. Fixed cells in the tube reference are introduced in the vicinity of the tube in order to avoid near-wall local mesh distortion. Dimensionless added mass and damping estimated numerically are compared to available analytical values in Figures 5 and 6 for several diameter ratios and Stokes numbers. Numerical results are in good agreement with expected solutions and the tube in fluid at rest features the expected behaviour. For Stokes number $St=5000$ dimensionless parameters are reported in Table 2. One gets an error smaller than 5% between numerical solution and analytical data of Sinyavaskii (1980).

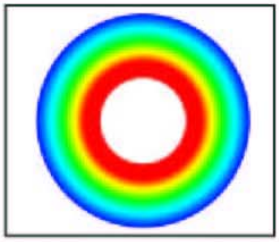

**Figure 4 : Mesh displacement.**

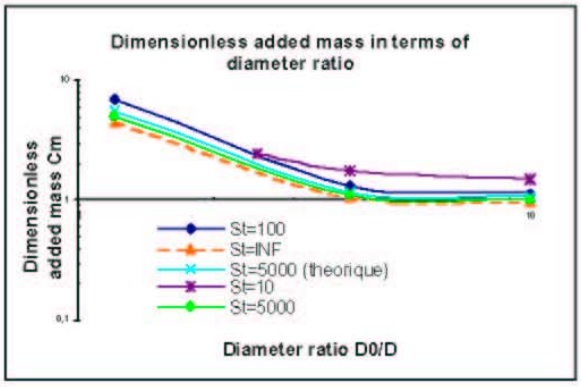


***Figure 5 : Dimensionless added mass in terms of diameter ratio for concentric tubes for different Stokes numbers for viscous fluid (St = 10, 100, 5000) and non viscous fluid (St = infinity). Comparison of numerical and analytical available solutions.***

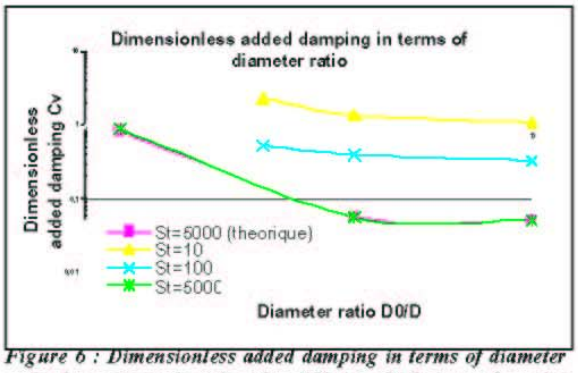


***Figure 6 : Dimensionless added damping in terms of diameter ratio for concentric tubes for different Stokes numbers for viscous fluid (St = 10, 100, 5000). Comparison of numerical and analytical available solutions.***

| Analytical results | Numerical results |
|---|---|
| Added mass | |
| 1.17333 | 1.09525 |
| Added damping | |
| 0.05793 | 0.06 |

***Table 2 : Dimensionless added mass and damping for concentric tubes with D0/D=4 and St = 5000.***

### 3.2 Eccentric tubes

In this test case, a tube diameter ratio $D_0/D=2$ configuration is considered and several cylinder eccentricity values are tested $e = 0, 0.3, 0.6$. Here the Reynolds circular number is imposed at $R_k=\frac{\omega D^2}{\nu}=50$. The dynamic viscosity $\nu$ is chosen in order to keep a reasonable tube frequency. Dimensional added mass and damping have the following form :

$m_a = \rho V C_m$

$C_v = -\frac{C_v}{\rho \pi R^2 \omega}$ (see Appendix 2)

In what follows the numerical results obtained with the partitioned procedure are compared to those obtained by Yang and Moran (1979) with an implicit monolithic procedure. The monolithic procedure relies on a finite element method coupling both fluid and structure computations in a strong coupling way.
Mesh and mesh displacement with the partitioned procedure are shown in Figures 7 and 8. Dimensionless added mass and damping are plotted in Figure 9. Numerical results obtained with the partitioned procedure and with the monolithic one are compared and according to the results, they are in good agreement.

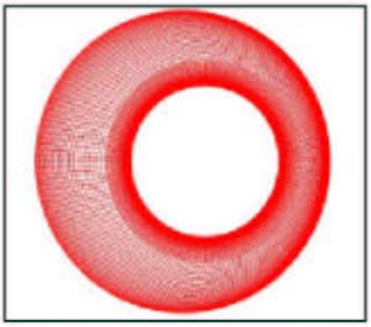

*Figure 7 : Mesh for tube with eccentricity e=0.3.*

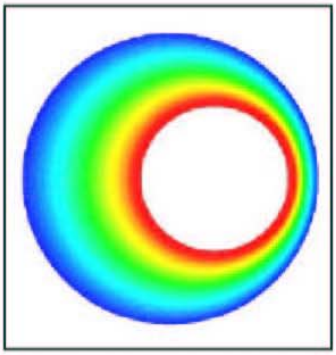

*Figure 8 : Mesh displacement in the x direction.*

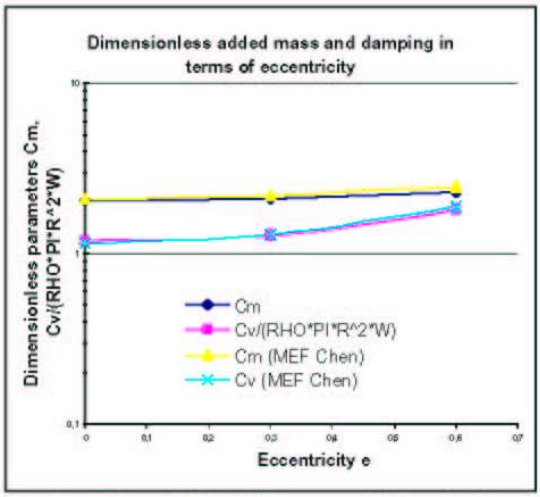


*Figure 9 : Dimensionless added mass and damping in terms of eccentricity for eccentric tubes. Comparison of numerical solutions with the numerical partitioned procedure and the numerical monolithic solution in Chen et al. (1987).*

### 3.3 Tube bundles

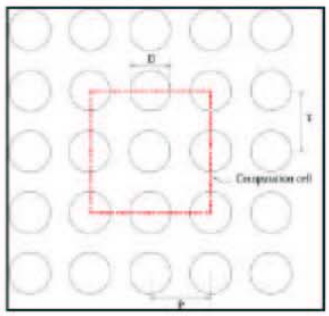

*Figure 10 : Experimental configuration for P/D = 1.5 (Weaver et al., 1985).*

A tube bundle configuration is studied and numerical identification of added mass and damping in fluid at rest for a single tube moving in a fixed tube array is investigated. The configuration is an in line square array with a pitch ratio diameter *P/D = 1.75* (Weaver and Abd-Rabbo, 1985). Numerical results obtained with the partitioned procedure are compared with available experimental results (Weaver and Abd-Rabbo, 1985).

The test case characteristics are given below :

$A = 1.0\ 10^{-5}$ mm : initial tube displacement amplitude

$\rho = 1000$ kg.m$^{-3}$ : fluid density

$\mu = 10\text{-}3$ : dynamic fluid viscosity

$D = 25.4$mm : tube diameter

$Lz = 300$ mm : tube length

$f_s = 25.5$ Hz +/- 0.2 Hz : structure frequency in air

$St = \frac{f_s D^2}{\nu} = 16000$ : Stokes number

$\delta_s = 0.014 +\text{-} 0.001$

$\delta_e = 0.037 +\text{-} 0.004$

In what follows one compares added damping estimated numerically and logarithmic increment in water measuring added damping. Fluid structure coefficients depend only on Stokes number and tube confinement. Structure mass and stiffness in air could be chosen arbitrarily and have to satisfy the given structure frequency $f_s$ in air.

In this computation, the fluid is newtonian and the flow is two-dimensional and incompressible. Periodic boundary conditions are used on a elementary 9-tubes computational cell in order to simulate an infinite tube bundle (figure 10). The explicit asynchronous code coupling scheme is used. Numerical results and experimental measurements are compared in Table 3.

| Experimental decrement (P/D=1.5) | Numerical results (P/D=1.5) |
|---|---|
| 0.037 | 0.03537 |

*Table 3 : Added damping estimated numerically and experimentally for a tube array with pitch ratio P/D = 1.5.*

Numerical results are in good agreement with experimental measurement with an error smaller than 10 %. A bigger computational cell could be used to improve numerical results.

## CONCLUSION

These studies provide a validation of the partitioned code coupling process in several configurations involving different Stokes numbers, boundary conditions and geometries.
The main objective of the present work is to contribute to the study of PWR (Pressurized Water Reactor) components who are subjected to complex flows causing possible vibrations and damages to the structure. To improve the code coupling process, further computations will be performed in tube bundles submitted to cross-flows. One of the main objective is to study numerically fluid-elastic instability development in tube bundles in cross flows responsible for possible wear problems and vibration fatigue.

## APPENDIX 1

### Post-processing for identification of fluid structure parameters :

A brief explanation of added mass and damping identification is explained in this appendix. A structure moving in a viscous fluid at rest in considered.

$$M_s \ddot{X} + C_s \dot{X} + K_s X = -M_a \ddot{X} - C_v \dot{X}$$

then :

$$(M_s + M_a)\ddot{X} + (C_s + C_v)\dot{X} + K_s X = 0$$

The characteristic equation is :

$$(M_s + M_a)r^2 + (C_s + C_v)r + K_s = 0$$

$$\Delta = (C_s + C_v)^2 - 4(M_s + M_a)K_s$$

A damped displacement is expected then $\Delta<0$ and the solutions of the characteristic equation are :

$$r_1 = \frac{-(C_s + C_v)}{2(M_s + M_a)} - i\sqrt{|\Delta|}\,\frac{1}{2(M_s + M_a)}$$

$$r_2 = \bar{r}_1$$

The structure displacement solution of a differential equation is:

$$X = a\exp\left(\frac{-(C_s + C_v)}{2(M_s + M_a)}t\right)\left[\exp\left(\frac{i\sqrt{|\Delta|}}{2(M_s + M_a)}t\right) + \exp\left(-\frac{i\sqrt{|\Delta|}}{2(M_s + M_a)}t\right)\right]$$

One defines the cylindrical frequency $\omega = \sqrt{\frac{K_s}{(M_s + M_a)}}$

with $\omega=2\pi f$ where $f$ is the structure frequency in fluid at rest.

One gets:

$$X = a\exp\left(\frac{-(C_s + C_v)}{2(M_s + M_a)}t\right)\cos\left(\sqrt{\omega^2 - \frac{(C_s + C_v)^2}{4(M_s + M_a)^2}}t\right)$$

The structure displacement has the following form:

$$X = a\exp(-\alpha t)\cos(w_p t)$$

with :

$$\alpha = \frac{C_s + C_v}{2(M_s + M_a)}$$

$$w_p = \sqrt{\omega^2 - \frac{(C_s + C_v)^2}{4(M_s + M_a)^2}}$$

Finally :

$$\omega = \sqrt{\alpha^2 + w_p^2}$$

$$M_a = \frac{K_s}{\omega} - M_s$$

$$C_v = 2\alpha(M_s + M_a) - C_s$$

Dimensionless added mass and added damping are expressed as follows:

$$M_{aa} = \frac{M_a}{L_z \rho D^2}$$

$$C_{aa} = \frac{C_a}{L_z \rho \pi R^2 \omega}$$

where $L_z$ designates tube length, $\rho$ structure density, D et R respectively moving tube diameter and tube radius. $M_{aa}$ et $C_{aa}$ are dimensionless added mass and damping.

## APPENDIX 2

### Analytical theory for identification of fluid structure parameters in concentric tubes :

Analytical solutions are based on the following theory and assumptions (Chen 1987). A viscous fluid and an incompressible flow are considered. Structure displacement is supposed to be small and Navier-Stokes equations are linearized :

$$\vec{\nabla}\vec{u} = 0$$

$$\frac{\partial \vec{u}}{\partial t} = -\frac{1}{\rho}\vec{\nabla}P + \frac{1}{\nu}\nabla^2\vec{u}$$

with $\vec{u}$ the velocity field and P the pressure.
The velocity and pressure of fluid are given by:

$$\vec{u} = \vec{\nabla}\phi + \vec{\nabla}x\vec{\psi}$$

$$P = -\rho\frac{\partial \phi}{\partial t}$$

$$\nabla^2\phi = 0$$

and $(\nabla^2 - \frac{1}{c^2}\frac{\partial}{\partial t})\vec{\psi} = 0$ c : sound velocity

The solution of this system is given by :

$$\nabla^4\psi - \frac{1}{\nu}\frac{\partial}{\partial t}\nabla^2\psi = 0 \qquad \text{(a)}$$

Using cylindrical coordinates, one gets :

$$u_r = -\frac{\partial\psi}{r\partial\theta} \;;\; u_\theta = \frac{\partial\psi}{\partial\theta}$$

On the fluid-structure interface, fluid velocity direction must be given by structure displacement, the two velocity components $u_r$ and $u_\theta$ are:

$$u_r = a\cos\theta\exp(i\omega t) \quad (b)$$

and

$$u_\theta = -a\sin\theta\exp(i\omega t) \quad \text{(c)}$$

Boundary conditions on fixed cylinder are :

At $r = D_0/2$ , $u_r = u_\theta = 0$ (d)

The exact solution of equation (a) is :

$$\psi = a[A_1(\frac{D^2}{r}) + A_2 r + A_3 DI_1(\lambda r) + A_4 DK_1(\lambda r)]\sin\theta\exp(i\omega t) \qquad \text{(e)}$$

with $\lambda = \sqrt{i\frac{\omega}{\nu}}$

$A_1$, $A_2$, $A_3$ and $A_4$ are arbitrary constants. They are expressed by the equations (b), (c), (d) and (e), with the coefficients $\alpha=\lambda D/2$, $\beta=\lambda D_0/2$, $\gamma=D_0/D$ and a function $\Delta$ in terms of modified Bessel function $I_i(j)$ and $K_i(j)$ $(i=0,1\ ,\ j=\alpha,\beta)$.

Then the fluid force acting on the cylinder per unit length is:

$g = M_a a\omega[Re(H)\sin\omega t + Im(H)\cos\omega t]$

This force can be expressed by using fluid velocity $\vec{u}$ :

$$g = -C_m M_a\frac{d^2u}{dt^2} - C_v\frac{du}{dt}$$

where

$C_m = Re(H)$,

$C_v = -M_a\omega Im(H)$,

$M_a = \rho\pi R^2$,

and

$H = \{2\alpha^2[I_0(\alpha)K_0(\beta) - I_0(\beta)K_0(\alpha)] - 4\alpha[I_1(\alpha)K_0(\beta) + I_0(\beta)K_1(\alpha)] + 4\alpha\gamma[I_0(\alpha)K_1(\beta) + I_1(\beta)K_0(\alpha)] - 8\gamma[I_1(\alpha)K_1(\beta) - I_1(\beta)K_1(\alpha)]\}/\{\alpha^2(1-\gamma^2)[I_0(\alpha)K_0(\beta) - I_0(\beta)K_0(\alpha)] - 2\alpha\gamma[I_0(\alpha)K_1(\beta) - I_1(\beta)K_0(\beta) + I_1(\beta)K_0(\alpha) - I_0(\beta)K_1(\beta)] + 2\alpha\gamma^2[I_0(\beta)K_1(\alpha) - I_0(\alpha)K_1(\alpha) + I_1(\alpha)K_0(\beta) - I_1(\alpha)K_0(\alpha)]\} - 1$

$H$ is a determinant ratio introducing modified Bessel functions 1 and 2 $I_i$ and $K_i$.

Two forces are associated with fluid motion :

$M_a a\omega Re(H)\sin\omega t$ ,in phase with acceleration, arises because the fluid is necessarily moving as the cylinder vibrates.

$M_a a\omega Im(H)\cos\omega t$, in opposite phase with the cylinder motion, is related to a mechanical damping.

$H$ depends on $\alpha$ and $\beta$. For large $\alpha$ and $\beta$, it is written :

$H = \{\alpha^2(1+D_0^2/D^2) - 8D_0/D]\sinh(\beta-\alpha) + 2\alpha(2-D_0/D+D_0^2/D^2)\cosh(\beta-\alpha) - (2D_0^2/D^2)(\alpha\beta)^{1/2} - 2\alpha(D_0/D)^{3/2}\}/\{\alpha^2(1-D_0^2/D^2)\sinh(\beta-\alpha) - 2\alpha(D_0/D)(1+D_0/D)\cosh(\beta-\alpha) + (2D_0^2/D^2)(\alpha\beta)^{1/2} + 2\alpha(D_0/D)^{3/2}\}$

Added mass and damping $C_m$ *and* $C_v$ are expressed in terms of $H$ depending on $D_0/D$ and on Reynolds number $R_k$ ($R_k = \omega D^2/\nu$).

Sinyavaskii et al. (1980) developed the following similar formula for $C_m$ and $C_v$ (it's an other solution):

$$C_m = \frac{D_0^2 + D^2}{D_0^2 - D^2} + \frac{4}{D}\left(\frac{2\nu}{\omega}\right)^{1/2}$$

and :

$$C_v = \frac{2\pi\mu D}{\sqrt{\frac{2\nu}{\omega}}}\left[\frac{D_0^4 + D^3 D_0}{(D_0^2 - D^2)^2}\right]$$

The latest formula of added mass and added damping are equivalent to the first expression of $H$ for high Stokes number :

$\mathrm{St} = \omega D^2/4\nu >> 1$ .

## REFERENCES


Abouri, D., Parry, A., Hamdouni, A., 2003. Fluid-rigid body dynamic interaction in complex industrial flow. Chapter Advances in fluid Mechanics: Fluid Structure interaction II, Wit Press, 295-305.

Chen, S.S., Wambsganss, M.W., Jendrzejczyk, J.A., 1976. Added mass and damping of a vibrating rod in confined viscous fluids. Journal of Applied Mechanics, Transaction of ASME, 43, 325-329.

Chen, S.S., 1987. Flow-Induced Vibration of circular cylindrical structures. Hemisphere publishing corporation.

Daim, F., Eymard, E., Hilhorst, D., Mainguy, M., Masson, R., 2002. A Preconditioned Conjugate Gradient based algorithm for coupling Geomechanical-Reservoir Simulation. Oil & Gas Science and Technology - Rev. IFP, 57, 5, 515-523.

Farhat, C., Lesoinne, M., Maman, N., 1995. Mixed explicit implicit time integration of coupled aeroelastic problems: three field formulation, geometric conservation and distribution solution, International Journal for Numerical Methods in Fluids. 21, 807-835.

Farhat, C., Lesoinne, M., 1997. Improved Staggered Algorithms for Serial and Parallel Solution of Three-Dimensional Nonlinear Transient Aeroelastic Problems. Center for Aerospace Structures - 97-11, University of Colorado, Boulder, Colorado., AIAA Journal.

Hermann, G.M., Steindorf, J., 1999. Efficient partitioned procedures for computation of fluid-structure interaction on parallel computers. Developments in Computational Mechanics with High Performance Computing, B.H.V, Civil-Comp Press, Edinburgh, S, 127-136.

Le Tallec, P., Mouro, J., 2001. Fluid structure interaction with large structural displacement, Comput. Methods Appl. Mech. Engrg, 190, 3039-3067.

Mani, S., 2003. Truncation error and energy conservation for fluid-structure interactions, Comput. Methods Appl. Mech. Engrg, 192, 4769-4804.

Piperno, S., Farhat, C., Larrouturou, B., 1995. Partitionned procedures for the transient solution of coupled aeroelastic problems. Part I: Model problem, theory and two-dimensional application. Comput.Methods Appl.Mech.Engrg, 124, 79-112.

Piperno, S., Farhat, C., 2001. Partitioned procedures for the transient solution of coupled aeroelastic problem- Part II: energy transfer analysis and three-dimensional applications. Comput.Methods Appl.Mech.Engrg, 190, 3147-3170.

Rogers, R.J., Taylor, C., Pettigrew, M.J., 1984. Fluid effects on multispan heat exchanger tube vibration. In ASME Pressure Vessel and Piping Conference, San Antonio, Texas.

Sinyavaskii, V.F.., Fedotovskii, V.S., Kukhtin, A.B., 1980. Oscillating of a Cylinder in a Viscous fluid. Prikladanaya Mekhanika , 16(1), 62-27.

Thomas, P.D., Lombard, C.K., 1979. Geometric Conservation Law and Its Application to Flow Computations on Moving Grids. AIAA Journal, 17, 1030:1037.

Weaver, D.S, Abd-Rabbo, A. 1985. A flow visualisation Study of a Square array of Tubes in Water Crossflow. Journal of Fluids Engineering, 107, 354-363.

Yang, C.I., Moran, T.J., 1979. Finite-Element Solution of Added Mass and Damping of Oscillation Rods in Viscous Fluids. Journal of Applied Mechanics. 46, 519-52

Yeh, T.T., Chen, S.S., 1978. The effect of fluid viscosity on coupled tube/fluid vibration. Journal of Sound and Vibration, 59(3), 453-467.

# CONCLUSIONS - PERSPECTIVES

# CONCLUSIONS – PERSPECTIVES

## 1. Principaux résultats et intérêts industriels

A la suite de ces travaux, on peut dire que le principal fait marquant est l'aboutissement à la création d'un outil prototype de simulation numérique des chaînages et des couplages fluide structure au sens large, mettant en œuvre des codes de calculs opérationnels et donc applicable à terme à la réalisation d'études à caractère industriel.

La démarche est innovante et les résultats obtenus confortent dès à présent l'industriel dans son engagement vers un programme de développement et de co-développement d'outils et de plateformes de couplages multi-physiques multi-échelles optimisés. Les configurations traitées sont certes académiques mais elles présentent un intérêt sur le plan industriel, a minima dans le cadre d'études locales éventuellement en similitude géométrique, mécanique ou hydraulique.

La phase d'industrialisation est dores et déjà engagée avec les travaux en cours d'intégration du prototype mis au point dans la plateforme généraliste de couplages *Salomé* destinée à terme à absorber toutes les évolutions futures, qu'elles soient de nature algorithmique, méthodologique ou physique. Parmi les principaux chantiers de développements en cours dans la continuité de ces travaux, on peut citer :

- l'axe couplage et parallélisme
- la thématique interface mobile et turbulence
- les extensions aux couplages multi-physiques multi-échelles

### 1.1. Couplage et parallélisme

Dans un contexte d'engagement de plus en plus systématique vers un parallélisme plutôt orienté à mémoire distribuée à ce jour, pour des outils multiples supportant tous types de formulations compatibles ou incompatibles et d'éléments conformes ou non conformes, la gestion des couplages dans un cadre distribué devient incontournable dans une perspective d'optimisation des performances des schémas de couplages. De telles évolutions requièrent des modifications profondes au niveau des algorithmes, aussi bien pour la gestion de la mémoire - avec le compromis à gérer : augmentation ou diminution de la mémoire en fonction du nombre de processeurs utilisés et de la taille des systèmes gérés au niveau de chaque processeur -, que pour le choix des modes de transferts de données entre processeurs, seuls les processeurs possédant des nœuds ou des éléments communs devant échanger des informations, avec la contrainte globale qui consiste à adopter une procédure d'échange symétrique entre émetteur et récepteur, qu'ils appartiennent à un même sous-système ou à des sous-systèmes couplés distincts, et distribuée en évitant le recours à des processeurs « maîtres », y compris pour l'avancée en temps du couplage. Un exemple d'utilisation d'une méthode par décomposition de domaines pour un couplage entre plusieurs sous-systèmes est illustré sur la Figure 53. L'extension de ces méthodes à tous types de couplages avec l'identification de critères systématiques permettant d'optimiser les performances des coupleurs parallèles en fonction de la nature des problèmes à gérer et des calculateurs utilisés n'en est qu'à ses débuts.

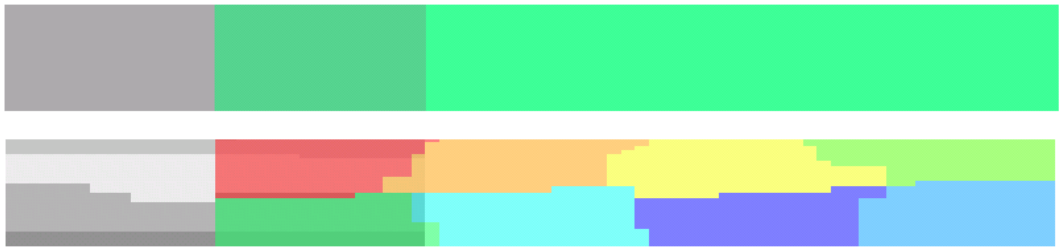

*Figure 53 : Exemple de gestion de couplage par une méthode de décomposition de domaines avec d'éventuelles zones de recouvrement surfacique ou volumique entre les domaines représentant les sous-systèmes couplés.*

### 1.2. Interface mobile et turbulence

Outre les aspects propres à la modélisation de la turbulence, - comme la validation des chargements pariétaux abordés dans le premier chapitre et encore non résolue pour l'ensemble des configurations à traiter (Figure 54 et Figure 55), la réduction de la taille du problème fluide avec par exemple l'utilisation de maillages non conformes compatibles avec le filtrage L.E.S. dans les directions axiales et transverses au cisaillement (Figure 56), l'optimisation du choix des modèles de turbulence avec la possibilité d'introduire localement des couplages entre modèles distincts (comme un couplage R.A.N.S. – L.E.S.), ou encore, en diphasique, la question sur les limites d'un modèle global homogène et la nécessité de recourir à une formulation locale fine augmentant le nombre de degrés de liberté du problème fluide, - la prise en compte de couplages fluide structure introduit une problématique supplémentaire sur les lois de parois mobiles, pour tout type de surface, tout type de maillage et tout type de modèle de turbulence, avec prise en compte des vitesses de glissement aux parois adaptées aux configurations à traiter.

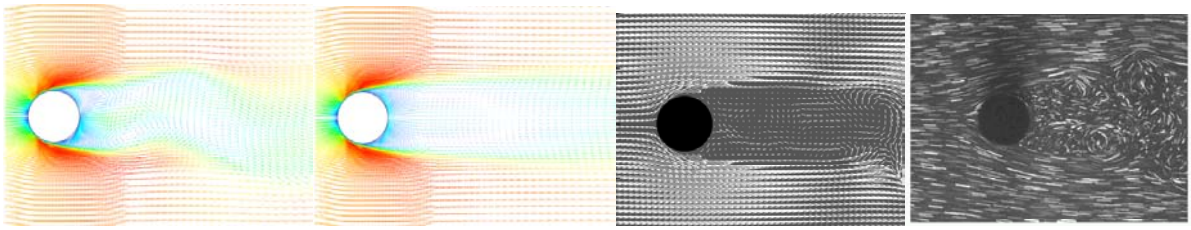

*(a)* *(b)* *(c)* *(d)*

*Figure 54 : Ecoulement derrière un cylindre : (a) LES, (b) LES moyennée, (c) DES, (d) Expérimental (Afgan et al. 2005).*

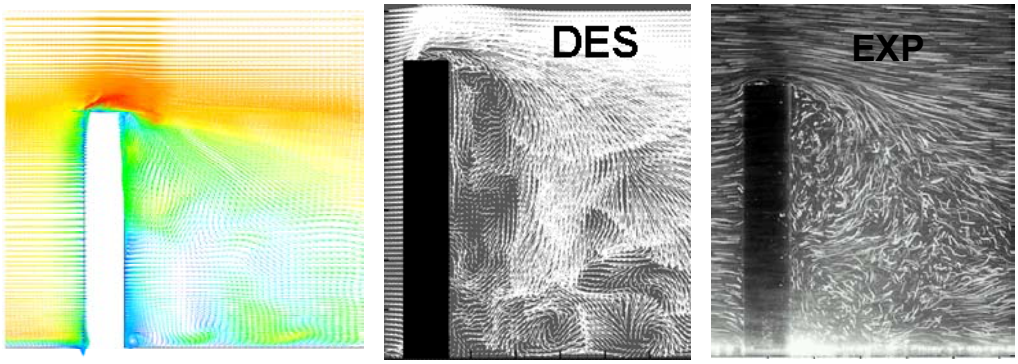


*(a)* *(b)* *(c)*

*Figure 55 : Ecoulement derrière un barreau : (a) LES, (b) DES, (c) Expérimental (Afgan et al. 2005).*

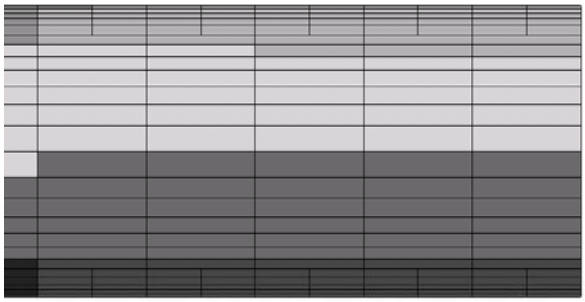

*Figure 56 : Exemple de maillage non conforme.*

### 1.3. Couplages multi-physiques multi-échelles

A fortiori la prise en compte de couplages multi-physiques quelconques faisant intervenir la thermohydraulique monophasique ou diphasique (Figure 57) et plusieurs autres disciplines comme la mécanique (Figure 58), la thermique (Figure 59), la neutronique ou la chimie introduit des difficultés nouvelles, non seulement au niveau de la supervision des couplages qui grâce à une architecture optimisée des plateformes doit supporter tout type de schéma d'avancée en temps pour les transferts de données entre solveurs, mais également du point de vue des modélisations physiques qui doivent rester toutes compatibles dans un contexte couplé, tout en étant pertinentes au sein de chaque sous-système. Ainsi la physique couplée peut introduire des interfaces particulières qui nécessitent des traitements singuliers pouvant impacter les méthodes numériques mises en œuvre de part et d'autre de l'interface. A titre d'exemple, on peut citer le cas du couplage fluide structure avec contact entre deux structures et grande déformation du domaine de calcul fluide de sorte qu'un formalisme A.L.E. ne convient pas, la topologie de la grille de calcul fluide ne pouvant rester inchangée au cours du temps. Une telle situation nécessite une méthode particulière pour le transfert de données entre solveurs fluide et structure et impacte directement chacun des solveurs. On peut citer l'exemple de la méthode Chimère (Figure 60) : son intégration au niveau du solveur fluide pour la résolution de problèmes de couplage avec une interface structure mobile requiert des modifications profondes comme la gestion de conditions aux limites au niveau des faces internes de la grille de calcul, ou encore la prise en compte de cellules fissiles, mixtes fluide structure pour les calculs à l'interface.

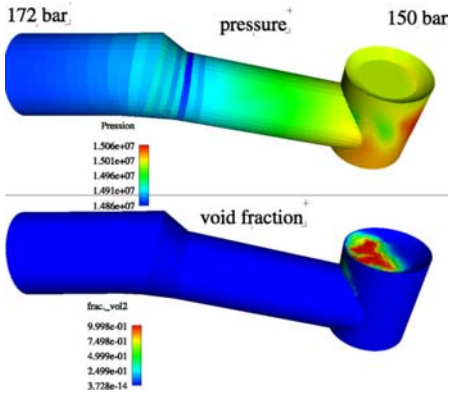


*Figure 57 : Simulation de création de vapeur au niveau du clapet d'un robinet dans des conditions thermohydrauliques caractéristiques d'un fonctionnement en ouverture rapide avec génération d'un effort de pression sur la tige de commande pouvant conduire à un problème de manœuvrabilité (Mimouni et al. 2006).*

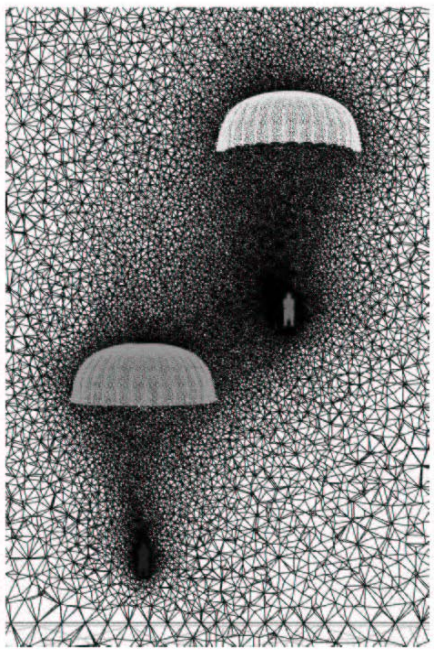

*Figure 58 :Exemple de couplage fluide structure en présence de plusieurs structures couplées.*

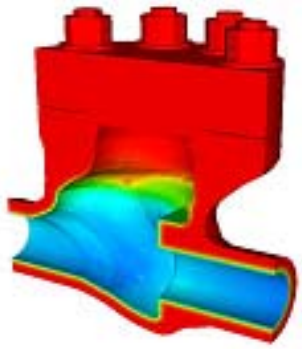

*Figure 59 : Exemple de couplage fluide structure par le biais de chargements pariétaux thermiques (Péniguel et al.).*

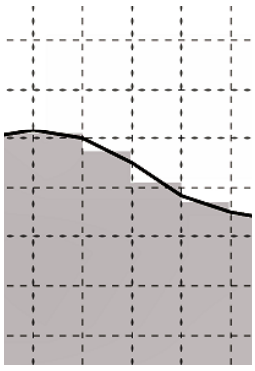

*Figure 60 : Exemple de gestion d'une interface fluide structure avec une formulation non A.L.E. de type Chimère.*

## 2. Perspectives d'applications et apports scientifiques

Au vu des premiers résultats obtenus en faisceaux de tubes, les applications directes de ces travaux relèveront du domaine des vibrations de structures induites par écoulements avec l'identification de vitesses critiques de départ en instabilité pour tout type de configuration de géométrie, fluide et structure quelconques (Figure 61). Des exemples d'applications sont fournis dans les Annexes 12 à 14.

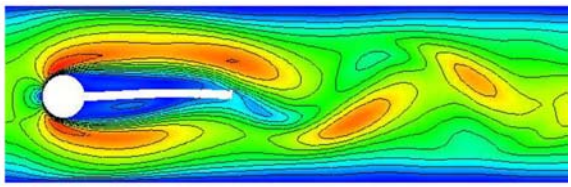

*Figure 61 : Exemple de départ en grand déplacement d'une lame flexible en aval d'un cylindre en présence d'un écoulement transverse (Hron et Turek 2006).*

### 2.1. Connaissance physique

Les futurs calculs couplés permettront-ils d'enrichir les cartes d'instabilités actuellement à la base de la plupart des études vibratoires des faisceaux de tubes de générateurs de vapeur, en régimes monophasiques et diphasiques, et pourtant reconnues incomplètes car basées uniquement sur une partie des paramètres adimensionnels de couplage (Figure 62 et Figure 63) ? Les études numériques paramétriques locales permettront-elles d'établir de nouvelles lois adimensionnelles fournissant des critères de stabilité systématiques pour tous types de configurations mettant en jeu des couplages forts ainsi que de nouvelles lois de transposition permettant d'extrapoler des observations faites sur maquettes dans des conditions de fonctionnement réelles, en particulier en réacteur (Baj 1998, Fujita et al. 2004, Figure 64) ? Permettront-elles également d'investiger des zones non accessibles par la mesure et pourtant riches en informations, comme la zone de post-instabilité des tubes suspectée stable dans certaines conditions, comme cela a pu être estimé à partir de techniques de contrôle actif (Caillaud 1999), et dont la connaissance permettrait d'envisager une extension du domaine d'exploitation des composants ?

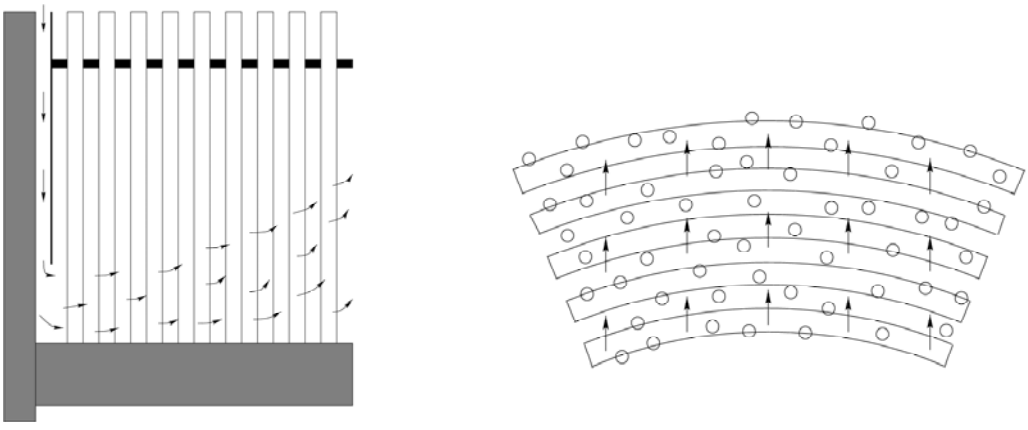

*Figure 62 : Représentation schématique de portion de faisceau de tubes de générateur de vapeur avec des écoulements monophasiques transverses ou obliques en partie basse (à gauche) et diphasiques transverses ou obliques dans la zone cintrée des tubes en partie haute (à droite).*

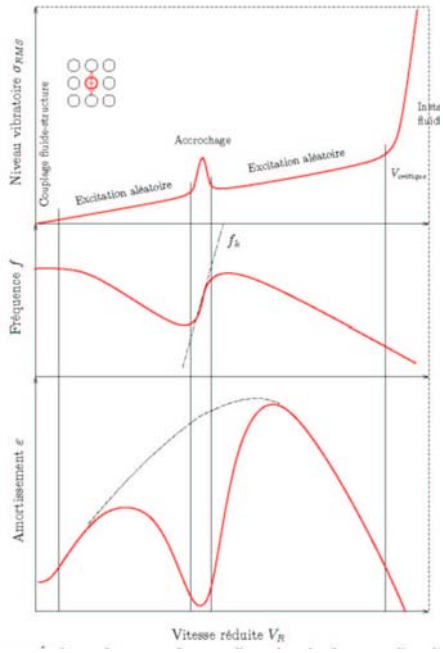


*Figure 63 : Evolution du niveau vibratoire, de la fréquence et de l'amortissement d'un tube dans un faisceau de tubes en présence d'un écoulement transverse.*

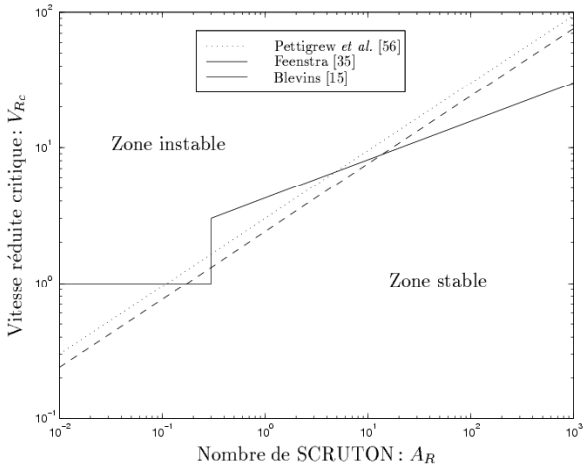


*Figure 64 : Exemple de carte d'instabilité pour un faisceau de tubes sous écoulement transverse fournissant la vitesse réduite critique en fonction du nombre de Scruton (défini à partir de la masse structure en eau, de l'amortissement structure en air, du diamètre du tube et de la masse volumique du fluide, Connors 1978).*

## 2.2. Evaluation des incertitudes

Jusqu'où faut-il aller dans la performance des calculateurs et dans la précision des schémas de calcul ? Sont-elles uniquement conditionnées par les contraintes des solveurs couplés ou le couplage modifie-t-il les niveaux d'incertitudes à prendre en compte ? Comment se propage l'incertitude sur l'entrée du solveur 1 en sortie du solveur 2 ? Par exemple, le niveau d'incertitude sur les chargements thermohydrauliques est-il le même que celui sur la réponse vibratoire induite et sur le seuil de vitesse critique, a priori très sensible aux données d'entrée (Figure 65) ?

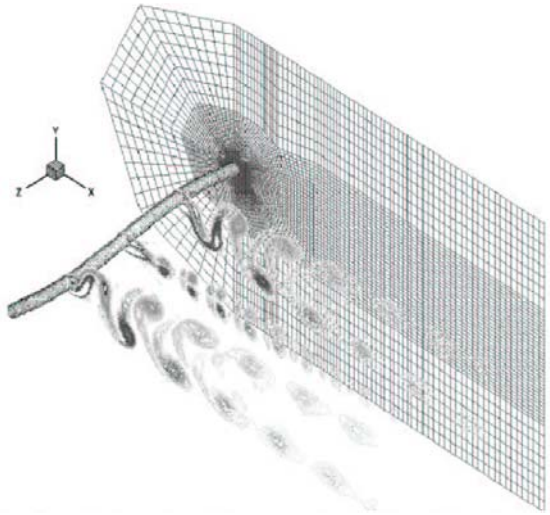

*Figure 65 : Exemple d'identification des sources d'incertitudes pour un écoulement turbulent autour d'un cylindre (Lucor 2004, Lucor et Karniadakis 2004).*

### 2.3. Progrès technologiques

Les réponses à toutes ces questions seront apportées par les évolutions futures des outils et des méthodes qui permettront d'envisager la réalisation d'études locales couplées, à des coûts de plus en plus réduits, facilitant le dimensionnement des composants et leur maintien en conditions opérationnelles, ouvrant peut-être la voie à une conception numérique de plus en plus systématique, toujours doublée d'une vérification expérimentale incontournable.

## 3. Perspectives de collaborations

Ces travaux sont le fruit de projets essentiellement conduits au sein d'EDF R&D et pilotés par les Départements Mécanique des Fluides, Energies et Environnement[19] et Analyses Mécaniques et Acoustiques[20]. Ils ont bénéficié de collaborations établies et entretenues avec des partenaires industriels et universitaires, tout particulièrement, à partir de 2001, le CEA et le Laboratoire de Mécanique de l'Université de Lille, et plus récemment, l'Université de La Rochelle, Schlumberger, CD-Adapco, DCN, l'IMFT, l'Université Paris VI ainsi que des interlocuteurs du Groupe De Recherche « Interactions Fluide Structure » créé en 2005.

Ils ont donné lieu à des participations à plusieurs conférences nationales et internationales ainsi qu'à la rédaction d'articles publiés dans des revues internationales avec comité de lecture.

Enfin ils ont toujours été accompagnés de tâches d'enseignement, qui se sont traduites notamment par la création d'un cours d'introduction à la simulation numérique des interactions et des couplages fluide structure associé à des travaux dirigés, des projets d'études et des travaux pratiques basés sur l'utilisation de l'outil de simulation des couplages fluide structure mis au point *Cosmethyc*. Ces enseignements ont été pour partie dispensés à l'Université de Paris XI, l'Université de La Rochelle, aux Mines de Douai ainsi qu'à l'ENPC dans le cadre d'ateliers en binômes.

[19] Département MFEE

[20] Département AMA

## Annexe 12 : Coupleur généraliste *Cosmethyc*

**Longatte, E.,** Huvelin, F., Souli, M. (2005). Code coupling for simulation of flow-induced vibrations. *1er Colloque du GDR Interactions Fluide Structure,* Sophia-Antipolis.

## Annexe 13 : Applications de *Cosmethyc*

**Longatte, E.**, Adobes, A., Souli, M. (2003). Steam generator tube vibrations : experimental determination versus ALE computation of fluidelastic forces. *PVP Conference*, Cleveland.

## Annexe 14 : Applications de *Cosmethyc*

Abouri, D., Parry, A., Hamdouni, A., **Longatte, E.** (2005). A stable fluid structure interaction algorithm : application to industrial problems. *JPVT, accepté*.

*Résumé pour le 1er colloque du GDR interactions fluide-structure – 26-27 sept. 2005*

# CODE COUPLING FOR SIMULATION OF FLOW-INDUCED VIBRATIONS

**Elisabeth LONGATTE[*], Fabien HUVELIN[*], Mhamed SOULI[**]**

*[*] EDF Research & Development Division,*
*Fluid Mechanics and Heat Transfer Department,*
*Chatou, France*
*elisabeth.longatte@edf.fr,fabien.huvelin@edf.fr*
*[**] Lille University, Mechanical Engineering Department*
*Villeneuve d'Ascq, France*
*mhamed.souli@univ-lille1.fr*

## 1 Introduction

Numerical simulation of industrial multi-physics problems is still a challenge to overcome because it may rely on code coupling and may require high computational resources for data transfers between codes. This issue is investigated in the present paper dealing with numerical simulation of fluid structure interactions and flow-induced vibrations in PWR components by using fluid structure code coupling. The purpose is to predict numerically tube bundle vibrations by using Computational Fluid Dynamics (CFD) and Computational Structure Dynamics (CSD) codes involving specific numerical methods for multi-physics problems.
As far as flow-induced vibrations are concerned, the purpose is to estimate thermo-hydraulics forces responsible for structure motion and in the same time to account for coupling between tube motion and fluid forces. Thanks to recent improvements in CFD, these simulations are now reachable in parts of industrial configurations involving basic geometry.
In the present paper computational process and numerical methods for simulation of flow-induced vibrations are presented. A specific attention is paid to time schemes ensuring code coupling with expected properties in terms of energy conservation and data transfer at the interface. Examples of application of the tools are proposed and results are discussed in specific configurations involving flexible tubes in the presence of fluid and flow.

## 2 Computational process

The purpose of the present work is to introduce a method for numerical prediction of flow-induced vibrations in industrial configurations. A fluid structure code coupling is involved in order to perform both fluid and structure computations in the same time and make data exchange possible thanks to convenient moving boundary conditions. There are three steps in the computation :

- At each time step of the calculation, the fluid problem is solved on the predicted computational domain and fluid forces acting on the flexible structure are estimated.
- Then these forces are introduced as inlet conditions into mechanical calculation providing the structure displacement and velocity.
- Finally these displacement and velocity are used as inlet conditions in the fluid calculation to deform the computational domain and actualize the geometry of the fluid problem.

Appropriate numerical methods are required to ensure data transfer between codes and three points are particularly investigated :

- boundary motion : fluid computation necessarily involves moving boundary treatment and an Arbitrary Euler Lagrange (ALE) formulation is introduced to account for structure motion effects on fluid computational domain displacement.

- Near-wall fluid forces : they are responsible for structure motion and must be estimated with accuracy in the vicinity of moving boundaries.
- Coupling process : time numerical schemes must be chosen to ensure energy conservation of fluid structure coupling system at each step of the calculation.

In mechanics one can describe fluid motion with two classical formulations : with an Eulerian formulation one considers a particular volume in space ; with a Lagrangian formulation one identifies and follows a particular region of fluid. The last formulation is not convenient in the presence of high magnitude motions. For problems involving moving wall boundaries it is necessary to have a middle formulation following the boundary motion and preserving the element shape in the same time. The ALE formulation has been introduced to ensure these capabilities (Souli [13], Longatte [5]).

Estimation of fluid forces is very important as structure response is directly generated by near-wall fluid forces. At each time step of the fluid calculation, fluid forces acting on the structure and responsible for its motion must be estimated with accuracy. A specific attention is paid to data transfer, projection and interpolation at each time step of calculation, especially when fluid and structure meshes do not coincide (Figure 1).

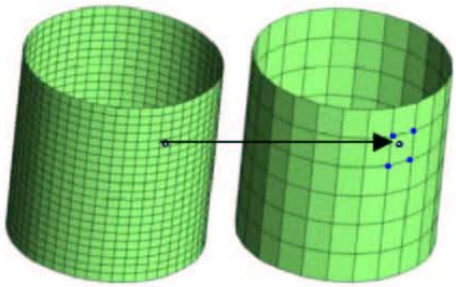

FIG. 1 – *Examples of fluid and structure meshes of the interface for data projection and interpolation*

For the coupling, the partitioned code coupling algorithm between fluid and structure solvers is presented in Figure 2. Explicit and implicit code coupling schemes with sub-cycling are possible. In the first step fluid forces acting on the structure are computed, then structure displacement is estimated and used as boundary condition for the next fluid step computation. Implicit code coupling scheme may require sub-cycling to avoid numerical damping induced by the partitioned coupling procedure.

## 3 Coupling schemes

The methodology for numerical simulation of fluid structure coupling can be split for each time step into three steps :
computation of the fluid forces acting on the structure
resolution of the mechanical equation
updating the fluid mesh motion thanks to an ALE formulation.

The calculation of structure motion at the time $t^{n+1}$ requires the computation of fluid forces acting on the structure. The time for computation of these forces depends on the chosen coupling scheme. The choice of this time is important because it may determine the ability of the scheme to conserve the energy or not at the interface.

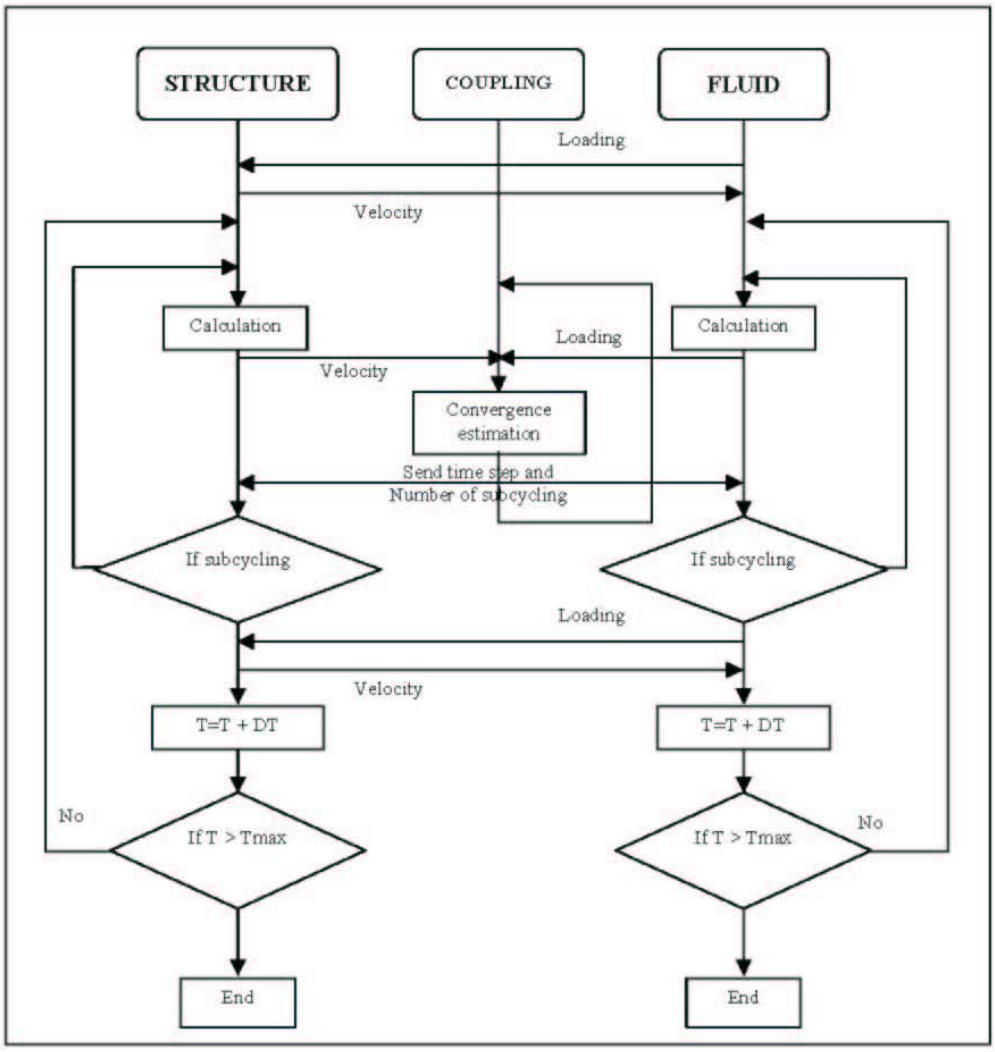


FIG. 2 – *Fluid structure code coupling algorithm*

The coupling scheme must be built to ensure energy conservation, or at least to minimize energy creation at the interface. Farhat [3], Piperno [8] introduced several explicit and implicit coupling schemes satisfying this property.
An explicit synchronous scheme computes a prediction of the structure displacement before the fluid force calculation at time $t^{n+1}$ as depicted in Figure 3.

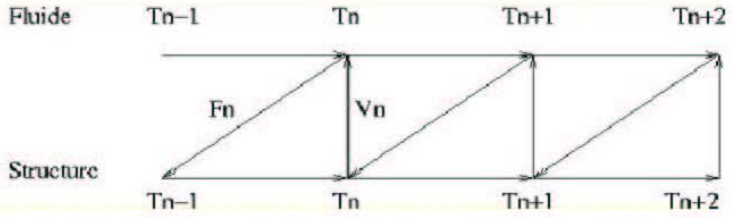


FIG. 3 –*Synchronous coupling scheme algorithm*

3

With an explicit asynchronous scheme coupling, fluid and structure problems are staggered in time. Fluid computation is performed at time $t^{n+1/2}$ while structure computation is performed at time $t^n$ (Figure 4). This scheme ensures the geometric conservation law (Piperno and Farhat [10]).

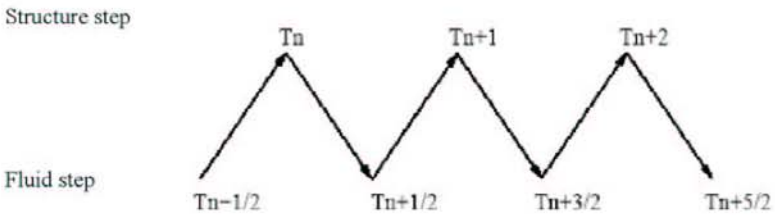


FIG. 4 – *Staggered coupling scheme algorithm*

An implicit coupling scheme is also possible (Abouri and al. [1], Le Tallec and Mouro [4], Piperno [8][9]). For each time step, this algorithm computes sub-cycling of an explicit scheme until convergence on a criterion based on the fluid force or on the structure velocity calculation. Each sub-cycling is computed with the value at time step $t^n$ except the position of fluid mesh which is taken at the previous sub-cycling. A fixed point algorithm is involved and ensures the convergence at each time step. This scheme features good properties in terms of energy conservation and it is often recommended. It is used in the work presented below.

## 4 Examples of application

In this part examples of application of the tools are presented. Several simplified configurations are considered involving tubes and tube bundles modeling parts of industrial components like heat exchangers, control rods or fuel assemblies. Internal and external flows are possible. Numerical results are illustrated. They are compared to available numerical, analytical or experimental data (Chen [2], Price and Païdoussis [11], Rogers et al. [13], Weaver et al. [14]). These studies show the ability of the tools to predict flow-induced vibrations in tubes and tube bundles in the presence of fluid at rest and flows (Longatte [6][7]).

### 4.1 Concentric tubes

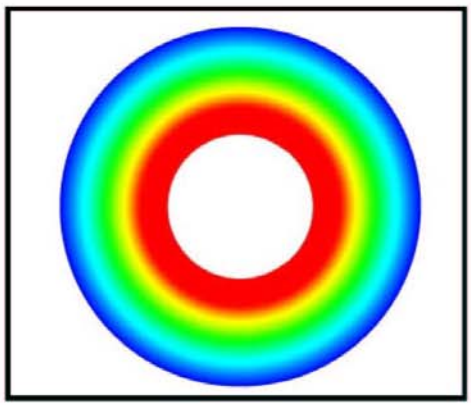

FIG. 5 – *Configuration involving a rigid tube moving in an annular fluid*

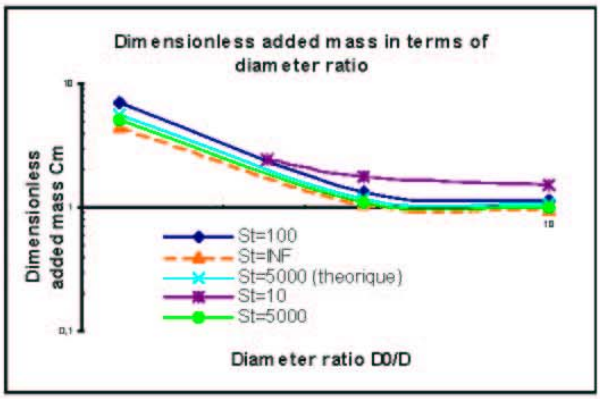


FIG. 6 –*Dimensionless added mass depending on internal and external tube diameter ratio for concentric tubes for several Stokes numbers for viscous fluid (St = 10, 100, 5000) and for non viscous fluid (St = infinity). Good agreement between numerical results (Longatte et al. [7]) and analytical solutions of Chen [2]*

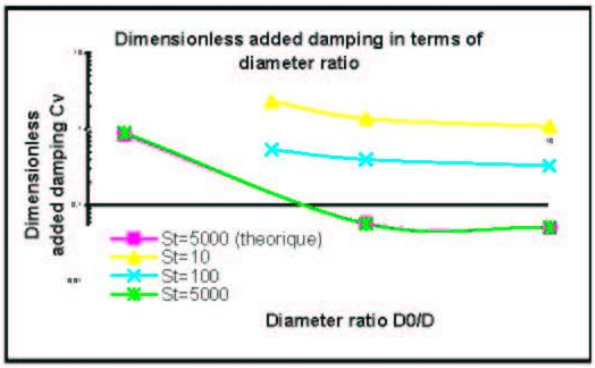


FIG. 7 – *Dimensionless added damping depending on internal and external tube diameter ratio for concentric tubes for several Stokes numbers for viscous fluid (St = 10, 100, 5000). Good agreement between numerical (Longatte et al. [7]) and analytical solutions of Chen [2]*

### 4.2 Eccentric tubes

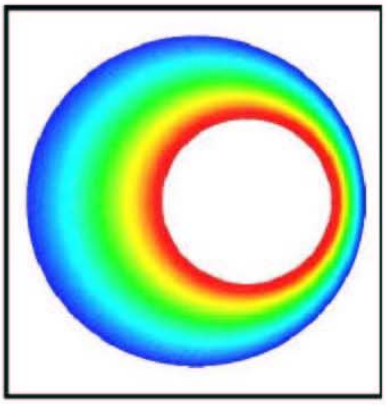

FIG. 8 – *Configuration involving a rigid tube moving in an annular eccentric fluid*

5

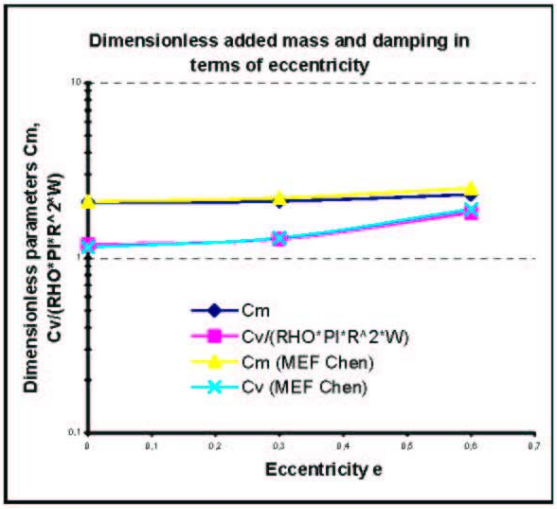


FIG. 9 – *Dimensionless added mass and damping depending on the eccentricity for eccentric tubes. Good agreement between numerical solution obtained with a numerical partitioned procedure (Longatte et al. [7]) and numerical monolithic solution obtained with strong coupling (Chen [2])*

### 4.3 Periodic tube bundle

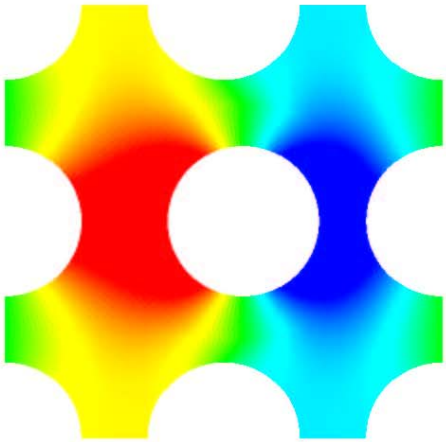

FIG. 10 –*Configuration involving a rigid tube moving in a fixed tube bundle represented by a periodic cell including 4 plain tubes*

| | *Experimental* | *Analytical* | *Numerical* |
|---|---|---|---|
| Frequency (Hz) | - | 20.3 | 20.5 |
| Damping (Hz) | 0.037± 0.004 | 0.037 | 0.036 |

TAB. 1 –*Tube frequency and damping for a single flexible tube in a fixed tube bundle in fluid at rest. Good agreement between numerical solutions obtained with a numerical partitioned procedure (Longatte et al. [6][7]), available analytical solutions (Chen [2], Rogers et al. [12]) and experimental data (Weaver [14])*

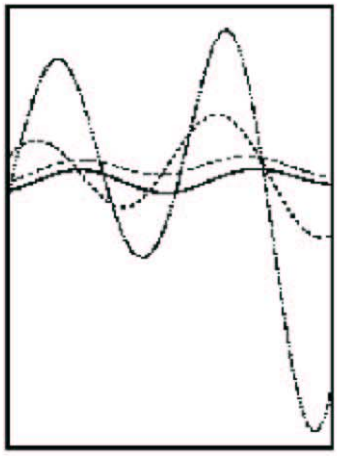

FIG. 11 – *Tube displacement of a single flexible tube in a fixed tube bundle in cross flow for several flow velocities obtained with a numerical partitioned procedure (Longatte et al. [6][7]). Stable and unstable tube behaviour above and below the critical flow velocity*

### 4.4 Hosepipe

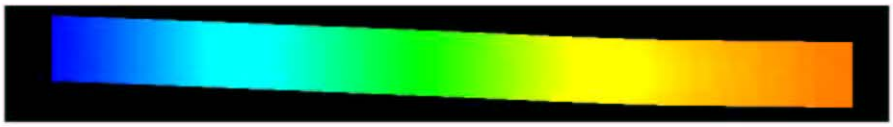

FIG. 12 – *Visualization of tube motion induced by an internal flow in an hosepipe estimated with the partitioned procedure*

## 5 Conclusion

A flow induced vibration prediction numerical method is presented in this paper. The fluid problem is solved by using an Arbitrary Lagrangian Eulerian (ALE) formulation and a coupling process between fluid and structure computations is involved in order to account for flow structure coupling. The approach is applied to numerical prediction of flexible tube and tube bundle vibrations in still water and flows. Numerical results are consistent with experimental predictions and available analytical solutions.
Further developments are carried out in order to improve code coupling process and flow modelling in the presence of turbulence and moving boundaries.

## References

[1] ABOURI, D., PARRY, A., HAMDOUNI, A., Fluid-rigid body dynamic interaction in complex industrial flow, *Chapter Advances in fluid Mechanics : Fluid Structure interaction II, Wit Press* (2003), 295-305

[2] CHEN, S.S., Flow-Induced Vibration of circular cylindrical structures, *Hemisphere publishing corporation* (1987).

[3] FARHAT, C., LESOINNE, M., MAMAN, N., Mixed explicit implicit time integration of coupled aeroelastic problems: three field formulation, geometric conservation and distribution solution, *International Journal for Numerical Methods in Fluids*, 21 (1995), 807-835.

[4] LE TALLEC, P., MOURO, J., Fluid structure interaction with large structural displacement, *Comput. Methods Appl. Mech. Engrg*, 190 (2001), 3039-3067.

[5] LONGATTE, E., BENDJEDDOU, Z., SOULI, M., Methods for numerical study of tube bundle vibrations in cross-flows, *Journal of Fluids and Structures*, 18 (2003), 513-528.

[6] LONGATTE, E., BENDJEDDOU, Z., VERREMAN V., SOULI, M., Explicit and implicit code coupling schemes in fluid structure interaction, *PVP Conference*, *Denver, PVP-2005-71647* (2005).

[7] LONGATTE, E., VERREMAN V., BENDJEDDOU, Z., SOULI, M., Comparison of strong and partitioned fluid structure code coupling methods, *PVP Conference*, *Denver, PVP-2005-71251* (2005).

[8] PIPERNO, S., FARHAT, C., LARROUTUROU, B., Partitionned procedures for the transient solution of coupled aeroelastic problems. Part I: Model problem, theory and two-dimensional application, *Comput. Methods Appl. Mech. Engrg*, 124 (1995), 79-112.

[9] PIPERNO, S., Explicit, implicit fluid, structure staggered procedures with a structural predictor and fluid subcycling for 2D inviscid areoelastic simulations. *International Journal for Numerical Methods in Fluids*, 25 (1997), 1207-1226.

[10] PIPERNO, S., FARHAT, C., Partitioned procedures for the transient solution of coupled aeroelastic problem - Part II: energy transfer analysis and three-dimensional applications, *Comput. Methods Appl. Mech. Engrg*, 190 (2001), 3147-3170.

[11] PRICE, S.J., PAÏDOUSSIS, M.P., A single flexible cylinder analysis for the fluid-elastic instability of an array of flexible cylinders in cross flow, *Journal of Fluids Engineering*, 108 (1986), 193-199.

[12] ROGERS, R.J., TAYLOR, C., PETTIGREW, M.J., Fluid effects on multispan heat exchanger tube vibration, *PVP Conference*, San Antonio (1984).

[13] SOULI, M., ZOLESIO, J.P., Arbitrary Lagrangian-Eulerian and free surface methods in fluid mechanics, *Comput.. Methods Appl. Mech. Engrg.,* 191 (2001), 451-466.

[14] WEAVER, D.S., ABD-RABBO, A., A flow visualisation study of a square array of tubes in water cross flow, *Journal of Fluids Engineering,* 107 (1985), 354-363.

PVP-Vol. 460, Emerging Technology in Fluids, Structures
and Fluid-Structure Interactions — 2003

PVP2003-1966

# STEAM GENERATOR TUBE VIBRATIONS : EXPERIMENTAL DETERMINATION VERSUS ALE COMPUTATION OF FLUIDELASTIC FORCES

Z. BENDJEDDOU*
Electricité de France - R&D Division
Fluid Mechanics and Heat Transfer Department
6 Quai Watier, 78400 Chatou, France
zaky.bendjeddou@edf.fr

A. ADOBES**
Electricité de France - R&D Division
Fluid Mechanics and Heat Transfer Department
6 Quai Watier, 78400 Chatou, France
andre.adobes@edf.fr

E. LONGATTE**
Electricité de France - R&D Division
Fluid Mechanics and Heat Transfer Department
6 Quai Watier, 78400 Chatou, France
elisabeth.longatte@edf.fr

M. SOULI***
Université des Sciences et Technologies de Lille
1, Boulevard Paul Langevin, Cité Scientifique
59655 Lille, France
mhamed.souli@univ-lille1.fr

## ABSTRACT

In heat exchanger tube bundles like in many others industrial applications, fluid structure interaction is a crucial problem to overcome. Flow-induced tube vibration in tube bundles is due to two main kinds of physical effects: (1) fluid-elastic forces caused by structure motion ; (2) turbulent forces due to vortex generation at high Reynolds numbers. The second component, turbulent excitation, is independent on structure motion and may generate wear and fatigue damage while the first component may lead to fluid-elastic instability inducing high amplitude displacement and possible tube short term failure. In this context many studies are carried out in order to develop methods for the identification of critical flow velocity in tube arrays.

In the present work two methods are presented : (1) the first one relies on experimental measurements, it is fitted with analytical modeling and provides fluid-elastic coefficients ; (2) the second one relies on numerical simulation using Computational Fluid Dynamics Codes (CFD) involving moving boundary techniques ; it provides fluid force estimates and in some cases it makes it possible to simulate tube vibrations.

The first part is devoted to experimental determination of fluid-elastic forces. A numerical method for prediction of fluid-elastic effects in fluid at rest is presented in the second section. Results of both methods are compared in the third part.

## NOMENCLATURE

| | |
|---|---|
| $C_d$ | dimensionless damping coefficient |
| $C_f$ | added damping per unit length [N.s.m$^{-2}$] |
| $C_k$ | dimensionless stiffness coefficient |
| $C_s$ | structural damping per unit length [N.s.m$^{-2}$] |
| $C_v$ | added damping in still water per unit length [N.s.m$^{-2}$] |
| $\tilde{C}_v$ | dimensionless added damping in still water |
| $\overline{\overline{D}}$ | fluid deformation tensor [s$^{-1}$] |
| $D_e$ | tube outer diameter [m] |
| $D_o$ | tube outer diameter in test facility [m] |
| $D_{eq}$ | equivalent tube diameter [m] |
| $D_i$ | tube inner diameter [m] |
| $f$ | tube frequency (Hz) |
| $fd$ | forced tube frequency (Hz) |
| $f_f$ | fluid-elastic force per unit length [N.m$^{-1}$] |
| $f_t$ | turbulent force per unit length [N.m$^{-1}$] |
| $fo$ | Imposed force amplitude per unit length [N.m$^{-1}$] |
| $K_s$ | structural stiffness per unit length [N.m$^{-2}$] |
| $K_f$ | added stiffness per unit length [N.m$^{-2}$] |
| $\overline{\overline{I}}$ | identity tensor |
| $L$ | tube length [m] |
| $M_a$ | added mass per unit length [kg.m$^{-1}$] |
| $\tilde{M}_a$ | dimensionless added mass |
| $M_s$ | structural mass per unit length [kg m$^{-1}$] |
| $P$ | pitch in square tube bundle [m] |
| $S$ | tube area [m$^2$] |
| $s$ | Laplace's variable |
| $St$ | Stokes number |
| $x$ | curvilinear abscissa along the tube |
| $xo$ | forced tube displacement |
| $U_o$ | pitch flow velocity in the test-facility[m s$^{-1}$] |
| $U$ | pitch flow velocity [m s$^{-1}$] |
| $Vr$ | dimensionless velocity $Vr = U/fD$ [-] |
| $\alpha$ | void fraction [-] |
| $\rho_o$ | external fluid density per unit length [kg m$^{-2}$] in test facility |
| $\rho_i$ | internal fluid density per unit length [kg m$^{-2}$] |
| $\rho_e$ | external fluid density per unit length [kg m$^{-2}$] |
| $\rho_{eq}$ | density of the equivalent tube per unit length [kg m$^{-2}$] |
| $\rho_t$ | tube density per unit length [kg m$^{-2}$] |
| $\overline{\overline{\sigma_f}}$ | fluid stress tensor [N.m$^{-2}$] |
| $\overline{\overline{\sigma_s}}$ | structure stress tensor [N.m$^{-2}$] |
| $\xi$ | "in flow" damping ratio [%] |

$\omega$ "in flow" circular frequency $\omega = 2\pi f$ [rad s$^{-1}$]

$\omega_d$ forced frequency in still water [rad s$^{-1}$]

$\omega_w$ circular frequency in still water [rad s$^{-1}$]

$\omega_s$ circular frequency in still air [rad s$^{-1}$]

## INTRODUCTION

Under operating conditions some Pressurized Water Reactor components are submitted to complex flows which make them vibrate and thereafter might in some cases eventually damage them by effect of wear or vibratory fatigue. Those damages potentially affecting nuclear safety, power plants operators steadily invest in research and development in order to be able to model better and better flow induced vibrations as well as subsequent degradation phenomena.

Since they are responsible for vibrations, special attention is paid to fluid forces, particularly to those that are motion dependent and govern instabilities, usually referred to as fluid-elastic forces.

The present paper first of all summarizes the methodology that is currently used by EDF, the French nuclear power plant operator, to estimate fluid-elastic forces acting on steam generator tube bundles. That methodology is based on dimensionless fluid force coefficients that need to be assessed from experiments. In a second step, the article presents a new methodology, still under elaboration and tested at EDF R&D Division, that consists in simultaneously simulating the thermohydraulics and the mechanics in a tube bundle vibrating under a cross flow, by using an Arbitrary Lagrange Euler (ALE) formulation for the fluid computation. That methodology rises up expectations because it should eventually allow one to explain the dispersion of data registered in the first methodology, thereafter highlighting the safety margins of it. In a third step, the paper finally tries to bridge the gap between the two methodologies by comparing some results of the two.

## 1 – EXPERIMENTAL DETERMINATION

Modeling the flow-induced vibrations of a tube inserted in a bundle that is submitted to an external cross-flow conveniently starts by splitting the fluid forces exerted by the external fluid on the tube into two categories (Gay et al., 1997) : the one of motion-dependent fluid forces referred to as "fluid-elastic forces" $f_f$, and the one of motion-independent fluid forces $f_t$, i.e. turbulent or two-phase excitation forces. In Laplace's domain, the motion of the tube can thereafter be described by the following equation :

$$M_s s^2 + C_s s + K_s = f_f(s) + f_t(s) \quad (1)$$

Motion-dependent fluid forces $f_f$ are supposed to affect the dynamic characteristics of the tube by modifying its mass, damping and stiffness. In Laplace's domain, one can therefore write them as :

$$f_f(s) = -M_a(\alpha)s^2 - C_f(\alpha,s,U)s + K_f(\alpha,s,U) \quad (2)$$

The added mass term $M_a$ is considered as depending only on void fraction, whereas the added damping and stiffness terms $C_f$ and $K_f$ are supposed to depend in addition on frequency and flow velocity.

Before solving equation (1), densities of the primary and secondary flows in the steam generator are in practice first computed by using a thermohydraulic two-phase software. Once those two quantities have been determined, the sum $\{M_s + M_a(\alpha)\}$ obtained by rearranging equations (1) and (2) is derived by assigning to the tube the following equivalent density per unit length $\rho_{eq}(x)$ :

$$\rho_{eq}(x) = \frac{1}{\left(D_e^2 - D_t^2\right)}\left[\rho_i(x)\, D_t^2 + \rho_t\left(D_e^2 - D_t^2\right) + D_{eq}^2 \rho_e(x)\right] \quad (3)$$

where $D_{eq}$ denotes a fictive diameter that allows one to derive the added mass due to the external fluid from the kind of arrangement.

As for the two terms $C_f$ and $K_f$ are concerned, they are obtained, for any given void fraction and flow velocity, by redimensioning dimensionless damping and stiffness coefficients denoted by $C_d$ and $C_k$. In practice $C_d$ and $C_k$ are assessed from experiments. They are derived from "in-flow" identified circular frequency, $\omega$, and damping ratio, $\xi$, as well as structural characteristics $M_s$, $C_s$, $K_s$ in still air and the hydrodynamic mass $M_a$ (Adobes et al. 2001) :

$$C_d = -\frac{4(M_s + M_a)\omega\xi - 2C_s}{\rho_o U_o D_o} \quad (4)$$

$$C_k = -\frac{2\left[(M_s + M_a)\omega^2 - K_s\right]}{\rho_o {U_o}^2} \quad (5)$$

$$M_a = M_s\left(\frac{\omega_s^2}{\omega_w^2} - 1\right) \quad (6)$$

## 2 - ALE COMPUTATION

### 2.1 - ALE formulation

ALE formulation is currently used to solve problems involving moving boundaries (free surface displacement, high velocity impact, off-shore structure motion, blood vessel deformation, explosion, Souli 2001, Souli 1999, Hughes et al. 1981, Hirt et al. 1974). It is therefore appropriate to deal with fluid structure interaction problems. In the present paper we use it to compute fluid-elastic forces exerted on a vibrating tube in a rigid tube bundle submitted to cross flow.

In the frame of Arbitrary Lagrangian Eulerian formulations, the fluid dynamic problem is solved as follows. One defines three domains in space and associated mappings from one domain to another (Figure 1). The first one is called the material domain $\Omega_m$. It follows the fluid particle motion according to Lagrangian formulation. The coordinates of a given fluid particule of the material domain are denoted by $X$ hereafter. The second one is called the spatial domain $\Omega_s$. It is immobile according to Eulerian formulation. The coordinates of a given observation point are denoted by $x$ hereafter. One can link Lagrangian and Eulerian coordinates :

$$x = x(X,t) \quad (7)$$

and define the material time derivative :

$$\left.\frac{\partial x}{\partial t}\right|_X = v(X,t) = v(x,t) \quad (8)$$

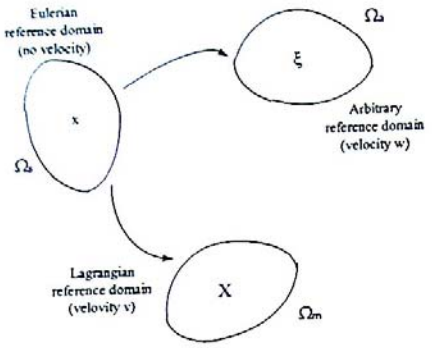


*Figure 1 : representation of spatial, material and arbitrary domains* $\Omega_s$, $\Omega_m$ *and* $\Omega_a$ *whose velocities are respectively 0, v and w.*

with $v$ denoting material velocity. Moreover the material time derivative of a given physical property $\phi$ can be written as :

$$\left.\frac{\partial\phi}{\partial t}\right|_X = \left.\frac{\partial\phi(X,t)}{\partial t}\right|_X = \left.\frac{\partial\phi(x,t)}{\partial t}\right|_x + \left.\frac{\partial\phi(x,t)}{\partial x_i}\right|_t .v_i(x_i,t) \qquad (9)$$

The third domain is called the arbitrary domain $\Omega_a$. It moves with an arbitrary velocity chosen to be different from the one of the material domain. Coordinate mapping between arbitrary and spatial domains reads as follows :

$$x = x(\zeta,t) \qquad (10)$$

and the arbitrary time derivative can be written as :

$$\left.\frac{\partial x}{\partial t}\right|_\zeta = w(\zeta,t) = w(x,t) \qquad (11)$$

with $w$ denoting arbitrary velocity and the arbitrary time derivative of a given physical property $\phi$ :

$$\left.\frac{\partial\phi(\zeta,t)}{\partial t}\right|_\zeta = \left.\frac{\partial\phi(x,t)}{\partial t}\right|_x + \left.\frac{\partial\phi(x,t)}{\partial x_i}\right|_t .w_i(x_i,t) \qquad (12)$$

In presence of vibrating structure boundaries, it is practical to choose an arbitrary domain $\Omega_a$ that coincides with structure boundaries. Owing to those notations, mass and momentum conservation equations in $\Omega_a$ are formulated as follows for an incompressible fluid :

$$div_x(v) = 0 \qquad (13)$$

$$\rho\left\{\left.\frac{\partial v}{\partial t}\right|_\zeta + (v-w).grad_x(v)\right\} = -grad_x(p) + div_x(\mu grad_x(v)) \qquad (14)$$

As shown in equations (13-14), ALE formulation consists in taking into account the mesh velocity $w$ in the advection term and in replacing the partial time derivative by the arbitrary partial time derivative in the left hand side. The arbitrary velocity is chosen to avoid element entanglement in the mesh. In the present work its is chosen to be the solution of a classical diffusion equation :

$$div(\lambda.gradw) = 0 \qquad (15)$$

with $\lambda$ designating a specific viscosity governing the diffusion of mesh deformation. It is chosen to keep appropriate mesh refinement in the full computational domain (Bendjeddou et al. 2002, Longatte et al 2002).

## 2.2 – Computation of fluid-elastic forces

As previously mentioned fluid forces may be split into two parts: turbulent forces non-depending on structure motion and fluid-elastic forces directly generated by structure motion. In the present paper we focus our attention on determination of fluid-elastic forces. Therefore the configuration to be considered involves a laminar flow in still water with minor turbulent effects. In this context one identifies fluid-elastic forces by investigating a forced tube motion in a two-dimensional flow at rest.

A computational domain represented by a periodic cell with four plain tubes including only one flexible tube is considered. The flexible tube motion is chosen to be harmonic with a fixed frequency $\omega_d=2\pi f_d$ and a displacement $x=x_o e^{i\omega t}$ . According to these notations fluid-elastic force may be written :

$$f_o e^{i\varphi} e^{i\omega_d t} = -M_a\ddot{x} - C_v\dot{x} = \left(M_a\omega_d{}^2 x_o - iC_v\omega_d x_o\right)e^{i\omega t} \qquad (16)$$

This is the summation of an added mass term characterized by *Ma* and an added damping term characterized by $C_v$ with insignificant stiffness effects as a flow at rest is investigated. According to equation (16) one may thus identify added mass and damping as follows :

$$M_a = \frac{f_o\cos\varphi}{\omega_d{}^2 x_o} \qquad (17)$$

$$C_v = -\frac{f_o\sin\varphi}{\omega_d x_o} \qquad (18)$$

with $\varphi$ designating the phase between $x$ and $f$.

This formulation requires the computation of near-wall fluid forces acting on the forced moving tube.

$$\vec{f}_f = \frac{1}{L}\int_S \bar{\bar{\sigma}}_f.\vec{n}_f dS \qquad (19)$$

with $\vec{n}_f$ designating unit local normal vector to tube wall. According to Stokes approximation the fluid stress tensor is defined by :

$$\bar{\bar{\sigma}}_f = -p\bar{\bar{I}} + 2\mu\bar{\bar{D}} \qquad (20)$$

## 2.3 - Moving boundary conditions

On moving boundary velocity and stress tensor continuities are ensured by :

$$\vec{u}_f = \vec{u}_s \qquad (21)$$

$$\overline{\overline{\sigma_s}}.\vec{n}_s + \overline{\overline{\sigma_f}}.\vec{n}_f = 0 \quad (22)$$

Rigid tubes are immobile and non-moving boundary conditions are written :

$$\vec{u}_f = \vec{0} \quad (23)$$

$$\vec{u}_s = \vec{0} \quad (24)$$

while periodic inlet and outlet conditions are introduced on other boundaries to simulate an infinite tube bundle with a periodic cell.

## 3 -RESULT COMPARISON

In the present section one compares fluid-elastic forces obtained by experimental determination and ALE computation. Moreover both added mass and added damping are compared to expected values predicted by well-known analytical laws in tube bundles. Finally a Stokes dependency of results is pointed out.

### 3.1 - Added mass

For high Stokes in tube bundles, analytical prediction of dimensionless added mass gives (Chen 1986):

$$\tilde{M}_a = \frac{\pi}{4}\frac{1+\left(\frac{D}{D_{eq}}\right)^2}{1-\left(\frac{D}{D_{eq}}\right)^2} + \sqrt{\frac{\pi}{St}} \quad (25)$$

with $D_{eq}$ designating the quantity defined by :

$$\frac{D_{eq}}{D} = f(\frac{P}{D}) = (1.07 + 0.56\frac{P}{D})\frac{P}{D} \quad (26)$$

Therefore an analytical expression for added mass is given by :

$$M_a = \rho D_e^2 L \tilde{M}_a \quad (27)$$

Experimental, numerical and analytical added mass values for a Stokes number $St = 18730$ and a pitch ratio $P/De = 1.44$ (Granger et al. 1993) are reported in Table 1. Numerical results are in good agreement with experimental and analytical predictions. The Stokes dependency of results is pointed out in Table 2. Numerical results are predictive in the sense that added mass does not depend on Stokes number as expected.

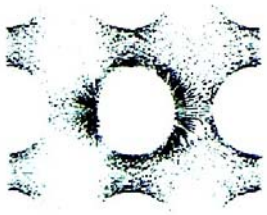

*Figure 2 : ALE computation of fluid-elastic forces : velocity fields coloured by pressure.*

*Table 1 : Comparison between added mass $M_a$ obtained with analytical law (equation 27), experimental determination (equation 6) and ALE computation (equation 17).*

| | Analytical results | Experimental results | Numerical results |
|---|---|---|---|
| Added mass $Ma\ (kg.m^{-1})$ | *0.508* | *0.464* | *0.412* |

*Table 2 : Comparison between added mass $M_a$ obtained with analytical law (equation 27 and ALE computation (equation 17) for three Stokes values.*

| Stokes | Analytical added mass | Numerical added mass |
|---|---|---|
| 13068 | *0.5092* | *0.4148* |
| 14036 | *0.5090* | *0.4140* |
| 15004 | *0.5086* | *0.4128* |

### 3.2 - Added damping

An analytical prediction for dimensionless added damping in tube bundle at high Stokes number is given by :

$$\tilde{C}_v = 2\pi^{\frac{3}{2}}\sqrt{St}\frac{1+\left(\frac{D}{D_{eq}}\right)^3}{\left(1-\left(\frac{D}{D_{eq}}\right)^2\right)^2} \quad (28)$$

Hence the expression for added damping :

$$C_v = \rho v D_{eq}\tilde{C}_v \quad (29)$$

According to experimental formulation presented in section 1 the expression of added damping is given by :

$$C_v = 2\left(M_s + M_a + M_i\right)\omega_e\xi_e - C_s \quad (30)$$

Analytical, experimental and numerical results in terms of added damping are reported in Table 3 for a Stokes number $St = 18730$ and a pitch ratio $P/De = 1.44$. Numerical results are consistent with those obtained experimentally. Due to the high Stokes dependency of added damping, the analytical law features a lack of consistency.

*Table 3 : Comparison between added damping $C_v$ obtained with analytical law (equation 29), experimental determination (equation 30) and ALE computation (equation 18).*

| | Analytical results | Experimental results | Numerical results |
|---|---|---|---|
| Viscosity damping $C_v\ (N.s.m^{-2})$ | *2.04* | *5.28* | *5.12* |

## CONCLUSION

In the present paper two methods for prediction of fluid-elastic forces are presented. Their results are compared in terms of added mass and added damping in fluid at rest. The first method called experimental determination is fitted with experimental measurements of tube frequency and damping in still air, in still water and in flow. The second method called ALE computation relies on a fully computational process involving specific moving boundary techniques. According to result comparison, numerical prediction of fluid-elastic parameters in fluid at rest are consistent with experiments and solutions features the expected behavior.

Further developments will be carried out to apply this numerical process to the prediction of fluid-elastic forces in presence of flows.

## REFERENCES

ADOBES A., GOSSE A., BARATTE C., 2001, "Qualification of motion dependent fluid forces coefficients", *ASME PVP conference, Atlanta.*

BENDJEDDOU Z., LONGATTE E., SOULI M., 2002, "Numerical simulation of tube bundle vibrations in cross flows", *ASME PVP Conference on Flow-Induced Vibrations,* Vancouver.

CHEN S.S., 1986, "Flow-induced vibration of circular cylindrical structures", *Hemisphere Publishing Corporation.*

GAY N., BARATTE C., FLESCH B., 1997, "An advanced tube wear and fatigue workstation to predict flow induced vibrations of steam generator tubes", *Conference ICONE 5,* 2289.

GRANGER S., CAMPISTRON R., LEBRET J., 1993, "Motion-dependent excitation mechanisms in square in -line tube bundle subject to water cross-flow : an experimental modal analysis", *J. Fluid. Struc.,* 7, 521-550.

HIRT C.W., AMSDERN A.A., COOK H.K., 1974, "An arbitrary Eulerian Lagrangian method for all flow speeds", *J. Comput. Phys.,* 14, 229-253.

HUGHES T.J.R., LIU W.K., ZIMMERMAN T.K., 1981, "Lagrangian Eulerian finite elements formulation for viscous flows", *J. Comput. Methods Appl. Mech. Engrg.,* 21, 329-349.

LONGATTE E., BENDJEDDOU Z., SOULI M., 2002, "Numerical simulation of tube bundle vibrations in cross flows", *ASME IMECE Conference,* New Orleans.

SOULI M., ZOLESIO J.P. 2001, "Arbitrary Lagrangian-Eulerian and free surface methods in fluid mechanics", *Comput. Methods Appl. Mech. Engrg.,* 2758.

SOULI M., OUAHSINE A., LEWIN L., 1999, "ALE formulation for fluid-structure interaction problems", *Comput. Methods Appl. Mech. Engrg.,* 190, 659-675.

# A Stable Fluid-Structure-Interaction Algorithm: Application To Industrial Problems

**D. Abouri**
CD-adapco, Paris Office, 31 rue Delizy, 93698 Pantin Cedex, France
e-mail: driss.abouri@fr.cd-adapco.com ; driss_abouri@yahoo.fr
**A. Parry**
Schlumberger Riboud Product Center, 1 rue Henri Becquerel, 92140 Clamart, France
e-mail: aparry@clamart.oilfield.slb.com

**A. Hamdouni**
University of La Rochelle, LEPTAB, Av. Michel Crépeau, 17042 La Rochelle, France
e-mail: ahamdoun@univ-lr.fr

**E. Longatte**
Electricité de France, Research and Development Division, 6 Quai Watier, 78400 Chatou, France
e-mail: elisabeth.longatte@edf.fr

## ABSTRACT

Fluid-structure interactions occur in a wide range of industrial applications, including vibration of pipe-work, flow meters, and positive displacement systems as well as many flow control devices. This paper outlines computational methods for calculating the dynamic interaction between moving parts and the flow in a flow-meter system. Coupling of phenomena is allowed without need for access to the source codes and is thus suitable for use with commercially available codes. Two methods are presented: one with an explicit integration of the equations of motion of the mechanism and the other, with implicit integration. Both methods rely on a Navier-Stokes equation solver for the fluid flow. The more computationally expensive, implicit method is recommended for mathematically stiff mechanisms such as piston movement. Industrial-application examples shown are for positive displacement machines, axial turbines, and steam-generator tube-bundle vibrations. The advances in mesh technology, including deforming meshes with nonconformal sliding interfaces, open up this new field of application of computational fluid dynamics (CFD) and mechanical analysis in flow meter design.

## 1 INTRODUCTION

There are many different groups of flow metering devices [1], some which include moving parts such as turbines and positive displacement meters and some which are static; for example, ultrasonic, fluidic, and pressure-drop based systems. In the present note we describe the application of CFD and mechanical analysis in the study of transient fluid-structure interaction. We focus on applications for measuring elements or on flow control devices with moving parts, in particular, those in which the moving parts play an important role in the measurement or control. We restrict the explanation to the case in which the components, moving relative to each other, do not undergo internal deformation; that is, the components are considered as rigid bodies. However, there is no limitation on the displacement of each rigid body. The principles developed are general and could be extended to include small or large internal deformations of the moving components. The method described is applied to an oscillating piston meter, a meter belonging to the positive displacement group.

Sayma *et al.* [2] presented a nonlinear analysis to predict turbine-forced response using a coupling method of the fluid and structural models; the structural response is described by a linear model. Blom [3] investigated time-lagged schemes where coupling was included by sequential solutions of fluid and structural models. In an implicit variant, the sequential solutions were repeated with updated interface boundary conditions until convergence was achieved. An algorithm was introduced to calculate fluid-structure interaction in a time-marching fashion where both fluid and structure have to be integrated in time simultaneously.

In this paper, two methods of applying a coupling algorithm are explained. The theory for fluid/rigid-body-interaction calculations is developed in Section 3. The explicit method and the more computationally intensive, implicit method, requiring the repetition of each time step, are presented. In Section 4, an industrial application of the implicit coupling algorithm is given for the oscillating piston meter, while the explicit scheme is employed to study the dynamics of an accelerating spinner used for flow indication. The fluid flow analysis software, STAR-CD™ [4] was used for the calculations included in this paper.

## 2 DESCRIPTION OF CALCULATION METHODS

### 2.1 Fluid/Rigid-Body Interaction Problem

A fluid-structure interaction problem shall be solved, in which the fluid occupies the domain $\Omega_f$, and the solid body, described in Lagrangian coordinates, occupies the domain $\Omega_s$ (Fig. 1). They have the common moving boundary $\Gamma(t) = \overline{\Omega}_f(t) \cap \overline{\Omega}_s(t)$, where the interaction takes place. On the remaining part of the boundaries $\Gamma_f$, $\Gamma_f^u$, and $\Gamma_f^\sigma$, we shall assume that appropriate boundary conditions have been specified, which makes the whole

STAR-CD™ is a registered trademark of Computational Dynamics Limited Corporation, United Kingdom.

problem well posed.

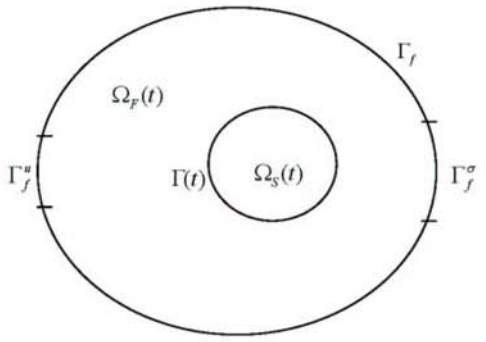


*Fig. 1: Fluid and solid domains.*

If one assumes that the fluid is incompressible, the flow-field variables are calculated from a set of equations that express in the spatial fluid domain $\Omega_F$ the conservation of fluid momentum and volume, the Navier-Stokes equations, as follows:

$$\begin{cases} div\, u = 0 \\ \rho_f \left( \dfrac{\partial u}{\partial t} + u \cdot \nabla u \right) = div\, \sigma_F + f \end{cases} \quad (1)$$

The body moves due to flow-induced forces. In addition to the fluid flow, the body motion is computed by solving the equations of motion (in general, six degrees of freedom):

$$\begin{cases} m \dfrac{dv_G}{dt} = F_z + F_f \\ J \dfrac{d\omega}{dt} + \omega \times (J\omega) = M_z + M_f \end{cases} \quad (2)$$

where $J$ is the operator of inertia of the solid $S$ in the centre of inertia (written in a reference frame related to the solid), $m$ is the mass of the solid, $F_z$ is the resultant of the external efforts solid/solid and gravity.

Initially the body shall be rigid; however, as shown in the latter part of the applications, the algorithm can be applied to flexible structures in which case, Eq. (2) is replaced by the continuum equations describing the dynamics of the flexible structure. The surface forces (pressure and shear) exerted by the fluid on the solid are given by :

$$\vec{F}_f = \int_\Gamma \sigma_F \cdot n_z d\gamma ,$$

where $\sigma_F$ is the constraint of Cauchy in the fluid :

$$\sigma_F = -pI + \upsilon \left( \nabla u + {}^t \nabla u \right)$$

and the moment of the efforts exerted by the fluid on the solid, to the centre of inertia G, is given by:

$$\vec{M}_f = \int_\Gamma \overrightarrow{GM} \times \sigma_F \cdot n_z d\gamma .$$

As the solid is rigid,

$$\forall M \in \Gamma(t),\ v(M) = v(G) + \omega \times \overrightarrow{GM} .$$

The nonslip condition is thus written as:

$$\forall x \in \Gamma(t),\ u(x) = v(G) + \omega \times x .$$

In addition, we have to have force equilibrium across the interface:

$$\sigma_F \cdot n_{|\Gamma(t)} = \sigma_z \cdot n_{|\Gamma(t)} ,$$

where $n_{|\Gamma(t)} = n_{z|\Gamma(t)} = -n_{F|\Gamma(t)}$ is the unitary normal vector of the solid wall $\Gamma$.

### 2.2 Arbitrary Lagrangian-Eulerian Formulation

In continuum mechanics, fluid motion is described by either of two classical formulations. In the Lagrangian approach, the independent variables are taken to be the initial position $a$ of a material point and time $t$. A Lagrangian description proves extremely useful in large deformation problems in solid mechanics. Nevertheless, this formulation includes severe distortions as the mesh deforms with the material. In the Eulerian description, the independent variables are spatial position $x$ and time $t$. The Eulerian approach is most often used in fluid mechanics. The mesh is fixed in space; so the description undergoes no distortion due to material motion.

For problems involving moving wall boundaries, it is necessary to have a middle formulation following the boundary motion and preserving the volume shape at the same time. To enable the computational mesh to remain regular, even in the presence of large structural displacements, Arbitrary Lagrangian-Eulerian (ALE) formulation has been introduced by Noh [5] and Hirt *et al.* [6] for finite difference formulation. Hughes *et al.* [7], Belytschko *et al.* [8], Liu and Huerta [9], and Benson [10] introduced the finite-element ALE formulation for incompressible viscous flows. Recently, the ALE method has been successfully applied to such moving boundary problems considering a rigid-body structure [11, 12]. The aim of the ALE formulation is to capture the advantages of both Lagrangian and Eulerian description while minimizing the disadvantages. The equations of motion are written in a form that accounts for the relative motion of the grid with respect to the fluid.

In the ALE description, each node is defined by the coordinates $\chi$. Figure 2 defines domains in space and associated mappings from one domain to another.

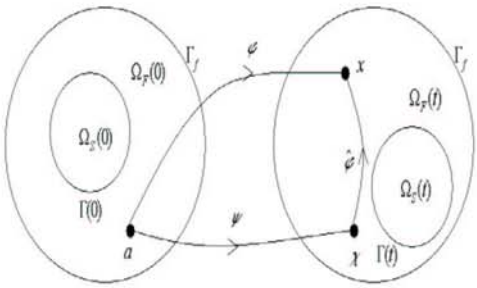


*Fig. 2: Representation of Eulerian, Lagrangian, and arbitrary reference domains.*

Therefore, the mapping $\varphi$ relates the Eulerian and Lagrangian space reference coordinates :

$$x = \varphi(a,t) .$$

Consider a physical property $g(x,t)$ expressed in the spatial

representation:

$$g(x,t) = g(\varphi(a,t),t) = \tilde{g}(a,t). \quad (3)$$

Now taking the time derivative of Eq. (3) with the material coordinates held fixed, we get:

$$\dot{g} = \left.\frac{\partial \tilde{g}}{\partial t}\right|_a = \left.\frac{\partial g}{\partial t}\right|_x + u \cdot \nabla_x g , \quad (4)$$

where $u = \left.\frac{\partial x}{\partial t}\right|_a$ is the material velocity.

Therefore, the mapping $\varphi$ relates the Eulerian and ALE space reference coordinates :

$$x = \hat{\varphi}(\chi,t) .$$

Thus, the physical property $g(x,t)$ can be expressed in the spatial representation as follows:

$$g(x,t) = g(\hat{\varphi}(\chi,t),t) = \hat{g}(\chi,t) \quad (5)$$

with the following time derivative expression :

$$\overset{\circ}{g} = \left.\frac{\partial \hat{g}}{\partial t}\right|_\chi = \left.\frac{\partial g}{\partial t}\right|_x + w \cdot \nabla_x g , \quad (6)$$

where $w = \left.\frac{\partial x}{\partial t}\right|_\chi$ is the mesh velocity.

Finally, we obtain a fundamental relationship that enables us to translate any law expressed in material (Lagrangian) variables into an equivalent law expressed in mixed variables :

$$\dot{g} = \overset{\circ}{g} + (u - w)\cdot \nabla_x g . \quad (7)$$

The arbitrary Lagrangian-Eulerian description may thus be viewed as a mapping of the initial configuration of the continuum into the current configuration of the reference frame. The Jacobian determinant $J = \det\left(\frac{\partial \varphi}{\partial a}\right)$ provides a link between mixed and material coordinates.

The Jacobian $J$ relates the current volume element $dV$ in the spatial frame to the associated volume element $dV_0$ in the referential frame :

$$dV = J(a,t)dV_0 , \text{ where } J(a,0) = 1.$$

One may show that the time rate of change of the mixed Jacobian is given by

$$J = \det\left(\frac{\partial \varphi}{\partial a}\right).$$

Consider a material coordinate $a$ taken to be the initial position, we get:

$$J(a,t)\rho_f(\varphi(a,t),t) = \rho_0(a)$$

that we write:

$$J\rho_f = \rho_0 .$$

Using the time derivative, we get the mass-conservation law:

$$\dot{\rho}_f + \rho_f \, div\, u = 0 . \quad (8)$$

Using this law and the relation in Eq. (7), we obtain the expression in the ALE formulation:

$$\overset{\circ}{\rho}_f + (u - w)\cdot \nabla_x \rho_f + \rho_f \, div\, u = 0 . \quad (9)$$

Using the same approach, we obtain the momentum-conservation law expressed in the ALE formulation.

In Eulerian form, we get:

$$\rho_f \left(\left.\frac{\partial u}{\partial t}\right|_x + u.\nabla u\right) = div\, u + f .$$

Using the relation in Eq. (7) for the physical property $u$, we obtain:

$$\dot{u} = \left.\frac{\partial u}{\partial t}\right|_x + u.\nabla u = \overset{\circ}{u} + (u - w)\cdot \nabla u .$$

Finally, Eq. (7) is a fundamental relationship that enables us to translate any law expressed in spatial (Eulerian) variables into an equivalent law expressed in mixed (ALE) variables:

$$\rho_f \left(\overset{\circ}{u} + (u - w)\cdot \nabla u\right) = div\, u + f .$$

Consider the relationship:

$$u(x,t) = u(\hat{\varphi}(\chi,t),t) = u \circ \hat{\varphi}(\chi,t) . \quad (10)$$

Now taking the time derivative of Eq. (10) with the mixed coordinates held fixed :

$$\overset{\circ}{u} = \left.\frac{\partial u \circ \hat{\varphi}}{\partial t}\right|_\chi .$$

Assuming incompressible fluid, the mass and momentum conservation equations are formulated as:

$$\begin{cases} div_x\, u = 0 & \text{in } \Omega_F(t) \\ \rho_f \left( \left.\frac{\partial u}{\partial t}\right|_\chi + (u - w)\cdot \nabla_x u \right) = div_x\, \sigma_F + f & \text{in } \Omega_F(t) \end{cases} . \quad (11)$$

The Geometric Conservation Law is invoked in the formulation $i$ to avoid errors induced by deformation of control volumes (see Thomas and Lombard [13] or Demirzic and Peric [14]). The surface of a control volume $V$ is described by $S$ and the surface vector $n$. In the case of moving grids, the space-conservation law (SCL) must be satisfied:

$$\frac{d}{dt}\int_V dV - \int_S w \cdot n dS = 0 .$$

To cope with large domain deformations and displacement, in addition to the ALE formulation, we need a means of treating sliding interfaces within the calculation domain of the fluid flow. Commercially available fluid-flow solvers are available with both these essential features for calculating fluid dynamics phenomena in domains undergoing large displacement or deformation. These methods are usually based on finite-element or finite-volume formulations.

The option of arbitrarily moving the mesh in the ALE description offers interesting possibilities. In fact, moving boundaries can be tracked with the accuracy characteristic of Lagrangian methods, and the interior mesh can be moved to avoid mesh distortion. Several procedures for mesh updating are explained in the literature [15–19]. Here in our application, the mesh motion is prescribed a priori based on the known rigid-body boundaries calculated at every instant.

### 2.3 Fully Implicitly Coupled Iteration Schemes

We assume that the domains for the fluid have been appropriately discretized. They shall be solved in a time-implicit manner.

The rigid-body movement is described by a set of ordinary differential equations of the form:

$$\begin{cases} m\dfrac{dv}{dt} = F(v,x,t) \\ \dfrac{dx}{dt} = v \end{cases}, \tag{12}$$

where $v$ is the velocity and $x$ is the position of the body.
In the context of transient fluid/rigid-body interaction, we have the choice of either explicit or implicit time integration of these ordinary differential equations. For example, the velocity equation is explicitly discretized as:

$$v_{n+1} = v_n + \Delta t \frac{F(v_n, x_n, t_n)}{m}. \tag{13}$$

Certain problems are better solved using an implicit discretization, particularly for problems with sensitive force-velocity behaviour, known as stiff problems in the mathematical sense. For stability reasons, we also prefer a time-implicit procedure for the overall time step. For example, the velocity equation is implicitly discretized as :

$$v_{n+1} = v_n + \frac{\Delta t}{2}\left(\frac{F(v_n, x_n, t_n) + F(v_{n+1}, x_{n+1}, t_{n+1})}{m}\right). \tag{14}$$

To calculate $v_{n+1}$, we must solve a nonlinear system :

$$G(v_{n+1}) = v_{n+1} - v_n - \frac{\Delta t}{2}\left(\frac{F(v_n, x_n, t_n) + F(v_{n+1}, x_{n+1}, t_{n+1})}{m}\right) = 0.$$

The most widely used and most robust method to accelerate convergence for the solution of a nonlinear system is the Newton-Raphson method. It requires the evaluation of derivatives approximated by finite differences. With the implicit method, the above equations are repeatedly applied until convergence is reached for each time step.

$$G(v_{n+1}) = 0$$
$$\begin{cases} v_{n+1}^0 \text{ initial guess} \\ v_{n+1}^{k+1} = v_{n+1}^k - \left[\nabla G(v_{n+1}^k)\right]^{-1} G(v_{n+1}^k) \end{cases}. \tag{15}$$

The Newton method is an iterative procedure. As a start, usually the initial value $v_{n+1}^0$ is predicted by an explicit scheme of the same order or simply from the result of the last time step ($v_{n+1}^0 = v_n$). In our application, $v_{n+1}^0$ is predicted with an explicit Adams-Bashforth scheme of order two :

$$v_{n+1}^0 = v_n + \frac{\Delta t}{2}\left(3\frac{F(v_n, x_n, t_n)}{m} - \frac{F(v_{n-1}, x_{n-1}, t_{n-1})}{m}\right). \tag{16}$$

Below is the description of the fully implicitly coupled iteration solution algorithm for nonlinear fluid/rigid-body interaction problems:

1. Explicit prediction of the interface velocity $v_{n+1}^0 = \left(v_{|\Gamma}\right)^{n+1}$ :

$$v_{n+1}^0 = \left(v_{|\Gamma}\right)^n + \frac{3}{2}\Delta t\left(a_{|\Gamma}\right)^n - \frac{1}{2}\Delta t\left(a_{|\Gamma}\right)^{n-1}. \tag{17}$$

2. Prediction of the interface position $x_{n+1} = x_n + \Delta t\, v_{n+1}^k$.
3. Compute fluid-mesh motion displacement based on the interface position $\Gamma_{n+1}$.
4. Computation of fluid-flow problem at $t_{n+1}$
   a. Kinematic compatibility condition on the interface:

$$\left(u_{|\Gamma}\right)^{n+1} = \left(v_{|\Gamma}\right)^{n+1} \tag{18}$$

   b. Computation of near-wall forces acting on the solid at $t_{n+1}$,

$$F_f^{n+1} = -\int_{\Gamma^{n+1}} \sigma_F^{n+1} \cdot n d\gamma. \tag{19}$$

5. Computation of solid problem at $t_{n+1}$
   a. Force equilibrium across the interface,

$$\sigma_F^{n+1} \cdot n_{|\Gamma_{n+1}} = \sigma_S^{n+1} \cdot n_{|\Gamma_{n+1}}. \tag{20}$$

   b. Update the velocity $v_{n+1}^k$ of the interface $\Gamma_{n+1}$ ; application of Eq. (15).
6. Check for convergence: If $\left\|v_{n+1}^k - v_{n+1}^{k-1}\right\| \le \varepsilon$, go to the next time step. Otherwise, again compute steps 2, 3, 4, and 5, updating the new velocity $v_{n+1}^k$ at $t_{n+1}$, computed at step 5.

A viable alternative approach to the Newton-Raphson method is to apply Eq. (14) instead of Eq. (15) to update $v_{n+1}^k$ in step 5. This is the basis of a sequential procedure with a larger convergence radius but less efficiency.
To realise the repetitions of the same time step we used a restart technique for moving mesh problems automated with an operating-system script. The calculation stages comprising initialisation, rigid-body dynamic analysis, mesh movement, and flow calculation are shown in the flow diagram in Fig. 3.

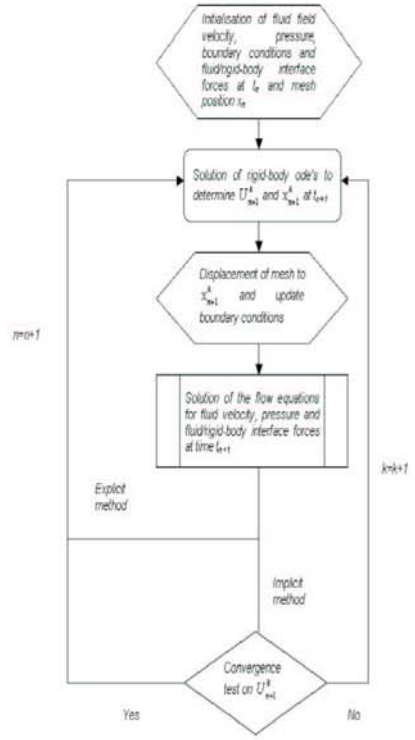


*Fig. 3: Flow diagram showing stages of the fluid-structure interaction calculation.*

### 2.4 Energy-Conserving And Stability Aspects

For fluid-structure-interaction problems with large displacements, it is necessary to have consistent and energy-conserving-interface boundary conditions at the moving fluid-solid interface. The coupling algorithm must be stable, and the discretization in time and space should respect the forces equilibrium at the fluid-solid interface. The fully implicit coupling algorithm developed in this paper respects this crucial property, taking the real velocity field at the interface as a test function for convergence. When the structure is assumed to be rigid, Abouri [20] demonstrated that the fully implicit scheme verifies that the variation of the sum of the kinetic energy of the system is equal to the difference between the energy introduced by the external boundary conditions and the energy dissipated by viscous effects inside the fluid. Grandmont [21] demonstrated this principle of energy conservation for the case of a linear elastic structure.

Le Tallec and Mouro [22] proposed a stability demonstration for an implicit fixed-point-relaxation algorithm; it coupled an implicit Euler treatment on the fluid domain and a midpoint rule for the structural equation. Similarly, Abouri [20] proposed a stability demonstration for the fully implicit coupling algorithm implemented here in the case of a rigid structure. The key point of the demonstration is to consider a global continuum-mechanics equation, including both fluids and solids, using variable functions for the physical quantities like density or velocity fields.

If a simple, explicit algorithm is used, we obtain a limitation in the time step and an unstable response. The explicit method is first-order accurate but only conditionally stable. In fact, the explicit staggering algorithm does not conserve energy at the interface because at each timestep the energy introduced by the fluid loading $\sigma_F^{n+1}$ on the structure is not equal to the energy change in the fluid. The difference between these two energies is

$$\int_{t^{n+1}} \sigma_F^{n+1}.(v_{n+1} - u_{n+1}) \cdot n d\gamma \,. \qquad (21)$$

For the explicit method, we have $\left(u_{|\Gamma}\right)^{n+1} = \left(v_{|\Gamma}\right)^n$. Therefore, the difference between the energies is $\int_{t^{n+1}} \sigma_F^{n+1}.(v_{n+1} - v_n) \cdot n d\gamma$, which is not equal to zero. The explicit coupling algorithm is not adequate to solve this type of problem because the delay between the two solvers, fluid and structure, creates energy dissipation. The kinematic condition implies equality of the velocities on the interface ($\left(u_{|\Gamma}\right)^{n+1} = \left(v_{|\Gamma}\right)^{n+1}$); the dynamic condition requires forces equilibrium across the interface ($\sigma_F^{n+1} \cdot n_{|\Gamma_{n+1}} = \sigma_S^{n+1} \cdot n_{|\Gamma_{n+1}}$). Those coupling conditions at the end of each new step are well fulfilled for the implicit scheme because the coupling variables are exchanged and the fluid domain is updated at each sub-iteration of each time step. The implicit method can be very useful to solve the fluid and the structure at the same time and to avoid energy dissipation created by an explicit method, owing to the delay between the two solvers.

## 3 APPLICATION TO COMPLEX INDUSTRIAL FLOWS

### 3.1 The Oscillating Piston Flow Meter

The moving element of this flow meter [23] consists of a hollow cylindrical piston with a horizontal mesh contained within a cylindrical working chamber provided with a cover (Fig. 4).

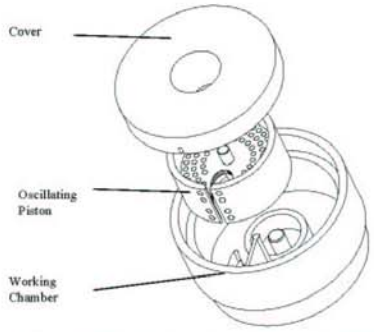


*Fig. 4: Three-dimensional view of working chamber and oscillating piston.*

A top view of an oscillating piston flow meter is shown in Fig. 5. The flow meter consists of a slotted piston, which oscillates in a working chamber comprising a partition or guide plate. A partition plate between the inlet and outlet ports forces incoming liquid to flow around a cylindrical measuring chamber and through the outlet port. The motion of the oscillating piston in the unit is transferred to a magnetic assembly in the measuring chamber, which is coupled to a follower magnet on the other side of the chamber wall. In one cycle, the angle $\theta$ undergoes one revolution. In fact, the piston is always moving in the same direction, and each revolution permits a certain volume of fluid to pass through the meter.

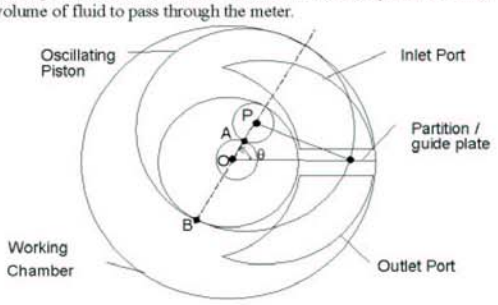


*Fig. 5: Schematic of an oscillating piston meter.*

### 3.2 Equations of Motion of the Mechanism and Treatment of Friction

The problem can be schematised by the slider-crank mechanism represented in Fig. 6. The connecting rod PQ is part of the oscillating piston.

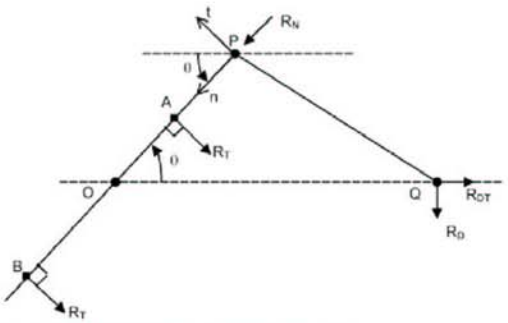


*Fig. 6: Free-body diagram of an oscillating piston.*

The equations of motion in normal (n), tangential (t) and axial (z) coordinates about O are:

$$\begin{aligned} F^n + G^n + R^n &= mr_{OP}\dot{\theta}^2 \\ F^t + G^t + R^t &= mr_{OP}\ddot{\theta} \\ M_F^z + M_C^z &= -\bar{I}^z\ddot{\beta} + mr_{OP}^2\ddot{\theta} \end{aligned} \quad , (22)$$

where

- $G$ = resultant body force due to weight according to the principle of Archimedes
- $F$ = resultant hydrodynamic force
- $M_F$ = resultant hydrodynamic moment about point O
- $R$ = reaction forces acting on the piston at contact lines
- $M_C$ = reaction force moment about point O
- $r_{OP}$ = distance between O and P
- $m$, $I$ = mass, moment of inertia about P of piston.

The friction in the n, t plane on the piston bottom or top surface can be expressed using the hypothesis that the repartition of the normal reaction force in the z direction is uniform. The choice of this treatment of friction for the plane contact on the bottom or top of the piston has proved to be useful when compared with experimental data.

### 3.3 Calculation Results

Inlet and outlet ports are positioned on the ends (top and/or bottom) of the working chamber to allow the positive displacement of fluid. The guide plate serves also to isolate the incoming and outgoing fluid. Figure 7 shows the mesh interface between two domains of fluid, one static (the inlet and outlet parts) and one deforming (the annular chamber with piston).

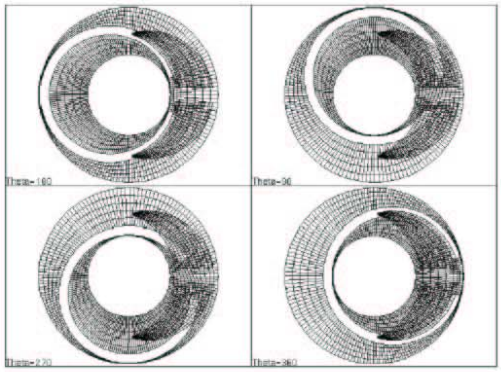

*Fig. 7: Evolution of mesh interface.*

Below are images of calculated results in an oscillating piston flow meter.
Figure 8 shows, at left, the velocity vectors in a plane through the meter and, at right, the contour pressure in a plane through the meter. We note the higher pressure (dark colour) in the inlet volumes to overcome piston friction, inlet and outlet losses, and inertial effects.

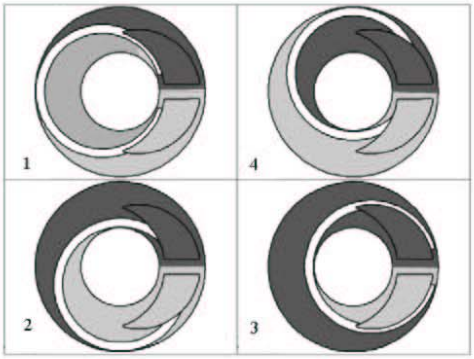


*Fig. 8: Piston movement cycle 1-2-3-4. Dark regions represent high-pressure inflow.*

The information available for the positive-displacement meter using the implicit approach are simulated calibration curves, pressure drops, forces acting on the components, and behaviour of meter in a time-varying consumption profile. The experiments offer quantitative data for detailed validation of the numerical solution.
Figure 9 shows the calculated calibration curve compared with experimental data in water at standard conditions. Comparisons were within 1%, which validates the fully coupled implicit algorithm.

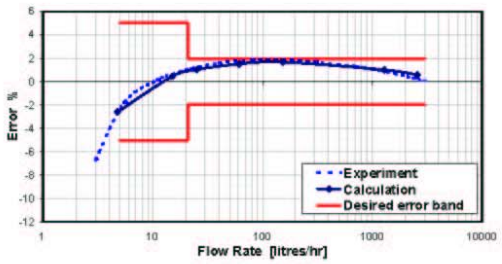


*Fig. 9: Comparison of predicted frequency against the measured frequency.*

### 3.4 Time and Space Discretization Tests

To demonstrate the robustness of the solution algorithm, time-step and grid-size dependence tests were carried out with the same boundary conditions and at high flow rate.
We compare the rotating velocity of the piston induced by fluid forces. We note that $N_r \times N_\theta \times N_z$ CV is the control volume number used with, respectively, $N_r$, $N_\theta$, and $N_z$ subdivisions in the direction $r$, $\theta$, and $z$ in the cylindrical reference frame related to the center of the box. Calculations were performed on four numerical grids which include one coarse grid with a $13 \times 90 \times 8$ CV and one refined grid with a $26 \times 270 \times 16$ CV.
For the coarse grid, three time increments were used : $\Delta t = T/82$, $\Delta t = T/164$ and $\Delta t = T/328$. Here $T$ represent the time period corresponding to one cycle of piston revolution.
Figure 10 shows a comparison of the rotating piston velocity calculated on the coarse grid with three different time steps during a revolution of approximately $T = 0.0492$ s. The close agreement of the results indicates that the temporal errors are small.

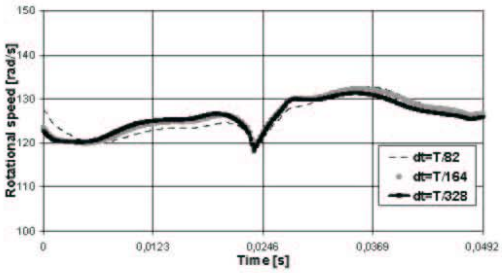


*Fig. 10: Comparison of predicted rotating piston velocity versus time using the coarse grid (13 × 90 × 8 CV) and various time steps.*

Figure 11 shows comparison between fine- and coarse-grid results during a revolution, both results obtained with $\Delta t = T/82$. As the grid is refined, the results converge to the same solution without any significant differences. These comparisons show that the spatial discretization errors are small enough to demonstrate the robustness of

the scheme.
Further grid refinement is necessary for numerically accurate results of particle tracking. However, in the optic of an optimisation form of the product, the numerical accuracy achieved with the grid with 13 × 180 × 8 CV and $\Delta t = T/82$ is sufficient to predict pressure drop or to derive calibration curves.

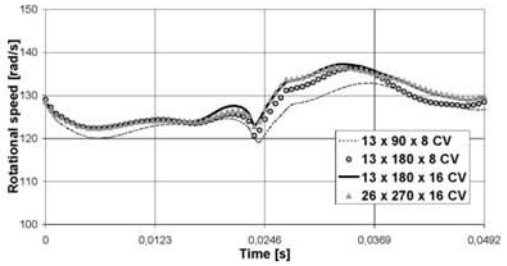


*Fig. 11: Comparison of predicted rotating piston velocity versus time using time step $\Delta t = T/82$ and various grids.*

### 3.5 Dynamics of a Spinner in a Conduit with Water Flow

The algorithm was used to calculate the dynamic response of an axial-flow spinner placed in a conduit used to indicate flow velocity. A lumped parameter analysis of such a spinner gives the classical equation:

$$I_{eff}\ddot{\theta} = \rho u A\left(\frac{\bar{r}u}{\tan\beta} - \bar{r}^2\dot{\theta}\right), \tag{23}$$

where $I_{eff}$ is the effective moment of inertia, including the mass of the fluid in the cylindrical volume swept by the blades, $\beta$ is the blade outlet flow angle, $\dot{\theta}$ is the spinner angular velocity, $u$ is the flow velocity, $\bar{r}$ is the effective blade radius, $A$ is the area of a plane disc normal to the flow and bounded by the blade root and tip radii, and ρ is the density of the fluid. The solution of the above equation compares well with the results from the explicit algorithm. As shown in Fig. 12, the error at terminal conditions is approximately 5%.

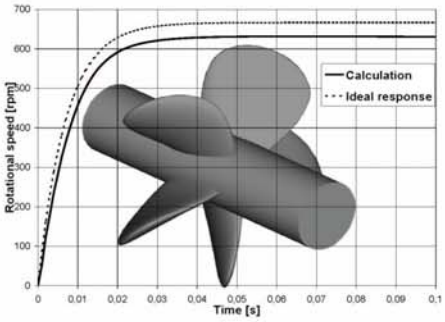


*Fig. 12: Dynamic response of the spinner (fluid is water, flow velocity = 1 m/s, initial spinner velocity = 0 rpm, β = 60 degrees, r = 8 mm).*

## 4 FURTHER VALIDATIONS

### 4.1 Fluid-Structure Interactions

The physical problem to be considered below deals with the prediction of steam-generator tube-bundle vibrations. In heat-exchanger-tube bundles, fluid-structure interaction is a crucial problem to overcome because fluid-structure and fluid-elastic effects may induce high amplitude displacements and lead to possible short-term failure through instability development. In this context, many studies are carried out to develop methods for the identification of critical flow velocity in tube arrays and to identify fluid-structure and fluid-elastic parameters in tubes and tube bundles. The results presented below are devoted to the identification of fluid-structure parameters of tubes and tube bundles in fluid without mean flows.

The dynamic equation governing the motion of a tube embedded in a fluid at rest can be written as follows, assuming the local flow remains laminar:

$$M_s\ddot{x} + C_s\dot{x} + K_s x = -M_a\ddot{x} - C_v\dot{x}, \tag{24}$$

where $M_s$, $M_a$, $C_s$, and $C_f$, respectively, represent tube mass, mass added by fluid, tube damping, and damping added by fluid. The following expressions describe the fluid structure parameters:

$$M_a = M_s\left(\frac{\omega_s^2}{\omega_e^2} - 1\right) \tag{25}$$

$$C_v = 2\left(M_s + M_a\right)\omega_e\xi_e - C_s, \tag{26}$$

where $\omega_s$ and $\omega_e$, respectively, represent the frequencies of tube alone and tube in fluid at rest, and $\xi_s$ and $\xi_e$ represent the associated damping ratios. Finally, dimensionless mass and damping terms are introduced to get results independent of the geometry defined by tube length, tube diameter, and pitch/diameter ratio.
The fluid-structure parameters in classical configurations involving concentric tubes and tube bundles are validated below. Numerical results are compared to available analytical or experimental data (Bendjeddou [24]).

### 4.2 Concentric Tubes

Fluid-structure interaction for a rigidly moving tube surrounded by an annular viscous fluid at rest is investigated (Fig. 13). A complete analytical and experimental study of this configuration was proposed by Chen *et al.* [25], Chen [26], and Yeh and Chen [27]. Analytical estimations of added mass and added damping are available. Different tube diameter ratio values $D_0/D$ were studied ($D_0/D$ = 1.2, 2.5, 4, and 10). In each case, different Stokes number values ($St$) were considered, such as $St$ = 10, 100, 5000, and ∞, corresponding to different dynamic viscosity values.

Dimensionless added mass and damping are numerically estimated and compared to available analytical values [25] in Figs. 14 and 15 for several values of the diameter ratio and the Stokes number. Numerical results are in good agreement with expected solutions, and the tube in fluid at rest features the expected behaviour.

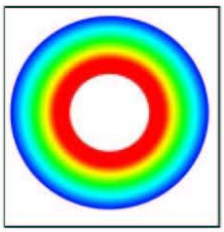

*Fig. 13: Mesh displacement for concentric tubes.*

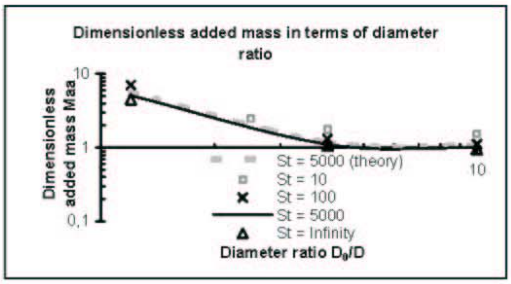


*Fig. 14: Dimensionless added mass in terms of diameter ratio for concentric tubes for different Stokes numbers for viscous fluid (St = 10, 100, 5,000) and nonviscous fluid (St = ∞). Comparison of numerical and available analytical solutions for St = 5,000 [25].*

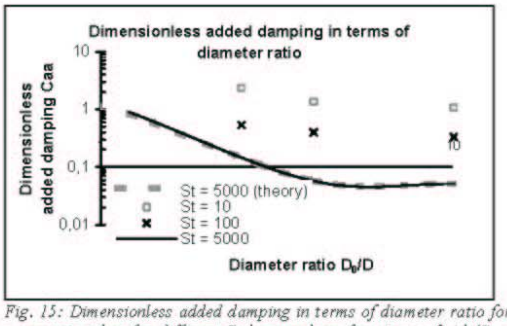


*Fig. 15: Dimensionless added damping in terms of diameter ratio for concentric tubes for different Stokes numbers for viscous fluid (St = 10, 100, 5,000). Comparison of numerical and available analytical solutions for St = 5,000 [25].*

### 4.3 Tube Bundles

Numerical identification of added mass and damping in fluid at rest for a single tube moving in a fixed tube bundle was investigated. The configuration involves an in-line square array with a pitch/diameter ratio (P/D) = 1.75, experimentally studied by Weaver and Abd-Rabbo [28]. The computational domain is shown in Fig. 16. The tube bundle is modelled by a periodic cell including two plain tubes with periodic inlet and outlet conditions, making it possible to simulate an infinite tube bundle in both cross directions.

Numerical damping is compared to available experimental data, while added mass is compared to a theoretical solution (Table 1). This analytical prediction is deduced from the law of Rogers *et al.* [29], which links fluid-structure parameters of tube bundles and concentric tubes.

According to the results, the expected trend was retrieved and the numerical solutions are in good agreement with predictions in terms of frequency and damping of the tube moving in fluid at rest.

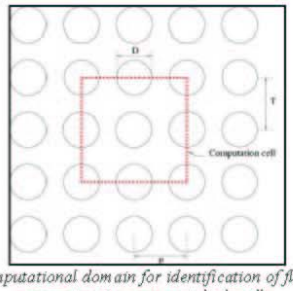


*Fig. 16: Computational domain for identification of fluid-structure parameters in a square tube bundle.*

*Table. 1: Frequency and damping for a single tube moving in a fixed tube bundle in fluid at rest with a pitch ratio P/D = 1.5 (Weaver [28]).*

| Tube bundle P/D = 1.5 | Numerical | Analytical (Chen [25]) | Experimental (Weaver [28]) |
|---|---|---|---|
| Frequency (Hz) | 20.55 | 20.3 | - |
| Damping (%) | 0.036 | 0.037 | 0.037 |

## 5 CONCLUSIONS

The present paper illustrates many potential applications for a numerical tool devoted to the simulation of fluid-structure interactions and flow-induced vibrations by using a fluid and structure code-coupling process. The implicit coupling algorithm has been demonstrated to be stable even for the case of stiff responses. Further development and validation will be performed to improve numerical schemes for coupling and to consider other industrial configurations.

## 6 REFERENCES

[1] **BS-7405** Selection and application of flowmeters for the measurement of fluid flow in closed conduits, 1991, *British Standards Institution.*

[2] **Sayma, A. I., Vahdati, M.,** and **Imregun, M.,** 2000, "Turbine forced response prediction using an integrated non-linear analysis," *Institution of Mechanical Engineers, Multi-body Dynamics Part K,* **214**(K1).

[3] **Blom, F.,** 1998, "A monolithical fluid-structure interaction algorithm applied to the piston problem," *J. Comput. Methods Appl. Mech. Engrg.* **167.**

[4] **STAR-CD,** 1999, "Methodology & User Guide", *Computational Dynamics Limited.*

[5] **Noh, W.F.**, 1964, "A time dependent two space dimensional coupled Eulerian Lagrangian code," *Meth. Comput. Phys. 3, Alder E. Fenbach and Rosenberg Editions.*

**[6] Hirt, C.W., Amsdern, A.A.** and **Cook, H.K.**, 1974, "An arbitrary Eulerian Lagrangian method for all flow speeds," *J. Comput. Phys.*, **14**, pp. [229-253].

[7] **Hughes, T.J.R., Liu, W.K.**, and **Zimmermann, T.K.**, 1981, "Lagrangian-Eulerian finite element formulation for incompressible viscous flows," *Computer Methods in Applied Mechanics and Engineering,* **29**, pp. [329-349].

[8] **Belyschko, T., Flanagran, D.F.** and **Kennedy, J.M.**, 1982, "Finite element method with user-controlled meshes for fluid-structure interactions," *Comput. Methods Appl. Mech. Engrg.*, **33**, pp. [689-723].

[9] **Liu, W.K.** and **Huerta, A.**, 1988, "Viscous flows for large free surface motion," *Comput. Methods Appl. Mech. Engrg.*, **69**, pp. [277-324].

[10] **Benson, D.**, 1989, "An efficient accurate, simple ALE method for non linear finite element programs," *Comp Meth in Appl Mech and Eng,* **33**, pp. [689-723].

[11] **Nomura, T.** and **Hughes, T.J.R.**, 1992, "An Arbitrary Lagrangian Eulerian finite element method for interaction of fluid and rigid body," *Comput. Methods Appl. Mech. Engrg.* **95**, pp. [115-138].

[12] **Sarrate, J., Huerta, A.** and **Donea, J.**, 1998, "Arbitrary Lagrangian-Eulerian formulation for fluid-multi rigid bodies interaction problems," *Computational Mechanics.*

**[13] Thomas, P.D.** and **Lombard, C.K.**, 1979, "Geometric conservation law and its application to flow computations on moving grids," *AIAA Journal 17,* **1030.**

[14] **Demirzic, I.** and **Peric, M.**, 1988, "Space Conservation Law In Finite Volume Calculations Of Fluid Flow," *Int. J. Numer. Methods in Fluids,* ***8***, pp. [1037-1050].

[15] **Souli, M., Ouahsine, A.** and **Lewin, L.**, 2000, "ALE formulation for fluid-structure interaction problems," *Comput. Methods Appl. Mech. Eng.* **190**, pp. [659-675].

[16] **Hughes, T.J.R.**, 1987, "The finite element method. Linear static and dynamic finite element analysis," *Englewood Cliffs, New Jersey : Prentice-Hall, Algorithms for hyperbolic and parabolic-hyperbolic problems,* pp. [490-567].

[17] **Blom, F.J.**, 1998, "Investigations on computational fluid-structure interaction, " *Thèse, Ecole polytechnique fédérale de Lausanne.*

[18] **Van Leer, B.**, 1982, "Flux-Vector Splitting for the Euler Equations," *Proc. 8th Int. Conf. On Numerical Methods in Fluid Dynamics, Springer Verlag,* pp. [507-512].

[19] **Batina, J.T.**, 1991, "Implicit flux-split Euler schemes for unsteady aerodynamic analysis involving unstructured dynamic meshes," *AIAA J.*, **29**, pp. [1836-1843].

[20] **Abouri, D.**, 2003, "A Fluid Rigid Body Interaction Algorithm : Application to Volumetric Flow Meter," *Thesis, University of Poitiers, France.*

[21] **Grandmont, C.**, 1998, "Analyse mathématique et numérique de quelques problèmes d'interaction fluide-structure, " *Thèse, Université de Paris VI.*

[22] **Le Tallec, P.** and **Mouro, J.**, 2001, "Fluid structure interaction with large structural displacements," *Comp. Meth. in applied mechanics and engineering.*, 190(24-25), pp. [3039–3067].

[23] **Linford, A.** ,1949, "Flow Measurement & Meters. N.Tetlow, London,".

[24] **Bendjeddou, Z.**, 2005, "Méthodologie pour la simulation numérique des vibrations induites par écoulements dans les faisceaux de tubes, " *Thèse, Université de Lille.*

[25] **Chen, S.S., Wambsganss, M.W., Jendrzejczyk, J.A.**, 1976, "Added mass and damping of a vibrating rod in confined viscous fluids," *Journal of Applied Mechanics, Transaction of ASME,* **43**, pp. [325-329].

[26] **Chen, S.S.**, 1987, "Flow-induced vibration of circular cylindrical structures," *Hemisphere publishing corporation*

[27] **Yeh, T.T., Chen, S.S.**, 1978, "The effect of fluid viscosity on coupled tube/fluid vibration," *Journal of Sound and Vibration,* **59(3)**, pp. [453-467].

[28] **Weaver, D.S, Abd-Rabbo, A., 1985,** "A flow visualisation study of a square array of tubes in water crossflow," *Journal of Fluids Engineering,* **107**,pp. [354-363].

[29] **Rogers, R.J., Taylor, C., Pettigrew, M.J.**, 1984, "Fluid effects on multispan heat exchanger tube vibration," *ASME Pressure Vessel and Piping Conference, San Antonio, Texas.*

# REFERENCES

# REFERENCES


Abouri, D. (2003). Un algorithme d'interaction fluide solide rigide : application à la volumétrie. *Thèse de doctorat*.

Abouri, D., Parry, A., Hamdouni, A. (2003). Fluid-rigid body dynamic interaction in complex industrial flow. *Advances in Fluid Mechanics : Fluid structure interaction II, Wit Press*, 295-305.

Addad Y., Benhamadouche S., Laurence D. (2003). The Negatively Buoyant Wall-Jet: LES Database, In Hanjalic, Nagano and Tummers. *Turbulence, Heat and Mass Transfer*, 4, 467-474, Beggel House, Inc.

Adobes, A., Gosse, A., Barrate, C. (2001). Qualification of motion dependent fluid forces coefficients. *PVP Conference*, Atlanta.

Andriambololona, H., Bosselut, D., Longatte, E. (2005). Insertion of a slim structure into a channel : simulation and parametric analysis. *EURODYN*, Paris.

Archambeau, F., Méchitoua, N., Sakiz, M. (2004). Code_Saturne : a finite volume code for the computation of turbulent incompressible flows – industrial applications. *International Journal on Finite Volumes*.

Axisa, F. (2001). Modélisation des systèmes mécaniques : Tome 4 : vibrations sous écoulements. *Hermes Sc. Publications*.

Bailly, C. (1994). Modélisation du rayonnement acoustique des écoulements turbulents libres subsoniques et supersoniques. *Thèse de doctorat*.

Bailly, C., Lafon, P., Candel, S. (1994). A stochastic approach to compute noise generation and radiation of free turbulent flows. *AIAA Conference*, 95-092.

Baj, F. (1998). Amortissement et instabilité fluide-élastique d'un faisceau de tubes sous écoulement diphasique. *Thèse de doctorat*, Université Paris VI.

Bastin, F. (1997). Etude numérique du bruit de jet rayonné par les structures cohérentes de la turbulence. *Thèse de doctorat*, Ecole Centrale Paris.

Béchara, W., Bailly, C., Lafon, P., Candel, S. (1994). Stochastic approach to noise modelling for free turbulent flows. *AIAA Journal*, 32(4), 455-463.

Bendjeddou, Z. (2005). Méthodologie pour la simulation numérique des vibrations induites par les écoulements dans les faisceaux de tubes. *Thèse de doctorat*, Université de Lille.

Benhamadouche, S., Laurence, D., Jarrin, N., Imran, A. (2005). Large Eddy Simulation of flow across in-line tube bundles. *NURETH-11*, Avignon.

Benhamadouche, S., Jarrin N. (2004). Ecoulement dans des faisceaux de tubes en configuration carrée avec la L.E.S. *EDF R&D,* HI-83/04/004.

Benhamadouche, S. and Laurence, D. (2003). LES, Coarse LES, and Transient RANS Comparisons on The Flow Across Tube Bundle. *International Journal of Heat and Fluid Flow*, 24 (4), 470-479.

Benhamadouche, S., Sakiz, M., Péniguel, C., Stéphan, J.M. (2003). Presentation of New Methodology of Chained Computations using Instationary 3D Approaches for the determination of Thermal Fatigue in a T-Junction of a PWR Nuclear Plant". *17th International*

*Conference on Structural Mechanics in Reactor Technology, SMIRT17,* Prague.

Benhamadouche, S., Jarrin, N., Fontes, J.P. (2002). Validation de la LES dans une version de développement de *Code_Saturne* : cas des canaux plans et des marches descendantes. *EDF R&D, HI-83/02/018*.

Benhamadouche, S. (2001). Implantation de la LES dans une version de développement de *Code_Saturne*. *EDF R&D, HI-83/01/25/A*.

Benhamadouche, S. (2001). Modélisation de sous-maille pour la LES - Validation avec la Turbulence Homogène Isotrope (THI) dans une version de développement de *Code_Saturne*. *EDF R&D*, HI-83/01/033.

Blevins, R.D. (1990). Flow-induced vibrations. *Krieger Publishing Company, second edition*.

Bogey, C., Bailly, C., Juvé, D. (2003). Noise investigation of a high subsonic, moderate Reynolds number jet using a compressible LES. *Theoretical and Computational Fluid Dynamics*, 16(4), 273-297.

Bogey, C., Bailly, C., Juvé, D. (2002). Computation of flow noise using source terms in linearized Euler's equations. *AIAA Journal*, 40(2), 235-243.

Caillaud, S. (1999). Excitation forcée et contrôle actif pour la mesure des forces fluide-élastiques. *Thèse de doctorat*, Université Pierre et Marie Curie, Paris VI.

Chen, S.C. (1987). Flow-Induced Vibration of Circular Cylindrical Structures. *Hemisphere Publishing Corporation,* Washington.

Chen, S.S., Yeh, T.T. (1977). The effect of fluid viscosity on coupled tube / fluid vibrations. *Journal of Sound and Vibration, 59, 453-467*.

Chen, S.S., Wambsganss M.W., Jendrzejczyk J.A. (1976). Added mass and damping of a vibrating rod in confined viscous fluids. *Journal of Applied Mechanics*, 43, 325-329.

Connors, H.J. (1978). Fluidelastic vibration of heat exchanger tube arrays. *Journal of Mechanical Design*, 100, 347-353.

Crouzet, F., Lafon, P., Buchal, T., Laurence, D. (2002). Aerodynamic Noise Prediction in Internal Flows Using LES Simulations and Euler Equations Acoustic Modelling. *8th AIAA/CEAS Aeroacoustics Conference*, Breckenridge, Colorado.

De Langre, E., (2002). Fluides et solides. *Ed. Ecole Polytechnique*.

Donea, J. (1982). An arbitrary lagrangian eulerian finite element method for transient dynamic fluid structure. *Computer Methods in Applied Mechanics and Engineering*, 33, 689-723.

Durand, C. (2005). Code_Aster, l'outil de modélisation en mécanique à EDF, *Giens*.

Farhat, C. Lesoinne, M., Le Tallec, P. (1998). Load and motion transfer algorithms for fluid structure interaction problems with non-matching discrete interfaces : momentum and energy conservation, optimal discretization and application to aeroelasticity. *Computer methods in applied mechanics and engineering,* 157, 95-114.

Farhat, C. Lesoinne, M., Stern, P., Lantéri, S. (1997). High performance solution of three-dimensional non linear aeroelastic problems via parallel partitioned algorithms : methodology and preliminary results. *Advances in Engineering Software,* 28, 43-61.

Farhat, C. Lesoinne, M., Maman, N. (1995). Mixed explicit implicit time integration of coupled aero elastic problems : three field formulation, geometric conservation and

distribution solution. *International Journal for Numerical Methods in Fluids*, 21, 807-835.

Farhat, C. Lesoinne, M. (1993). Automatic partitioning of unstructured meshes for parallel solution of problems in computational mechanics. *International Journal for Numerical Methods in Engineering*, 36, 745-764.

Feenstra, P.A., Weaver, D.S, Nakamura, T. (2003). Vortex shedding and fluid elastic instability in a normal square tube array excited by two-phase cross flow. *Journal of Fluids and Structures*, 17, 793-811.

Fernandez Varela, M.A. (2001). Modèles simplifiés d'interaction fluide structure. *Thèse de doctorat*, Université Paris IX.

Fischer, M., Stolz., J., Strohmeier, K. (2003). Three-dimensional simulation of tube bundle vibration induced by cross flow in real apparatus. *PVP Conference*, Cleveland.

Fujita, K., Wakita, T. (2004). Fluid elastic vibration analysis of circular cylinder arrays based on hybrid method using CFD and analytical solution. *FIV Conference*. Paris.

Gibert, R.J. (1988). Vibrations des structures. Interactions avec les fluides. Sources d'excitation aléatoires. *Eyrolles*.

Gloerfelt, X., Bogey, C., Bailly, C. (2006). Cavity noise, chapter 6.3, in LES for Acoustics, ed. by C. Wagner, T. Hüttl & P. Sagaut. *Cambridge University Press*, 311-322.

Granger, S., Perotin, L. (1997). An inverse method for the identification of a distributed random excitation acting on a vibrating structure: Part 1: Theory. *ASME Conference, Symposium on Fluid-Structure Interactions*.

Granger, S., Perotin, L. (1997). An inverse method for the identification of a distributed random excitation acting on a vibrating structure: Part 2: Flow-induced vibration application. *ASME Conference, Symposium on Fluid-Structure Interactions*.

Granger, S. and Gay, N. (1996). An unsteady semi-analytical model for cross flow induced vibration in tube bundle : comparison with experiment. *Flow induced vibrations*, Rotterdam.

Granger, S. and Païdoussis, M.P. (1996). An improvement to the quasi-steady model with application to cross flow induced vibration in tube array. *Journal of Fluid Mechanics*, 320, 163-184.

Greffet, N. (2001). Simulation couplée fluide structure appliquée aux problèmes d'instabilité non linéaire sous écoulement. *Thèse de doctorat*, Ecole Normale Supérieure de Cachan.

Guimet, V. (1998). Analyse numérique et simulation de problèmes d'interaction fluide structure en régime incompressible. *Thèse de doctorat*, Université Paris VI.

Hadj-Sadok, C. (1994). Forces fluide-élastiques dans un faisceaux de tubes soumis à un écoulement transversal. *Thèse de doctorat*, Université Pierre et Marie Curie, Paris VI.

Hémon, P. (1999). An improvement of the time-delayed quasi-steady model for the oscillations of circular cylinders in cross flow. *Journal of fluids and Structures*, 13, 291-307.

Hron, J., Turek, S. (2006). Proposal for numerical benchmarking of fluid structure interaction between elastic object and laminar incompressible flow. *In H.-J. Bungartz and M. Schäfer, editors, LNCSE series, Springer, to appear*.

Hugues, T.J.R., Liu, W.K., Zimmermann, T.K. (1981). Lagrangian Eulerian finite element formulation for incompressible viscous flows. *Computer Methods in Applied Mechanics and Engineering*, 29, 329-349.

Huvelin, F., Longatte, E., Verreman, V., Souli, M. (2006). Numerical simulation of dynamic instability for a pipe conveying fluid. *PVP Conference*, Vancouver.

Laurence, D. (2002). Large Eddy Simulation of Industrial Flows? Closure Strategies for turbulent and transitional flows, B. *Launder and N. Sandham Eds, Cambridge U.P.,* 392-406, ISBN 0 521 79208 8.

Le Tallec, P., Mouro, J. (1996). Fluid structure interaction with large structural displacements. *Computer Methods in Applied Mechanics and Engineering*, 190 (24-25), 3039-3067.

Liang, C., Papadakis, G. (2004). Large eddy simulation of cross flow over inline and staggered tube bundles. *FIV Conference*. Paris.

Longatte, E., Verreman, V., Souli, M. (2006). Numerical tool for simulation of flow-induced vibrations, part I : Theory. *Journal of Fluids and Structures, soumis*.

Longatte, E., Verreman, V., Souli, M. (2006). Numerical tool for simulation of flow-induced vibrations, part II : Application. *Journal of Fluids and Structures, soumis*.

Longatte, E., Verreman, V., Bendjeddou, Z., Souli, M. (2005). Comparison of strong and partitioned fluid structure code coupling methods. *PVP Conference*, Denver.

Longatte, E., Bendjeddou, Z., Verreman, V., Souli, M. (2005). Explicit and implicit code coupling schemes in fluid structure interaction. *PVP Conference*, Denver.

Longatte, E., Huvelin, F., Souli, M. (2005). Code coupling for simulation of flow-induced vibrations. *1er Colloque du GDR Interactions Fluide Structure*, Sophia-Antipolis.

Longatte, E., Bendjeddou, Z., Souli, M. (2004). Comparison of code coupling scheme for simulation of fluid structure problems. *PVP Conference*, San Diego.

Longatte, E., Bendjeddou, Z., Souli, M. (2003). Application of Lagrangian Eulerian formulations to flow-induced vibration problems. *Journal of Pressure Vessel Technology*.

Longatte, E., Bendjeddou, Z., Souli, M. (2003). Methods for numerical study of tube bundle vibrations in cross-flows. *Journal of Fluids and Structures*, 18 (5), 513-528.

Longatte, E., Laurence, D., Barré, F., Ledac, P. (2001). Application of Large Eddy Simulation to a flow-induced vibration problem. *PVP Conference*, Atlanta.

Longatte, E. (1998). Modélisation de la propagation et de la génération du bruit au sein des écoulements turbulents internes. *Thèse de doctorat*, Ecole Centrale Paris.

Lucor, D. (2004). Generalized Polynomial chaos : applications to random oscillators and flow-structure interactions. *Ph. D. Thesis, Brown University*.

Lucor, D., Karniadakis, G. (2004). Predictability and uncertainty in flow-structure interactions. *European Journal of Mechanics/B Fluids*, 23/1, 41-49.

Maman, N., Farhat, C. (1995). Matching fluid and structure meshes for aeroelastic computations : a parallel approach. *Computers and Structures*, 54-4, 779-785.

Mimouni, S., 2006, Modélisation 3D de la cavitation et validation dans le code Neptune CFD. *EDF R&D, HI-81/05/04/A*.

Morand, H., Ohayon, R. (1995). Fluid structure interaction – Applied numerical methods. *John Wiley & Sons and Masson Editions*.

Moulinec, C., Pourquié, M.J.B.M., Boersma, B.J. and Nieuwstadt, F.T.M. (2001). Diagonal Cartesian Method on staggered grids for a DNS in a tube bundle. *Direct and Large-Eddy Simulation IV*, Enschede.

Mureithi, N.W., Zhang, C., Pettigrew, M.J. (2004). Fluidelastic instability tests on an array of tubes preferentially flexible in the flow direction. *FIV Conference*. Paris.

Païdoussis, M.P. (2004). Fluid-structure interactions : slender structures and axial flow. *Academic Press*.

Péniguel, C., Sakiz, M., Benhamadouche, S. (2003). Projet DOMZOME T2 00 04 : Etude thermohydraulique L.E.S. et thermique du piquage RRA de Civaux (ancienne configuration) pour un bêta de 10% à l'aide des logiciels *Code_Saturne* et *Syrthes*. *EDF R&D, HI-83/03/018*.

Péniguel, C., Sakiz, M., Benhamadouche, S. (2003). Projet DOMZOME T2 00 04 : Etude thermohydraulique L.E.S. et thermique de la maquette FATHER à l'aide des logiciels *Code_Saturne* et *Syrthes* . *EDF R&D, HI-83/03/019*.

Pettigrew, M. J. and Taylor, C.E. (2004). Damping of Heat Exchanger Tubes in two-phase flows : review and design guidelines. *Journal of Pressure Vessel Technology*, 126 (4), 523-533.

Piperno, S. and Farhat, C. (2001). Partitioned procedures for the transient solution of coupled aeroelastic problems. Part II : energy transfer analysis and three-dimensional applications. *Comput. Methods Appl. Mech. Engrg., 190, 3147-3170*.

Piperno, S. (1997). Explicit, implicit fluid, structure staggered procedures with a structural predictor and fluid subcycling for 2D inviscid areoelastic simulations. *International Journal for Numerical Methods in Fluids, 25, 1207-1226*.

Piperno, S., Farhat, C. (1997). Design and evaluation of staggered portioned procedures for fluid structure interaction simulations. *INRIA, 3241*.

Piperno, S., Farhat, C., Larrouturou, B. (1995). Partitioned procedures for the transient solution of coupled aeroelastic problems. Part I : model problem, theory and two-dimensional application. *Comput. Methods Appl. Mech. Engrg., 124, 79-112*.

Price, S.J. Païdoussis, M. P. (1997). An improved mathematical model for the stability of cylinder flows subject to cross-flow. *Journal of Sound and Vibration,* 97(4), 615-640.

Price, S.J., Païdoussis, M.P. (1989). The flow-induced response of a single flexible cylinder in an in-line array of ridig cylinders. *Journal of Fluids and Structures, 3, 61-82*.

Price, S.J., Païdoussis, M.P. (1986). A single-flexible-cylinder analysis for the fluidelastic instability of an array of flexible cylinders in cross flow. *Journal of Fluids Engineering, 108, 193-199*.

Price, S.J. and Païdoussis, M.P (1984). An improved mathematical model for the stability of cylinder rows subjected to cross flow. *Journal of Sound and Vibration*, 97, 615-640.

Price, S.J. Païdoussis, M. P. (1984). The aerodynamic forces acting on groups of two and three circular cylinder when subject to a cross-flow, *Journal of Wind Enginnering and Industrial Aerodynamics, 17, 329-347*.

Renou, J.Y., 1998, Une méthode eulérienne pour le calcul numérique de forces fluide-élastiques. *Thèse de doctorat*, Université Paris VI.

Rogers, J., Taylor, C., Pettigrew, M.J. (1994). Two-phase flow-induced vibration : an overview. *Journal of Pressure and Vessel Technology*, 116, 233-253.

Rollet-Miet, P. (1997). Simulation des Grandes Echelles sur maillages non structurés pour géométries complexes, *Thèse de doctorat*, Ecole Centrale de Lyon.

Schäfer, M., Lange, H., Heck, M. (2005). Implicit partitioned fluid structure interaction

coupling. *1er Colloque du GDR Interactions Fluide Structure*, Sophia-Antipolis.

Schäfer, M., Teschauer, S. (2001). Numerical simulation of coupled fluid solid problems. *Computer Methods in Applied Mechanics and Engineering*, 190, 3645-3667.

Sigrist, J.F. (2004). Modélisation et simulation numérique d'un problème couplé fluide structure non linéaire. Application au dimensionnement de structures nucléaires de propulsion navale. *Thèse de doctorat*. Ecole Centrale de Nantes.

Sigrist, J.F., Melot, V., Laine., C, Peseux, B. (2004). Numerical simulation of fluid structure problem by coupling fluid finite volume and structure finite element or modal approach. *FIV Conference*. Paris.

Simonin, O., Barcouda M. (1988). Measurements and prediction of turbulent flow entering a staggered tube bundle", *Fourth Int. Symp. on App. of Laser Anemometry to fluid mechanics,* Lisbon.

Souli, M., Zolesio, J.P. (2001). Arbitrary Lagrangian-Eulerian and free surface methods in fluid mechanics. *Computer Methods in Applied Mechanics and Engineering*, 191, 451-466.

Souli, M. (2000). ALE and fluid structure interaction capabilities in LS-Dyna. *PVP Conference*, Atlanta.

Souli, M., Ouahsine, A., Lewin, L . (2000). ALE formulation for fluid structure interaction problems. *Computer Methods in Applied Mechanics and Engineering*, 190, 659-675.

Tanaka, H., Takahara, S. (1981). Fluid elastic vibration of tube array in cross flow. *Journal of Sound and Vibration*, 77, 19-37.

Thomas, P.D., Lombard, C.K. (1979). Geometric conservation law and its application to flow computation on moving grids. *AIAA Journal*, 17, 1030-1037.

Van Herpe, F. (1993). Numerical estimation of the sound produced by a fluid flow in a duct obstructed by a diaphragm. *Ph.D. Thesis*, Cambridge University.

Yang, C.I., Moran, T.J. (1979). Finite element solution of added mass and damping of oscillation rods in viscous fluids. *Journal of Applied Mechanics*, 46, 519-523.

Weaver, D.S., Fitzpatrick, J.A., Elkashlan, H. (1986). Strouhal numbers for heat exchanger tube arrays in cross flow. *Journal of Pressure Vessel Technology*, 109, 219-223.

# PROGRAMME DE COURS EN IFS

# PROGRAMME DE COURS EN IFS

**Partie I. Méthodes numériques pour l'interaction fluide structure**

Chapitre 1. Vibrations linéaires d'une structure
*1. Hypothèses générales*
*2. Formulation forte et formulation faible du problème*
*3. Discrétisation par la méthode des éléments finis*
*4. Formulation discrète. Problème modal et temporel*
*5. Exemple d'application : modes de flexion d'une poutre élastique*

Chapitre 2. Vibrations linéaires d'un fluide
*1. Hypothèses générales*
*2. Formulation forte et formulation faible du problème*
*3. Discrétisation par la méthode des éléments finis*
*4. Formulation discrète. Problème modal et temporel*
*5. Exemple d'application : modes acoustiques d'une cavité cylindrique*
*6. Exemple d'application : modes de ballottement d'un réservoir cylindrique*

Chapitre 3. Structure couplée avec un fluide incompressible
*1. Hypothèses générales*
*2. Formulation forte et formulation faible du problème*
*3. Discrétisation par couplage éléments finis/éléments finis*
*4. Formulation discrète. Problème modal et temporel*
*5. Exemple d'application : poutre élastique couplée avec un fluide contenu dans une cavité cylindrique*
Chapitre 4. Dynamique vibratoire d'un système couplé fluide structure
*1. Hypothèses générales*
*2. Formulations non symétriques*
*3. Formulations symétriques*
*4. Exemple d'application : poutre élastique couplée avec un fluide compressible sans surface libre*
*5. Exemple d'application : poutre élastique couplée avec un fluide incompressible avec surface libre*

Chapitre 5. Etude dynamique de problèmes d'interaction fluide structure
*1. Méthodes modales*
*2. Méthodes directes*
*3. Exemple d'application : fluide incompressible avec surface libre soumis à un choc*
*4. Exemple d'application : poutre élastique et fluide incompressible soumis à un choc*
*5. Exemple d'application : poutre élastique et fluide compressible soumis à un choc*

Chapitre 6. Applications industrielles
*1. Calcul des modes propres d'une hélice marine*
*2. Réponse au séisme d'un réacteur nucléaire*

**Partie II. Méthodes numériques pour le couplage fluide structure**

Chapitre 1. Dynamique d'un fluide réel
*1. Hypothèses générales*
*2. Modélisation mathématique des équations de conservation*
*3. Méthodes de discrétisation temporelle et spatiale*
*4. Exemple d'application : écoulement de Couette cylindrique*
*5. Exemple d'application : ballottement d'un fluide dans un réservoir cylindrique*

Chapitre 2. Dynamique d'un fluide en présence d'une frontière mobile
*1. Hypothèses générale*
*2. Modélisation des parois mobiles et frontières libres*
*3. Méthodes de discrétisation temporelle et spatiale*
*4. Exemple d'application : oscillations forcées d'un cylindre dans d'un fluide parfait en milieu confiné*
*5. Exemple d'application : cylindre impulsé dans un fluide visqueux non confiné*

Chapitre 3. Vibrations d'une structure couplée avec un fluide initialement au repos
*1. Position du problème*
*2. Méthodes de couplage*
*3. Résolution explicite, implicite*
*4. Exemple d'application : oscillations libres d'un cylindre dans d'un fluide parfait en milieu confiné*
*5. Exemple d'application : oscillations d'une poutre avec surface libre*

Chapitre 4. Vibrations d'une structure couplée avec un fluide en écoulement
*1. Position du problème*
*2. Méthodes de chaînage et de couplage*
*3. Problématiques liées à la turbulence*
*4. Exemple d'application : vibration d'une poutre induite par la turbulence*

Chapitre 5. Applications industrielles
*1. Vibration d'un tube en présence d'un fluide au repos dans un faisceau de tubes*
*2. Vibrations d'un tube induites par un écoulement dans un faisceau de tubes*

**Partie III. Méthodes numériques pour le couplage fortement non linéaire**

Chapitre 1. Dynamique non linéaire d'une structure
*1. Hypothèses générales*
*2. Formulation mathématique*
*3. Discrétisation par la méthode des éléments finis*
*4. Intégration en temps : méthode explicite*
*5. Exemple d'application : impact d'un cylindre creux*

Chapitre 2. Dynamique non linéaire d'un fluide
*1. Hypothèses générales*
*2. Formulation mathématique*
*2. Résolution numérique : discrétisation spatiale et temporelle*
*3. Traitement des problèmes fluide multi-phasique*

*4. Exemple d'application : ballottement d'un fluide*

Chapitre 3. Algorithmes de contact en dynamique non linéaire
*1. Problématique*
*2. Algorithmes de gestion des contacts*
*3. Application aux problèmes couplés fluide/structure*

Chapitre 4. Réponse d'un fluide à un impact d'une structure rigide
*1. Problématique*
*2. Méthode de résolution numérique*
*3. Exemple d'application : impact d'une bille sur un fluide non borné*

Chapitre 5. Réponse d'un système couplé fluide/structure à un impact
*1. Problématique*
*2. Méthode de résolution numérique*
*3. Exemple d'application : choc sur un réservoir fluide déformable*

Chapitre 6. Applications industrielles